UNIVERSITY OF CALIFORNIA

Santa Barbara

INVESTIGATING THE HOMO-OLIGOMERIZATION OF THE HUMAN ADENOSINE A2A RECEPTOR

A dissertation submitted in partial satisfaction of the

requirements for the degree Doctor of Philosophy

in Chemistry

by

Khanh Dinh Quoc Nguyen

Committee in charge:

Professor Song-I Han, Co-Chair

Professor Michelle O'Malley, Co-Chair

Professor Frederick Dahlquist

Professor Lior Sepunaru

Professor Arnab Mukherjee

December 2021

The dissertation of Khanh Dinh Quoc Nguyen is approved.

_____
Arnab Mukherjee

_____
Lior Sepunaru

_____
Frederick Dahlquist

_____
Michelle O'Malley, Committee Co-Chair

_____
Song-I Han, Committee Co-Chair

December 2021

Investigating the Homo-Oligomerization of the Human Adenosine A_{2A} Receptor

by

Khanh Dinh Quoc Nguyen

ACKNOWLEDGMENTS

Completion of the Ph.D. program wraps up not only my graduate school journey but also my first chapter in America and my 23-year-long education stage. Therefore, I will write a prolonged text to express my gratitude towards the many people who have helped me all these years, even though it is rather futile no matter how many words I put down.

First of all, I would like to acknowledge the several mentors of whom I have been lucky enough to be a student. Coming from Vietnam, I would not have been able to pursue a Ph.D. degree in America had it not been for Ms. Thu Ho, my first English teacher, who had laid a concrete foundation of English education for me to build on and become a proficient speaker and writer of the language. During these junior high school years, Mr. Thuy Tran had had an immense impact in training me to become a critical and logical thinker with his intricate Math problems. In high school, Ms. Lien Le was the first teacher to show me how challenging yet intriguing Chemistry is, while Ms. Hanh Nguyen and my classmates brought me probably the best year of my early education journey. As importantly, Ms. Bich Vu has been a mentor and a dear friend of mine for fifteen long years, teaching me critical lessons in life and playing a big part in shaping who I am right now.

Starting the journey in America, Prof. Mark Trudell, my first research mentor, enlightened me with the various ways medicinal chemistry and drug discovery can save lives. Although I no longer pursue his expertise in organic chemistry, my ultimate scientific goal and philosophy were solidly shaped during the two years I was his mentee. At the University of New Orleans, I also owe it to Prof. Matthew Tarr and Prof. Hank Hauck, who had given me valuable advice during the confusing transition time. Later at UC Santa Barbara, my difficult decision to shift focus towards Biophysics had been made much easier with the excellent mentorship from my two Ph.D. advisors, Prof. Songi Han and Prof. Michelle O'Malley. Prof. Han cares so deeply about my unique challenges that after my time as her student, I have grown tremendously not only as a researcher but also as a person. Meanwhile, I am greatly indebted to Prof. O'Malley for her profound knowledge and insights associated with biological systems, which have been and will be the major focus of my scientific career. I also want to thank Prof. Frederick Dahlquist for the many scientific discussions with me since my first year, Prof. Lior Sepunaru for the thought-provoking and brainstorming one-to-one meetings, Prof. Arnab Mukherjee for his valuable questions, ideas, and support, and Prof. Irene Chen for being a very kind and supportive committee member during the first three years of my Ph.D. program. It has been a great experience working and doing research with the faculty at UC Santa Barbara.

My collaborative projects have been fruitful thanks to many excellent researchers who have greatly contributed to the studies presented in this dissertation. Dr. Nicole Schonenbach was my first mentor on the studies associated with the adenosine A_{2A} receptor, and much of

my first knowledge and experience in Biophysics were taught by her. Michael Vigers has been the first and most productive collaborator with me regarding the C-terminus and cryo-EM projects, as well as a good friend of mine since year one. Dr. Susanna Seppälä has given me so many helpful ideas and support, including but not limited to the truncation of the C-terminus and the use of SMA nanodiscs. The power saturation project was successful thanks to the help of Dr. Ryan Barnes and Dr. Xinpeng Cheng, while the DEER measurements were adeptly conducted with the help of Dr. Timothy Keller and Karen Tsay. Dr. Li Xing (IMRI at UC Irvine) gave me the first hands-on experience with cryo-EM, while Dr. Chung-Ta Han and Maxwell Berkow have provided me with the essential knowledge and training to work with proteorhodopsin. I also thank Prof. Bradley Chmelka for always holding me to the highest standards both in class and in our research collaboration. At West Virginia University, I have had the pleasure to work with Prof. Blake Mertz and Dr. Eric Sefah through a collaboration sparked at the BPS conference, which represents my personal experience in how sharing and collaborating can greatly advance science. I was supported both academically and financially through an NIH grant involving BlueLight Therapeutics. Jennifer Hoover, Rohan Katpally, and Elsa Winslow worked with me during their undergraduate studies; I will miss them very much and have no doubt they will find great success in their future careers.

I would also like to acknowledge all the past and current members of the Han group and the O'Malley group whose time overlaps with mine. I will miss dearly the scientific discussion and guidance, the personal support, the cakes, the cards, and the experience I received from them. Furthermore, I also received help from members of other labs, especially Dr. Nicholas Bartelli and Dr. Martin Kurnik. I also had great experience with everyone in my class, especially Dr. Jason Yun, with whom I shared not only my office but also many graduate school stories.

My graduate school journey has been much more upbeat thanks to soccer, music, and most importantly, friendship. My passion for soccer has brought me through tough times, and I thank all my teammates as well as everyone with whom I have played the sports. The Santa Barbara Revels, especially Susan Keller and Erin McKibben, gave me my first opportunity to perform singing and acting on stage with actual tickets and audience, and that will be an unforgettable experience. I have had the honor of being friends with many in the small but tight Vietnamese community in Santa Barbara, and I will keep in touch with them all. I save special thanks to Nam, my best friend since high school until now, who has supported me unconditionally regardless of whether he understands what I do. Phung has also been one of those rare friends that share my journey from Vietnam to America, and I thank her for that. Furthermore, the members of the Vietnamese Chemical Association have always encouraged during this journey, and I hope I will be a part of this for many more years.

Besides, my time in graduate school, especially the final two years, would have been much more difficult without Quan. I forever cherish not only the many meals she cooked and hours she commuted, but also her heartfelt support and companionship. I'm so glad to have shared perhaps the most critical part of my time in graduate school with her, and there will be more to come.

Finally, and most importantly, a big part of this achievement belongs to my family. The warm support that I received from my relatives in New Orleans helped me navigate through the first three difficult years in America. My extended family in Vietnam have cheered me on since day one, and I heard they were glad to hear me graduate. Then there's my parents and siblings, who have been my greatest emotional support system. Although they may not understand my research, my parents comprehend me as a person more than anyone else in the world. I have been told that I carry with me a great deal of hopes and expectations from my family during my adventure in America, and I have used that thought many times to motivate myself. However, I'm sure the only expectation they have is to see me happy, and I wish them the same.

Vita of KHANH D. Q. NGUYEN

Department of Chemistry and Biochemistry
University of California – Santa Barbara
Santa Barbara, CA 93106

Physical Science Building – North 4650-B
(669) 294-1413
kdnamycin@gmail.com

Education

University of California – Santa Barbara — **Santa Barbara, CA**
PhD in Chemistry, Biophysical Chemistry — 2021
- *Outstanding Departmental Service (Jun 2019)*

University of New Orleans — **New Orleans, LA**
BS in Chemistry, Medicinal Chemistry, GPA: 3.94/4.00 — 2016
- *Jim & Sonia Miller Scholarship (Apr 2016)*
- *Chemistry Senior Award (Apr 2016)*
- *Privateer Transfer Scholarship (Fall 2014 – Spring 2016)*

Ho Chi Minh City University of Pedagogy — **Ho Chi Minh City, Vietnam**
Completed 50% of requirements for a BA degree in English Education — 2011 – 2013
- *Departmental Writing Award – First Prize (Apr 2013)*

Professional Experience

Graduate Student Researcher — Jul 2016 – Dec 2021
UCSB – Department of Chemistry and Biochemistry — Santa Barbara, CA
Advisors: Prof. Song-I Han and Prof. Michelle A. O'Malley

The human adenosine A_{2A} receptor ($A_{2A}R$) serves as an excellent target to conduct modeling studies into oligomerization of GPCRs, as there is solid evidence that this particular member of GPCR family forms homo-oligomers and heteromers, playing an impactful role in several CNS disorders. Using various biophysical tools including SEC, cw-EPR, DEER, and cryo-EM, my goal is to identify the oligomeric interface of $A_{2A}R$, establish experimental read-out for $A_{2A}R$ activity, and evaluate functional impact of the oligomeric state and membrane environment on $A_{2A}R$.

Undergraduate Student Researcher — Sep 2015 – Apr 2016
University of New Orleans – Department of Chemistry — New Orleans, LA
Advisor: Prof. Mark L. Trudell

The project involves a new method of *N*-alkylation of amines with alcohols using a catalytic system consisting of $[Cp^*IrCl_2]_2$ and a weak base. My participation in this project is the extensive amount of work on a wide variety of amino acids, with multiple primary alcohols as alkylating agents in the presence of $[Cp^*IrCl_2]_2$ and K_2CO_3 as a base. 12/14 reactions gave desired products (some of which are novel compounds) with a yield of up to ~40%. The application of this catalytic system has never been done on amino acids before, which makes this basic research a very useful approach for the synthesis of these compounds and for further studies on amino acids.

Teaching Assistant — Apr 2013 – Jun 2013
British Council and Yola Institute — Ho Chi Minh City, Vietnam

Main duty was to support teaching English to young learners in Vietnam. Planned and ran international projects and activities and was also a resource to help students improve their English.

Publications

Published Manuscript

1. **Nguyen, K. D. Q.**; Vigers, M.; Sefah, E.; Seppälä, S.; Hoover, J. P.; Schonenbach, N. S.; Mertz, B.; O'Malley, M. A.; Han, S. Homo-Oligomerization of the Human Adenosine A_{2A} Receptor Is Driven by the Intrinsically Disordered C-Terminus. *eLife* 2021, 10:e66662 (DOI: 10.7554/eLife.66662).

Manuscripts in Preparation

3. **Nguyen, K. D. Q.**; Vigers, M.; Tsay, K.; Winslow, E.; O'Malley, M. A.; Han, S. Visualizing the Dimeric Interface of the Human Adenosine A_{2A} Receptor with DEER and cryo-EM. *In Preparation.*
2. Han, C.-T.*; **Nguyen, K. D. Q.***; Hussain, S.*; Berkow, M.; Kiani, A.; Kinnebrew. M.; Idso, M. N.; Baxter, N.; Chang, E.; Aye, E.; Winslow, E.; Chmelka, B.; Mertz, B.; Han, S. Lipid-Based Membrane Mimetics and Oligomerization Have Distinct Impacts on the Functional Properties of Proteorhodopsin. *In Preparation.*
1. Schonenbach, N. S.; **Nguyen, K. D. Q.**; Duran, A. M.; Yoo, J. I.; Meiler, J.; Han, S.; O'Malley, M. A. Engineering GPCR Variants with Simultaneous Multi-Point Mutations via Molecular Modeling and Combinatorial Mutagenesis. *In Preparation.*

Presentations

Poster Presentations

4. "Human Adenosine A_{2A} Receptor – Structural and Functional Consequences"
   Khanh D. Q. Nguyen, Susanna Seppälä, Michael Vigers, Timothy J. Keller, Jennifer P. Hoover, Nicole S. Schonenbach, Michelle A. O'Malley, Song-I Han
   12th Annual Amgen-Clorox Graduate Student Symposium, UCSB (Oct 2019)
3. "Dimerization of Human Adenosine A_{2A} Receptor – Impact of the C-Terminus"
   Khanh D. Q. Nguyen, Susanna Seppälä, Michael Vigers, Nicole S. Schonenbach, Michelle A. O'Malley, Song-I Han
   63rd Annual Biophysical Society Meeting, Baltimore, MD (Mar 2019)
2. "Revealing Impact of C-Terminus in Dimerization of Human Adenosine A_{2A} Receptor"
   Khanh D. Q. Nguyen, Michael Vigers, Nicole S. Schonenbach, Song-I Han, Michelle A. O'Malley
   11th Annual Clorox-Amgen Graduate Student Symposium, UCSB (Oct 2018)
1. "Role of Disordered C-Terminus in Dimerization of Human Adenosine A_{2A} Receptor"
   Khanh D. Q. Nguyen, Nicole S. Schonenbach, Justin I. Yoo, Michael Vigers, Song-I Han, Michelle A. O'Malley
   62nd Annual Biophysical Society Meeting, San Francisco, CA (Feb 2018)

Oral Presentations

12. "Homo-Oligomerization of the Human Adenosine A_{2A}R Is Driven by the Intrinsically Disordered C-Terminus"
    Khanh D. Q. Nguyen, Michael Vigers, Eric Sefah, Susanna Seppälä, Jennifer P. Hoover, Nicole S. Schonenbach, Blake Mertz, Michelle A. O'Malley, Song-I Han
    ASBMB Protein Data Bank 50th Celebration Symposium, Virtual (May 2021)
11. "Oligomerization of the Human Adenosine A_{2A}R Is Driven by the Intrinsically Disordered C-Terminus"
    Khanh D. Q. Nguyen, Michael Vigers, Eric Sefah, Susanna Seppälä, Jennifer P. Hoover, Nicole S. Schonenbach, Blake Mertz, Michelle A. O'Malley, Song-I Han
    6th University of California Chemical Symposium, Virtual (Mar 2021)
10. "Oligomerization of the Human Adenosine A_{2A}R Is Driven by the Intrinsically Disordered C-Terminus"
    Khanh D. Q. Nguyen, Michael Vigers, Eric Sefah, Susanna Seppälä, Jennifer P. Hoover, Nicole S. Schonenbach, Blake Mertz, Michelle A. O'Malley, Song-I Han
    65th Annual Biophysical Society Meeting, Virtual (Feb 2021)
9. "What a Ph.D. in Biophysics Looks Like"
   Khanh D. Q. Nguyen
   SciTrek Weekly Seminar, Virtual (Jan 2021)

8. "Human Adenosine $A_{2A}R$ Dimerization Is Driven by Its C-Terminus"
   Khanh D. Q. Nguyen, Susanna Seppälä, Michael Vigers, Nicole S. Schonenbach, Jennifer P. Hoover, Rohan Katpally, Michelle A. O'Malley, Song-I Han
   5th University of California Chemical Symposium, Lake Arrowhead, CA (Mar 2020)
7. "Human Adenosine $A_{2A}R$ Dimerization Is Driven by a C-Terminal Motif"
   Khanh D. Q. Nguyen, Susanna Seppälä, Michael Vigers, Nicole S. Schonenbach, Jennifer P. Hoover, Rohan Katpally, Michelle A. O'Malley, Song-I Han
   64th Annual Biophysical Society Meeting, San Diego, CA (Feb 2020)
6. "Dimerization of Human Adenosine A_{2A} Receptor Is Driven by Intrinsically Disordered C-Terminus"
   Khanh D. Q. Nguyen, Susanna Seppälä, Jennifer P. Hoover, Nicole S. Schonenbach, Michelle A. O'Malley, Song-I Han
   9th Chemical Sciences Student Seminar, UCSB (Dec 2019)
5. "Graduate School and Research in Biophysical Chemistry – How Do We Cure Diseases?"
   Khanh D. Q. Nguyen
   Chemistry Club Seminar, UCSB (Oct 2019)
4. "Elucidating the Role of the C-Terminus in Dimerization of a GPCR – Adenosine A_{2A} Receptor"
   Khanh D. Q. Nguyen, Susanna Seppälä, Michael Vigers, Timothy J. Keller, Jennifer P. Hoover, Nicole S. Schonenbach, Michelle A. O'Malley, Song-I Han
   8th Chemical Sciences Student Seminar, UCSB (May 2019)
3. "When Proteins Hold Hands and Dance"
   Khanh D. Q. Nguyen
   7th Grad Slam, Preliminary Round & Semi-Final Round, UCSB (Apr 2019)
2. "Elucidating the Role of the C-Terminus in $A_{2A}R$ Dimerization"
   Khanh D. Q. Nguyen, Susanna Seppälä, Michael Vigers, Timothy J. Keller, Jennifer P. Hoover, Nicole S. Schonenbach, Michelle A. O'Malley, Song-I Han
   4th University of California Chemical Symposium, Lake Arrowhead, CA (Mar 2019)
1. "Dimerization of a Membrane Protein GPCR Using EPR – Generation of Cysteine-Free Constructs and Complications"
   Khanh D. Q. Nguyen, Nicole S. Schonenbach, Justin I. Yoo, Michael Vigers, Song-I Han, Michelle A. O'Malley
   7th Chemical Sciences Student Seminar, UCSB (Nov 2017)

Honors/Awards

Outstanding Departmental Service — Jun 2019
Department of Chemistry and Biochemistry, UC Santa Barbara
Awarded for exceptional leadership and outstanding commitment to the mission of the Department during the 2018–2019 academic year

Phi Lambda Upsilon Honor Society — Sep 2017
Department of Chemistry and Biochemistry, UC Santa Barbara
Awarded to students majoring in chemistry who rank in the top 20 percent of their class

Jim & Sonia Miller Scholarship — Apr 2016
Department of Chemistry, University of New Orleans
A limited scholarship of up to $2,000 awarded to students with a BS Chemistry major

UNO Chemistry Senior Award — Apr 2016
Department of Chemistry, University of New Orleans
An honorable award to recognize the senior-year student with the best academic performance in 2016

Phi Beta Kappa Honor Society — Apr 2016
Department of Chemistry, University of New Orleans
Awarded to senior-year students with outstanding academic performance

Undergraduate Award in Inorganic Chemistry — Apr 2015
Department of Chemistry, University of New Orleans
Awarded the student with the best academic performance in Inorganic Chemistry courses at undergraduate level

Privateer Transfer Scholarship Fall 2014 – Spring 2016
University of New Orleans
Out-of-state tuition waiver of up to $14,000/year for international transfer student

Professional Memberships and Affiliations

International EPR Society (IES) 2018 – present
Biophysical Society (BPS) 2017 – present
American Chemical Society (ACS) 2017 – present

Volunteer Experience

University of California Chemical Symposium Dec 2019 – present
Head of Social Marketing and Communications

- Design and manage website for marketing (see more at https://www.ucchemsym.org).
- Promote events on various social platforms, including Twitter, Instagram, and Facebook.
- Manage database to facilitate programming and internal operation.

Vietnamese Chemical Association Jul 2019 – present
Head of Social Marketing

- Lead the branding and marketing aspects from foundation, including the **Young Chemists Conference 2021** (see more at https://www.yccvietnam.org).
- Invite speakers and host multiple scientific and professional webinars.
- Design graphical posters and create content to promote activities on various social platforms.

Chemical Sciences Student Seminar - UCSB Sep 2019 – present
Committee Member

- Schedule speakers.
- Arrange and attend practice talks to provide feedback.

The Association of Vietnamese Students and Professionals in the United States Jun 2019 – present
Content Writer

- Write introduction and recap contents for multiple events of national statures.
- Scheduled and monitored the Soccer Tournament.
- Is part of the judge committee for multiple writing contests.

Santa Barbara Revels Jul 2019 – present
Board Member/Solstice Singer

- Sing and perform songs written in Spanish, Italian, English, and Latin.
- Participate in fundraising and administrative tasks.

Teaching Experience

Department of Chemistry and Biochemistry, UCSB

- Laboratory Techniques in Biophysical Chemistry *CHEM 112L* Spring 2018
- Laboratory Techniques in Biochemistry *CHEM 125L* Winter 2017
- Introductory Biochemistry Laboratory *CHEM 110L* Fall 2017
- General Chemistry Laboratory 2 *CHEM 1BL* Winter 2016
- General Chemistry Laboratory 1 *CHEM 1AL* Fall 2016

Technical Skills

Scientific Research

- Molecular cloning
- Membrane protein expression in *E. coli* and *S. cerevisiae*
- Membrane protein purification using detergent (DDM, CHAPS, and CHS) or nanodiscs (SMALPs)
- Biochemical techniques: total protein stain, Western Blotting, BCA assay, confocal microscopy
- Magnetic resonance spectroscopy: cw- and pulsed EPR, specifically power saturation and DEER
- Chromatography: IMAC, ligand-affinity, SEC
- Electron microscopy: negative-staining TEM and cryo-EM
- Computational knowledge: LaTeX, PyMOL, Chimera, VMD, EMAN2.

Social Marketing and Communications

- Social marketing on Facebook, Twitter, Instagram, LinkedIn, and YouTube
- Graphic design with Adobe Illustrator and Canva
- Webpage design and management with Squarespace and Drupal

Mentoring

Jennifer Hoover, biochemistry, UC Santa Barbara — Sep 2018 – Jul 2019
Rohan Katpally, chemical engineering, UC Santa Barbara — Oct 2019 – May 2020
Elsa Winslow, biochemistry, UC Santa Barbara — Jul 2020 – present

References

Song-I Han
Professor, Department of Chemistry and Biochemistry, UC Santa Barbara
(805) 893-4858
songi@chem.ucsb.edu

Michelle A. O'Malley
Associate Professor, Department of Chemical Engineering, UC Santa Barbara
(805) 893-4769
momalley@engineering.ucsb.edu

Mark L. Trudell
Distinguished Professor, Department of Chemistry, University of New Orleans
(504) 280-7337
mtrudell@uno.edu

ABSTRACT

Investigating the Homo-Oligomerization of the Human Adenosine A_{2A} Receptor

Khanh Dinh Quoc Nguyen

Oligomerization of G protein-coupled receptors (GPCRs) is a widespread phenomenon whose discovery generates a plethora of alternative targets for new therapeutic approaches towards human diseases. Nevertheless, challenges still exist in the characterization of these complexes, especially in terms of driving factors of formation, interfaces, and functional consequences. Despite their significance, structural and functional studies of GPCR oligomers have been hindered by their dynamic nature and their generally low suitability for biophysical techniques.

Among these receptors, the human adenosine A_{2A} receptor ($A_{2A}R$) serves as an excellent target to conduct modeling studies into oligomerization of GPCRs, as there is solid evidence that this receptor forms homo- and hetero-oligomers both *in vitro* and *in vivo*. Its intrinsically disordered C-terminus is removed in all structural studies of $A_{2A}R$ for stability and homogeneity purposes, but a C-terminal mutation has been shown to prevent $A_{2A}R$ oligomer formation. We first aimed to understand the role of the C-terminus in driving the oligomerization of $A_{2A}R$. Size-exclusion chromatography (SEC) was applied as the primary method to quantify the oligomer levels of multiple variants of $A_{2A}R$ with strategic mutations and truncations on the C-terminus. We discovered that the C-terminus of $A_{2A}R$ drives receptor

homo-oligomerization via multiple types of covalent and non-covalent interactions. Computational analysis revealed that $A_{2A}R$ dimers are formed via multiple interfaces, all involving the C-terminus. Variation of ionic strength of the buffer indicated depletion interactions via the C-terminus to be the main driving force of $A_{2A}R$ oligomerization. Experiments on the C-terminus *sans* the transmembrane (TM) helices demonstrated that $A_{2A}R$ C-terminus in and of itself can form insoluble aggregate at high salt concentrations.

The inclusion of the C-terminus enables the production and isolation of $A_{2A}R$ oligomers, yet also further complicates biophysical and structural studies of this receptor. Electron paramagnetic resonance (EPR) spectroscopy offers unique capability of probing how the dynamic C-terminus is involved at the multiple interfaces of $A_{2A}R$ oligomers. Much effort had been made using cell sorting in engineering properly folded $A_{2A}R$ variants void of free cysteines to facilitate biophysical characterization by EPR, but the structure and function of these variants needed to be thoroughly investigated. We discovered that these $A_{2A}R$ mutants, selected with an agonist-based assay, showed reduced binding activity to antagonist. Further characterization with EPR power saturation experiments demonstrated that various extracellular disulfide bonds were disrupted in these variants, suggesting that the removed transmembrane cysteines may serve a role in maintaining the proper structure and function of the receptor.

Moving forward, we next sought to visualize the oligomeric interfaces of $A_{2A}R$ and the structural role of the intrinsically disordered C-terminus by combining continuous-wave (CW) EPR with cryogenic electron microscopy (cryo-EM). CW-EPR revealed that a C-terminal residue was immobilized as $A_{2A}R$ formed oligomers, suggesting that the C-terminus is directly

involved at the oligomeric interface of the receptor. The related technique double electron electron resonance (DEER) revealed a large intermolecular distance between two C-terminal cysteines, suggesting that $A_{2A}R$ oligomers are not stabilized by direct disulfide bonds between the C-termini. Early cryo-EM data collection yielded a low-resolution 3D structure of $A_{2A}R$ dimers that showed the involvement of the TM regions at the interfaces. Therefore, it appears that both the C-terminus and the TM helices of $A_{2A}R$ contribute to forming the oligomeric interfaces of the receptor.

Finally, in search of a membrane mimetic platform that can retain the native structure and function of $A_{2A}R$ oligomers, styrene maleic acid (SMA) lipid polymers were employed as a promising detergent-free method to isolate transmembrane proteins. We sought to assess the functional impact of extracting directly from the native host environment $A_{2A}R$ and proteorhodopsin (PR), a model bacterial transmembrane proton pump. We discovered that SMA-solubilized $A_{2A}R$ exhibited reduced binding activity to antagonist, likely due to the lack of functional cholesterol. For PR, SMA could only capture the monomeric form of the receptor and could not solubilize the functionally important hexameric form. Further analyses demonstrated that solubilizing PR with SMA severely reduced its active population and disrupt its photocycle properties. Taken together, despite retention of the native host membranes, SMA appeared to have negative impacts on the functional properties of both $A_{2A}R$ and PR.

TABLE OF CONTENT

LIST OF TABLES

LIST OF FIGURES

Figure 1-8. Analysis of (A) disorder and (B) protein binding probability of the C-terminus of A2AR (in box) using computational software. Y-axis values > 0.5 indicate disordered and putative binding regions. Increased disorder and decreased protein binding probability suggests destabilization of protein-protein association upon C394S mutation. (A) PONDR VSL2 suggests high disorder for the C-terminus, with the mutation C394S increasing its disorder. (B) ANCHOR predicts that the C-terminus is strongly prone to protein binding, with the mutation C394S decreasing this probability.

Figure 2-1. Depletion interactions can occur via two mechanisms: (A) overlapping of exclusion volume and (B) dehydration. Both mechanisms are driven by entropy, favoring protein-protein association.

Figure 2-2. Visual summary of the entire process of cloning, expression, purification, and separation of A2AR oligomeric species. Plasmids containing the A2AR gene is linearized with BsaBI, then transformed into the genome of *S. cerevisiae*. Protein expression is induced with galactose-containing media. Cells are then harvested with centrifugation, lysed with mechanical beads, and solubilized in an optimized system of detergent micelles containing DDM, CHAPS, and CHS. IMAC with Ni-NTA resin is used to obtain a semi-pure mixture of A2AR, which is then subjected to ligand-affinity chromatography with a high-affinity antagonist (XAC) to select for ligand-active receptor. Finally, the various oligomeric species of A2AR is separated and isolated with SEC for further biophysical characterization. (Figure courtesy of Dr. Nicole S. Schonenbach.)

Figure 2-3. (A) Representative total protein stain (upper panel) and western blot (lower panel) of A2AR-WT during purification. Positive ((+) ctrl) and negative ((–) ctrl) controls consist of 5 OD cell lysate of *S. cerevisiae* BJ5464 cells expressing and not expressing A2AR WT, respectively. “IMAC FT” indicates the flow-through from IMAC step. “XAC inactive” and “XAC active” indicate the fractions that do not and do bind to XAC during the ligand-affinity chromatography step. (B) Representative western blot of A2AR-WT during SEC separation. The fractions are matched to the distinct oligomeric peaks in the SEC chromatogram. Each lane on the blot is from 0.5 mL fractions eluted from a Superdex 200 10/300 GL (GE

Healthcare) column. MagicMark protein ladder (LC5602) is used as the molecular weight standard.

Figure 2-4. Method for collecting SEC data and assessing A2AR oligomerization. The SEC data is recorded every second as absorbance at 280 nm. The baseline is corrected to ensure uniform fitting and integration across the peaks. The areas under the curve, resulting from a multiple-Gaussian curve fit, express the population of each oligomeric species. The reported standard errors of integration are within a 95% confidence interval and are calculated from the variance of the fit, not experimental errors. The levels of HMW oligomer and dimer are expressed relative to the monomeric population in arbitrary units. A representative calculation defining the oligomer levels is given in the box.

Figure 2-5. (A) Curve fitting using OriginLab of all A2AR variants used in the main text of this study, listed by the order they appear. By default, each oligomeric peak is fitted with one curve using Gaussian distribution and displayed by different color shades, with the HMW oligomer eluted first (dark orange), followed by the dimer (lighter orange), followed by the monomer (lightest orange). However, the HMW oligomer peak in some cases cannot be fitted with one curve and thus is fitted with two curves instead. This discrepancy can be explained by variation in HMW oligomerization order among the variants. The identity of each peak is confirmed with western blotting. The value and error from the curve fitting of each peak are given in Table 2-1. (B) Data distribution of all variants used in this study in comparison to five experimental replicates of A2AR-WT. The C-terminally truncated mutants are represented by different shades of green in increasing darkness corresponding to the increased length of the C-terminus, with the lightest shade representing the mutant with the shortest C-terminus (A316ΔC) and the darkest shade for the mutant with the longest C-terminus (P395ΔC). The levels of dimer and HMW oligomer are expressed relative to the monomeric population in arbitrary unit, with reported errors calculated from the variance of the fit, not experimental variation. There are significant variations in the dimer and HMW oligomer levels among the WT replicates, stemming from experimental errors. These variations are mitigated when the two parameters are added, as the data distribution becomes more uniform. Also, the

oligomerization levels of the WT replicates are consistently higher than the mutated and truncated variants.

Figure 2-6. Residue C394 helps stabilize A2AR oligomerization via disulfide bonds. (A) The effect of C394X substitutions on A2AR oligomerization. The levels of dimer (dark colors) and HMW oligomer (light colors) are expressed relative to the monomeric population in arbitrary units, with reported errors calculated from the variance of the fit, not experimental variation. (B) Line densitometry of Western Blot bands on SEC-separated dimeric populations of A2AR-WT and Q372ΔC with and without 5 mM TCEP. The level of dimer is expressed relative to the monomeric population in arbitrary units similarly to the SEC analysis. MagicMark protein ladder (LC5602) is used as the molecular weight standard.

Figure 2-7. Truncation of the C-terminus does not affect membrane localization of A2AR. Confocal microscopy images of *S. cerevisiae* cells expressing A2AR WT, A316ΔC, and V334ΔC tagged with a C-terminal green fluorescent protein trafficking to the plasma membrane.

Figure 2-8. Truncating the C-terminus systematically affects A2AR oligomerization. **(A)** Depiction of where the truncation points are located on the C-terminus, with region 354–359 highlighted (in black) showing critical residues. **(B)** The levels of dimer and HMW oligomer are expressed relative to the monomeric population as an arbitrary unit and plotted against the residue number of the truncation sites, with reported errors calculated from the variance of the fit, not experimental variation. Region 354–359 is emphasized (in black and gray) due to a drastic change in the dimer and HMW oligomer levels. **(C)** The dependence of A2AR oligomerization on three consecutive charged residues ^{355}ERR$^{357.}$ The substitution of residues ^{355}ERR^{357} to ^{355}AAA^{357} is referred to as the ERR:AAA mutations. The levels of dimer and HMW oligomer are expressed relative to the monomeric population as an arbitrary unit, with reported errors calculated from the variance of the fit, not experimental variation.

Figure 2-9. Non-bonded interactions of the extended C-terminus of A2AR play a critical role in stabilization of the dimeric interface. (A) Dimer configurations from cluster analysis in GROMACS of the 394-residue variant identify two major clusters involving either 1) the C-

terminus of one protomer and the C-terminus, ICL2, and ICL3 of the second protomer or 2) the C-terminus of one protomer and ICL2, ICL3, and ECL2 of the second protomer. Spheres: residues forming intermolecular electrostatic contacts. (B) Average number of residues that form electrostatic contacts as a function of sequence length of A2AR. (C) Average number of residues that form hydrogen bonds as a function of sequence length of A2AR. The criteria for designating inter-A2AR contacts as electrostatic interactions or hydrogen bonds are described in detail in 2.2 above.

Figure 2-10. The effects of ionic strength on the oligomerization of various A2AR variants reveal the involvement of depletion interactions. The levels of dimer and HMW oligomer are expressed relative to the monomeric population as an arbitrary unit and plotted against ionic strength, with reported errors calculated from the variance of the fit, not experimental variation. NaCl concentration is varied to achieve ionic strengths of 0.15, 0.45, and 0.95 M.

Figure 2-11. The dimer/oligomerization of A2AR is a thermodynamic process where the dimer and HMW oligomer once formed are kinetically trapped. (A) SEC chromatograms of the consecutive rounds of SEC performed on A2AR-WT and Q372ΔC. The first rounds of SEC are to separate the dimer/oligomer population and the monomer population, while the second rounds of SEC are performed on these SEC-separated populations to assess their stability and reversibility. The total oligomer level is expressed relative to the monomeric population in arbitrary units. (B) Energy diagram depicting A2AR oligomerization progress. The monomer needs to overcome an activation barrier (EA), driven by depletion interactions, to form the dimer/oligomer. Once formed, the dimer/oligomer populations are kinetically trapped by disulfide linkages.

Figure 2-12. The A2AR C-terminus is prone to aggregation. (A) Absorbance at 450 nm of the A2AR C-terminus in solution, with NaCl and GdnHCl concentrations varied to achieve ionic strengths 0–4 M. Inset: the solution at ionic strength 4 M achieved with NaCl. The Hofmeister series is provided to show the ability of cations to salt out (blue) or salt in (red) proteins. (B) SYPRO orange fluorescence of solutions containing the A2AR C-terminus as the temperature was varied from 20 to 70°C (grey). The change in fluorescence, measured in relative

fluorescence unit (RFU), was calculated by taking the first derivative of the fluorescence curve (black).

Figure 2-13. (A) Hydropathy plot against A2AR residue number showing the hydrophobicity of A2AR C-terminus, scored with ProtScale using method described by Kyte & Doolittle, window size of 3. Positive scores represent hydrophobicity and negative scores hydrophilicity. (B) The non-polar residues in A2AR C-terminus. (C) Average number of residues that form non-polar contacts as a function of sequence length of A2AR. The criteria for designating inter-A2AR contacts as non-polar interactions are described in detail in 2.2.

Figure 2-14. (A) Representative snapshot of A2AR-C394ΔC dimers shows salt bridge formation between a sample trajectory. The insets are close-ups of the salt bridges, which can be both intra- and intermolecular. The last inset shows a network of salt bridges with the charged cluster ^{355}ERR^{357} involved. (B) Helical tilt angles for TM7 helix in A2AR as a function of protein length. Systematic truncations of the C-terminus lead to rearrangement of the heptahelical bundle. The participation of the C-terminus in A2AR dimerization increases the tilting of the TM7 domain, which is in closest proximity to the C-terminus.

Figure 2-15. Helical tilt angles for TM1–6 helices in A2AR as a function of protein length. Systematic truncations of the C-terminus lead to rearrangement of the heptahelical bundle, propagated to the entire receptor and is especially pronounced in helices proximal to the C-terminus, *i.e.*, TM1, TM2, TM7. For almost all TM helices, a noticeable shift in tilt angle occurs upon modeling the full-length (394 residues) variant. This behavior is fundamentally different from the conventional model of GPCR activation, in which TM 1, 2, 4, and 7 remain rigid, with TM5 and TM6 undergoing an outward tilt/rotation to enable binding to the cognate G protein. Relaxation of the heptahelical bundle (*i.e.*, an increase in helical tilt) as a function of protein length and dimerization could potentially be critical to our understanding of the activation mechanism of A2AR, as past studies have overwhelmingly focused on activation of the monomer.

Figure 3-1. Reaction of the nitroxide spin label with cysteine to attach the label onto the protein via disulfide bond. The dot represents the free electron in the N–O bond stabilized by the methyl groups in vicinity.

Figure 3-2. Snake diagram of A2AR secondary structure, highlighting TM cysteine residues that were mutated in this study. The human adenosine A2A receptor contains 15 cysteines in total. The pink cysteines are on the extracellular side and are disulfide-bonded, thus are not accessible to nitroxide spin labels. The blue transmembrane and the orange C-terminal cysteines are all exposed to spin label. Estimated location of the lipid membrane is indicated by the two black dash-dot lines.

Figure 3-3. (A) Pipeline for construction, expression, and enrichment of TM-Cys-free A2AR Library. Illustration summary of steps to conduct mutagenesis, cloning, transformation, expression, and fluorescent ligand binding screen A2AR library designed for site-saturation mutagenesis at 6 transmembrane sites within A2AR. (B) Summary of FACS analysis of 13 library variants, ranked qualitatively by the percent of cells within the sorting gate (*i.e.*, ligand binding) relative to the average of three wild-type (WT) controls. Out of 100,000 events in each sample, variants that exhibited greater than 80% of the wild-type population of cells within the sorting gate were selected for further characterization, indicated by a shaded box with dashed lines.

Figure 3-4. Agonist-active TM-Cys-free A2AR Variants Exhibit Reduced Affinity to Antagonist XAC and Incomplete Disulfide Formation. (A) Representative Western Blots of A2AR variants purified and analyzed for antagonist binding via xanthine amine congener (XAC) ligand affinity column. Negative control (–) is cell lysate for wild-type BJ5464 S. cerevisiae strain without the A2AR receptor. Positive control (WT) is cell lysate for BJ5464 expressing the wild-type A2AR. "XAC Inactive" indicates improperly folded A2AR that has poor/reduced affinity to the XAC ligand affinity column. "XAC Active" indicates receptor that sufficiently bound to the affinity column. (B) EPR spectra for spin labeled A2AR library variants.

Figure 3-5. Power saturation experiments reveal differences in solvent exposure of spin labeled A2AR variants. (A–D) CW-EPR spectra for A2AR-WT, A2AR-C394L, A2AR-C394S/C28M/C254S, and A2AR-TM-Cys-Free-53, respectively. The mobile (m) and immobile (i) components in these CW-EPR spectra indicate the mobility of the spin label in these variants. (E–H) Power saturation profiles for A2AR-WT, A2AR-C394L, A2AR-C394S/C28M/C254S, and A2AR-TM-Cys-Free-53, respectively. The first integral values are normalized by the highest value in each curve and plotted against the square root of microwave power. In F, G, and H, the power curve in the presence of NiEDDA of each variant (orange) is overlaid with that of A2AR-WT (green). Solvent accessibility of each variant is assessed by how similar its power curve in NiEDDA is to that of A2AR-WT.

Figure 3-6. The agonist-biased TM-Cys-Free variants of A2AR do not bind to the agonist adenosine amine congener. (A) Ligand-affinity chromatograms of A2AR-WT bound to XAC and ADAC. The protein is detected at 280 nm wavelength. Fractions 1–8 contain the inactive flow-through, while fractions 9–17 contain the active protein, which is saturated by the signals from the ligands. ADAC-affinity chromatogram (right) shows a much larger area under the curve of the inactive fractions compared with XAC-affinity chromatogram (left). (B) Western Blot analysis of SDS-PAGE of all fractions from ADAC-affinity chromatography. No bands were observed in the “ADAC Active” fractions. MagicMark protein ladder (LC5602) is used as the molecular weight standard.

Figure 3-7. Visualization of A2AR-WT bound to XAC (PDB ID: 3REY) and adenosine (PDB ID: 2YDO) with PyMOL. The terminal amine group on XAC is clearly exposed, enabling attachment onto the resin. No crystal structure of A2AR bound to ADAC is available. Based on the structure of A2AR bound to adenosine, the point that would be attached to the amine congener on adenosine is directed towards the protein itself. Due to electron delocalization, attachment of the amine congener creates a planar structure that extends directly into the protein, leaving the terminal amine group unavailable for resin attachment.

Figure 4-1. Four-pulse DEER sequence. Pump (red) and observer (blue) microwave pulses are used to selectively excite distinct spin populations, A and B. A two pulse Hahn echo is formed by exciting A spins at the observer frequency. A pump pulse is subsequently applied to flip the

B spins followed by a varying time delay, t, resulting in a modulation of the echo amplitude of A spins. At some delay, τ_2, the echo is refocused by an additional pulse at the observer frequency. The DEER experimental trace, $\boldsymbol{V(t)}$, is the integral of refocused echo as a function of pump pulse position, t.

Figure 4-2. CW-EPR spectra for A2AR-WT and C394S normalized by protein concentration to emphasize the difference in signal intensity and spin labeling efficiency upon removal of residue C394. Mobile and immobile features are indicated as "m" and "i", respectively. The mobile:immobile ratio indicates tertiary contacts experienced by the side chain of the MTSL label. The center peak linewidth is designated as ΔH0 as an indicator of side chain mobility.

Figure 4-3. CW-EPR measurements of SEC-separated A2AR monomer, dimer, and higher-order oligomers, labeled with MTSL. The spectra are normalized by the intensity of the center peak. Mobile and immobile spectral features are indicated, and the mobile:immobile ratio can indicate tertiary contacts experienced by the side chain of the MTSL label.

Figure 4-4. Distance distributions from DEER measurements of SEC-separated MTSL-labeled A2AR-WT dimers with at 0.15 mM and 0.95 mM ionic strength. The sample is dominantly labeled at site C394, and hence the targeted distance was the intermolecular distance between residues C394. The mutant C394S is used as a negative control for signals from residue C394. The spectra are denoised with Tikhonov regularization.

Figure 4-5. TEM images at 100,000X magnification under negative stain of SEC-separated monomer vs. dimer forms of A2AR. The image of the monomer fraction (A) shows particles of high contrast and consistent size (~7 nm in diameter), while the image of the dimer fraction (B) shows significantly larger particles, with white arrows pointing at particles that are ~15 nm in size (particle sizes may vary depending on different orientations on the EM grid). Preliminary data shows that our sample preparation is free of interference from the buffer or contaminants.

Figure 4-6. Preliminary cryo-EM data collection of SEC-separated A2AR dimers. 2D classification is performed on RELION 2.0 using ~4,000 auto picked particles from a reference.

Representative particles of A2AR monomer and dimer are provided. Final model (gray hollow sphere) was found to assume a C2 symmetry with the size approximately two times larger than the cryo-EM structure of A2AR monomer (purple, PDB ID: 6GDG128).

Figure 5-1. Common membrane mimetic platforms for transmembrane protein solubilization. The protein is indicated in blue. Detergent micelle and amphipol are non-bilayer systems, while bicelle, MSP nanodisc, and SMA nanodisc are bilayer systems. (Figure from Dörr, J. M. et al, *Eur. Biophys. J.* 2016, 45, 3–21.)

Figure 5-2. Chemical structure of the SMA polymer at 50% ionization. The S:MA ratio (n/m) varies among different types of SMA. (Figure from Scheidelaar et al, *Biophys. J.* 2016, 111, 1974–1986.)

Figure 5-3. Proteorhodopsin acts as a light-activated proton transporter, increasing the proton concentration on the exterior of the cell. ATP synthase is among the proteins that rely on proton gradient to carry out their functions.

Figure 5-4. Western Blot analysis of SDS-PAGE of A2AR solubilized with SMALPs to track the presence of A2AR at every step from lysis to sterilization prior to ligand-affinity chromatography. Positive ((+) ctrl) and negative ((–) ctrl) controls consist of 5 OD cell lysate of *S. cerevisiae* BJ5464 cells expressing and not expressing A2AR WT, respectively. "SMALP'd A2a" indicates A2AR-containing *S. cerevisiae* membranes after SMA application but before ultracentrifugation. "2nd Centri" indicates the supernatant containing solubilized A2AR after ultracentrifugation. "Pellet 2nd Centri" indicates the pellet containing non-solubilized materials. "IMAC FT" and "IMAC Elute" indicate the flow-through and elute from IMAC step. "Desalt" indicates the desalted sample, and "Sterile" indicates the sterilized sample prior to ligand-affinity chromatography. Line densitometry was performed on the bands representing the supernatant containing solubilized A2AR and the pellet containing non-solubilized A2AR. MagicMark protein ladder (LC5602) is used as the molecular standard weight.

Figure 5-5. Western Blot analysis of SDS-PAGE of A2AR solubilized in SMALPs and in DDM detergent during purification with ligand-affinity column. “XAC inactive” and “XAC active” indicate the fractions that do not and to bind to XAC during the ligand-affinity chromatography step. MagicMark protein ladder (LC5602) is used as the molecular standard weight.

Figure 5-6. SMALPs effectively solubilizes *E. coli* membranes regardless of the size of the embedded protein, but can only capture the monomeric form of PR. (A) Visualization of the PR-WT and PR-E50Q samples before and after SMA application. The 60,000 × g ultracentrifugation yields the supernatant, which contains the solubilized materials, and the pellet, which contains the non-solubilized debris. (B) The weights of the pellets before and after SMA application of the PR-WT and PR-E50Q samples were normalized by the buffer volume before centrifugation (in mg/mL buffer). (C) Western Blot analysis of SDS-PAGE and visualization of SMA-solubilized PR-WT and PR-E50Q samples. MagicMark protein ladder (LC5602) is used as the molecular standard weight.

Figure 5-7. (A) pH-dependent absorbance transitions of PR E50Q in SMALPs (solid red line) at 570 nm, compared with those of PR E50Q in DDM detergent (dashed blue line) and in POPC/POPG liposomes (dashed pink line). (B) Transient absorbance data of PR E50Q extracted with SMALPs directly from *E. coli* membrane. Measurements were performed at pH 8.0 and 10.0 at ~293 K. The transient absorbance changes at 410, 470, 550, and 590 nm were collected after PR is photoactivated by a green-light pulse laser.

Figure 5-8. (A) Measurements of the diameters of PR hexamer and monomer using PyMOL. Measurements are done on the crystal structure of blue light-absorbing proteorhodopsin (PDB ID: 4JQ6). (B) Dimensions of styrene-maleic acid lipid particles consisting of DMPC synthetic lipids and a SMA polymer with a S:MA ratio of 2, as determined from small-angle neutron scattering experiments (Figure adapted from Jamshad, M. et al, *Nano Res.* 2015, 8, 774–789.)

Figure 6-1. Cartoon representation of the experimental setup of SHG assay. A SHG-active dye is conjugated via cysteine to the protein molecule, which is then attached to a supported biotin surface via a Avidin-tag. The SHG intensity is dictated by the angle θ between the transition

dipole moment of the dye and the z axis perpendicular to the surface. This change in SHG intensity can be monitored and compared between when the protein is and is not bound to a ligand, indicating conformational changes upon activation. (Figure adapted from Young, T. A. et al, *Methods Enzymol.* 2018, 610.)

Figure 6-2. The molecular structure of CHEAPS involves linking the cholesterol moiety native in cell membranes with zwitterionic sulfobetaine segment via an ester bond. The lack of hydrogen bond donors and acceptors render this molecule highly soluble in water containing detergents or amphiphilic polymers. (Figure from Trinh, T. K. H. et al, *Biochim Biophys Acta* 2021, 1865, 129908.)

Figure 6-3. (A) Synthesis of SMA-QA polymer by modifications of SMA polymer. The structure of SMA-QA contains a quaternary ammonium moiety that does not increase the local proton concentration when the nanodiscs are formed. (B) The size of the nanodiscs formed by SMA-QA can be tuned by varying the concentration of the polymer. (Figure adapted from Ravula, T. et al, *Angew. Chem. Int. Ed.* 2018, 57, 1342–1345.)

Chapter 1 | INTRODUCTION

1.1. G PROTEIN-COUPLED RECEPTORS

G protein-coupled receptors (GPCRs) are the largest and most diverse superfamily of proteins in every eukaryotic cell. The coupling of G proteins to these receptors evolved even before the plant/fungi/animal split (~1.2 billion years ago)(Römpler et al. 2007). Often referred to as seven-transmembrane receptors, they transmit signals induced by not only a multitude of neurotransmitters and hormones but also light, smell, and taste. At least 4% of the entire human protein-coding genome have been predicted by genomics to code for GPCRs(Bjarnadóttir et al. 2006). Due to its vast size and extensive participation in many biological pathways, this superfamily of receptors is the most important validated drug targets in medicine(Römpler et al. 2007). In fact, GPCRs are involved in countless diseases and are the primary(Hazell et al. 2012) target of approximately 40% of all modern medicinal drugs(Overington, Al-Lazikani, and Hopkins 2006; Rask-Andersen, Masuram, and Schiöth 2014). Nevertheless, only 4 out of 24 novel drugs approved by FDA in 2013 target GPCRs(Mullard 2014), and this low percentage is attributable to a lack of thorough understanding of their functional consequences, which arise from structural changes at the molecular level.

1.1.1. Biology

Found only in eukaryotes, GPCRs play crucial roles in a wide variety of important physiological processes including, but not limited to, homeostasis modulation(Hazell et al. 2012), regulation of immune system activity(Sharma, Akhade, and Qadri 2013), sensory signaling(Liman 2006), and even cancer(Dorsam and Gutkind 2007). These receptors function by sensing and binding to extracellular molecules, which causes a conformational change that

triggers their interaction with the coupled G proteins, eventually resulting in cellular signaling and responses. Their ligands include amino acids and ions (*e.g.*, glutamate, γ-butyric acid (GABA), Ca^{2+}), lipids (*e.g.*, LPA, PAF, prostaglandins, leukotrienes)[19], peptides and proteins (*e.g.*, angiotensin, bradykinin, endorphins), biogenic amines (*e.g.*, noradrenaline, dopamine, serotonin, acetylcholine), among various other types of molecules (*e.g.*, odorants, pheromones, nucleotides, opiates). The binding of a ligand to a GPCR allows the receptor to act as a guanine nucleotide exchange factor (GEF) that can then activate the associated G protein by replacing the GDP bound on the G protein with a GTP. This exchange of molecules leads to the dissociation of the G protein's α subunit from the β and γ subunits, allowing the G protein to interact with downstream intracellular proteins. This results in phosphorylation cascades of signaling molecules, producing second messengers such as cyclic adenosine monophosphate (cAMP), 1,2-diacylglycerol (DAG), and inositol 1,4,5-triphosphate (IP_3). Activation of the downstream effector is terminated when the bound GTP molecule is hydrolyzed, allowing the trimeric G protein to reform and interact with other GPCRs (**Figure 1-1**).

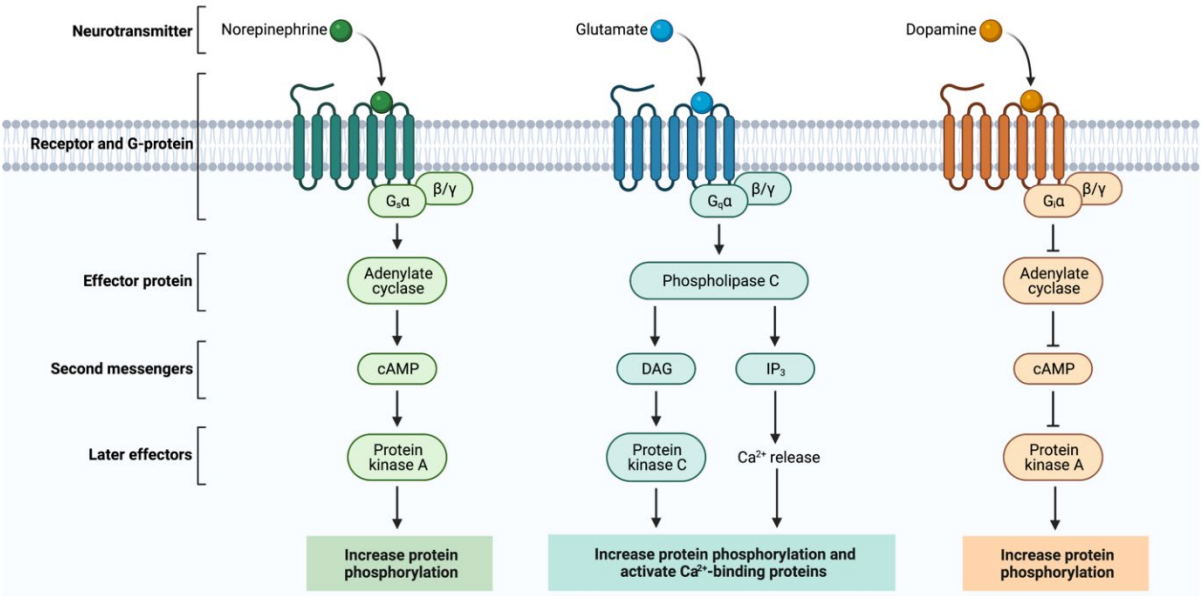

Figure 1-1. Various effector pathways of GPCRs. Depending on the types of G protein the GPCR interacts with, different downstream signaling pathways are activated. The three most common types of G proteins include G_s, G_q, and $G_{i/o}$.

GPCRs are deactivated by phosphorylation at the C-terminal end by G protein-coupled receptor kinases (GRKs), leading to the binding of β-arrestins, which sterically blocks the coupling of G proteins(Lefkowitz 2007). Since the binding site of β-arrestins and G proteins are the same, their coupling to the GPCR is competitive and thus can dictate the active/inactive equilibrium of the GPCR(Edelstein and Changeux 2016). Additionally, the preference of the GPCR to interact with either G proteins or β-arrestins can be mediated by different ligands, leading to various downstream signaling effects, including rapid G protein activation, long-term β-arrestin-mediated responses, internalization of the GPCR, etc. (Lefkowitz 2007).

1.1.2. Families and Classifications

Although all GPCRs share the same seven transmembrane (TM) helix (heptahelical) structure, they differ in other respects, primarily in the length of the extracellular N-terminus and the location of the ligand binding domain. There is significant sequence homology among the members in the same family, but those across different families have little similarity. Classically, the GPCR superfamily is grouped into six families:

- Family A (rhodopsin-like) comprises the largest group of GPCRs, accounting for nearly 85% of the gene encoding GPCRs. It includes most monoamine, neuropeptide, and chemokine receptors. Family A GPCRs have short N-terminus, with ligands bound to the TM helices or to extracellular loops (ECLs).
- Family B (secretin) includes GPCRs regulated by peptide hormones such as calcitonin, secretin, and glucagon. This family is characterized by members with longer N-termini as the primary ligand-binding domain(George, O'Dowd, and Lee 2002).
- Family C (glutamate) is a small receptor family that includes metabotropic glutamate receptors, $GABA_B$ receptors, and Ca^{2+}-sensing receptors. Receptors in this family have exceptionally long N-termini incorporating ligand-binding region.
- Family D (fungal mating pheromone) consists of members that are specific to peptide pheromones, which control cell division and conjugation in the yeast *Saccharomyces cerevisiae*(Thorner 1980).
- Family E (cAMP) includes receptors responsible for the aggregation of individual *Dictyostelium discoideum* (slime molds) cells into a multicellular organism(Klein et al. 1988).

- Family F (Frizzled/Taste2) serves in several biological pathways and facilitates the sensation of taste.

1.1.3. Structure

The first high-resolution structure of a GPCR was that of rhodopsin, obtained in 2000 at a resolution of 2.8 Å(Palczewski et al. 2000). Since then, the difficulties of crystalizing GPCRs have been overcome(Weis and Kobilka 2008), allowing X-ray crystallography to blossom in the structure determination of such difficult targets. With the additional help from cryogenic electron microscopy (cryo-EM) in recent years, structural biologists have been able to obtain 321 experimental structures of 60 different GPCRs from 9 species("GPCR-EXP for Experimentally-Solved and Predicted GPCR Structures" 2019). Also, ligand binding mechanism and the conformational changes induced by activation can now be sensibly studied using fluorescence methods(Lohse et al. 2009; Bockenhauer et al. 2011). These significant breakthroughs have helped scientists gain a sharper picture of how GPCRs work and eventually how to design better ligands that intervene in this process as desired.

GPCRs are usually made up of a single polypeptide chain of 350–450 residues, sometimes up to 1,000 residues. Considering structure, GPCRs mainly consist of an extracellular N-terminus, a seven-transmembrane domain (TMD) bundle connected by three ECLs and three intracellular loops (ICLs), and an intracellular C-terminus (**Figure 1-2**). Varying greatly in lengths and amino acid sequences(Lagerström and Schiöth 2008), the N-terminus has a few known functions, such as enhancing specificity in hydrophobic ligand recognition(Hurst et al. 2010) (rhodopsin(Palczewski et al. 2000) and $S1P_1$ receptor(M. A. Hanson et al. 2012)), participating in ligand binding (class B GPCRs(Runge et al. 2003;

Grauschopf et al. 2000; Grace et al. 2007; Robberecht et al. 1992)), and even alone serving as ligand-binding domain (class C GPCRs(Takahashi et al. 1993; Hammerland et al. 1999; Bräuner-Osborne et al. 1999; O'Hara et al. 1993; Malitschek et al. 1999)). The seven TM helices form the ligand-binding pocket with the ECLs and the G protein-coupling region with the ICLs, especially the ICL3(Katritch, Cherezov, and Stevens 2012; Rasmussen et al. 2011). Communication between the ligand-binding pocket and the G protein-coupling region is enabled also by the receptor core, which assumes a tertiary structure that undergoes a change in the relative orientations among their helical domains, leading to an eventual structural rearrangement on the cytoplasmic side of the receptor that facilitates the coupling of G proteins. Furthermore, the canonical presence of disulfide bonds in the ECLs greatly contributes to receptor stability and activity(O'Malley et al. 2010a; De Filippo et al. 2016; Zhang et al. 1999; Perlman et al. 1995; Cook and Eidne 1997).

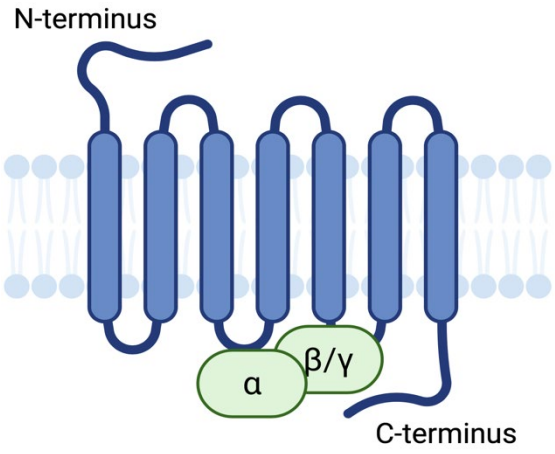

Figure 1-2. General structure of a GPCR. It consists of a single polypeptide chain with an extracellular N-terminus, a seven-transmembrane-helix domain connected by three extracellular loops and three intracellular loops, and an intracellular C-terminus. The heterotrimeric G protein binds to the receptor on the intracellular side.

The C-terminus in many GPCRs is a long, variable, intrinsically disordered structure(Veli-Pekka Jaakola et al. 2005) protein segment, which suggests that it may contain peptide motifs that help with partner recognition and binding(Gsponer and Madan Babu 2009). For example, the six-residue polybasic motif (KKKRRK) in the C-terminus of M_3 muscarinic receptor and other G_q-coupled receptors is crucial for their preassembly with G_q heterotrimers(K. Qin et al. 2011). Moreover, serine and threonine residues in the C-terminus of many GPCRs are often targets of phosphorylation, which is necessary for the recruitment of β-arrestins for receptor desensitization(Oakley et al. 1999; 2001; Nobles et al. 2011; Luttrell and Lefkowitz 2002).

1.1.4. Oligomerization of GPCRs

It has been long recognized that the activity of GPCRs can be regulated by structural modifications, among which oligomerization is a key factor that leads to major functional changes or even is required for proper functioning, as exemplified by the studies of $GABA_B$ receptors(Margeta-Mitrovic, Jan, and Jan 2000),(White et al. 1998), α-factor receptor(Overton and Blumer 2000), opioid receptor(Waldhoer et al. 2005), or chemokine receptor(Wu et al. 2010) (**Figure 1-3**). In fact, oligomerization is not limited to the formation of homo-oligomers, as scientists have widely accepted the concept of "receptor hetero-oligomer", which referred to the resulted substantial changes in biochemical and functional characteristics as receptors of the same or different families combine among themselves to form high-order entities(Agnati 2003; Ferré et al. 2007; Pin et al. 2007). In fact, there is a published list of requirements, proposed by the International Union of Basic and Clinical Pharmacology, for a multimeric receptor to be accepted by the science community. At least two of the following criteria should

be met, which includes: (1) physical association in native environment; (2) colocalization of the two protomers in the same subcellular unit of the same cell; (3) physical interaction of the two protomers in native tissue demonstrated by coimmunoprecipitation, energy transfer techniques, or transgenic animals expressing fluorescently labeled proteins; (4) evidence of functions uniquely exhibited by the heteromer; and (5) *in vivo* interaction proved by knockout animals or RNAi technology(Pin et al. 2007).

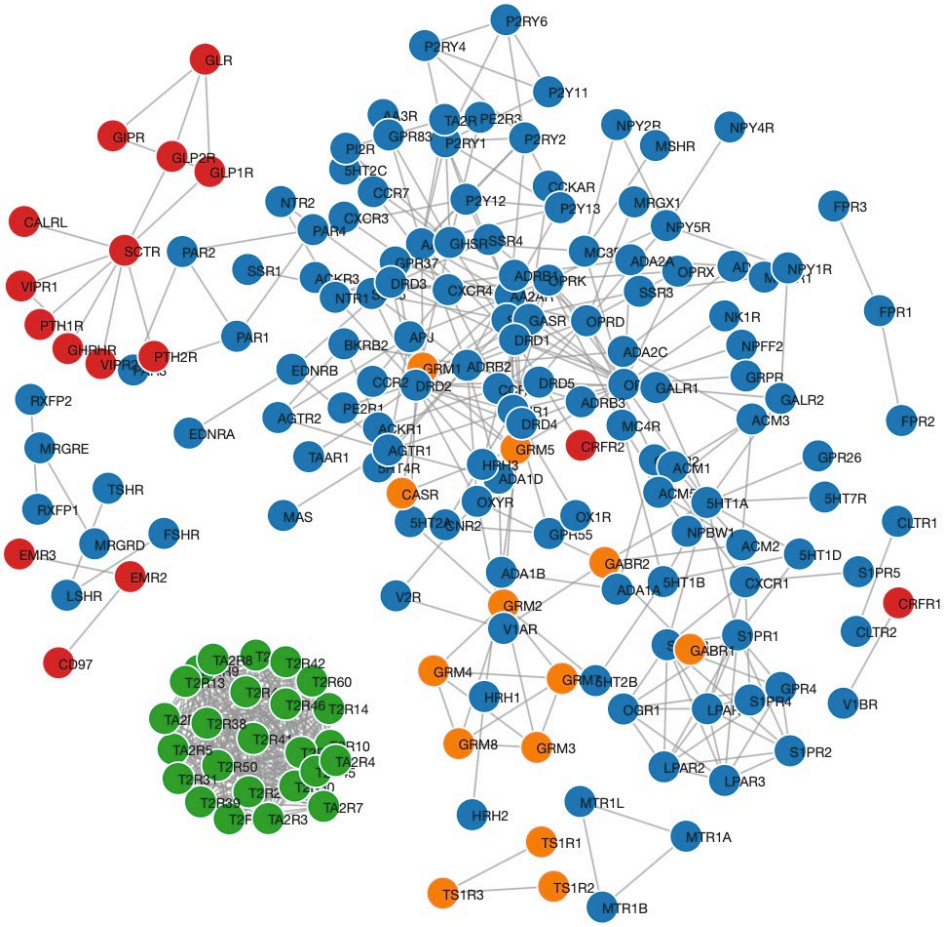

Figure 1-3. There exists an intricate network of oligomers among GPCRs, in which one member can form oligomers with many others. (Figure from www.gpcr-hetnet.com)

How many active protomers are needed to couple to and activate a G protein? In the case of family C GPCRs, dimerization is obligatory for the receptor to form a physiologically functional complex. The $GABA_B$ receptor is composed of two subunits GbR_1 and GbR_2, one needed for ligand binding and the other for G protein coupling, making both subunits required for the formation of a fully active receptor complex(Margeta-Mitrovic, Jan, and Jan 2000; Robbins et al. 2001; Ng et al. 1999). Taste T_1 receptor has also been shown to detect sweet and umami only as heteromers(Prezeau et al. 2010; Nelson et al. 2001). When it comes to class A GPCRs, the monomeric form is usually sufficient to perform a physiological function. However, there is vast evidence that confirms the existence of functional homo- and hetero-oligomers of class A GPCRs, including those formed between adenosine A_1R-dopamine D_1R(Gines et al. 2000), D_1R-D_2R(Beaulieu, Espinoza, and Gainetdinov 2015), D_2R homo-oligomers(Strange 2005), D_1R-D_3R(Marcellino et al. 2008), $A_{2A}R$-D_2R(Kamiya et al. 2003), serotonin 5-$HT_{2C}R$ homo-dimers(Herrick-Davis et al. 2015), or even a trimeric $mGlu_5R$-D_2R-$A_{2A}R$ complex(Cabello et al. 2009), and so on.

Not only that, this multitude of GPCR oligomeric species may also adopt multiple interfaces. Using molecular dynamics (MD) simulations, it was shown that the β_2-adrenergic receptor (β_2AR) dimers can form via six distinct interfaces, some of which are more energetically favorable than others(Ghosh, Sonavane, and Joshi 2014a). Similarly, the crystal structure of the turkey β_1AR showed that this receptor dimerizes via two different interfaces, one formed by TMD4/TMD5 and the other by TMD1/TMD2/H8 (helix 8)(J. Huang et al. 2013). This phenomenon was also observed in the crystal structure of μ-opioid receptor (μ-OR), in which the protomers appear to dimerize via two interfaces(Manglik et al. 2012). Besides, various studies also suggest that such multiple oligomeric interfaces may dynamically

rearrange to activate receptor function. For example, the metabotropic glutamate receptors (mGluRs) have been shown to undergo major ligand-induced rearrangement of dimeric interfaces from TMD4/TMD5 to TMD6; this rearrangement is in fact required for receptor activity(Xue et al. 2015). Furthermore, a recent study combining experimental and computational data suggested that neurotensin receptor 1 (NTS_1R) dimers are formed via multiple interfaces that coexist and interconvert when the receptor is activated(Dijkman et al. 2018).

It is not the sheer physical interaction between the protomers that gives emphasis to GPCR oligomerization, as this phenomenon transforms how GPCRs function in many ways. The basic molecular mechanism leading to the functional changes of these receptor assemblies appear to be allosteric interactions(Changeux and Christopoulos 2016). As an example, the dimerization of cell chemokine receptor CCR_{2B} and CCR_5 causes the latter to bind monocyte chemoattractant protein-1 (MCP-1), which is not a native ligand of CCR_5(L. El-Asmar 2004). Another study showed that in the βAR-AT_1R heterodimer, inhibition of one subunit leads to blockade of the other subunit(Barki-Harrington, Luttrell, and Rockman 2003). An MD simulation study discovered that the dimers of the muscarinic M_2 receptor exhibit higher conformational flexibility that enhances ligand binding compared with the monomeric form, indicating positive cooperativity(Shivnaraine et al. 2016). Moreover, GPCR oligomerization can also affect the preference of the receptor complex to couple with different types of G proteins. For example, D_1R and D_2R are natively linked to G_s and G_i, respectively, but their heterodimeric complex is coupled to $G_{q/11}$, eliciting a novel pathway that leads to an increase in intracellular calcium level(S. P. Lee et al. 2004). More impressively, as in the case of the κ

opioid receptor, its dimerization with neurotensin receptor 1 switches κOR's downstream effector from G protein to β-arrestin 2(H. Liu et al. 2016).

Since oligomerization of GPCRs can lead to drastic changes in downstream signaling, its implication in diseases and drug discovery is immense. Hasbi et al., 2014 was able to design an interfering peptide that disrupts the interaction between the D_1R and D_2R in the same heteromer, a complex that has been linked to drug addiction and depression, resulting in anti-depressant effects(Hasbi et al. 2014). In the case of CB_1R-5-$HT_{2A}R$ heterodimer, disrupting this complex results in the beneficial pain-relieving effect disconnected from the harmful anxiolytic and amnesic impacts usually exhibited by delta-9-tetrahydrocannabinol (THC), thus enhancing the therapeutic potential of THC(Viñals et al. 2015). Furthermore, μOR-δOR dimer exhibited enhanced β-arrestin recruitment, counteracting the impairment of internalization of individual receptors due to chronic morphine exposure(Gomes et al. 2004). As a result, μOR-δOR dimer could be a valid target for treatment of conditions that requires long-term use of morphine.

In brief, the aforementioned examples showed clear evidence of how GPCR oligomerization leads to completely altered downstream signaling effects and thus different neurological and pathological behaviors in the human body. Apparently, the molecular mechanism of oligomerization and its functional consequences should be at the center of attention when it comes to research into GPCRs.

1.1.5. Difficulties in Biophysical and Structural Studies of GPCRs

Despite their importance, many structural and biophysical aspects of GPCR oligomers are still poorly understood or debated, such as the driving factors of their formation, the oligomeric interfaces, or their functional consequences. The dynamic nature of their conformations and interfaces suggests that the interactions at play should be reversible, rendering non-covalent interactions such as hydrogen bonds, electrostatic interactions, and hydrophobic interactions particularly important. Indeed, electrostatic interactions have been shown to be crucial in the formation of GPCR dimers ($A_{2A}R$-D_2R, $A_{2A}R$-CB_1R, and CB_1R-D_2R) and trimers ($A_{2A}R$-D_2R-CB_1R)(Navarro et al. 2010; Ciruela et al. 2004; Woods and Ferré 2005). In terms of functional outcomes, allostery modulation upon receptor oligomerization would be maximized if the allosteric sites are made up of flexible, non-covalent interactions. In that sense, protein regions that dynamically fluctuate would be more apt than "rigid" structures in enabling GPCR oligomerization and the consequent allosteric modulation of functions. The occurrence of intrinsic disorder in proteins has been demonstrated as necessary for structure formation and assemblies(Milles et al. 2018; Wicky, Shammas, and Clarke 2017; Szasz et al. 2011; Goldenberg and Argyle 2014; S. Qin and Zhou 2013; Cino, Karttunen, and Choy 2012; Soranno et al. 2014; Zosel et al. 2020), as well as the allosteric coupling of many protein families(Motlagh et al. 2014; Hilser and Thompson 2007; Eginton et al. 2015), as detailed later in **Chapter 2**.

Most difficulties associated with the study of GPCR oligomers stem from the heterogeneity in their conformations and assemblies. Most notably, there exist major hurdles in applying well-established structural tools, such as X-ray crystallography and nuclear magnetic resonance (NMR) spectroscopy, in solving the structures of GPCR oligomeric

complexes. The harsh and non-physiological condition involved in the crystallization procedure may render the resulted structure physiologically irrelevant. Additionally, significant modifications required for successful crystallization often involve removal of intrinsically disordered regions, thus excluding a lot of information about dynamics in protein assembly or conformational changes. Meanwhile, NMR spectroscopy can be used to probe dynamic features of proteins, but the deciphering of NMR spectra could prove taxing due to spectral overlap between the loop regions and the TM domains(Fox and Columbus 2013).

Two other viable options to study the dynamics of GPCR assembly and conformation are electron paramagnetic resonance (EPR) spectroscopy and cryo-EM. At the cost of lower resolution, EPR and the related technique double electron-electron resonance (DEER) can be exploited to investigate the mobility and dynamic of disordered regions as well as distances among protomers in an oligomeric GPCR complex. However, this technique requires the substitution of free endogenous cysteines in the investigated protein, which could lead to structural and functional changes, as detailed later in **Chapter 3**. Meanwhile, unlike EPR and X-ray crystallography, cryo-EM does not require harmful modifications or truncation of disordered protein regions. However, most GPCRs are ~50 kDa in size in their monomeric form, so the contrast on the cryo-EM micrographs would be poor even for a trimer of GPCRs. Furthermore, the detergent micelles commonly used in isolating GPCRs could result in altered structure and function, as detailed later in **Chapter 5**.

1.2. THE HUMAN ADENOSINE A_{2A} RECEPTOR

After many years of intense research since 1929, when adenosine was discovered to have pronounced effects on many biological pathways(Drury and Szent-Györgyi 1929), it is now well demonstrated that adenosine is among the most crucial neurotransmitters in the human body. This naturally occurring nucleoside binds to the adenosine receptors, members of the GPCR family that are divided into four subtypes: A_1, A_{2A}, A_{2B}, and A_3. Among these receptors, the human adenosine A_{2A} receptor serves as an excellent target to conduct modeling studies into oligomerization of GPCRs, as there is solid evidence that this receptor forms homo-oligomers(Canals et al. 2003; Schonenbach et al. 2016) as well as heteromers, especially with D_2 receptor(Ferré et al. 2016; Kamiya et al. 2003), playing an impactful role in several central nervous system (CNS) disorders(Morelli et al. 2007; Ferré et al. 2004; Vallano et al. 2011; Schwarzschild et al. 2006). Nevertheless, since the monomeric form is sufficient for ligand binding(V.-P. Jaakola et al. 2008), the exact mechanism of this interaction as well as its functional consequences, which should be at the spotlight, remains elusive.

1.2.1. Biology and Therapeutic Impacts

In the human body, $A_{2A}R$ is abundant in the striatum, the nucleus accumbens, and the olfactory tubercle(Kull et al. 2000). Its endogenous ligand is adenosine, while other more familiar binding molecules include caffeine and theophylline, both of which are antagonists. Upon agonist binding, $A_{2A}R$ activates G_s protein, which stimulates the production of adenylyl cyclase to generate cAMP, turning on protein kinase A (PKA). The effect of $A_{2A}R$ on G_s leads to an upregulation of cAMP, which plays a critical role in vasodilation(Schindler et al. 2005), decreased dopaminergic activity in the CNS(Yao et al. 2002), etc. (**Figure 1-4**).

Due to its critical role in regulating blood flow, $A_{2A}R$ is targeted to stimulate the heart to help patients achieve the required heart rate during treadmill exercise. In fact, adenosine has been widely accepted as a pharmacologic stress agent to induce coronary arterial vasodilation(Cerqueira 2004). Regadenoson, a more $A_{2A}R$-specific agonist(Palle et al. 2002), was approved by FDA in 2008 for myocardial perfusion imaging and bears the trade name Lexiscan. At lower doses, $A_{2A}R$ agonists inhibit inflammation by modulating the activity of various inflammatory cells, including neutrophils, macrophages, T cells, etc., and thus can be used to treat inflammation(Lappas, Sullivan, and Linden 2005). Meanwhile, $A_{2A}R$ antagonists give hope mostly to patients suffering from Parkinson's disease (PD), which is caused by a lack of dopaminergic activity, leading to impairment in motor functions. Blockade of $A_{2A}R$ leads to enhanced D_2R-dependent downstream signaling(Pollack and Fink 1995) and reduces the risk of motor fluctuations and hallucinations associated with long-term use of drugs directly targeting D_2R(Antonini and Cilia 2009). However, many of the $A_{2A}R$ antagonists designed for treatment of PD, such as preladenant, vipadenant, tozadenant, or istradefylline, never made it to the market due to toxicity or lack of efficacy in human trials(de Lera Ruiz, Lim, and Zheng 2014).

1.2.2. Structure and Conformational Changes upon Activation

Like any other GPCRs, A_{2A} receptor consists of a seven-transmembrane-helix core connected by three ICLs and three ECLs. Succeeding the 7^{th} helix is a short helix 8 that lies parallel to the surface of the lipid membrane. Its N-terminus is insignificant in length, while the C-terminus is 122-residue long and intrinsically disordered. The structure of $A_{2A}R$ is further stabilized by a network of four highly-conserved extracellular disulfide bonds(V.-P. Jaakola et

al. 2008). X-ray structures of $A_{2A}R$ bound to ligands revealed that its binding pocket is formed by the extracellular part of TMD5, 6, and 7(V.-P. Jaakola et al. 2008; Doré et al. 2011; Xu et al. 2011).

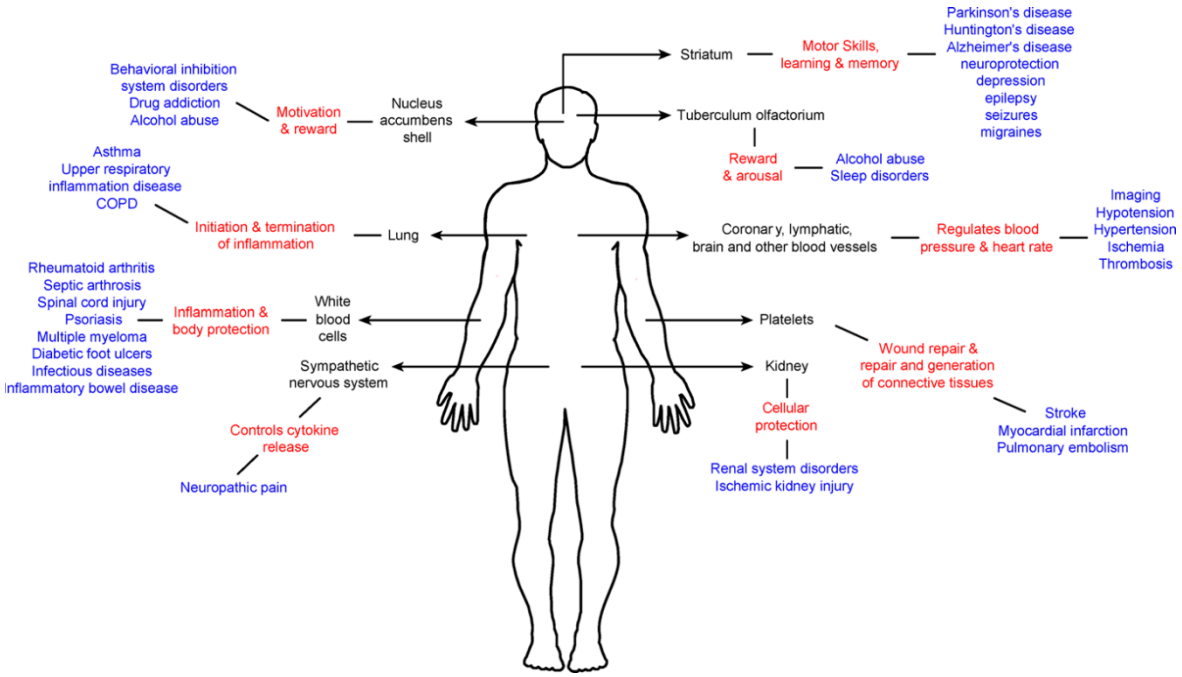

Figure 1-4. Adenosine A_{2A} receptor is abundant in many locations in the human body and thus has various therapeutic implications depending on where it is found. (Figure from de Lera Ruiz, M.; Lim, Y.-H.; Zheng, J. *J. Med. Chem.* 2014, *57*, 3623–3650.)

Most papers describing available crystal structures of $A_{2A}R$ agree that its conformational changes upon activation mainly involve movements of TMD3, 5, 6, and 7(V.-P. Jaakola et al. 2008; Doré et al. 2011; Xu et al. 2011; Hino et al. 2012; Sun et al. 2017; Carpenter et al. 2016). In fact, an ionic lock is formed between TMD3 and 6 (R102/R107 and E228)(Doré et al. 2011; Sun et al. 2017), and this combination of movements is required to break this ionic lock for the G-protein to bind to the receptor(Ye et al. 2016). TMD5 and 6,

connected by ICL3, sit most closely to the core of the receptor(Doré et al. 2011). Again, this emphasizes the importance of investigating the role of ICL3 upon activation.

It has been suggested that $A_{2A}R$ can be partially or fully activated upon binding to specific ligands(Doré et al. 2011). In fact, a ^{19}F NMR study done on $A_{2A}R$-A316ΔC (a variant truncated at position A316), with V229C labeled (next to E228, which is involved in the ionic lock), suggested that an ensemble of four states were found in equilibrium: two inactive states in millisecond exchange, consistent with a formed (S_1) and a broken (S_2) ionic lock, and two active states (S_3 and $S_{3'}$)(Ye et al. 2016). Activation of $A_{2A}R$ is found to be via conformational selection, which means that the four states all exist in the apo form in equilibrium, and addition of different types of ligand shift the equilibrium to different states – antagonist binding shifts the equilibrium to S_1 and S_2, partial agonist shifts it to S_3 (a "less open" conformation), while agonist shifts it to $S_{3'}$ (a "more open" and therefore fully agonist-binding conformation)(Ye et al. 2016). Upon activation, there is a concomitant proton uptake from the aqueous environment to the conserved D(E)RY motif on TM3. As a result, the population of the four states is also pH-dependent(Ye et al. 2016).

1.2.3. Oligomerization of $A_{2A}R$

$A_{2A}R$ has been shown by bimolecular fluorescence complementation (BiFC) and fluorescence resonance energy transfer (FRET) to exist as homodimers and even higher-order oligomers at the plasma membrane in living neuronal cells(Vidi et al. 2008). Such homo-oligomers of $A_{2A}R$, like other GPCR oligomeric complexes, can form via multiple interfaces. Using computational method, Fanelli and Felline predicted three $A_{2A}R$ dimer interfaces(Fanelli and Felline 2011) (**Figure 1-5**) as follows:

- DIM1 (H1-H1/H2-H2): (a) the ECL end of TM1 and TM3, (b) the ICL end of TM1, (c) the ECL half of TM2.
- DIM2 (H1-H4/H2-H2): (a) TM1 and TM4, (b) ECL ends of TM2 and TM3, (c) ECL half of TM2.
- DIM3 (H6-H6/H6-H7): (a) ICL half of TM6 of monomer A to ICL halves of TM6 and TM7 and vice versa, (b) ECL halves of TM6 and TM7, (c) H8 and both ICL3 and the ECL extension of TM6.

According to this study, DIM1 and DIM2 seem to enhance antagonist-mediated communication of $A_{2A}R$, while DIM3 appears to reduce this. The impairing effect of DIM3 architecture is expected to be even more remarkable for the agonist-bound forms, as the TMD6 movement required for receptor activation would be hindered in this architecture(Fanelli and Felline 2011). In fact, a BiFC study strongly supported that TMD5 and 7 are not included in the $A_{2A}R$ homodimer interfaces(Bonaventura et al. 2015). The evidence above makes DIM3 less convincing as a pursuit. However, this deduction contradicts with a study working with peptide, which suggested that TMD5 peptides of $A_{2A}R$ *per se* can form dimers and that a mutation M193A significantly reduced the dimer/monomer ratio as shown on sodium dodecyl sulphate–polyacrylamide gel electrophoresis (SDS-PAGE), suggesting that M193 is involved in the dimerization of $A_{2A}R$(Thévenin et al. 2005). A recent study using computational prediction method also revealed that M193A (but not M193I) completely changed the contact interface between TMD5, thus supporting that TMD5 is involved in $A_{2A}R$ dimerization(Altwaijry et al. 2017). Also, using bioluminescence resonance energy transfer (BRET) and information on TM interfaces based on crystal structures of other GPCRs, TMD4/5 interface was modeled to be the $A_{2A}R$ (and A_1R) homodimer interface(Navarro et al.

2016). Another prominent study recently demonstrated that $A_{2A}R$ oligomers can adopt eight distinct interfaces that interconvert when the receptor is activated or when there are changes in the local membrane environment, with TMD4/5 again involved in the most commonly formed interfaces(Song, Duncan, and Sansom 2020). As a result, DIM1 and DIM2 seem more worthwhile to pursue if this computational study is used as a guide, while TMD5 remains to be investigated as a possible homodimer interface.

Furthermore, Schonenbach et al., 2016, employing a tandem two-step affinity chromatography approach followed by SEC-MALS and EPR measurements, demonstrated that $A_{2A}R$ exists as three distinct oligomer species and that residue C394 may have a critical stabilizing effect on the dimer species, since the mutation C394S disrupts this architecture(Schonenbach et al. 2016) (**Figure 1-6**).

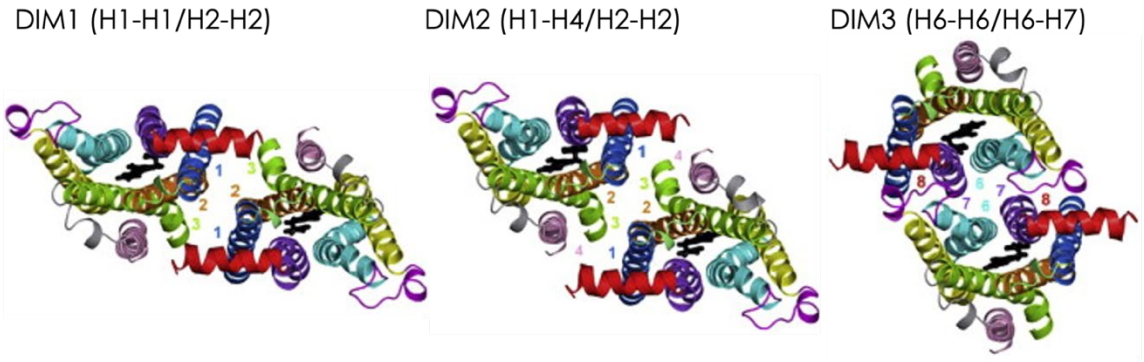

Figure 1-5. $A_{2A}R$ may adopt multiple oligomeric interfaces as suggested via MD simulations. Fanelli and Felline predicted that there exist three interfaces for $A_{2A}R$ dimers (shown here as seen from the intracellular side in a direction perpendicular to the membrane plane). Numbers indicate the receptor portions that participate the most in the interface. (Figure from Fanelli and Felline, *Biochim. Biophys. Acta Biomembr.* **2011**, 1808, 1256–1266.)

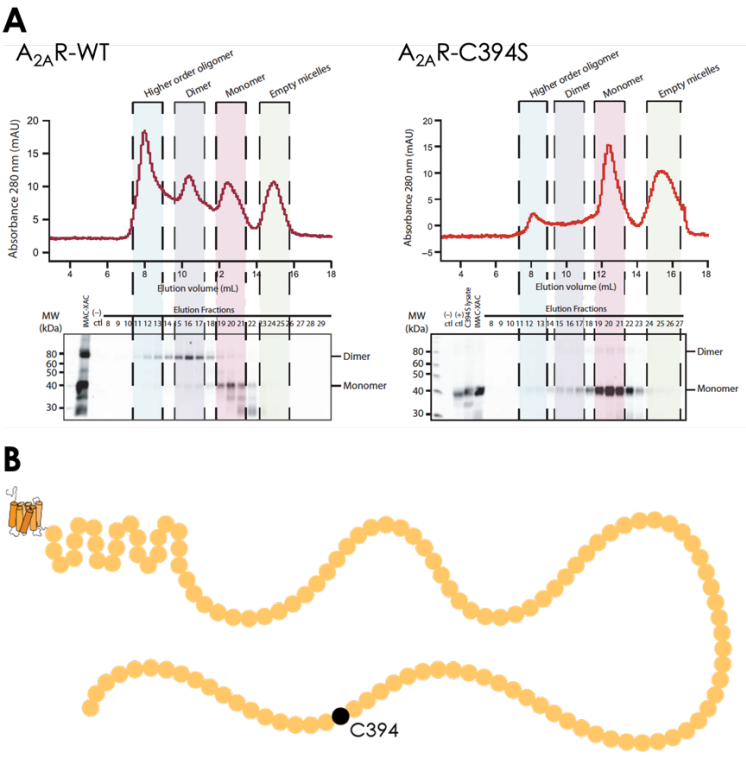

Figure 1-6. (A) Active $A_{2A}R$ can be separated by SEC with peaks representing distinct oligomeric species as indicated. Dimer and higher-order oligomer are clearly observed in $A_{2A}R$-WT but are almost completely abolished upon the mutation C394S. (Figure from Schonenbach, N. S. *et al*. *FEBS Lett.* **2016**, *590*, 3295–3306.) **(B)** The 122-residue long C-terminus of $A_{2A}R$ with residue C394 indicated.

Besides homo-oligomers, $A_{2A}R$ can also form hetero-oligomers with many other GPCRs, including A_1R as well as various dopamine receptors and purinoreceptors (**Figure 1-7**). Its most well-known partner is D_2 receptor: heterodimerization(Kamiya et al. 2003) and even heterotetramerization(Casadó-Anguera et al. 2016a) between $A_{2A}R$ and D_2R have been reported. Recently, TMD5 of both $A_{2A}R$ and D_2R was strongly suggested to form part of the oligomeric interface by a study using BiFC(Bonaventura et al. 2015). It is important to note that TMD5 is adjacent to ICL3, which has been at the limelight of attention in elucidating $A_{2A}R$ function. Other studies with pull-down assay, mass spectrometry (MS)(Ciruela et al. 2004),

BRET(Borroto-Escuela, Romero-Fernandez, et al. 2010; Navarro et al. 2010) and ligand-binding assay(Bonaventura et al. 2015) (with mutations at specific sites) indicated that $A_{2A}R$-D_2R heteromerization is dictated by a strong electrostatic interaction between an Arg-rich epitope from ICL3 of D_2R (217–222) and two adjacent DD 401–402 or a phosphorylated S374 in the C-terminus of $A_{2A}R$(Bonaventura et al. 2015; Ciruela et al. 2004; Borroto-Escuela, Romero-Fernandez, et al. 2010; Navarro et al. 2010).

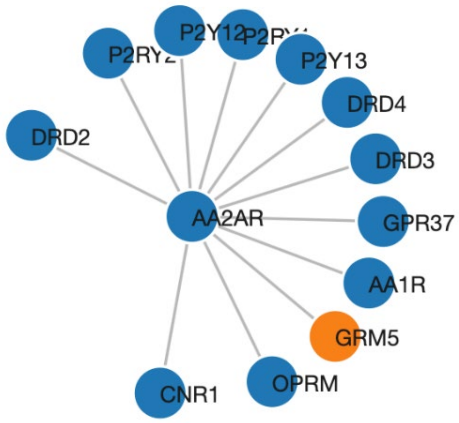

Figure 1-7. The human adenosine A_{2A} receptor can undergo oligomerization with many other GPCRs, most prominently the dopamine and purinergic receptors. (Figure from www.gpcr-hetnet.com)

It is also worthy to mention that $A_{2A}R$ has also been found to oligomerize with the angiotensin AT_1R (a possible target to treat tardive dyskinesia)(Oliveira et al. 2017), metabotropic glutamate $mGlu_5R$(Ferré et al. 2002), dopamine D_3R(Torvinen 2004), cannabinoid CB_1R(Ferré et al. 2009), adenosine $A_{2B}R$ ($A_{2A}R$ ligand recognition is blocked upon this interaction)(Hinz et al. 2018), or form even a heterotrimeric CB_1R-D_2R-$A_{2A}R$ complex(Navarro et al. 2008).

1.2.4. The Intrinsically Disordered C-Terminus

The C-terminus is a unique structural feature of $A_{2A}R$: in contrast to many other GPCRs and, specifically to the other members of the adenosine receptor family, $A_{2A}R$ has an unusually long C-terminus (122 residues compared with only 34 residues in A_1 receptor). High-resolution crystal structures and most previous structural studies of $A_{2A}R$ up to now involve the truncation of this long C-terminus to enhance conformational and thermostability of the receptor.

Most class A GPCRs have one or two palmitoylated cysteines in the C-terminus close to the end of the TMD7 to stabilize this segment in an α-helical conformation (helix 8). Instead of these canonical cysteines, $A_{2A}R$ only has one cysteine (C394) very close to the end of the C-terminus that is not involved in the stabilization of the helix 8(Zezula and Freissmuth 2009). It has been shown that the mutation C394S significantly reduced the dimer/oligomerization of the receptor, as quantified with size-exclusion chromatography (SEC)(Schonenbach et al. 2016). Furthermore, the C-terminus of $A_{2A}R$ has been characterized in terms of disorder and protein binding probability using computational software PONDR VSL2 and ANCHOR, respectively. As shown in **Figure 1-8**, the C-terminus of $A_{2A}R$-WT showed high disorder and strong propensity to protein binding. As outlined in **1.1.5 above**, intrinsically disordered regions appear to promote protein-protein interactions via non-covalent bonds. Upon C394S mutation, $A_{2A}R$ C-terminus showed increased disorder and decreased protein binding probability, suggesting destabilization of protein-protein interaction in agreement with the aforementioned study(Schonenbach et al. 2016). Therefore, we hypothesized that the intrinsically disordered C-terminus of $A_{2A}R$ may promote protein-protein association, leading to homo- or hetero-oligomerization of this receptor with other GPCRs.

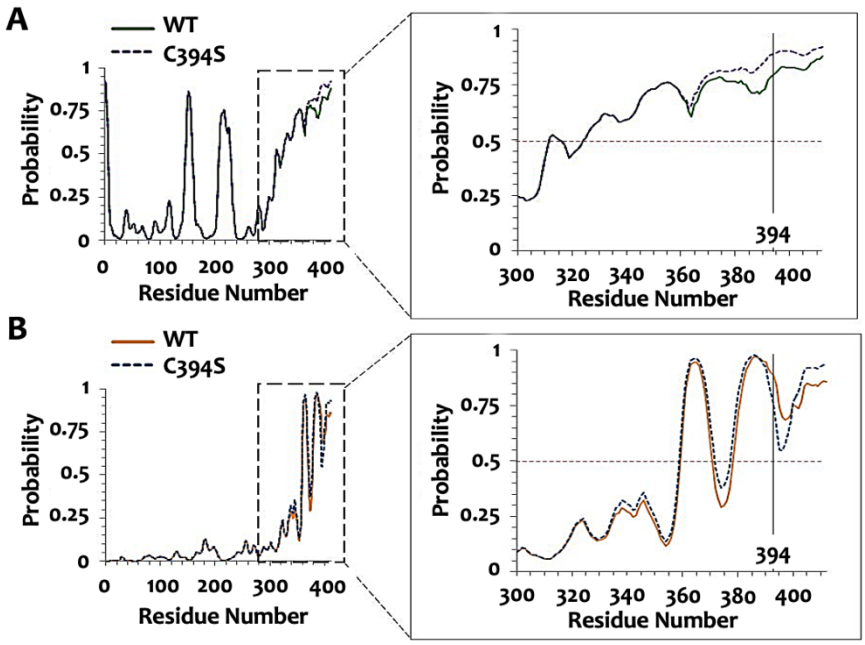

Figure 1-8. Analysis of **(A)** disorder and **(B)** protein binding probability of the C-terminus of $A_{2A}R$ (in box) using computational software. Y-axis values > 0.5 indicate disordered and putative binding regions. Increased disorder and decreased protein binding probability suggests destabilization of protein-protein association upon C394S mutation. **(A)** PONDR VSL2 suggests high disorder for the C-terminus, with the mutation C394S increasing its disorder. **(B)** ANCHOR predicts that the C-terminus is strongly prone to protein binding, with the mutation C394S decreasing this probability.

1.3. APPROACH AND PROJECT GOALS

The preliminary data presented above suggest that a thorough structural study on the full-length construct of $A_{2A}R$ be carried out, as it will provide an original perspective on the oligomerization of not only A_{2A} receptor but also GPCRs in general. **The hypothesis** is that (1) there is a specific mechanism that allows the intrinsically disordered C-terminus to stabilize $A_{2A}R$ oligomers and that (2) the interfaces among $A_{2A}R$ oligomers directly involve the C-terminus. To answer these perplexing questions, I aim to address two underlying questions:

- Identifying the role of the C-terminus in $A_{2A}R$ oligomerization, either at the interface or as a critical structural feature in stabilizing $A_{2A}R$ oligomers, can be key to answering a lot of questions, given the unique length and unusual behavior of this C-terminus (*e.g.*, the C-terminal C394 residue is important for oligomerization (**1.2.4 above**))
- Mapping the network of connection at the oligomeric interface is crucial to probe the dynamics and mechanism of $A_{2A}R$ oligomerization, as the stability and even dissociation constants for the complex, together with how to disrupt and further control the oligomerization and activity of $A_{2A}R$, can be determined.

To understand the role of the C-terminus in $A_{2A}R$ oligomerization, one should first learn the specific residues that are involved, together with the mechanism of bonding associated with each residue. The first logical speculation is covalent disulfide bonding involving the C-terminal cysteine C394. However, non-covalent interactions may also be of importance due to their potential role in accommodating dynamic protein assembly and conformational changes (see **1.2.4 above**). One approach to understand how the C-terminus affects $A_{2A}R$ dimerization is to systematically truncate the C-terminus and assess oligomeric

distribution using SEC. Impact of different parts of the C-terminus on oligomerization can be evaluated, which will help narrow the specific segments needed and potentially the specific residues. Once a list of residues needed for oligomerization is known, it should be easier to understand the overall mechanism of bonding. This effort will be described in detail in **Chapter 2**.

As mentioned in **1.2.4 above**, GPCRs are notoriously challenging targets in biophysical and structural studies due to their dynamic nature and the generally low suitability for biophysical techniques. EPR and DEER are most probing protein dynamics, especially when the intrinsically disordered C-terminus is involved. In **Chapter 3**, I will describe the characterization of the $A_{2A}R$ constructs void of free cysteines that are required for the employment of EPR and DEER, as well as the role of its TM cysteines in maintaining receptor structure and function. Furthermore, styrene maleic acid (SMA) copolymers, a novel nanodisc platform, offer a promising avenue towards detergent-free isolation of $A_{2A}R$ that retains its native structure and function. **Chapter 5** explains efforts in applying SMA to isolate and stabilize $A_{2A}R$ as well as proteorhodopsin, a model bacterial transmembrane proton pump. The findings described in these two chapters offer valuable insights into sample preparation of $A_{2A}R$ for further structural analysis.

In order to elucidate $A_{2A}R$ dimer/oligomer interface, one should first identify which residues are involved in the interaction. A logical prediction of such residues has been made using MD simulations, from which three possible dimeric interfaces have been identified, indicated based on the regions most involved in the interaction as H1 (helix 1)-H1/H2-H2 (DIM1), H1-H4/H2-H2 (DIM2), and H6-H6/H6-H7 (DIM3) dimers(Fanelli and Felline 2011).

Additionally, a number of experimental and computational studies on the hetero-oligomerization of $A_{2A}R$ with other GPCRs such as angiotensin II type 1 AT_1R, dopamine D_2R, and adenosine A_1R provide agree that the TMD5, 6, and 7 of $A_{2A}R$ are most likely to participate in these interfacial interactions(Casadó-Anguera et al. 2016a; Navarro et al. 2016; Oliveira et al. 2017). This great amount of preliminary data makes it conducive to carry out dynamic studies of the $A_{2A}R$ homodimer interface. The role of the C-terminus, which may or may not be at the actual interface, should be investigated alongside. From here, the immediate plan is to visualize the interface of the $A_{2A}R$ dimers. One method is to use cryo-EM to directly visualize this interface, which seems to be promising as our sample preparation has been proved to exceed the quality required to obtain good cryo-EM images. The potential role of cryo-EM in this project is limited by the poor resolution, an inherent problem for a membrane protein like $A_{2A}R$, as only secondary structures can be seen. However, this finding from cryo-EM will allow inter-$A_{2A}R$ distance measurements with double electron electron resonance (DEER) at Q-band (33–50 GHz) using nitroxides (for 4–7 nm distance) and W-band (50–75 GHz) using Gd^{3+} probes (for 2.5–3.5 nm distance) to characterize the interfaces of detergent-constituted $A_{2A}R$. Subsequently, continuous wave EPR (cw-EPR) lineshape analysis at 240 GHz can be performed on $A_{2A}R$ to obtain mobility information to compare and support the results from the distance measurements. **Chapter 4** aims to describe the preliminary data obtained from this approach to visualize the oligomeric interfaces of $A_{2A}R$.

Chapter 2 | HOMO-OLIGOMERIZATION OF THE HUMAN ADENOSINE A_{2A} RECEPTOR IS DRIVEN BY THE INTRINSICALLY DISORDERED C-TERMINUS

2.1. INTRODUCTION

G protein-coupled receptors (GPCRs) have long been studied as monomeric units, but accumulating evidence demonstrates that these receptors can also form homo- and hetero-oligomers with far-reaching functional implications. The properties emerging from these oligomers can be distinct from those of the monomeric protomers in ligand binding(Laïla El-Asmar et al. 2005; Casadó-Anguera et al. 2016b; Guitart et al. 2014; Yoshioka, Saitoh, and Nakata 2001), G protein coupling(Cristóvão-Ferreira et al. 2013; Cordomí et al. 2015; González-Maeso et al. 2007; S. P. Lee et al. 2004; Rashid et al. 2007), downstream signaling(H. Liu et al. 2016; Hilairet et al. 2003; Rozenfeld and Devi 2007; Borroto-Escuela, Narvaez, et al. 2010), and receptor internalization/desensitization(Ecke et al. 2008; Stanasila et al. 2003; Faklaris et al. 2015). With the vast number of genes identified in the human genome(Takeda et al. 2002), GPCRs are able to form a daunting number of combinations with unprecedented functional consequences. The existence of this intricate network of interactions among GPCRs presents major challenges and opportunities for the development of novel therapeutic approaches(Dorsam and Gutkind 2007; Farran 2017; Schonenbach, Hussain, and O'Malley 2015; Ferré et al. 2014; Bräuner-Osborne, Wellendorph, and Jensen 2007; George, O'Dowd, and Lee 2002). Hence, it is crucial to identify the driving factors of GPCR oligomerization,

such that this process can be more deliberately controlled to facilitate structure-function studies of GPCRs.

GPCR oligomers with multiple interfaces(Song, Duncan, and Sansom 2020; Ghosh, Sonavane, and Joshi 2014b; Periole et al. 2012; Fanelli and Felline 2011; W. Liu et al. 2012) can give rise to myriad ways by which these complexes can be formed and their functions modulated. In the crystal structure of the turkey β_1-adrenergic receptor (β_1AR), the receptor appears to dimerize via two different interfaces, one formed via TM4/TM5 (transmembrane domains 4/5) and the other via TM1/TM2/H8 (helix 8) contacts(J. Huang et al. 2013). Similarly, in the crystal structure of the antagonist-bound μ-opioid receptor (μ-OR), the protomers also dimerize via two interfaces; however, only one of them is predicted to induce a steric hindrance that prevents activation of both protomers(Manglik et al. 2012), hinting at interface-specific functional consequences. A recent computational study predicted that the adenosine A_{2A} receptor (A_{2A}R) forms homodimers via three different interfaces and that the resulting dimeric architectures can modulate receptor function in different or even opposite ways(Fanelli and Felline 2011). All the above-mentioned interfaces are symmetric, meaning that the two protomers are in face-to-face orientations, hence forming strictly dimers. Asymmetric interfaces, reported in M_3 muscarinic receptor(Thorsen et al. 2014), rhodopsin(Fotiadis et al. 2006; 2003; Liang et al. 2003), and opsin(Liang et al. 2003), are in contrast formed with the protomers positioning face-to-back, possibly enabling the association of higher-order oligomers.

Not only do GPCRs adopt multiple oligomeric interfaces, but various studies also suggest that these interfaces may dynamically rearrange to activate receptor function(Xue et

al. 2015). According to a recent computational study, $A_{2A}R$ oligomers can adopt eight different interfaces that interconvert when the receptor is activated or when there are changes in the local membrane environment(Song, Duncan, and Sansom 2020). Similarly, a recent study that combined experimental and computational data proposed that neurotensin receptor 1 (NTS_1R) dimer is formed by "rolling" interfaces that co-exist and interconvert when the receptor is activated(Dijkman et al. 2018). Clearly, meaningful functional studies of GPCRs require exploring their dynamic, heterogeneous oligomeric interfaces.

The variable nature of GPCR oligomeric interfaces suggests that protomers of GPCR oligomers may be connected by tunable interactions. In this study, we explore the role of an intrinsically disordered region (IDR) of a model GPCR that could engage in diverse non-covalent interactions, such as electrostatic interactions, hydrogen bonds or hydrophobic interactions. These non-covalent interactions are readily tunable by external factors, such as pH, salts, and solutes, and further can be entropically enhanced by depletion interactions(Asakura and Oosawa 1958; Yodh et al. 2001; Marenduzzo, Finan, and Cook 2006), leading to structure formation and assembly(Milles et al. 2018; Wicky, Shammas, and Clarke 2017; Szasz et al. 2011; Goldenberg and Argyle 2014; S. Qin and Zhou 2013; Cino, Karttunen, and Choy 2012; Soranno et al. 2014; Zosel et al. 2020). In a system where large protein molecules and small solute particles typically coexist in solution, assembly of the protein molecules causes their excluded volumes to overlap and the solvent volume accessible to the non-protein solutes to increase, raising the entropy of the system (**Figure 2-1A**). The type and concentration of solutes or ions can also remove water from the hydration shell around the proteins, further enhancing entropy-driven protein-protein association in what is known as the hydrophobic effect (**Figure 2-1B**) (Charles Tanford 1980; C Tanford 1978; Pratt and Chandler

1977; van der Vegt and Nayar 2017). This phenomenon is applied in the precipitation of proteins upon addition of so-called salting-out ions according to the Hofmeister series(Hofmeister 1888; Hyde et al. 2017; Yang 2009). The ability of IDRs to readily engage in these non-covalent interactions motivates our focus on the potential role of IDRs in driving GPCR oligomerization.

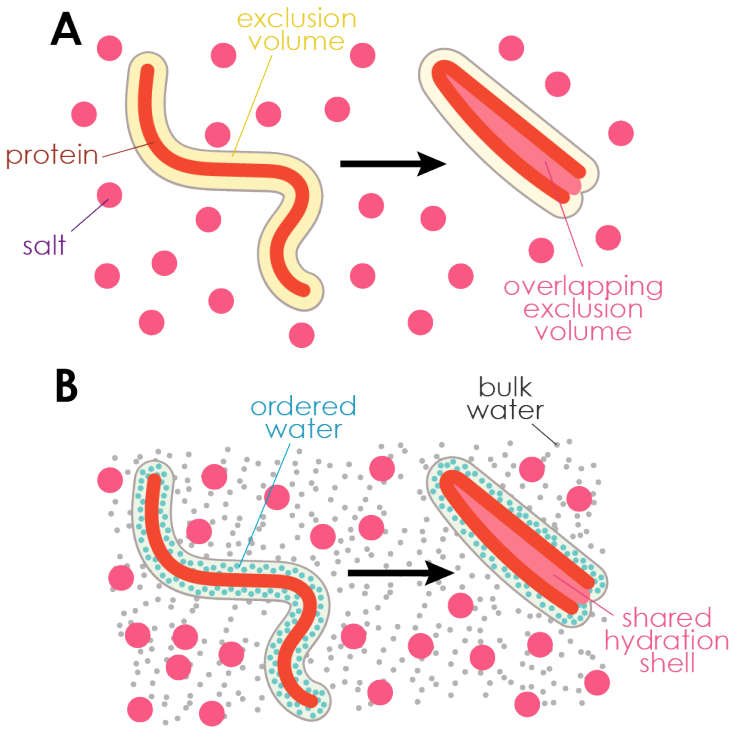

Figure 2-1. Depletion interactions can occur via two mechanisms: **(A)** overlapping of exclusion volume and **(B)** dehydration. Both mechanisms are driven by entropy, favoring protein-protein association.

The cytosolic carboxy (C-)terminus of GPCRs is usually an IDR(Tovo-Rodrigues et al. 2014; Veli-Pekka Jaakola et al. 2005). Varying in length among different GPCRs, the C-terminus is commonly removed in structural studies of GPCRs to enhance receptor stability and conformational homogeneity. A striking example is $A_{2A}R$, a model GPCR with a particularly long, 122-residue, C-terminus that is truncated in all published structural biology

studies(Song, Duncan, and Sansom 2020; Fanelli and Felline 2011; Garcıa-Nafrıa et al. 2018; Sun et al. 2017; Lebon et al. 2011; Xu et al. 2011; Doré et al. 2011; V.-P. Jaakola et al. 2008; Carpenter et al. 2016; Hino et al. 2012). However, evidence is accumulating that such truncations—shown to affect GPCR downstream signaling(Koretz et al. 2021; Navarro, Cordomí, Brugarolas, et al. 2018; A. Jain, McGraw, and Robinson 2020)—may abolish receptor oligomerization(Schonenbach et al. 2016; Cvejic and Devi 1997). A study using immunofluorescence has demonstrated that C-terminally truncated $A_{2A}R$ does not show protein aggregation or clustering on the cell surface, a process readily observed in the wild-type form(Burgueño et al. 2003). Our recent study employing a tandem three-step chromatography approach uncovered the impact of a single residue substitution of a C-terminal cysteine, C394S, in reducing the receptor homo-oligomerization in vitro(Schonenbach et al. 2016). In the context of heteromerization, mass spectrometry and pull-down experiments have demonstrated that $A_{2A}R$-D_2R dimerization occurs via direct electrostatic interactions between the C-terminus of $A_{2A}R$ and the third intracellular loop of D_2R(Ciruela et al. 2004). These results all suggest that the C-terminus may participate in $A_{2A}R$ oligomer formation. However, no studies to date have directly and systematically investigated the role of the C-terminus, or any IDRs, in GPCR oligomerization.

This study focuses on the homooligomerization of the human adenosine $A_{2A}R$, a model GPCR, and seeks to address: (i) whether the C-terminus engages in $A_{2A}R$ oligomerization, and if so, (ii) whether the C-terminus forms multiple oligomeric interfaces. We use size-exclusion chromatography (SEC) to assess the oligomerization levels of $A_{2A}R$ variants with strategic C-terminal modifications: mutations of a cysteine residue C394 and a cluster of charged residues ^{355}ERR^{357}, as well as systematic truncations at eight different sites along its length. We

complemented our experimental study with an independent molecular dynamics (MD) simulation study of $A_{2A}R$ dimers of five C-terminally truncated $A_{2A}R$ variants designed to mirror the experimental constructs. We furthermore examined the oligomerization level of select C-terminally modified $A_{2A}R$ variants under conditions of varying ionic strength ranging from 0.15 to 0.95 M. To verify whether the $A_{2A}R$ oligomer populations are thermodynamic products, we performed a series of SEC analyses on SEC-separated monomer and dimer/oligomer populations to observe their repopulation into monomer and dimer/oligomer populations. Finally, to test whether the C-termini directly and independently promote $A_{2A}R$ oligomerization, we recombinantly expressed the entire $A_{2A}R$ C-terminal segment *sans* the transmembrane portion of the receptor and investigated its solubility and assembly properties with increasing ion concentration and temperature. This is the first study designed to uncover the role of the intrinsically disordered C-terminus on the oligomerization of a GPCR.

2.2. MATERIALS AND METHODS

2.2.1. Key Resources Table

Reagent type (species) or resource	Designation	Source or reference	Identifiers	Additional information
Recombinant DNA reagent	pITy (plasmid)	(Parekh, Shaw, and Wittrup 1996)		
Strain, strain background (*Saccharomyces cerevisiae*)	BJ5464	Robinson Lab – Carnegie Mellon University		
Strain, strain background (*Escherichia coli*)	BL21 (DE3)	Sigma, St. Louis, MO, USA	#CMC0014	
Chemical compound, drug	DDM	Anatrace, Maumee, OH, USA	#D310	
Chemical compound, drug	CHAPS	Anatrace, Maumee, OH, USA	#C216	
Chemical compound, drug	CHS	Anatrace, Maumee, OH, USA	#CH210	
Chemical compound, drug	Xanthine amine congener	Sigma, St. Louis, MO, USA	#X103	
Chemical compound, drug	Theophylline	Sigma, St. Louis, MO, USA	#T1633	
Commercial assay, kit	Affigel 10 resin	BioRad, Hercules, CA, USA	#1536099	
Commercial assay, kit	Tricorn Superdex 200 10/300 GL column	GE Healthcare, Pittsburgh, PA, USA	#17-5175-01	
Antibody	Anti-$A_{2A}R$, clone 7F6-G5-A2 (Mouse monoclonal)	Millipore, Burlington, MA, USA	#05-717	(1:500) dilution
Antibody	Anti-Mouse IgG H&L DyLight 550 (Goat monoclonal)	Abcam, Cambridge, MA, USA	#ab96880	(1:600) dilution
Software, algorithm	MODELLER 9.23	(Eswar et al. 2006)		
Software, algorithm	martinize.py script	(de Jong et al. 2013)		
Software, algorithm	ELNeDyn elastic network	(Periole et al. 2009)		
Software, algorithm	MARTINI coarse-grained force field v2.2	(Monticelli et al. 2008)		
Software, algorithm	GROMACS 2016	(Abraham et al. 2015)		
Software, algorithm	backward.py script	(Wassenaar et al. 2014)		
Software, algorithm	LINCS	(Hess et al. 1997)		
Software, algorithm	CHARMM36 and TIP3P force fields	(Best et al. 2012; Jorgensen et al. 1983)		

Software, algorithm	LOOS	(Romo and Grossfield 2009)		
Software, algorithm	VMD	(Humphrey, Dalke, and Schulten 1996)		

2.2.2. Cloning, Gene Expression, and Protein Purification

The entire process of cloning, gene expression, protein purification, and separation of oligomeric species is visually depicted in **Figure 2-2**.

The multi-integrating pITy plasmid(Parekh, Shaw, and Wittrup 1996), previously used for overexpression of $A_{2A}R$ in *Saccharomyces cerevisiae*(O'Malley et al. 2009), was employed in this study. pITy contains a Gal1–10 promoter for galactose-induced expression, a synthetic pre-pro leader sequence which directs protein trafficking(Clements et al. 1991; Parekh, Forrester, and Wittrup 1995), and the yeast alpha terminator. The genes encoding $A_{2A}R$ variants with 10-His C-terminal tag were cloned into pITy downstream of the pre-pro leader sequence, using either splice overlapping extension(Bryksin and Matsumura 2010) or USER cloning using X7 polymerase(Nørholm 2010; Nour-Eldin et al. 2006). The plasmids were then transformed into *S. cerevisiae* strain BJ5464 (MATα ura3-52 trp1 leu2Δ1 his3Δ200 pep4::HIS3 prb1Δ1.6R can1 GAL) (provided by the lab of Anne Robinson at Carnegie Mellon University) using the lithium-acetate/PEG method(Gietz 2014). Transformants were selected on YPD G-418 plates (1% yeast extract, 2% peptone, 2% dextrose, 2.0 mg/mL G-418).

Receptor was expressed and purified following the previously described protocol(Niebauer and Robinson 2006). In brief, from freshly streaked YPD plates (1% yeast extract, 2% peptone, 2% dextrose), single colonies were grown in 5-mL YPD cultures overnight at 30ºC. From these 5-mL cultures, 50-mL cultures were grown with a starting OD of 0.5 overnight at 30ºC. To induce expression, yeast cells from these 50-mL cultures were

centrifuged at 3,000 × g to remove YPD before resuspended in YPG medium (1% yeast, 2% peptone, 2% D-galactose) at a starting OD of 0.5. The receptor was expressed for 24 hours overnight at 30ºC with 250 r.p.m shaking. Cells were pelleted by centrifugation at 3,000 × g, washed in sterile PBS buffer, and pelleted again before storage at –80ºC until purification.

Mechanical bead lysis of cells was done, per 250 mL of cell culture, by performing 12 pulses of 60 s intense vortexing (with at least 60 s of rest in between pulses) in 10 mL 0.5-mm zirconia silica beads (BioSpec, Bartlesville, OK, USA; #11079105z), 25 mL of lysis buffer (50 mM sodium phosphate, 300 mM sodium chloride, 10% (v/v) glycerol, pH = 8.0, 2% (w/v) n-Dodecyl-β-D-maltopyranoside (DDM; Anatrace, Maumee, OH, USA; #D310), 1% (w/v) 3-[(3-Cholamidopropyl)dimethylammonio]-1-propanesulfonate (CHAPS; Anatrace; #C216), and 0.2% (w/v) cholesteryl hemisuccinate (CHS; Anatrace; #CH210) and an appropriate amount of 100x Pierce Halt EDTA-free protease inhibitor (Pierce, Rockford, IL, USA #78439)). Beads were separated using a Kontex column. Unlysed cells were removed by centrifugation at 3,220 × g for 10 min. Receptor was let solubilized on rotary mixer for 3 hours before cell debris was removed by centrifugation at 10,000 × g for 30 min. Solubilized protein was incubated with Ni-NTA resin (Pierce; #88221) overnight. Protein-resin mixture was then washed extensively in purification buffer (50 mM sodium phosphate, 300 mM sodium chloride, 10% (v/v) glycerol, 0.1% (w/v) DDM, 0.1% (w/v) CHAPS and 0.02% (w/v) CHS, pH = 8.0) containing low imidazole concentrations (20–50 mM). $A_{2A}R$ was eluted into purification buffer containing 500 mM imidazole. Prior to further chromatographic purification, imidazole was removed using a PD-10 desalting column (GE Healthcare, Pittsburgh, PA, USA; # 17085101).

Ligand affinity resin was prepared as previously described for purification of active $A_{2A}R$.(O'Malley et al. 2007), (Weiß and Grisshammer 2002) In brief, 8 mL of isopropanol-washed Affigel 10 resin (BioRad, Hercules, CA, USA; #1536099) was mixed gently in an Erlenmeyer flask for 20 h at room temperature with 48 mL of DMSO containing 24 mg of xanthine amine congener (XAC, high-affinity $A_{2A}R$ antagonist, K_D = 32 nM; Sigma, St. Louis, MO, USA; #X103). The absorbance at 310 nm of the XAC-DMSO solution before and after the coupling reaction was measured in 10 mM HCl and compared to a standard curve. The amount of resin bound to ligand was estimated to be 5.6 μM. The coupling reaction was quenched by washing the resin with DMSO, then with Tris-HCl 50 mM (pH = 7.4), then with 20% (v/v) ethanol. The resin was packed into a Tricorn 10/50 column (GE Healthcare) under pressure via a BioRad Duoflow FPLC (BioRad).

For purification of active $A_{2A}R$, the column was equilibrated with 4 CV of purification buffer. The IMAC-purified $A_{2A}R$ was desalted and diluted to 5.5 mL before applied to a 5-mL sample loop on the BioRad Duoflow FPLC, from which the sample was loaded onto the column at a rate of 0.1 mL/min. Inactive $A_{2A}R$ was washed from the column by flowing 10 mL of purification buffer at 0.2 mL/min, followed by 16 mL at 0.4 mL/min. Active $A_{2A}R$ was eluted from the column by flowing purification buffer containing 20 mM theophylline (low-affinity $A_{2A}R$ antagonist, K_D = 1.6 μM; Sigma; #T1633). Western blot analysis was performed to determine 4-mL fractions with active $A_{2A}R$ collected with a BioFrac fraction collector (BioRad), which were then concentrated through a 30-kDa MWCO centrifugal filter (Millipore, Billerica, MA, USA; # UFC803096) and desalted to remove excess theophylline. For the experiments where the salt concentrations were varied, the buffer exchange was done also by this last desalting step.

2.2.3. Size-Exclusion Chromatography

To separate oligomeric species of active $A_{2A}R$, a prepacked Tricorn Superdex 200 10/300 GL column (GE Healthcare; #17-5175-01) connected to a BioRad Duoflow FPLC was equilibrated with 60 mL of running buffer (150 mM sodium chloride except for the ionic strength experiments where NaCl concentration is adjusted to achieve the desired ionic strengths, 50 mM sodium phosphate, 10% (v/v) glycerol, 0.1% (w/v) DDM, 0.1% (w/v) CHAPS, 0.02% (w/v) CHS, pH = 8.0) at a flow rate of 0.2 mL/min. 0.5-mL fractions were collected with a BioFrac fraction collector in 30 mL of running buffer at the same flow rate. The subsequent SEC analysis performed on the SEC-separated oligomeric populations also followed this protocol.

2.2.4. SEC Peak Analysis

SEC chromatograms were analyzed using OriginLab using the nonlinear curve fit (Gaussian) function. The area under the curve and the peak width were manually defined in cases where the SNR of the SEC trace were too low. The R^2 values reached > 0.96 for most cases. The population of each oligomeric species was expressed as the integral of each Gaussian this curve fit of the SEC signal. The HMW oligomer peak in some cases could not be fitted with one curve and thus was fitted with two curves instead. The reported standard errors were calculated from the variance of the fit and did not correspond to experimental errors. The results are detailed in **Figure 2-5** and **Table 2-1**.

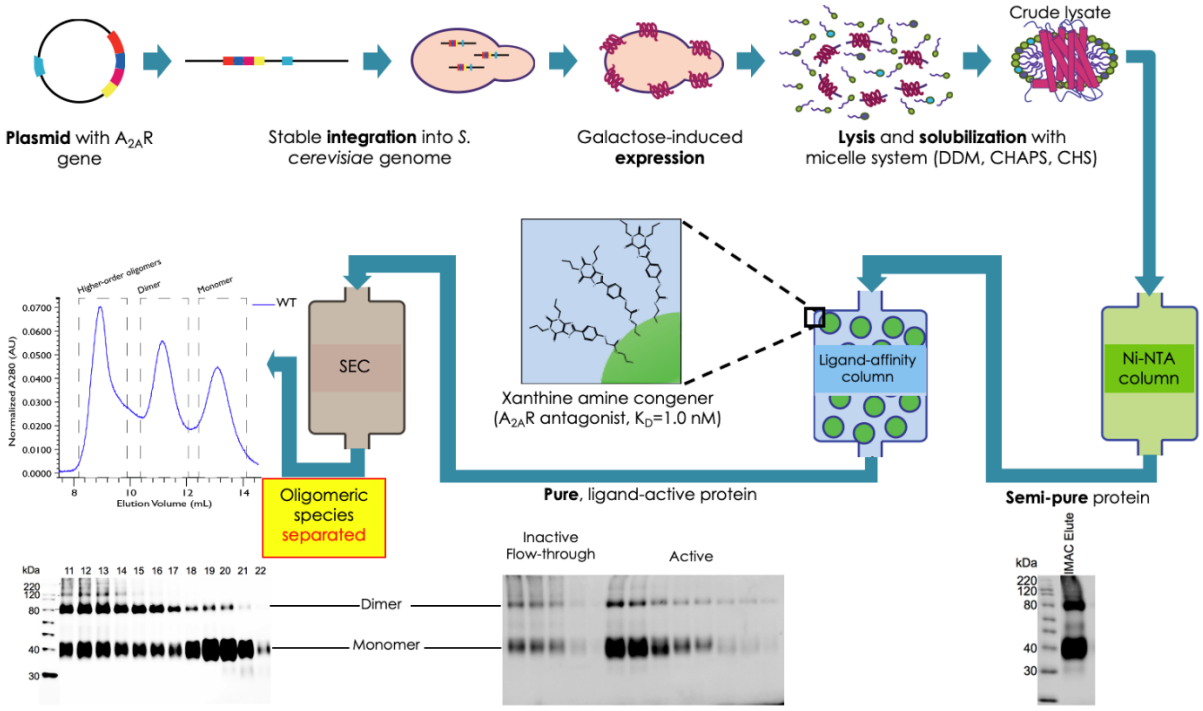

Figure 2-2. Visual summary of the entire process of cloning, expression, purification, and separation of $A_{2A}R$ oligomeric species. Plasmids containing the $A_{2A}R$ gene is linearized with BsaBI, then transformed into the genome of *S. cerevisiae*. Protein expression is induced with galactose-containing media. Cells are then harvested with centrifugation, lysed with mechanical beads, and solubilized in an optimized system of detergent micelles containing DDM, CHAPS, and CHS. IMAC with Ni-NTA resin is used to obtain a semi-pure mixture of $A_{2A}R$, which is then subjected to ligand-affinity chromatography with a high-affinity antagonist (XAC) to select for ligand-active receptor. Finally, the various oligomeric species of $A_{2A}R$ is separated and isolated with SEC for further biophysical characterization. (Figure courtesy of Dr. Nicole S. Schonenbach.)

2.2.5. SDS-PAGE and Western Blotting

10% SDS-PAGE gels were hand-casted in BioRad Criterion empty cassettes (BioRad; #3459902, 3459903). Lysate controls were prepared by lysis of 5 OD cell pellets with 35 μL of YPER (Fisher Scientific, Waltham, MA, USA # 8990) at RT for 20 min, incubation with 2x Laemmli buffer (4% (w/v) SDS, 16% (v/v) glycerol, 0.02% (w/v) bromophenol blue, 167 M

Tris, pH 6.8) at 37ºC for 1 h, and centrifugation at 3,000 × g for 1 min to pellet cell debris. Protein samples were prepared by incubation with 2x Laemmli buffer at 37ºC for 30 min. For all samples, 14 μL (for 26-well gel) or 20 μL (for 18-well gel) was loaded per lane, except for 7 μL of Magic Mark XP Western protein ladder (Thermo Scientific, Waltham, MA, USA; #LC5602) as a standard. Electrophoresis was carried out at 120 V for 100 min. Proteins were transferred to 0.2-μm nitrocellulose membranes (BioRad; # 170-4159) via electroblotting using a BioRad Transblot Turbo, mixed MW protocol. Membranes were blocked in Tris-buffered saline with Tween (TBST; 150 mM sodium chloride, 15.2 mM Tris-HCl, 4.6 mM Tris base, pH = 7.4, 0.1% (v/v) Tween 20 (BioRad; #1706531)) containing 5% (w/v) dry milk, then probed with anti-$A_{2A}R$ antibody, clone 7F6-G5-A2, mouse monoclonal (Millipore, Burlington, MA, USA; #05-717) at 1:500 in TBST with 0.5% (w/v) dry milk. Probing with secondary antibody was done with a fluorescent anti-mouse IgG H&L DyLight 550 antibody (Abcam, Cambridge, MA, USA; #ab96880) at 1:600 in TBST containing 0.5% (w/v) milk.

Western blot was analyzed with Image Lab 6.1 software (Bio-rad), with built-in tool to define each sample lane and to generate an intensity profile. Peaks were manually selected and integrated with the measure tool to determine the amount of protein present.

2.2.6. Confocal Microscopy

Yeast cells expressing fluorescently tagged $A_{2A}R$ were cultured for confocal imaging following the same protocol as above, but only induced into 5 mL of YPG. After 20 hours of expression, enough cells for an OD of 1 in 1 mL were pelleted at 4,000 × g and resuspended in 1 mL sterile phosphate buffer saline (PBS) (137 mM sodium chloride, 2.7 mM potassium chloride, 10 mM sodium phosphate, 1.8 mM potassium phosphate). Samples of diluted cell

slurry (250 μL) were aliquoted onto chambered slides (Labtek) pre-coated with poly-L-lysine and allowed to settle for 10 minutes at room temperature. Confocal images of GFP-tagged $A_{2A}R$ variants were collected on an Olympus Fluoview 1000 Spectral Confocal at the NRI-MCDB Microscopy Facility at UC Santa Barbara, using a 10-mW argon laser at 488 nm excitation and detected with a 530 nm filter under a 60x objective.

2.2.7. Coarse-Grained MD Simulations

Initial configuration of $A_{2A}R$ was based on the crystal structure of the receptor in the active state (PDB 5G53). Since this structure does not include the entire C-terminus, we resorted to using homology modeling software (*i.e.*, MODELLER 9.23) (Eswar et al. 2006) to predict the structures of the C-terminus. After removing all non-receptor components, the first segment of the C-terminus consisting of residues 291–314 were modeled as a helical segment parallel to the cytoplasmic membrane surface while the rest of the C-terminus was modeled as intrinsically disordered. MODELLER is much more accurate in structural predictions for segments less than 20 residues. This limitation necessitated that we run an equilibrium MD simulation for 2 μs to obtain a well equilibrated structure that possesses a more viable starting conformation. To validate our models of all potential variants of $A_{2A}R$, we calculated the RMSD and RMSF for each respective system. Default protonation states of ionizable residues were used. The resulting structure was converted to MARTINI coarse-grained topology using the martinize.py script(de Jong et al. 2013). The ELNeDyn elastic network(Periole et al. 2009) was used to constrain protein secondary and tertiary structures with a force constant of 500 kJ/mol/nm^2 and a cutoff of 1.5 nm. To optimize loop refinement of the model, a single copy was embedded in a 1-palmitoyl-2-oleoyl-sn-glycero-3-phosphocholine (POPC) bilayer using

the insane.py script, solvated with MARTINI polarizable water, neutralized with 0.15 M NaCl, and a short MD (1.5 μs) run to equilibrate the loop regions. Subsequently, two monomers of the equilibrated $A_{2A}R$ were randomly rotated and placed at the center of a 13 nm × 13 nm × 11 nm (xyz) box, 3.5 nm apart, with their principal transmembrane axis aligned parallel to the z axis. The proteins were then embedded in a POPC bilayer using the insane.py script. Sodium and chloride ions were added to neutralize the system and obtain a concentration of 0.15 M NaCl. Total system size was typically in the range of 34,000 CG particles, with a 280:1 lipid:protein ratio. Ten independent copies were generated for each $A_{2A}R$ truncated variant.

v2.2 of the MARTINI coarse-grained force field(Monticelli et al. 2008) was used for the protein and water, and v2.0 was used for POPC. All coarse-grained simulations were carried out in GROMACS 2016(Abraham et al. 2015) in the NPT ensemble (P = 1 atm, T = 310 K). The Bussi velocity rescaling thermostat was used for temperature control with a coupling constant of τ_t = 1.0 ps(Bussi, Donadio, and Parrinello 2007), while the Parrinello-Rahman barostat(Martoňák, Laio, and Parrinello 2003) was used to control the pressure semi-isotropically with a coupling constant of τ_t = 12.0 ps and compressibility of 3 x 10^{-4} bar^{-1}. Reaction field electrostatics was used with Coulomb cut-off of 1.1 nm. Non-bonded Lennard-Jones interactions were treated with a cut-off of 1.1 nm. All simulations were run with a 15 fs timestep, updating neighbor lists every 10 steps. Cubic periodic boundary conditions along the x, y and z axes were used. Each simulation was run for 8 μs.

2.2.8. Atomistic MD Simulations

Three snapshots of symmetric dimers of $A_{2A}R$ for each respective truncated variant were randomly selected from the CG simulations as starting structures for backmapping. Coarse-grained systems were converted to atomistic resolution using the backward.py script(Wassenaar et al. 2014). All simulations were run in Gromacs2019 in the *NPT* ensemble (P = 1 bar, T = 310 K) with all bonds restrained using the LINCS method(Hess et al. 1997). The Parrinello-Rahman barostat was used to control the pressure semi-isotropically with a coupling constant of τ_t = 1.0 ps and a compressibility of 4.5 x 10^{-5} bar^{-1}, while the Bussi velocity rescaling thermostat was used for temperature control with a coupling constant of τ_t = 0.1 ps. Proteins, lipids, and solvents were separately coupled to the thermostat. The CHARMM36 and TIP3P force fields(Best et al. 2012; Jorgensen et al. 1983) were used to model all molecular interactions. Periodic boundary conditions were set in the x, y, and z directions. Particle mesh Ewald (PME) electrostatics was used with a cut-off of 1.0 nm. A 2-fs time step was used for all atomistic runs, and each simulation was run for 50 ns.

2.2.9. Analysis of Computational Results

All trajectories were post-processed using gromacs tools and in-house scripts. We ran a clustering analysis of all dimer frames from the CG simulations using Daura et. al.'s clustering algorithm(Daura et al. 1999) implemented in GROMACS, with an RMSD cutoff of 1.5 Å. An interface was considered dimeric if the minimum center of mass distance between the protomers was less than 5 Å. This method uses an RMSD cutoff to group all conformations with the largest number of neighbors into a cluster and eliminates these from the pool, then repeats the process until the pool is empty. We focused our analysis on the most populated

cluster from each truncated variant. Electrostatic interactions in the dimer were calculated from CG systems with LOOS(Romo and Grossfield 2009) using a distance cutoff of 5.0 Å. Transmembrane helical tilt angles were also calculated in LOOS from CG simulations. Hydrogen bonds were calculated from AA simulations using the hydrogen bonds plugin in VMD(Humphrey, Dalke, and Schulten 1996), with a distance cutoff of 3.5 Å and an angle cutoff of 20º. Only C-terminal residues were included in hydrogen bond analysis. PyMOL(*The PyMOL Molecular Graphics System, Version 2.0 Schrödinger, LLC.*, n.d.) was used for molecular visualizations.

2.2.10. Assessing $A_{2A}R$ Oligomerization with Increasing Ionic Strength

Na_2HPO_4 and NaH_2PO_4 in the buffer make up an ionic strength of 0.15 M, to which NaCl was added to increase the ionic strength to 0.45 M and furthermore to 0.95 M. The $A_{2A}R$ variants were purified at 0.45 M ionic strength and then exchanged into buffers of different ionic strengths using a PD-10 desalting column prior to subjecting the samples to SEC. The buffer composition is detailed below.

Buffers	***Components***	***Conc. (mM)***	***Ionic Strength (mM)***
0.15 M Ionic Strength	**NaCl**	**0**	**0**
	NaH_2PO_4	4	4
	Na_2HPO_4	49	146
0.45 M Ionic Strength	**NaCl**	**300**	**300**
	NaH_2PO_4	4	4
	Na_2HPO_4	49	146
0.95 M Ionic Strength	**NaCl**	**800**	**800**
	NaH_2PO_4	4	4
	Na_2HPO_4	49	146

2.2.11. Isolated C-Terminus Purification

Escherichia coli BL21 (DE3) cells (Sigma; #CMC0014) were transfected with pET28a DNA plasmids containing the desired $A_{2A}R$ sequence with a 6x His tag attached for purification. Cells from glycerol stock were grown in 10 mL luria broth (LB, Sigma Aldrich, L3022) overnight at 37°C and then used to inoculate 1 L of fresh LB and 10 μg/mL kanamycin (Fisher Scientific, BP906). Growth of cells were performed at 37°C, 200 rpm until optical density at λ = 600 nm reached 0.6–0.8. Expression was induced by incubation with 1 mM isopropyl-β-D-thiogalactoside (Fisher Bioreagents, BP175510) for 3 hrs.

Cells were harvested with centrifugation at 5000 rpm for 30 min. Harvested cells were resuspended in 25 mL Tris-HCl, pH = 7.4, 100 mM NaCl, 0.5 mM DTT, 0.1 mM EDTA with 1 Pierce protease inhibitor tablet (Thermo Scientific, A32965), 1 mM PMSF, 2 mg/mL lysozyme, 20 μg/mL DNase (Sigma, DN25) and 10 mM $MgCl_2$, and incubated on ice for 30 min. Samples were then incubated at 30ºC for 20 minutes, then flash frozen and thawed 3 times in LN_2. Samples were then centrifuged at 10,000 rpm for 10 min to remove cell debris. 1 mM PMSF was added again, and the resulting supernatant was incubated while rotating for at least 4 hrs with Ni-NTA resin. The resin was loaded to a column and washed with 25 mL 20 mM sodium phosphate, pH = 7.0, 1 M NaCl, 20 mM imidazole, 0.5 mM DTT, 100 μM EDTA. Purified protein was eluted with 15 mL of 20 mM sodium phosphate, pH = 7.0, 0.5 mM DTT, 100 mM NaCl, 300 mM imidazole. The protein was concentrated to a volume of 2.5mL and was buffer exchanged into 20 mM ammonium acetate buffer, pH = 7.4, 100 mM NaCl using a GE PD-10 desalting column. Purity of sample was confirmed with SDS-PAGE and western blot.

2.2.12. Aggregation Assay to Assess $A_{2A}R$ C-Terminus Assembly

Absorbance was measured at 450 nm using a Shimadzu UV-1601 spectrophotometer with 120 μL sample size. Prior to reading, samples were incubated at 40°C for 5 minutes. Samples were vigorously pipetted to homogenize any precipitate before absorbance was measured. Protein concentration was 50 μM in a 20 mM ammonium acetate buffer (pH = 7.4).

2.2.13. Differential Scanning Fluorimetry

DSF was conducted with a Bio-rad CFX90 real-time PCR machine. A starting temperature 20ºC was increased at a rate of 0.5ºC per 30 seconds to a final temperature of 85ºC. All samples contained 40 μL of 40 μM $A_{2A}R$ C-terminus, 9x SYPRO orange (ThermoFisher S6650), 200 mM NaCl, and 20 mM MES. Fluorescence was detected in real-time at 570 nm. All samples were conducted in triplicate.

2.2.14. Hydrophobicity and Charge Profile of C-Terminus

The hydrophobicity profile reported in **Figure 2-13** was determined with ProtScale using method described by Kyte & Doolittle(Kyte and Doolittle 1982), window size of 3.

2.3. RESULTS

This study systematically investigates the role of the C-terminus on $A_{2A}R$ oligomerization and the nature of the involved interactions through strategic mutations and truncations at the C-terminus as well as modulation of the ionic strength of solvent. All experiments were done at 4°C unless stated otherwise. The experimental assessment of $A_{2A}R$ oligomerization relies on size-exclusion chromatography (SEC) analysis.

2.3.1. SEC Quantifies $A_{2A}R$ Oligomerization

We performed SEC analysis on a mixture of ligand-active $A_{2A}R$ purified from a custom synthesized antagonist affinity column (**Figure 2-3A**). Distinct oligomeric species were separated and eluted in the following order: high-molecular-weight (HMW) oligomer, dimer, and monomer (**Figure 2-4** and **Figure 2-3B**). This peak assignment has been verified with SEC-MALS (multi-angle light scattering) experiments, as detailed in a previous publication(Schonenbach et al. 2016). The population of each oligomeric species was quantified as the integral of each Gaussian from a multiple-Gaussian curve fit of the SEC signal. The reported standard errors were calculated from the variance of the fit that do not correspond to experimental errors (see **Table 2-1** and **Figure 2-5** for SEC data corresponding to all $A_{2A}R$ variants in this study). As this study sought to identify the factors that promote $A_{2A}R$ oligomerization, the populations with oligomeric interfaces (*i.e.*, dimer and HMW oligomer) were compared with those without such interfaces (*i.e.*, monomer). Hence, the populations of the HMW oligomer and dimer were expressed relative to the monomer population in arbitrary units as monomer-equivalent concentration ratios, henceforth referred to as population levels (**Figure 2-4**).

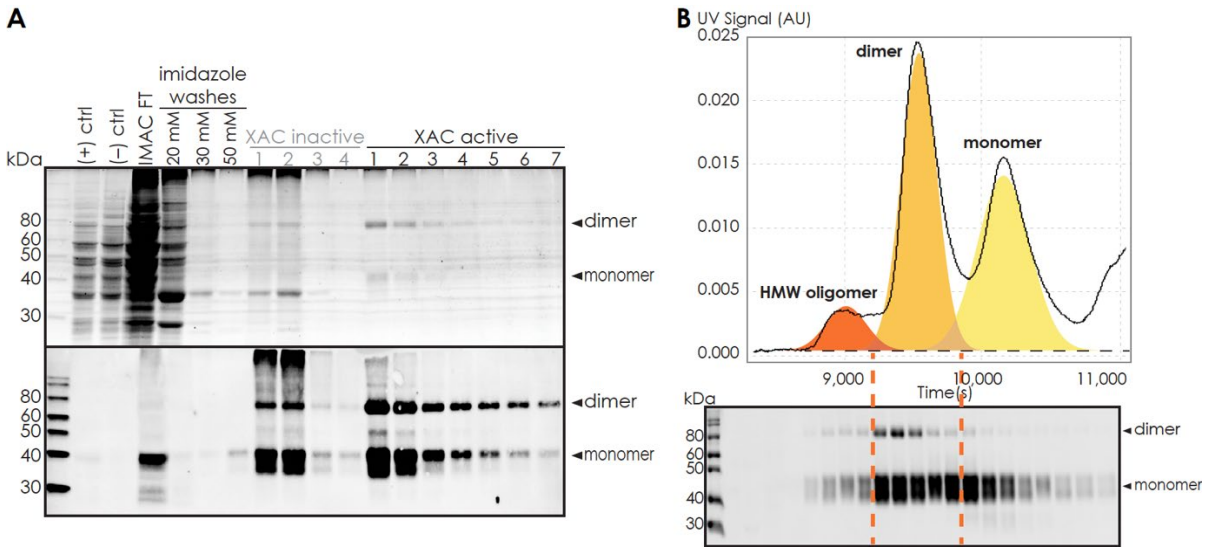

Figure 2-3. (A) Representative total protein stain (upper panel) and western blot (lower panel) of A2AR-WT during purification. Positive ((+) ctrl) and negative ((–) ctrl) controls consist of 5 OD cell lysate of *S. cerevisiae* BJ5464 cells expressing and not expressing $A_{2A}R$ WT, respectively. "IMAC FT" indicates the flow-through from IMAC step. "XAC inactive" and "XAC active" indicate the fractions that do not and do bind to XAC during the ligand-affinity chromatography step. **(B)** Representative western blot of $A_{2A}R$-WT during SEC separation. The fractions are matched to the distinct oligomeric peaks in the SEC chromatogram. Each lane on the blot is from 0.5 mL fractions eluted from a Superdex 200 10/300 GL (GE Healthcare) column. MagicMark protein ladder (LC5602) is used as the molecular weight standard.

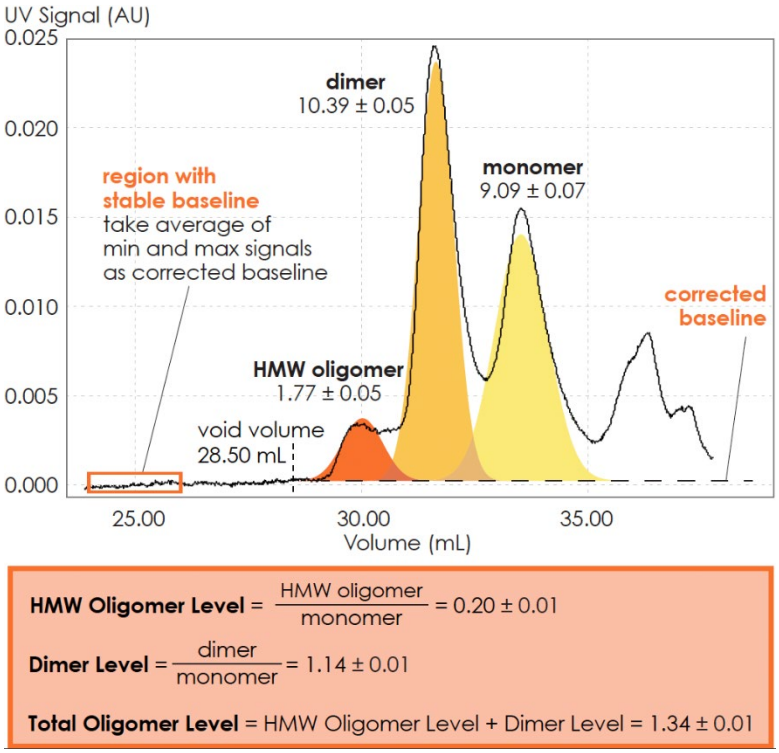

Figure 2-4. Method for collecting SEC data and assessing $A_{2A}R$ oligomerization. The SEC data is recorded every second as absorbance at 280 nm. The baseline is corrected to ensure uniform fitting and integration across the peaks. The areas under the curve, resulting from a multiple-Gaussian curve fit, express the population of each oligomeric species. The reported standard errors of integration are within a 95% confidence interval and are calculated from the variance of the fit, not experimental errors. The levels of HMW oligomer and dimer are expressed relative to the monomeric population in arbitrary units. A representative calculation defining the oligomer levels is given in the box.

Table 2-1. Results from curve fitting using OriginLab and calculations of the HMW oligomer and dimer levels for all $A_{2A}R$ variants used in the main text of this study. The variants are grouped by the order they appear and numbered corresponding to **Figure 2-5**. The levels of dimer and HMW oligomer are expressed relative to the monomeric population in arbitrary units as monomer-equivalent concentration ratios. The errors are calculated from the variance of the fit, not experimental variations, and are within 95% confidence interval. Only the WT replicates are represented with standard deviation as experimental variations (last row; n = 5; mean ± SD).

Fig	Variants	No.	HMW Oligomer Level	Dimer Level	Total Oligomer Level	[HMW Oligomer]	[Dimer]	[Monomer]
2-6A	WT	1	0.20 ± 0.01	1.14 ± 0.01	1.34 ± 0.01	1.77 ± 0.05	10.39 ± 0.05	9.09 ± 0.07
	C394S	2	0.28 ± 0.06	0.57 ± 0.01	0.85 ± 0.06	1.66 ± 0.35	3.36 ± 0.07	5.90 ± 0.06
	C394A	3	0.31 ± 0.08	0.28 ± 0.06	0.59 ± 0.10	0.49 ± 0.11	0.44 ± 0.10	1.57 ± 0.08
	C394L	4	0.78 ± 0.01	0.43 ± 0.01	1.21 ± 0.01	9.09 ± 0.13	5.07 ± 0.07	11.73 ± 0.09
	C394M	5	0.50 ± 0.08	0.38 ± 0.03	0.88 ± 0.09	2.70 ± 0.42	2.05 ± 0.18	5.44 ± 0.05
	C394V	6	0.64 ± 0.01	0.23 ± 0.01	0.88 ± 0.01	9.94 ± 0.13	3.65 ± 0.06	15.44 ± 0.07
2-8B	WT	1	0.20 ± 0.01	1.14 ± 0.01	1.34 ± 0.01	1.77 ± 0.05	10.39 ± 0.05	9.09 ± 0.07
	P395ΔC	7	0.58 ± 0.01	1.15 ± 0.01	1.73 ± 0.02	3.34 ± 0.05	6.69 ± 0.05	5.80 ± 0.06
	Q372ΔC	8	0.22 ± 0.01	0.65 ± 0.01	0.87 ± 0.01	1.64 ± 0.05	4.95 ± 0.05	7.59 ± 0.06
	N359ΔC	9	0.28 ± 0.01	0.81 ± 0.01	1.09 ± 0.01	2.31 ± 0.06	6.72 ± 0.05	8.30 ± 0.06
	P354ΔC	10	0.42 ± 0.01	0.19 ± 0.01	0.62 ± 0.02	2.17 ± 0.05	0.99 ± 0.05	5.12 ± 0.05
	G349ΔC	11	0.48 ± 0.02	0.09 ± 0.01	0.58 ± 0.02	2.23 ± 0.07	0.42 ± 0.06	4.60 ± 0.03
	G344ΔC	12	0.44 ± 0.10	0.06 ± 0.06	0.50 ± 0.12	0.80 ± 0.18	0.11 ± 0.11	1.81 ± 0.04
	V334ΔC	13	0.04 ± 0.01	0.10 ± 0.01	0.14 ± 0.01	0.29 ± 0.06	0.83 ± 0.06	8.23 ± 0.06
	A316ΔC	14	0.03 ± 0.01	0.03 ± 0.01	0.06 ± 0.01	0.08 ± 0.02	0.08 ± 0.02	2.89 ± 0.02
2-8C	WT	15	0.88 ± 0.04	0.49 ± 0.01	1.37 ± 0.01	5.37 ± 0.22	2.98 ± 0.07	6.10 ± 0.04
	WT-ERRAAA	16	0.66 ± 0.03	0.29 ± 0.01	0.95 ± 0.03	3.76 ± 0.16	1.64 ± 0.08	5.72 ± 0.07
	N359ΔC	17	0.68 ± 0.04	0.33 ± 0.03	1.01 ± 0.05	1.10 ± 0.06	0.53 ± 0.04	1.61 ± 0.04
	N359ΔC-ERRAAA	18	0.38 ± 0.03	0.48 ± 0.02	0.85 ± 0.04	1.05 ± 0.08	1.32 ± 0.06	2.78 ± 0.05
2-10	WT 0.15 M	19	0.07 ± 0.01	0.09 ± 0.01	0.16 ± 0.02	0.19 ± 0.04	0.27 ± 0.04	2.87 ± 0.04
	WT 0.45 M	15	0.88 ± 0.04	0.49 ± 0.01	1.37 ± 0.04	5.37 ± 0.22	2.98 ± 0.07	6.10 ± 0.04
	WT 0.95 M	20	2.20 ± 0.04	1.31 ± 0.02	3.51 ± 0.05	14.54 ± 0.25	8.62 ± 0.11	6.60 ± 0.06
	WT-ERRAAA 0.15 M	21	0.17 ± 0.05	0.02 ± 0.01	0.19 ± 0.05	0.62 ± 0.17	0.07 ± 0.01	3.73 ± 0.03
	WT-ERRAAA 0.45 M	16	0.47 ± 0.08	0.45 ± 0.04	0.92 ± 0.09	2.55 ± 0.45	2.45 ± 0.23	5.45 ± 0.07

	WT-ERRAAA 0.95 M	22	1.20 ± 0.03	0.38 ± 0.01	1.58 ± 0.03	7.41 ± 0.18	2.37 ± 0.08	6.21 ± 0.04
	N359ΔC 0.15 M	23	0.11 ± 0.01	0.11 ± 0.01	0.21 ± 0.02	0.72 ± 0.08	0.71 ± 0.08	6.67 ± 0.07
	N359ΔC 0.45 M	17	0.68 ± 0.04	0.33 ± 0.03	1.01 ± 0.05	1.10 ± 0.06	0.53 ± 0.04	1.61 ± 0.04
	N359ΔC 0.95 M	24	0.04 ± 0.01	0.04 ± 0.01	0.09 ± 0.01	0.51 ± 0.05	0.59 ± 0.05	11.90 ± 0.06
	V334ΔC 0.15 M	25	0.13 ± 0.01	0.08 ± 0.01	0.21 ± 0.01	0.65 ± 0.04	0.41 ± 0.03	5.03 ± 0.03
	V334ΔC 0.45 M	13	0.04 ± 0.01	0.10 ± 0.01	0.14 ± 0.01	0.29 ± 0.06	0.83 ± 0.06	8.23 ± 0.06
	V334ΔC 0.95 M	26	0.09 ± 0.02	0.15 ± 0.04	0.23 ± 0.01	0.85 ± 0.19	1.41 ± 0.34	9.68 ± 0.27
WT Replicates (with Variations from the Fit)			1.16 ± 0.05	0.65 ± 0.03	1.81 ± 0.06	9.45 ± 0.39	5.34 ± 0.20	8.16 ± 0.04
			0.98 ± 0.03	0.57 ± 0.01	1.56 ± 0.04	6.44 ± 0.20	3.76 ± 0.09	6.55 ± 0.04
			1.48 ± 0.05	0.57 ± 0.01	2.05 ± 0.05	12.02 ± 0.35	4.66 ± 0.06	8.12 ± 0.05
			0.20 ± 0.01	1.14 ± 0.01	1.34 ± 0.01	1.77 ± 0.05	10.39 ± 0.05	9.09 ± 0.07
			0.88 ± 0.04	0.49 ± 0.01	1.37 ± 0.04	5.37 ± 0.22	2.98 ± 0.07	6.10 ± 0.04
WT Replicates (with Experimental Variations: Mean ± SD; n = 5)			0.94 ± 0.47	0.68 ± 0.26	1.63 ± 0.30	7.01 ± 3.92	5.42 ± 2.92	7.60 ± 1.24

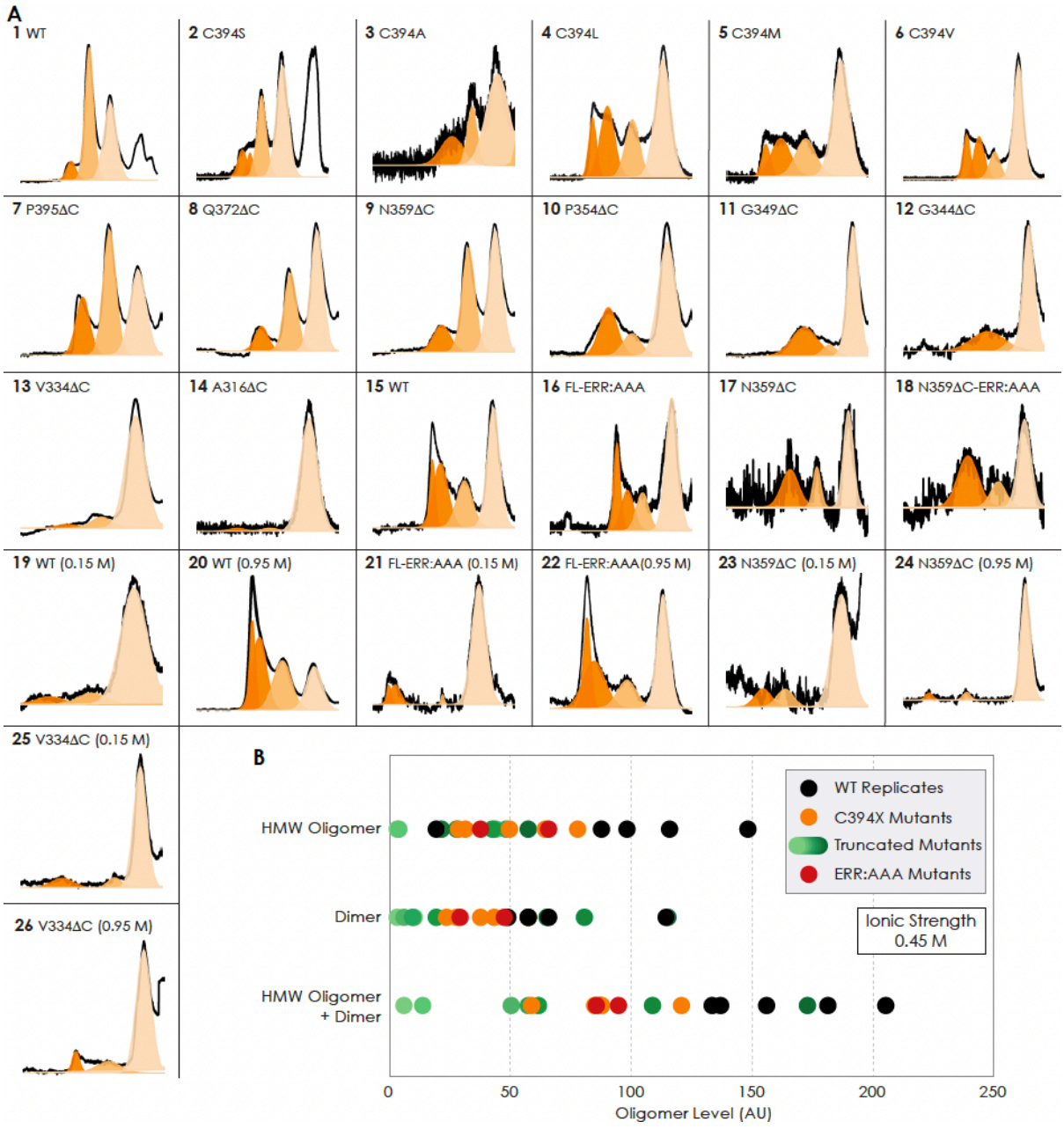

Figure 2-5. (A) Curve fitting using OriginLab of all $A_{2A}R$ variants used in the main text of this study, listed by the order they appear. By default, each oligomeric peak is fitted with one curve using Gaussian distribution and displayed by different color shades, with the HMW oligomer eluted first (dark orange), followed by the dimer (lighter orange), followed by the monomer (lightest orange). However, the HMW oligomer peak in some cases cannot be fitted with one curve and thus is fitted with two curves instead. This discrepancy can be explained by variation in HMW oligomerization order among the variants. The identity of each peak is confirmed with western

blotting. The value and error from the curve fitting of each peak are given in **Table 2-1**. **(B)** Data distribution of all variants used in this study in comparison to five experimental replicates of A_{2A}R-WT. The C-terminally truncated mutants are represented by different shades of green in increasing darkness corresponding to the increased length of the C-terminus, with the lightest shade representing the mutant with the shortest C-terminus (A316ΔC) and the darkest shade for the mutant with the longest C-terminus (P395ΔC). The levels of dimer and HMW oligomer are expressed relative to the monomeric population in arbitrary unit, with reported errors calculated from the variance of the fit, not experimental variation. There are significant variations in the dimer and HMW oligomer levels among the WT replicates, stemming from experimental errors. These variations are mitigated when the two parameters are added, as the data distribution becomes more uniform. Also, the oligomerization levels of the WT replicates are consistently higher than the mutated and truncated variants.

2.3.2. C-Terminal Amino Acid Residue C394 Contributes to $A_{2A}R$ Oligomerization

To investigate whether the C-terminus of $A_{2A}R$ is involved in receptor oligomerization, we first examined the role of residue C394, as a previous study demonstrated that the mutation C394S dramatically reduced $A_{2A}R$ oligomer levels(Schonenbach et al. 2016). The C394S mutation was replicated in our experiments, alongside other amino acid substitutions for the cysteine, namely alanine, leucine, methionine, or valine, generating five $A_{2A}R$-C394X variants. The HMW oligomer and dimer levels of $A_{2A}R$ wild-type (WT) were compared with those of the $A_{2A}R$-C394X variants. We found that the dimer level of $A_{2A}R$-WT was significantly higher than that of the $A_{2A}R$-C394X variants (WT: 1.14; C394X: 0.24–0.57; **Figure 2-6A**). A similar result, though less pronounced, was observed when the HMW oligomer and dimer levels were considered together (WT: 1.34; C394X: 0.59–1.21; **Figure 2-6A**). This suggests that residue C394 plays a role in $A_{2A}R$ oligomerization, and even more prominently in $A_{2A}R$ dimerization.

To test whether residue C394 stabilizes $A_{2A}R$ dimerization by forming disulfide linkages, we incubated the SEC-separated dimers of $A_{2A}R$-WT and $A_{2A}R$-Q372ΔC with 5 mM of the reducing agent TCEP, followed by SDS-PAGE and Western Blotting. The population of each species was determined as the area under the densitometric trace. The dimer level was then expressed as monomer-equivalent concentration ratios in a manner similar to that of the SEC experiment described above. Upon incubation with TCEP, the dimer level of the $A_{2A}R$-WT sample decreased from 1.14 to 0.51 (**Figure 2-6B**). This indicates that disulfide bond formation via residue C394 is one possible mechanism for $A_{2A}R$ dimerization. Interestingly, the dimer level of the $A_{2A}R$-Q372ΔC sample also decreased from 0.68 to 0.22 (**Figure 2-6B**). This suggests that there may exist other inter-$A_{2A}R$ disulfide bonds that do not involve residue

C394. Still, in both cases, a clearly visible population of $A_{2A}R$ dimer persists, even after reduction of disulfide bonds via TCEP (**Figure 2-6B**), suggesting that there must be additional interfacial sites that help drive $A_{2A}R$ dimer/oligomerization.

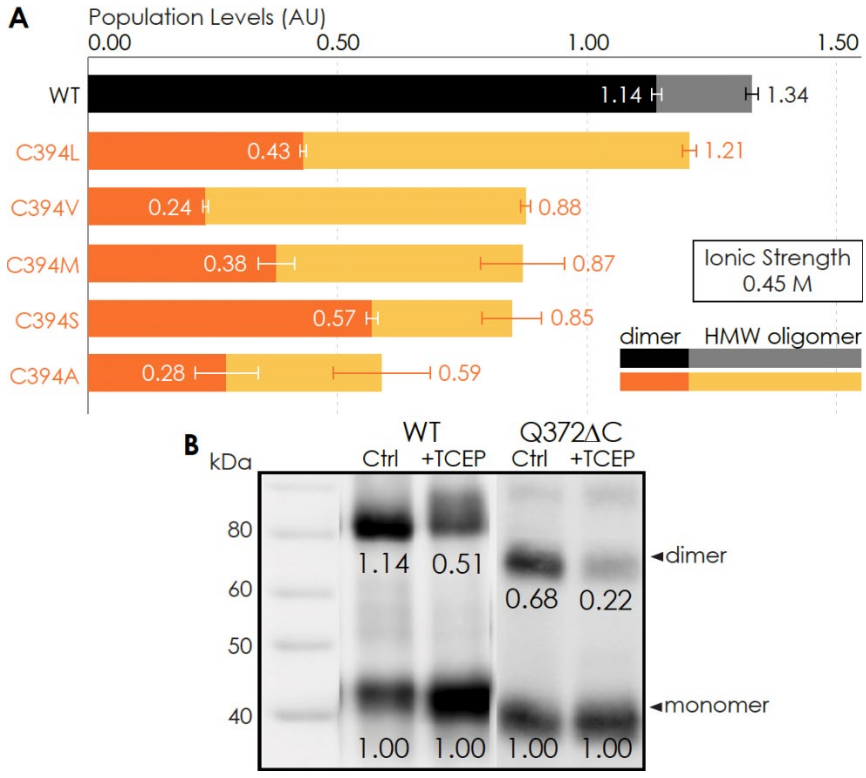

Figure 2-6. Residue C394 helps stabilize $A_{2A}R$ oligomerization via disulfide bonds. **(A)** The effect of C394X substitutions on $A_{2A}R$ oligomerization. The levels of dimer (dark colors) and HMW oligomer (light colors) are expressed relative to the monomeric population in arbitrary units, with reported errors calculated from the variance of the fit, not experimental variation. **(B)** Line densitometry of Western Blot bands on SEC-separated dimeric populations of $A_{2A}R$-WT and Q372ΔC with and without 5 mM TCEP. The level of dimer is expressed relative to the monomeric population in arbitrary units similarly to the SEC analysis. MagicMark protein ladder (LC5602) is used as the molecular weight standard.

2.3.3. C-Terminus Truncation Systematically Reduces $A_{2A}R$ Oligomerization

To determine which interfacial sites in the C-terminus other than the disulfide-bonded cysteines drive $A_{2A}R$ dimer/oligomerization, we carried out systematic truncations at eight sites along the C-terminus (A316, V334, G344, G349, P354, N359, Q372, and P395), generating eight $A_{2A}R$-ΔC variants (**Figure 2-8A**). The $A_{2A}R$-A316ΔC variant corresponds to the removal of the entire disordered C-terminal region and is used in all published structural studies of $A_{2A}R$ (Martynowycz et al. 2020; Song, Duncan, and Sansom 2020; Garcıa-Nafrıa et al. 2018; Sun et al. 2017; Carpenter et al. 2016; Hino et al. 2012; Xu et al. 2011; Lebon et al. 2011; Doré et al. 2011; V.-P. Jaakola et al. 2008; Fanelli and Felline 2011). Confocal microscopy revealed that the largest truncations at sites A316 and V334 did not affect membrane localization of the receptor compared with $A_{2A}R$-WT (**Figure 2-7**).

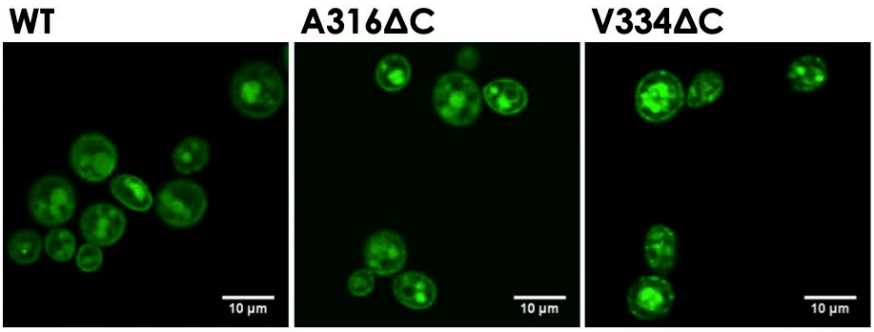

Figure 2-7. Truncation of the C-terminus does not affect membrane localization of $A_{2A}R$. Confocal microscopy images of *S. cerevisiae* cells expressing $A_{2A}R$ WT, A316ΔC, and V334ΔC tagged with a C-terminal green fluorescent protein trafficking to the plasma membrane.

Using the SEC analysis described earlier (**2.3.1 above**), we evaluated the HMW oligomer and dimer levels of the $A_{2A}R$-ΔC variants relative to that of the $A_{2A}R$ full-length-wild-type (FL-WT) control. Both the dimer and the total oligomer levels of $A_{2A}R$ decreased progressively with the shortening of the C-terminus, with almost no oligomerization detected upon complete truncation of the C-terminus at site A316 (**Figure 2-8B**). This result shows that the C-terminus drives $A_{2A}R$ oligomerization, with multiple potential interaction sites positioned along its length.

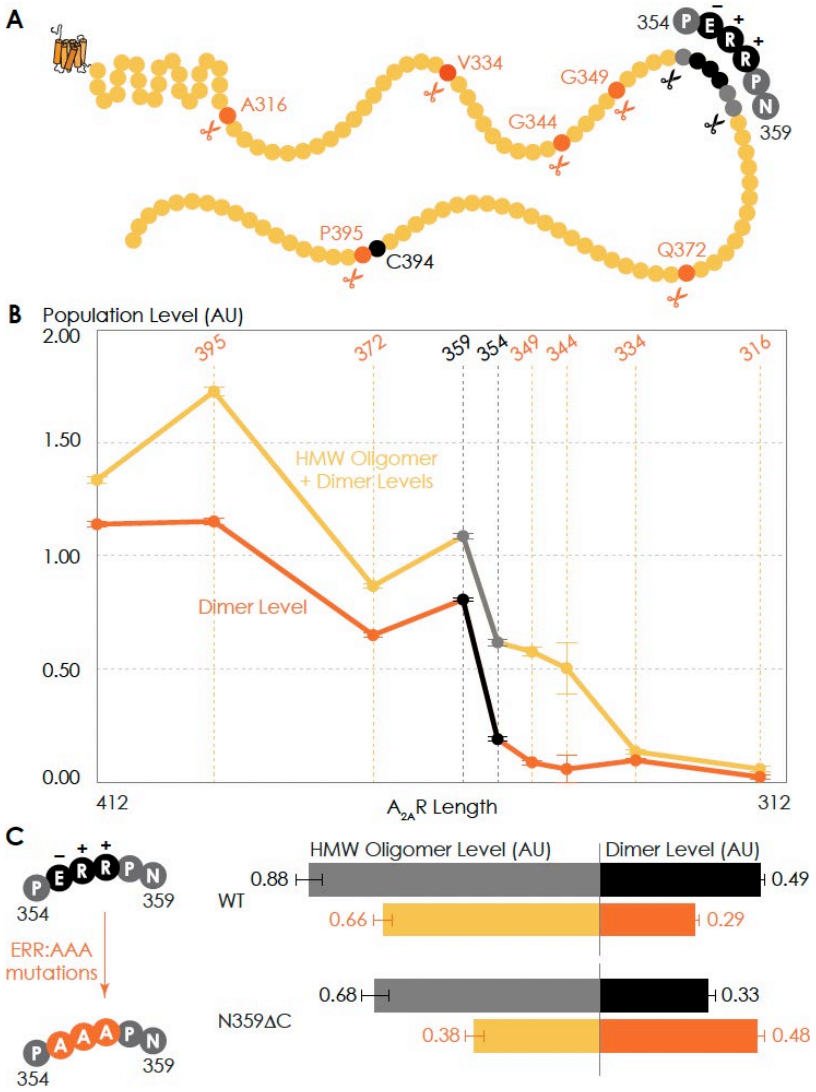

Figure 2-8. Truncating the C-terminus systematically affects $A_{2A}R$ oligomerization. **(A)** Depiction of where the truncation points are located on the C-terminus, with region 354–359 highlighted (in black) showing critical residues. **(B)** The levels of dimer and HMW oligomer are expressed relative to the monomeric population as an arbitrary unit and plotted against the residue number of the truncation sites, with reported errors calculated from the variance of the fit, not experimental variation. Region 354–359 is emphasized (in black and gray) due to a drastic change in the dimer and HMW oligomer levels. **(C)** The dependence of $A_{2A}R$ oligomerization on three consecutive charged residues ^{355}ERR^{357}. The substitution of residues ^{355}ERR^{357} to ^{355}AAA^{357} is referred to as the ERR:AAA mutations. The levels of dimer and HMW oligomer are expressed relative to the monomeric population as an arbitrary unit, with reported errors calculated from the variance of the fit, not experimental variation.

Interestingly, there occurred a dramatic decrease in the dimer level between the N359 and P354 truncation sites, from a value of 0.81 to 0.19, respectively (**Figure 2-8B**). A similar result, though less pronounced, was observed on the total oligomer level, with a decrease from 1.09 to 0.62 for the N359 and P354 truncation sites, respectively (**Figure 2-8B**). Clearly, the C-terminal segment encompassing residues 354–359 (highlighted in black in **Figure 2-8A**) is a key constituent of the $A_{2A}R$ oligomeric interface.

Since segment 354–359 contains three consecutive charged residues (^{355}ERR^{357}; **Figure 2-8A**), which could be involved in electrostatic interactions, we hypothesized that this ^{355}ERR^{357} cluster could strengthen inter-protomer $A_{2A}R$-$A_{2A}R$ association. To test this hypothesis, residues ^{355}ERR^{357} were substituted by ^{355}AAA^{357} on $A_{2A}R$-FL-WT and $A_{2A}R$-N359ΔC to generate $A_{2A}R$-ERR:AAA variants (**Figure 2-8C**). We then compared the HMW oligomer and dimer levels of the resulting variants with controls (same $A_{2A}R$ variants but without the ERR:AAA mutations). We found that the ERR:AAA mutations had varied effects on the dimer level: decreasing for $A_{2A}R$-FL-WT (ctrl: 0.49; ERR:AAA: 0.29) but increasing for $A_{2A}R$-N359ΔC (ctrl: 0.33; ERR:AAA: 0.48) (**Figure 2-8C**). In contrast, the ERR:AAA mutations reduced the HMW oligomer level of both $A_{2A}R$-FL-WT (ctrl: 0.88; ERR:AAA: 0.66) and $A_{2A}R$-N359ΔC (ctrl: 0.68; ERR:AAA: 0.38) (**Figure 2-8C**). Consistently, the ERR:AAA mutation lowered the total oligomer level of both $A_{2A}R$-FL-WT (ctrl: 1.37; ERR:AAA: 0.94) and $A_{2A}R$-N359ΔC (ctrl: 1.01; ERR:AAA: 0.85) (**Figure 2-8C**). These results suggest that the charged residues ^{355}ERR^{357} participate in $A_{2A}R$ oligomerization, with a greater effect in the context of a longer C-terminus and for forming higher-order oligomers. The question then arises as to what types of interactions are formed along the C-terminus that help stabilize $A_{2A}R$ oligomerization.

2.3.4. C-Terminus Truncation Disrupts Complex Network of Non-Bonded Interactions Necessary for $A_{2A}R$ Dimerization

Given that the structure of $A_{2A}R$ dimers or oligomers are unknown, we next used MD simulations to seek molecular-level insights into the role of the C-terminus in driving $A_{2A}R$ dimerization and to gain an understanding of what types of interactions and sites may be involved in this process. First, to explore $A_{2A}R$ dimeric interface, we performed coarse-grained (CG) MD simulations using the Martini force field (see **2.2.10 above** for details). The Martini force field can access the length and time scales relevant to membrane protein oligomerization, albeit at the expense of atomic-level details. We carried out a series of CGMD simulations on five $A_{2A}R$-ΔC variants designed to mirror the experiments by systematic truncation at five sites along the C-terminus (A316, V334, P354, N359, and C394). Our results revealed that $A_{2A}R$ dimers were formed with multiple interfaces, all involving the C-terminus only (**Figure 2-9A**). The transmembrane heptahelical bundles were not a part of the dimeric interfaces as they all showed distances greater than the minimum distance criterion of 7 Å for interacting helices. The vast majority of $A_{2A}R$ dimers were symmetric, with the C-termini of the protomers directly interacting with each other. A smaller fraction of the dimers had asymmetric orientations, with the C-terminus of one protomer interacting with other parts of the other protomer, such as ICL2 (the second intracellular loop) and ICL3 (**Figure 2-9A**).

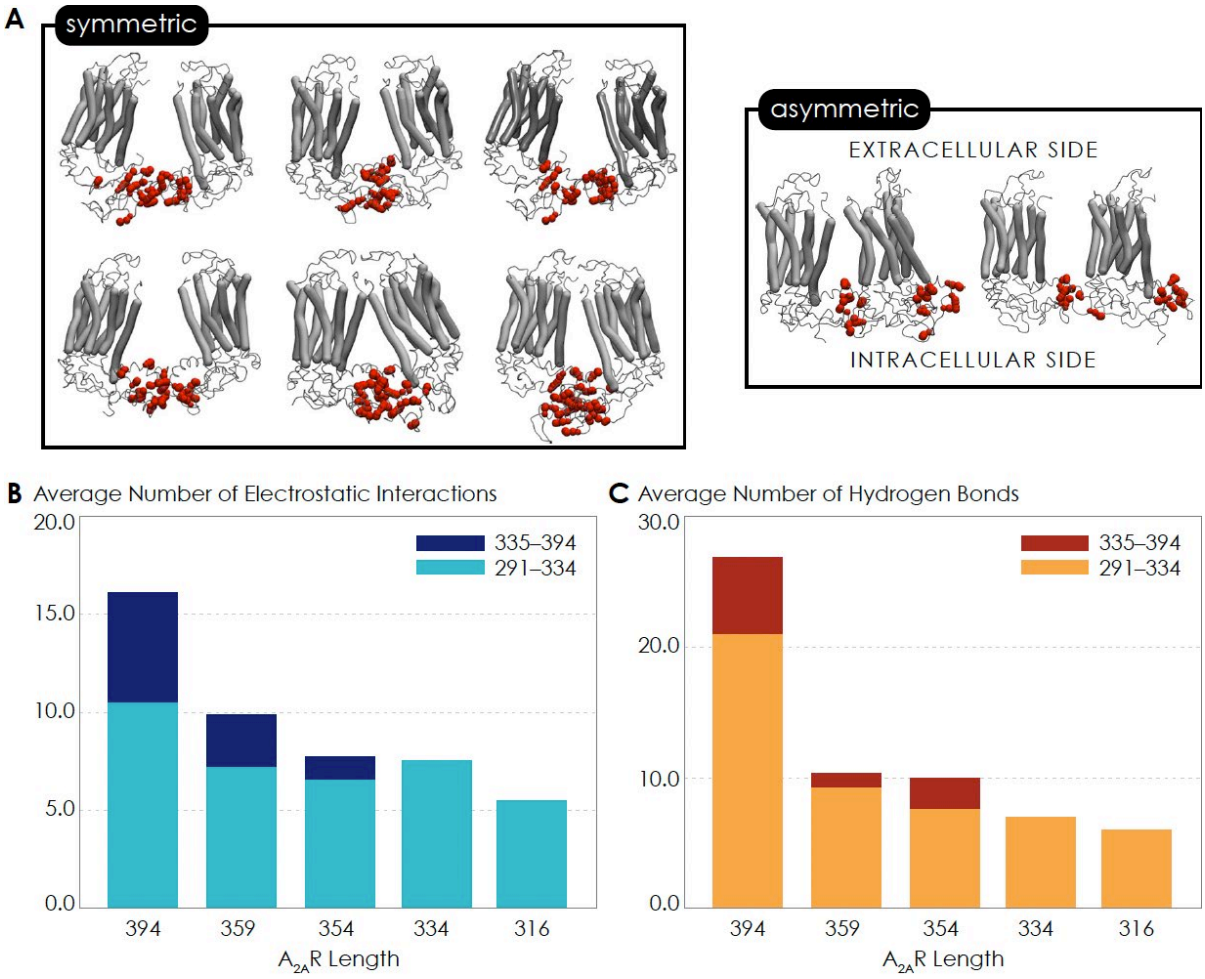

Figure 2-9. Non-bonded interactions of the extended C-terminus of $A_{2A}R$ play a critical role in stabilization of the dimeric interface. **(A)** Dimer configurations from cluster analysis in GROMACS of the 394-residue variant identify two major clusters involving either 1) the C-terminus of one protomer and the C-terminus, ICL2, and ICL3 of the second protomer or 2) the C-terminus of one protomer and ICL2, ICL3, and ECL2 of the second protomer. Spheres: residues forming intermolecular electrostatic contacts. **(B)** Average number of residues that form electrostatic contacts as a function of sequence length of $A_{2A}R$. **(C)** Average number of residues that form hydrogen bonds as a function of sequence length of $A_{2A}R$. The criteria for designating inter-$A_{2A}R$ contacts as electrostatic interactions or hydrogen bonds are described in detail in **2.2 above.**

Our observation of multiple $A_{2A}R$ oligomeric interfaces, which is consistent with previous studies(Fanelli and Felline 2011; Song, Duncan, and Sansom 2020), suggests that tunable, non-covalent intermolecular interactions may be involved in receptor dimerization. We first dissected two key non-covalent interaction types: electrostatic and hydrogen bonding interactions. Electrostatic interactions were calculated from CGMD simulations, while hydrogen bonds were quantified from atomistic MD simulation as the CG model merges all hydrogens into a coarse-grained bead and hence cannot report on hydrogen bonds. This analysis was performed on the symmetric dimers as they constituted the more dominant population. With the least truncated $A_{2A}R$ variant containing the longest C-terminus, $A_{2A}R$-C394ΔC, we observed an average of 15.9 electrostatic contacts (**Figure 2-9B**) and 26.7 hydrogen bonds (**Figure 2-9C**) between the C-termini of the protomers. This result shows that both electrostatic interactions and hydrogen bonds can play important roles in $A_{2A}R$ dimer formation.

Upon further C-terminus truncation, the average number of both electrostatic contacts and hydrogen bonds involving C-terminal residues progressively declined, respectively reaching 5.4 and 6.0 for $A_{2A}R$-A316ΔC (in which the disordered region of the C-terminus is removed) (**Figure 2-9B** and **C**). This result is consistent with the experimental result, which demonstrated a progressive decrease of $A_{2A}R$ oligomerization with the shortening of the C-terminus (**Figure 2-8B**). Interestingly, upon systematic truncation of the C-terminal segment 335–394, we observed in segment 291–334 a steady decrease in the average number of electrostatic contacts, from 10.4 to 7.4 (**Figure 2-9B**). This trend was even more pronounced with hydrogen bonding contacts involving segment 291–334 decreasing drastically from 21.0 to 7.0 as segment 335–394 was gradually removed (**Figure 2-9C**). This observation that

truncation of a C-terminal segment reduces inter-$A_{2A}R$ contacts elsewhere along the C-terminus, indicates that an allosteric mechanism of dimerization exists, in which an extended C-terminus of $A_{2A}R$ stabilizes inter-$A_{2A}R$ interactions near the heptahelical bundles of the dimeric complex. These results demonstrate that $A_{2A}R$ dimers can be formed via multiple interfaces and stabilized by an allosteric network of electrostatic interactions and hydrogen bonds along much of its C-terminus.

2.3.5. Ionic Strength Modulates Oligomerization of C-Terminally Truncated $A_{2A}R$

So far, we have demonstrated that the C-terminus clearly plays a role in forming $A_{2A}R$ oligomeric interfaces. However, it remains unclear what the driving factors of $A_{2A}R$ oligomerization are and whether the oligomeric populations are thermodynamic products. The variable nature of $A_{2A}R$ oligomeric interfaces suggests that the main driving forces must be non-covalent interactions, such as electrostatic interactions and hydrogen bonds. Modulating the solvent ionic strength is an effective method to identify the types of non-covalent interaction(s) at play. Specifically, with increasing ionic strength, electrostatic interactions are weakened (based on Debye-Hückel theory, most electrostatic bonds at a distance greater than 5 Å are screened out at an ionic strength of 0.34 M at 4°C) and depletion interactions are enhanced with salting-out salts, while hydrogen bonds remain relatively impervious. For this reason, we subjected various $A_{2A}R$ variants (FL-WT, FL-ERR:AAA, N359ΔC, and V334ΔC) to ionic strength ranging from 0.15 to 0.95 M by adding NaCl (buffer composition shown in

2.2.10 above). The HMW oligomer and dimer levels of the four $A_{2A}R$ variants were determined and plotted as a function of ionic strengths.

The low ionic strength of 0.15 M should not affect hydrogen bonds or electrostatic interactions if present. We found that the dimer and total oligomer levels of all four variants were near zero (**Figure 2-10**). This is a striking experimental observation: despite being shown to play a role in stabilizing $A_{2A}R$ dimers according to our MD simulations (**Figure 2-9B** and **C**), we can conclude that electrostatic and hydrogen-bonding interactions are not the dominant driving force for $A_{2A}R$ association. The question remains whether depletion interactions could facilitate $A_{2A}R$ oligomerization.

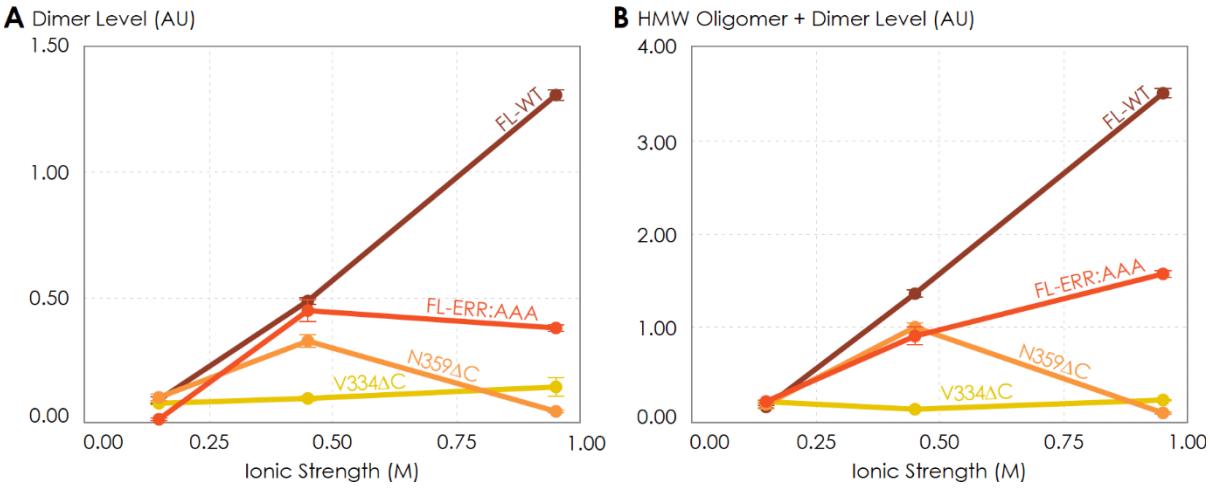

Figure 2-10. The effects of ionic strength on the oligomerization of various $A_{2A}R$ variants reveal the involvement of depletion interactions. The levels of dimer and HMW oligomer are expressed relative to the monomeric population as an arbitrary unit and plotted against ionic strength, with reported errors calculated from the variance of the fit, not experimental variation. NaCl concentration is varied to achieve ionic strengths of 0.15, 0.45, and 0.95 M.

At higher ionic strengths of 0.45 M and 0.95 M, the dimer and total oligomer levels of $A_{2A}R$-V334ΔC still remained near zero (**Figure 2-10**). In contrast, we observed a progressive

and significant increase in the dimer and total oligomer levels of A_{2A}R-FL-WT with increasing ionic strength (**Figure 2-10**). This result indicates A_{2A}R oligomerization is driven by depletion interactions enhanced with increasing ionic strength, and that these interactions must involve the C-terminal segment after residue V334.

Upon closer examination, we recognize that at the very high ionic strength of 0.95 M, the increase in the dimer and total oligomer levels was robust for A_{2A}R-FL-WT, but less pronounced for A_{2A}R-FL-ERR:AAA (**Figure 2-10**). Furthermore, this high ionic strength even had an opposite effect on A_{2A}R-N359ΔC, with both its dimer and total oligomer levels abolished (**Figure 2-10**). These results indicate that the charged cluster ^{355}ERR^{357} and the C-terminal segment after residue N359 promote the depletion interactions to drive A_{2A}R oligomerization. Taken together, we can conclude that A_{2A}R oligomerization is more robust when the C-terminus is fully present and the ionic strength higher, suggesting that depletion interactions via the C-terminus are strong driving factors of A_{2A}R oligomerization.

The discussion of depletion interactions as driving factors assumes that A_{2A}R dimer/oligomer populations are thermodynamics products at equilibrium with the A_{2A}R monomer population. However, some of the A_{2A}R dimer/oligomer populations may be kinetically stabilized. To address this question, we tested the stability and reversibility of A_{2A}R oligomers by performing a second round of SEC on the monomer and dimer/oligomer populations of the A_{2A}R-WT and Q372ΔC variants. We found that the SEC-separated monomers repopulate into dimer/oligomer, with the total oligomer level after redistribution comparable with that of the initial samples for both A_{2A}R-WT (initial: 2.87; redistributed: 1.60) and Q372ΔC (initial: 1.49; redistributed: 1.40) (**Figure 2-11A**). This observation indicates that

$A_{2A}R$ oligomer is a thermodynamic product with a lower free energy compared with that of the monomer (**Figure 2-11B**). This agrees with the results we have shown in **Table 2-1** that the oligomer levels of $A_{2A}R$-WT are consistent among replicates (1.34–2.05) and that $A_{2A}R$ oligomerization can be modulated with ionic strengths via depletion interactions (**Figure 2-10**).

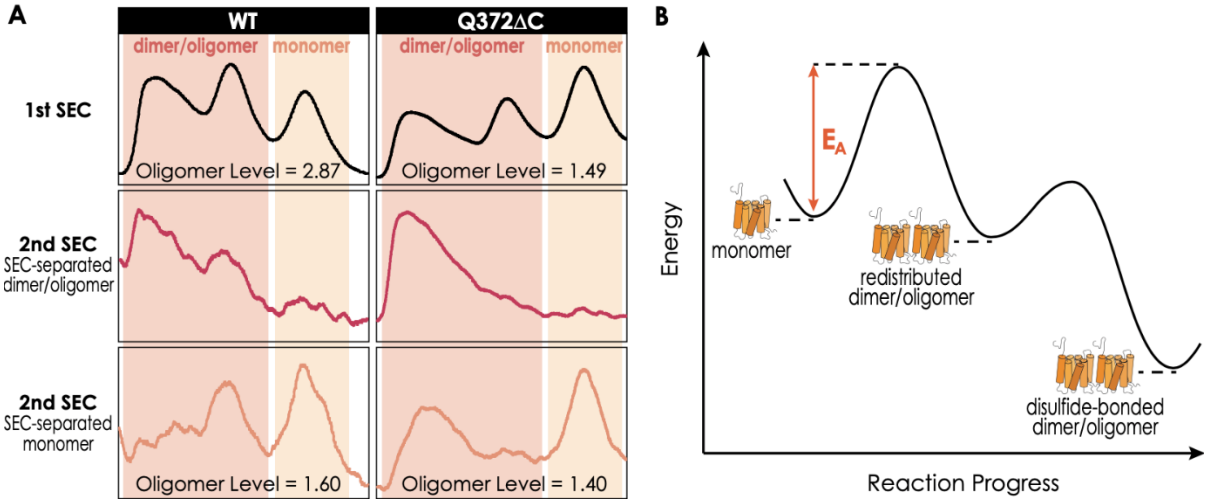

Figure 2-11. The dimer/oligomerization of $A_{2A}R$ is a thermodynamic process where the dimer and HMW oligomer once formed are kinetically trapped. **(A)** SEC chromatograms of the consecutive rounds of SEC performed on $A_{2A}R$-WT and Q372ΔC. The first rounds of SEC are to separate the dimer/oligomer population and the monomer population, while the second rounds of SEC are performed on these SEC-separated populations to assess their stability and reversibility. The total oligomer level is expressed relative to the monomeric population in arbitrary units. **(B)** Energy diagram depicting $A_{2A}R$ oligomerization progress. The monomer needs to overcome an activation barrier (E_A), driven by depletion interactions, to form the dimer/oligomer. Once formed, the dimer/oligomer populations are kinetically trapped by disulfide linkages.

In contrast, the SEC-separated dimer/oligomer populations do not repopulate to form monomers (**Figure 2-11A**). This observation is consistent with a published study of ours on $A_{2A}R$ dimers(Schonenbach et al. 2016), indicating that once the oligomers are formed, some are kinetically trapped and thus cannot redistribute into monomers. We believe that disulfide

linkages are likely candidates to kinetically stabilize $A_{2A}R$ oligomers, as demonstrated by their redistribution into monomers only in the presence of a reducing agent (**Figure 2-6B**).

Taken together, we suggest that $A_{2A}R$ oligomerization is a thermodynamic process (**Figure 2-11B**), with the free energy of the dimer/oligomers lowered by depletion forces that hence increase their population relative to that of the monomers (there always exists a distribution between the two). Once formed, the redistributed dimer/oligomer populations may be kinetically stabilized by disulfide linkages. The question then arises whether inter-$A_{2A}R$ interactions are primarily a result of the C-termini directly interacting with one another. This question motivated us to carry out a study focused on investigating the behavior of $A_{2A}R$ C-terminus *sans* the transmembrane domains.

2.3.6. The Isolated $A_{2A}R$ C-Terminus Is Prone to Aggregation

To test whether $A_{2A}R$ oligomerization is driven by direct depletion interactions among the C-termini of the protomers, we assayed the solubility and assembly properties of the stand-alone $A_{2A}R$ C-terminus—an intrinsically disordered peptide—*sans* the upstream transmembrane regions. Since depletion interactions can be manifested via the hydrophobic effect(van der Vegt and Nayar 2017), we examined whether this effect can also drive the assembly of the $A_{2A}R$ C-terminal peptides.

It is an active debate whether the hydrophobic effect can be promoted or suppressed by ions with salting-out or salting-in tendency, respectively(Thomas and Elcock 2007; Graziano 2010; Zangi, Hagen, and Berne 2007; Grover and Ryall 2005). We increased the solvent ionic strength using either sodium (salting-out) or guanidinium (salting-in) ions and assessed the aggregation propensity of the C-terminal peptides using UV-Vis absorption at 450 nm, which

indicates the turbidity of the solution. We first observed the behavior of the C-terminus with increasing salting-out NaCl concentrations. At NaCl concentrations below 1 M, the peptide was dominantly soluble, despite showing slight aggregation at NaCl concentrations between 250–500 mM (**Figure 2-12A**). At NaCl concentrations above 1 M, $A_{2A}R$ C-terminal peptides strongly associated into insoluble aggregates (**Figure 2-12A**). Consistent with the observations made with the intact receptor (**Figure 2-10**), the $A_{2A}R$ C-terminus showed the tendency to progressively associate and eventually precipitate with increasing ionic strengths, suggesting that depletion interactions drive the association and precipitation of the peptides. We next observed the behavior of the C-terminus with increasing concentrations of guanidine hydrochloride (GdnHCl), which contains salting-in cations that do not induce precipitation and instead facilitate the solubilization of proteins(Heyda et al. 2017; Baldwin 1996). Our results demonstrated that the $A_{2A}R$ C-terminus incubated in 4 M GdnHCl showed no aggregation propensity (**Figure 2-12A)**, validating our expectation that salting-in salts do not enhance depletion interactions. These observations demonstrate that the C-terminal peptide in and of itself, outside the context of the lipid membrane and TM domain, can directly interact with other C-terminal peptides to form self-aggregates in the presence of ions, and presumably solutes, that have salting-out effects.

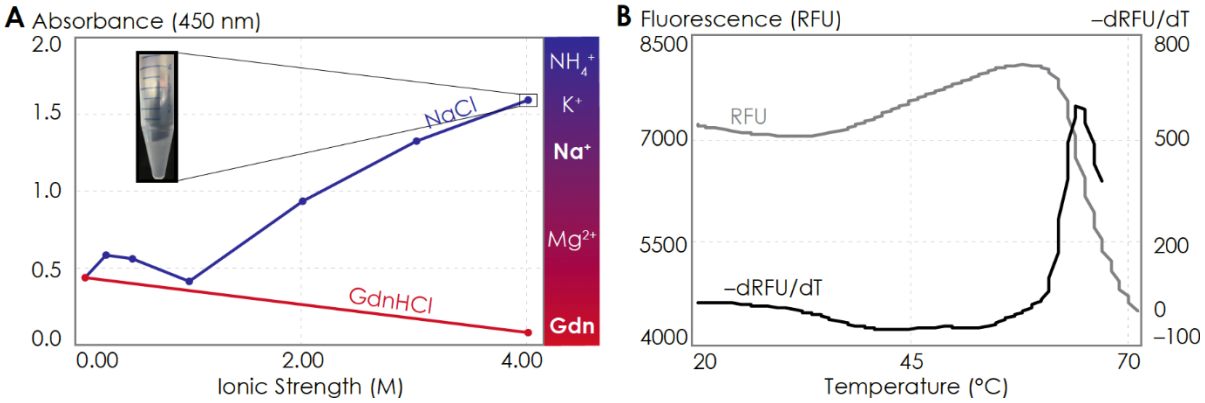

Figure 2-12. The $A_{2A}R$ C-terminus is prone to aggregation. **(A)** Absorbance at 450 nm of the $A_{2A}R$ C-terminus in solution, with NaCl and GdnHCl concentrations varied to achieve ionic strengths 0–4 M. Inset: the solution at ionic strength 4 M achieved with NaCl. The Hofmeister series is provided to show the ability of cations to salt out (blue) or salt in (red) proteins. **(B)** SYPRO orange fluorescence of solutions containing the $A_{2A}R$ C-terminus as the temperature was varied from 20 to 70°C (grey). The change in fluorescence, measured in relative fluorescence unit (RFU), was calculated by taking the first derivative of the fluorescence curve (black).

Attractive hydrophobic interactions among the hydrophobic residues are further enhanced when the water that solvate the protein surface have more favorable interactions with other water molecules, ions or solutes than with the protein surface, here the truncated C-terminus(Larsen, Olson, and Goodsell 1998; Tsai and Nussinov 1997; Tsai et al. 1997). We explored the possible contribution of hydrophobic interactions to the aggregation of the C-terminal peptides using both experimental and computational approaches. Using differential scanning fluorimetry (DSF), we gradually increased the temperature to melt the C-terminal peptides, exposing any previously buried hydrophobic residues (**Figure 2-13A** and **B**), which then bound to the SYPRO orange fluorophore, resulting in an increase in fluorescence signal. Our results showed that as the temperature increased, a steady rise in fluorescence was observed (**Figure 2-12B**), indicating that multiple hydrophobic residues were gradually exposed to the SYPRO dye. However, at approximately 65°C, the melt peak signal was

abruptly quenched (**Figure 2-12B**), indicating that the hydrophobic residues were no longer exposed to the dye. This observation suggests that, at 65°C, enough hydrophobic residues in the C-terminal peptides become exposed such that they collapse on one another (thus expelling the bound dye molecules), resulting in aggregation. This experimental result is further supported by our CGMD computational analysis of C-terminal non-polar contacts found in $A_{2A}R$ symmetrical dimers (**Figure 2-13C**). Specifically, we observed an average of 60 non-polar contacts for $A_{2A}R$-C394ΔC. This number progressively declined upon further C-terminus truncation, reaching 15 for $A_{2A}R$-A316ΔC. Clearly, the hydrophobic effect can cause $A_{2A}R$ C-terminal peptides to directly associate. These results demonstrate that $A_{2A}R$ oligomer formation can be driven by depletion interactions among the C-termini of the protomers by non-polar contacts.

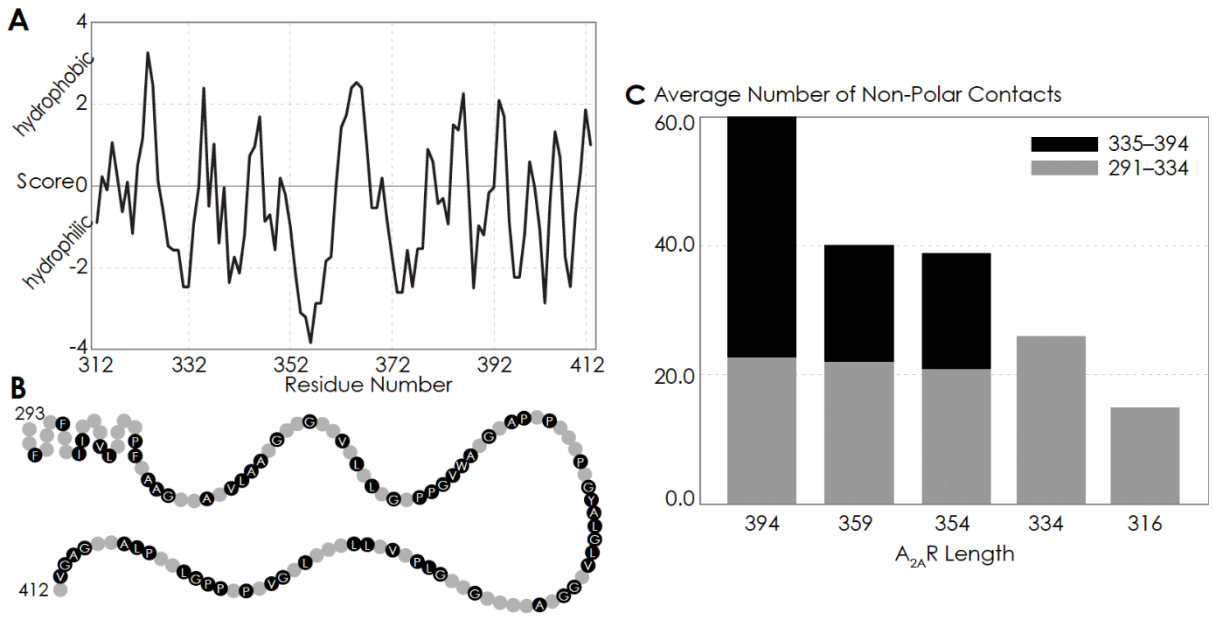

Figure 2-13. (A) Hydropathy plot against $A_{2A}R$ residue number showing the hydrophobicity of $A_{2A}R$ C-terminus, scored with ProtScale using method described by Kyte & Doolittle, window size of 3. Positive scores represent hydrophobicity and negative scores hydrophilicity. **(B)** The non-polar residues in $A_{2A}R$ C-terminus. **(C)** Average number of residues that form non-polar contacts as a function of sequence length of $A_{2A}R$. The criteria for designating inter-$A_{2A}R$ contacts as non-polar interactions are described in detail in **2.2**.

2.4. DISCUSSION

The key finding of this study is that the C-terminus of $A_{2A}R$, removed in all previously published structural studies, directly responsible for receptor oligomerization. Using a combination of experimental and computational approaches, we demonstrate that the C-terminus stabilizes $A_{2A}R$ oligomers via a combination of disulfide linkages, hydrogen bonds, electrostatic interactions, and hydrophobic interactions. This diverse combination of interactions is greatly enhanced by depletion interactions, forming a network of malleable bonds that drives $A_{2A}R$ oligomerization and gives rise to multiple oligomeric interfaces.

Intermolecular disulfide linkages play a role in $A_{2A}R$ oligomerization, potentially by kinetically trapping the receptor oligomers. Among the seven cysteines that do not form intramolecular disulfide bonds(De Filippo et al. 2016; Naranjo et al. 2015; O'Malley et al. 2010a), residue C394 is largely involved in stabilizing $A_{2A}R$ oligomers (**2.3.2 above**). Indeed, this cysteine is highly conserved and a C-terminal cysteine is almost always present in $A_{2A}R$ homologs(Pándy-Szekeres et al. 2018), suggesting that it may serve an important role *in vivo*. There may also exist inter-$A_{2A}R$ disulfide linkages that do not involve residue C394 at all, as the SEC-separated dimer/oligomer populations of $A_{2A}R$-Q372ΔC, which lack residue C394, were still resistant to TCEP reduction (**Figure 2-6B**) and appear to be kinetically trapped (**Figure 2-11**). Such disulfide linkages may involve other cysteines in the hydrophobic core of $A_{2A}R$, namely $C28^{1.54}$, $C82^{3.30}$, $C128^{4.49}$, $C185^{5.46}$, $C245^{6.47}$, or $C254^{6.56}$. Many examples exist where disulfide linkages help drive GPCR oligomerization, including the CaR-$mGluR_1$ heterodimer(Gama, Wilt, and Breitwieser 2001), homodimers of $mGluR_5$(Romano, Yang, and O'Malley 1996), M_3R(Zeng and Wess 1999), V_2R(Zhu and Wess 1998), 5-HT_4R(Berthouze

et al. 2007) and 5-HT_{1D}R(Xie et al. 1999), and even higher-order oligomers of D_2R(Guo et al. 2008). Although unconventional cytoplasmic disulfide bonds have been reported(Saaranen and Ruddock 2013; Locker and Griffiths 1999), no study has shown how such linkages would be formed *in vivo*, as the cytoplasm lacks the conditions and machinery required for disulfide bond formation(Gaut and Hendershot 1993; Hwang, Sinskey, and Lodish 1992; Helenius, Marquardt, and Braakman 1992; Creighton, Hillson, and Freedman 1980).

The electrostatic interactions that stabilize A_{2A}R oligomer formation come from multiple sites along the C-terminus. From a representative snapshot of a A_{2A}R-C394ΔC dimer from our MD simulations (**Figure 2-14A**), we could visualize not only the intermolecular interactions calculated from the CGMD simulations (**Figure 2-9B**), but also intramolecular salt bridges. In particular, the ^{355}ERR^{357} cluster of charged residues lies distal from the dimeric interface but still forms several salt bridges (**Figure 2-14A**, inset). This observation is supported by our experimental results showing that substituting this charged cluster with alanines reduces the total A_{2A}R oligomer levels (**Figure 2-7C**). However, it is unclear how such salt bridges involving this ^{355}ERR^{357} cluster are enhanced by depletion interactions (**Figure 2-10**), as electrostatic interactions are usually screened out at high ionic strengths. In our MD simulations, we also observed networks of salt bridges along the dimeric interface, for example between K315 of one monomer and D382 and E384 of the other monomer (**Figure 2-14A**, inset). The innate flexibility of the C-terminus could facilitate the formation of such salt bridges, which then help stabilize A_{2A}R dimers.

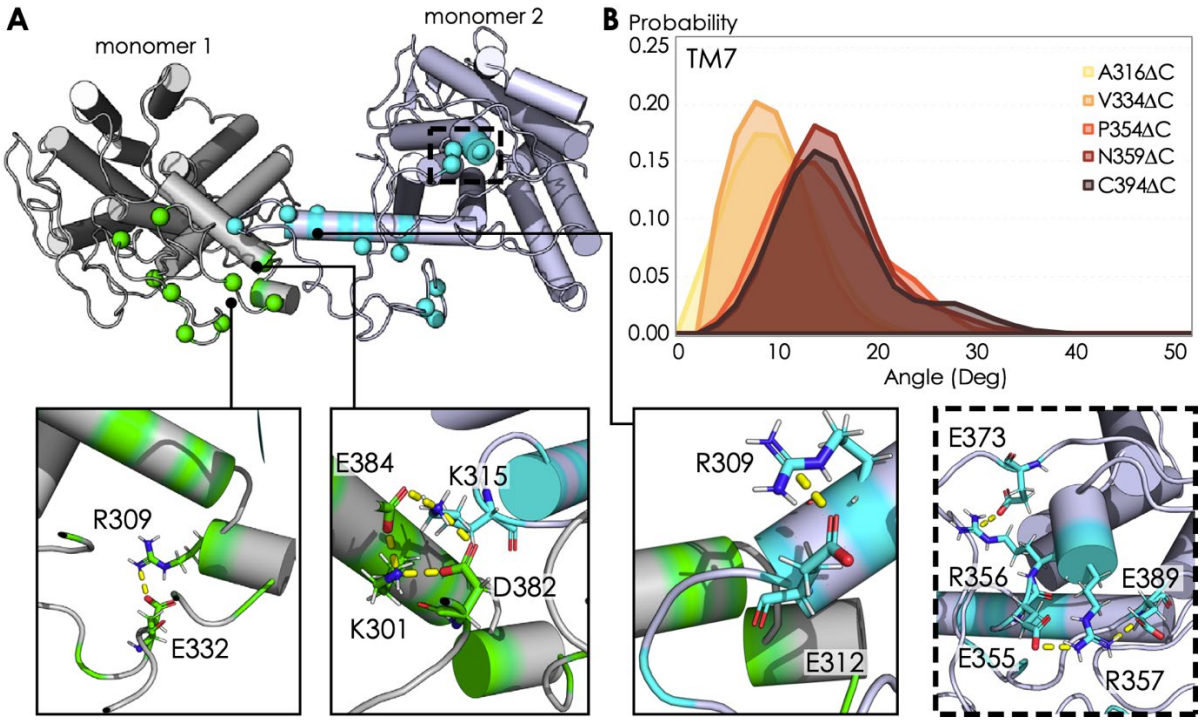

Figure 2-14. (A) Representative snapshot of $A_{2A}R$-C394ΔC dimers shows salt bridge formation between a sample trajectory. The insets are close-ups of the salt bridges, which can be both intra- and intermolecular. The last inset shows a network of salt bridges with the charged cluster ^{355}ERR^{357} involved. **(B)** Helical tilt angles for TM7 helix in $A_{2A}R$ as a function of protein length. Systematic truncations of the C-terminus lead to rearrangement of the heptahelical bundle. The participation of the C-terminus in $A_{2A}R$ dimerization increases the tilting of the TM7 domain, which is in closest proximity to the C-terminus.

Our finding that $A_{2A}R$ forms homo-oligomers via multiple interfaces (**Figure 2-9A**) agrees with the increasing number of studies reporting multiple and interconverting oligomeric interfaces in $A_{2A}R$ and other GPCRs(Song, Duncan, and Sansom 2020; Ghosh, Sonavane, and Joshi 2014b; Periole et al. 2012; Fanelli and Felline 2011; W. Liu et al. 2012; J. Huang et al. 2013; Manglik et al. 2012; Thorsen et al. 2014; Fotiadis et al. 2006; 2003; Liang et al. 2003; Xue et al. 2015; Dijkman et al. 2018). When translated to *in vivo* situations, GPCR oligomers can also transiently associate and dissociate(Kasai et al. 2018; Tabor et al. 2016; Möller et al.

2020; Vilardaga et al. 2008). Such conformational changes require that the oligomeric interfaces be formed by interactions that can easily be modulated. This is consistent with our study, which demonstrates that depletion interactions via the intrinsically disordered, malleable C-terminus drive $A_{2A}R$ oligomerization. Because depletion interactions can be readily tuned by environmental factors, such as ionic strength, molecular crowding, and temperature, the formation of GPCR oligomeric complexes could be dynamically modulated in response to environmental cues to regulate receptor function.

Not only did we find multiple $A_{2A}R$ oligomeric interfaces, we also found that these interfaces can be either symmetric or asymmetric. This finding is supported by a growing body of evidence that there exists both symmetric and asymmetric oligomeric interfaces for $A_{2A}R$(Song, Duncan, and Sansom 2020) and many other GPCRs. Studies using various biochemical and biophysical techniques have shown that heterotetrameric GPCR complexes can be formed by dimers of dimers, including μOR-δOR(Golebiewska et al. 2011), CXC_4R-CC_2R(Armando et al. 2014), CB_1R/D_2R(Bagher et al. 2017) as well as those involving $A_{2A}R$, such as A_1R-$A_{2A}R$(Navarro, Cordomí, Brugarolas, et al. 2018; Navarro et al. 2016) and $A_{2A}R$-D_2R(Navarro, Cordomí, Casadó-Anguera, et al. 2018). The quaternary structures identified in these studies required specific orientations of each protomer, with the most viable model involving a stagger of homodimers with symmetric interfaces(Cordomí et al. 2020). On the other hand, since symmetric interfaces limit the degree of receptor association to dimers, the HMW oligomer of $A_{2A}R$ observed in this(Song, Duncan, and Sansom 2020) and other studies(Schonenbach et al. 2016; Vidi et al. 2008) can only be formed via asymmetric interfaces. It is indeed tempting to suggest that the formation of the HMW oligomer of $A_{2A}R$ may even arise from combinations of different interfaces. In any case, the wide variation of

GPCR oligomerization requires the existence of both symmetric and asymmetric oligomeric interfaces.

The ultimate question to answer is how oligomerization alters $A_{2A}R$ function. In the case of $A_{2A}R$, displacement of the transmembrane domains have been demonstrated to be the hallmark of receptor activation(Eddy et al. 2018; Sušac et al. 2018; Prosser et al. 2017; Ye et al. 2016), but no studies have linked receptor oligomerization with the arrangement of the TM bundles in $A_{2A}R$. Our MD simulations revealed that C-terminus truncation resulted in structural changes in the heptahelical bundles of $A_{2A}R$ dimers. Specifically, as more of the C-terminus was preserved, we observed a progressive increase in the helical tilt of TM7 (**Figure 2-14B**). This change in helical tilt occurred for the entire heptahelical bundle, with an increase in tilt for TM1, TM2, TM3, TM5, and TM7, and a decrease in tilt for TM4 and TM6 (**Figure 2-15**). The longer C-terminus in the full-length $A_{2A}R$ permits greater rearrangements in the transmembrane regions, leading to the observed change in helical tilt. Furthermore, in the cellular context, it has been demonstrated that truncation of the C-terminus significantly reduced receptor association with $G\alpha_s$ and cAMP production in cellular assays(Koretz et al. 2021). These results hint at potential conformational changes of $A_{2A}R$ upon oligomerization, necessitating future investigation on functional consequences.

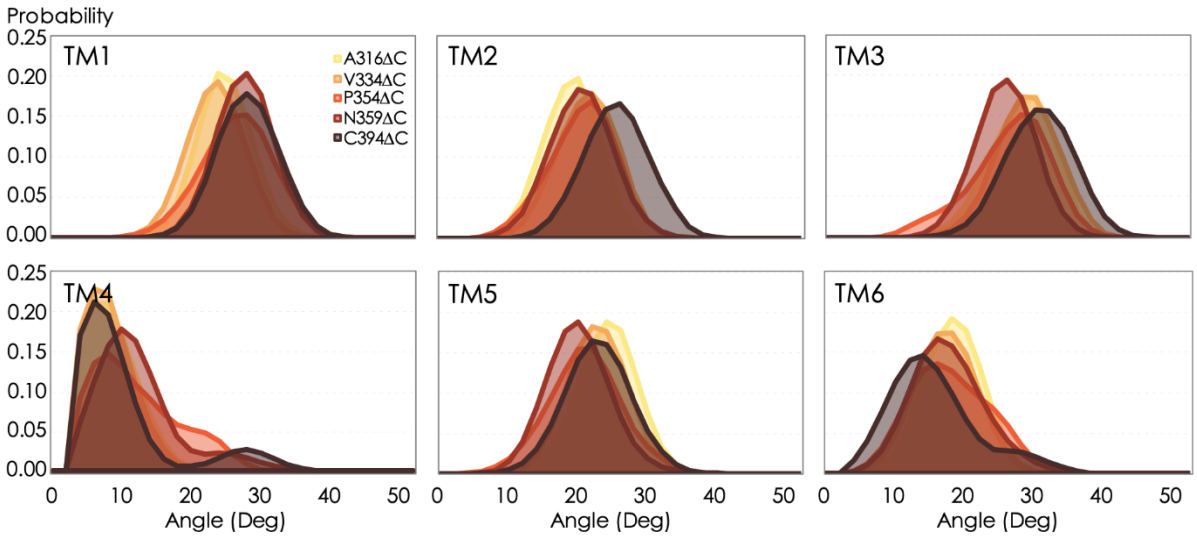

Figure 2-15. Helical tilt angles for TM1–6 helices in $A_{2A}R$ as a function of protein length. Systematic truncations of the C-terminus lead to rearrangement of the heptahelical bundle, propagated to the entire receptor and is especially pronounced in helices proximal to the C-terminus, *i.e.*, TM1, TM2, TM7. For almost all TM helices, a noticeable shift in tilt angle occurs upon modeling the full-length (394 residues) variant. This behavior is fundamentally different from the conventional model of GPCR activation, in which TM 1, 2, 4, and 7 remain rigid, with TM5 and TM6 undergoing an outward tilt/rotation to enable binding to the cognate G protein. Relaxation of the heptahelical bundle (*i.e.*, an increase in helical tilt) as a function of protein length and dimerization could potentially be critical to our understanding of the activation mechanism of $A_{2A}R$, as past studies have overwhelmingly focused on activation of the monomer.

Like all biophysical studies of membrane proteins in non-native environments, a drawback in our study is the question whether the above results, conducted in detergent micelles, can be translated to bilayer or cellular context. It has been demonstrated that the propensity of membrane proteins to associate and oligomerize is greater in lipid bilayers compared to that in detergent micelles(Popot and Engelman 1990). Furthermore, in the cellular context, $A_{2A}R$ has been shown to assemble into homo-oligomers in transfected HEK293 cells(Canals et al. 2003) and in Cath.A differentiated neuronal cells(Vidi et al. 2008), while C-terminally truncated $A_{2A}R$ shows no protein aggregation or clustering on the cell surface, in contrast with its WT form(Burgueño et al. 2003). Therefore, we speculate that $A_{2A}R$ oligomerization will be present in the lipid bilayer and cellular environment. Regardless, given that most biophysical structure-function studies of GPCRs are conducted in detergent micelles and other artificial membrane mimetics, it is critical to understand the role of the C-terminus in the oligomerization of $A_{2A}R$ reconstituted in detergent micelles.

C-terminal truncations prior to crystallization and structural studies may be the main reason for the scarcity of GPCR structures featuring oligomers. In that context, this study offers valuable insights and approaches into how the oligomerization of $A_{2A}R$ and potentially of other GPCRs can be tuned by modifying the intrinsically disordered C-terminus and varying salt types and concentrations. The presence of $A_{2A}R$ oligomeric populations with partial C-terminal truncations means that one can now study its oligomerization with less perturbation from the C-terminus. We also present evidence that the multiple C-terminal interactions that drive $A_{2A}R$ oligomerization can be easily modulated by ionic strength and specific salts (**Figure 2-10** and **Figure 2-12A**). Given that ~75% and ~15% of all class-A GPCRs possess a C-terminus of > 50 and > 100 amino acid residues(Mirzadegan et al. 2003), respectively, it will be worthwhile

to explore the prospect of tuning GPCR oligomerization not only by shortening the C-terminus but also with simpler approaches such as modulating ionic strength and the surrounding salt environment.

2.5. CONCLUSION

This study emphasizes for the first time the definite impact of the C-terminus on $A_{2A}R$ oligomerization, which can be extended to include the oligomers formed by other GPCRs with a protracted C-terminus. We have shown that the oligomerization of $A_{2A}R$ is strongly driven by depletion interactions along the C-terminus, further modulating and enhancing the multiple interfaces formed via a combination of hydrogen, electrostatic, hydrophobic, and covalent disulfide interactions. The task remains to link $A_{2A}R$ oligomerization to functional roles of the receptor. From a structural biology standpoint, visualizing the multiple oligomeric interfaces of $A_{2A}R$ in the presence of the full-length C-terminus is key to investigating whether these interfaces give rise to different oligomer functions.

Chapter 3 | CHARACTERIZATION OF CYSTEINE-FREE CONSTRUCTS OF THE HUMAN ADENOSINE A_{2A} RECEPTOR FOR STUDIES USING ELECTRON PARAMAGNETIC RESONANCE SPECTROSCOPY

So far, this thesis has provided deeper insights into how the intrinsically disordered C-terminus promotes the oligomerization of the human adenosine A_{2A} receptor ($A_{2A}R$). As mentioned in **1.3 above**, the second aim of this thesis is to visualize the oligomeric interfaces of $A_{2A}R$ and decipher the structural role of the C-terminus at such interfaces. This chapter seek to describe the challenges associated with structural studies of GPCR oligomers using electron paramagnetic resonance (EPR) spectroscopy, a biophysical technique with unique capabilities of provide dynamic information into the role of the disordered C-terminus in $A_{2A}R$ oligomer formation.

3.1. INTRODUCTION

3.1.1. Methods to Study Membrane Protein Structure

Membrane proteins play a crucial role in a vast number of biological processes. Nearly 30% of all open reading frames in eukaryotic cells have been predicted to encode for membrane proteins(Wallin and Heijne 1998). Changes in structure of these proteins due to mutations or improper folding is linked with a multitude of human diseases, including cystic fibrosis, depression, cardiovascular diseases, Alzheimer's and Parkinson's, cancer, among many others. G protein-coupled receptors (GPCRs) in particular are targeted by ~40% of all modern drugs(Overington, Al-Lazikani, and Hopkins 2006; Rask-Andersen, Masuram, and Schiöth 2014). The field of drug discovery has benefited greatly from methods such as high-throughput screening (HTS) or computational methods, but it is structural information from three-

dimensional (3D) atomic structures that reveals how drug candidates bind to proteins and what conformational changes proteins consequently undergo.

X-ray crystallography and nuclear magnetic resonance (NMR) spectroscopy are the two most used techniques for obtaining structural information on biological targets. However, both techniques have limitations critical to deciphering structures of membrane proteins, especially of GPCRs. NMR is excellent at capturing dynamics and structure of proteins, but it is only useful and easy to perform on targets of ≤ 50 kDa in size. As the protein gets as large as the typical size of a GPCR, the slow tumbling rate results in band broadening and intensity loss, decreasing spectral resolution. This problem can be overcome by applying certain pulse sequences to cancel out unwanted signals, but such method cannot mitigate the significant increase in linewidth caused by interference from detergent micelles typically used to solubilize membrane proteins (Torres, Stevens, and Samsó 2003). An alternative to sidestep the problem of slow tumbling is to use solid-state NMR by magic-angle spinning (MAS), which is spinning the sample at 40–100 kHz on an axis 54.74º relative to the magnetic field B_0, such that the sample undergoes only anisotropic motions. However, the amount of sample that can be packed into a MAS rotor is physically limited, as the rotor must be small enough to be spun at such ultra-high speed. Together with the presence of the required amount of membrane mimetics detergent, such sample limitation poses serious problems associated with low sensitivity, requiring prolonged data acquisition time.

Meanwhile, although X-ray crystallography can provide valuable structural information of proteins, it usually takes years to obtain a crystal structure that reflects a membrane protein at high enough resolution (< 3 Å). Although structural details are needed to

visualize $A_{2A}R$ oligomeric interfaces, X-ray crystallography is not the optimal method for several reasons. First, the detergent system used to solubilize membrane proteins can undergo phase separation upon increase of precipitant concentration in the hanging-drop method, negatively impacting crystallization(Lacapère et al. 2007). Secondly, the micelles surrounding the protein can hinder crystal contacts, although this problem can be overcome by co-crystallizing the protein with antibody fragments(Hunte and Michel 2002). Thirdly, due to weak crystal contact and the presence of amphiphilic detergent molecules, the protein crystals are often unstable and sensitive to temperature, thus difficult to handle(Lacapère et al. 2007). (Note that all of the above three reasons are associated with the use of detergent micelles, adding to the various problems posed by this membrane mimetic platform in membrane protein structure determination. Efforts to replace detergent micelles with styrene maleic acid (SMA) lipid polymers, a promising nanodisc platform, will be discussed in **Chapter 5.**)

Last but most importantly, as mentioned in **Chapter 2**, the intrinsically disordered C-terminus is critical for the formation of $A_{2A}R$ oligomers. Crystalizing the full-length wild-type form of $A_{2A}R$ means crystalizing the long and intrinsically disordered C-terminus of the protein. This is not a practical goal, as intrinsically disordered proteins (IDPs) usually fail to crystalize due to the inherent flexibility. Even when successfully crystalized, their numerous conformations cannot be captured by just a single snapshot(Timsit et al. 2006). In fact, all crystal structures of $A_{2A}R$ up to date required the truncation of the C-terminus(V.-P. Jaakola et al. 2008; Hino et al. 2012; Sun et al. 2017; Xu et al. 2011; Doré et al. 2011; Carpenter et al. 2016), which essentially excludes the purpose of this project. As a result, X-ray crystallography is insufficient to probe the role of protein disorder in not only GPCR oligomerization but also conformational changes of proteins.

Apart from X-ray crystallography and NMR spectroscopy, cryogenic electron microscopy (cryo-EM) is the other viable option for the purpose of the project. This method involves plunge-freezing the sample within milliseconds to prevent ice crystal formation, which can destroy the protein of interest(Thompson et al. 2016). Cryo-EM exceeds the limitations of crystallography in the sense that it does not require thermostabilizing mutations and special conditions to induce crystallization, which are harmful for proteins in general. Also, no C-terminus truncation is needed so images of $A_{2A}R$ dimers can be captured. However, to membrane proteins, especially GPCRs, there still exist major hurdles to employing cryo-EM for structural studies. These challenges will be further discussed in **Chapter 4**, but can be listed briefly: (1) $A_{2A}R$ dimers do not exceed the size required (> 150 kDa) for the particle to be recognized in the low-contrast micrographs; (2) the detergent and salt required to stabilize the receptor in the current protocol may scatter the electrons so much that it becomes hard to tell apart the protein particles from the buffer atoms using phase contrast; (3) micelle is a dynamic and deformable structure, which may decrease the rigidity of the $A_{2A}R$ dimer structure of interest, making it difficult to identify the dimer for automatic particle boxing in single particle analysis.

3.1.2. Electron Paramagnetic Resonance in Structural Biology

Electron paramagnetic resonance (EPR) spectroscopy and other EPR-based techniques, on the other hand, serve as a potential solution to overcome these obstacles and to obtain both structural and dynamic information on various biological systems(Klug and Feix 2008). EPR spectroscopy does not suffer from the restriction in size and optical properties of the protein since it offers sensitivity of 50- to several hundred-fold higher than that of NMR. Additionally,

EPR measurements can be performed on samples of many different types(Hustedt and Beth 1999), including membrane-embedded proteins, to answer structural and dynamic questions that could not be probed by conventional techniques(Hustedt and Beth 1999; Bordignon and Steinhoff 2007; Hubbell et al. 1996). Furthermore, continuous-wave (CW) EPR spectroscopy of spin-labeled molecules can provide information about the motion as well as distances between different paramagnetic centers in the system(Klare 2013).

EPR and the related techniques require a label to be incorporated into the system of interest to make it "EPR-active". This incorporation of labels with unpaired electrons is performed by introducing a cysteine residue into a recombinant protein via site-directed mutagenesis, which is then conventionally reacted with a paramagnetic nitroxide reagent to generate an EPR-active side chain(Klare 2013) (**Figure 3-1**). In order for this incorporation to be site-specific, a method referred to as site-directed spin labeling (SDSL), all accessible free cysteines must be removed, usually by mutating them to serines (which can form hydrogen bond) or alanines (relatively non-reactive).

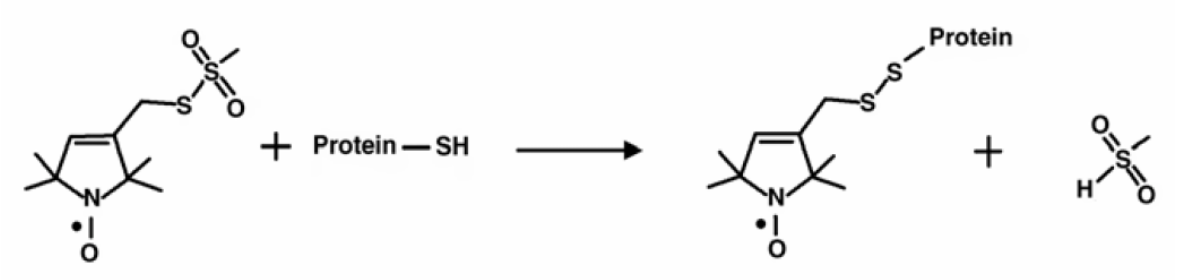

Figure 3-1. Reaction of the nitroxide spin label with cysteine to attach the label onto the protein via disulfide bond. The dot represents the free electron in the N–O bond stabilized by the methyl groups in vicinity.

3.1.3. Fluorescent-Activated Cell Sorting (FACS) to Screen for Cysteine-Free $A_{2A}R$ Constructs

The A_{2A} receptor contains 15 cysteine residues in total, with eight forming four disulfide bonds on the extracellular loops (ECLs) of the receptor, six in the transmembrane (TM) domains, and one C394 on the C-terminus. Since the spin labeling procedure uses the same chemistry of disulfide bond formation, the extracellular cysteines are not available for spin labeling. The other seven, on the other hand, are very much exposed to spin labeling, as cw-EPR measurements of $A_{2A}R$-WT and $A_{2A}R$-C394S showed significant background signals(Schonenbach et al. 2016).

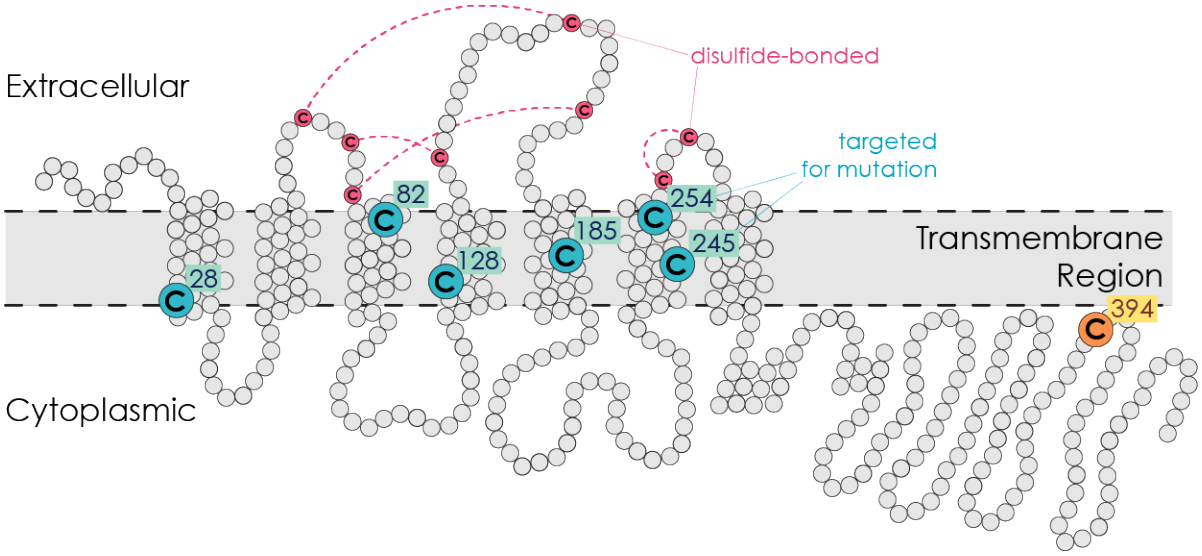

Figure 3-2. Snake diagram of $A_{2A}R$ secondary structure, highlighting TM cysteine residues that were mutated in this study. The human adenosine A_{2A} receptor contains 15 cysteines in total. The pink cysteines are on the extracellular side and are disulfide-bonded, thus are not accessible to nitroxide spin labels. The blue transmembrane and the orange C-terminal cysteines are all exposed to spin label. Estimated location of the lipid membrane is indicated by the two black dash-dot lines.

To make $A_{2A}R$ EPR-inactive (with no cysteines available for spin labeling), these seven free cysteines needed to be substituted. Modeling and simulation (in this case with RosettaDesign) were considered a good approach to identify the best mutations to remove cysteines without disrupting the function of the protein. However, Rosetta modeling could only predict combinations of mutations that are thermodynamically favorable for the associated constructs to traffic to the membrane of the heterologous expressing system. To this end, FACS became a much more robust experimental platform to screen for mutants with so many simultaneous mutations. The technique involves having the fluid containing the cells to be sorted injected into a flow cytometer through a laser beam. Depending on the properties of interest, wanted cells are often tagged with a fluorophore that scatters the laser beam differently, thus sorted into a separate batch one at a time. In this case, the FACS-based agonist binding assay developed used the following three criteria: (1) good expression, (2) membrane localization, and (3) ligand binding (**Figure 3-3A**). All three criteria had to be met for the cells carrying the cysteine-free $A_{2A}R$ constructs to be collected during cell sorting.

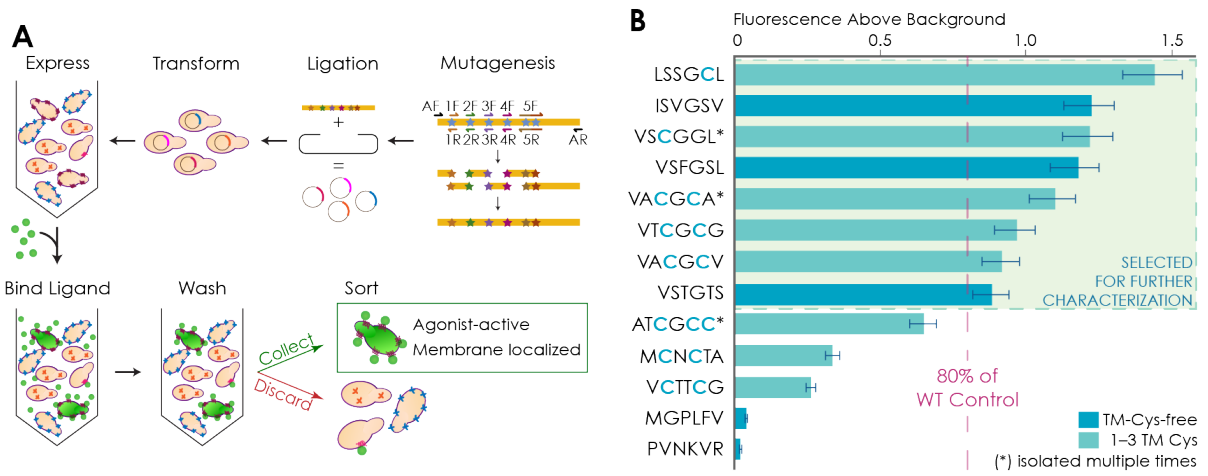

Figure 3-3. (A) Pipeline for construction, expression, and enrichment of TM-Cys-free $A_{2A}R$ Library. Illustration summary of steps to conduct mutagenesis, cloning, transformation, expression, and fluorescent ligand binding screen $A_{2A}R$ library designed for site-saturation mutagenesis at 6 transmembrane sites within $A_{2A}R$. **(B)** Summary of FACS analysis of 13 library variants, ranked qualitatively by the percent of cells within the sorting gate (*i.e.*, ligand binding) relative to the average of three wild-type (WT) controls. Out of 100,000 events in each sample, variants that exhibited greater than 80% of the wild-type population of cells within the sorting gate were selected for further characterization, indicated by a shaded box with dashed lines.

After three rounds of sorting, 50 colonies were randomly chosen for sequencing analysis, yielding 13 variants for further functional characterization (**Figure 3-3B**). These variants include three identified multiple times (ATCGCC, VACGCA, and VSCGGL), five containing no TM cysteines, and five containing 1–3 TM cysteines with no bulky or charged amino acid substitutions. The ligand binding activity of these variants was verified individually by FACS analysis using the same ligand binding protocol as for library sorting. Approximately 100,000 events were analyzed, reporting the percent of cells that exhibited fluorescence intensity high enough to place them within the sorting gate (relative fluorescence above background). Variants' agonist binding activities were compared to wild-type agonist binding by dividing the percent of variant cells within the gate by the average percent of wild-type cells

within the gate. These normalized relative fluorescence intensities for each variant reported in **Figure 3-3B** indicate whether variant cells bound FITC-APEC as well as or better than wild-type (≥ 1) or not as well (< 1). These mean fluorescence intensities do not necessarily translate directly to agonist binding affinity, but rather a combined effect of agonist binding and expression levels. In other words, variants that bind to FITC-APEC with slightly lower affinities could still yield a normalized relative fluorescence ≥ 1 if it is expressed more highly than wild-type. False positives were observed (variants PVNKVR and MGPLFV) due to the nature of cell sorting within a sorting gate set to allow a small percentage (≤ 0.5%) of negative control cells to be collected during sorting. Eight out of 13 select variants had considerable normalized fluorescence (89–145%) relative to that of $A_{2A}R$-WT (**Figure 3-3B**). These include three completely void of TM cysteines, two retaining only one TM cysteine, and three with two TM cysteines. The variant with the highest normalized fluorescence relative to WT (145%; sequence LSSGCL) retained only the highly conserved $C245^{BW6.47}$ cysteine.

Although the above results were promising toward engineering a TM-Cys-free $A_{2A}R$ variant that expresses well in yeast, binds ligand, and has lower predicted energy than wild-type $A_{2A}R$, the FITC-APEC ligand used to enrich the library is an agonist with high affinity to $A_{2A}R$. As such, the nature of this FACS-based screen allowed for the enrichment of "active structure" variants, which could increase the chances of observing reduced antagonist binding, as has been observed previously(Magnani et al. 2008). Furthermore, such simultaneous elimination of cysteines could disrupt the receptor's function or structure, which are partially maintained by cysteines linked via hydrogen bonds or disulfide bonds(O'Malley et al. 2010a; De Filippo et al. 2016).

3.1.4. Goals and Approaches

To ensure that the FACS-sorted $A_{2A}R$ variants were EPR-dark, cw-EPR was employed on these cysteine-free constructs. It was later revealed that the cysteine-free $A_{2A}R$ variants were still spin labeled, which can only be explained by the nitroxide label being attached to the remaining extracellular cysteines. These ECL cysteines were more exposed to the solvent phase compared to the TM cysteines. As a result, the spin label molecules attached to the ECL cysteines can be distinguished from those attached to the TM cysteines using the power saturation technique.

In terms of function, the cysteine-free $A_{2A}R$, the variants were expressed, purified, and subjected to ligand-affinity chromatography using an antagonist (XAC), which was used to purify $A_{2A}R$-WT and other variants(Schonenbach et al. 2016). Attempts to build an agonist-based ligand-affinity column to enhance protein yield will also be presented below.

3.2. MATERIALS AND METHODS

3.2.1. Expression of $A_{2A}R$ Variants in *S. cerevisiae*

Variants of the human adenosine A_{2A} receptor ($A_{2A}R$) tagged with 10 C-terminal histidines (pITy-A_{2A}R-10His) or GFP-10His(pITy-A_{2A}R-eGFP-10His) were cloned and expressed in the vacuolar protease deficient *S. cerevisiae* strain BJ5464 (MATα ura3-52 trp1 leu2Δ1 his3Δ200 pep4::HIS3 prb1Δ1.6R can1 GAL) (provided by the lab of Anne Robinson at Carnegie Mellon University) and purified as described previously(Schonenbach et al. 2016). Expression screens were performed by selecting four colonies from transformation plates and cultured overnight at 30°C in 5 mL of YPD (1% w/v yeast extract, 2% w/v peptone, 2% dextrose) with shaking at 250 rpm. Expression was induced in 5 mL of YPG (1% yeast, 2% peptone, 2% galactose) at an initial optical density at 600 nm (OD) of 0.5 and allowed to grow for 24 hours. After 24 hours, 5 OD of cells were pelleted and prepared for SDS-PAGE. Western blotting was carried out with an anti-GFP antibody conjugated to horseradish peroxidase (HRP) (Abcam, ab6663). Colonies for each variant that exhibited the highest expression levels by Western blot analysis were cryo-preserved.

For expression, *S. cerevisiae* BJ5464 transformed with $A_{2A}R$ variants were grown at 30°C overnight in 5 mL of YPD with shaking at 250 rpm. These overnight cultures were then sub-cultured into 50 mL of YPD at an initial OD of 0.5 and allowed to grow for 24 hours. Cells from these 50-mL cultures were pelleted at 2,000 × g for 5 minutes and resuspended in 1-L YPG expression cultures at an initial OD of 0.5. Cells in the induction medium were grown for 24 hours at 30°C with shaking at 250 rpm. Cells were harvested by centrifugation at 2,000 × g for 5 minutes, washed in sterile phosphate buffer saline (PBS) (137 mM sodium chloride, 2.7

mM potassium chloride, 10 mM sodium phosphate dibasic, 1.8 mM potassium phosphate monobasic, pH 7.4) buffer and centrifuged again before storage at –80°C until needed for protein preparation.

3.2.2. Purification of $A_{2A}R$ Variants

Cells were lysed using mechanical bead lysis in lysis buffer (50 mM sodium phosphate, 300 mM sodium chloride, 10% v/v glycerol, pH = 8.0) containing 2% (w/v) *n*-dodecyl-β-D-maltopyranoside (DDM), 1% (w/v) 3-[(3-cholamidopropyl)dimethylammonio]-1-propanesulfonate (CHAPS), and 0.2% (w/v) cholesteryl hemisuccinate (CHS) (Anatrace, Maumee, OH #D310, C216, CH210, respectively) and an appropriate quantity of 100X Pierce Halt EDTA-free protease inhibitor #78439). After removing unlysed cells and cell debris by centrifugation at 3,200 × g for 10 minutes, solubilized protein in this supernatant was gently mixed with Nickel NTA resin (Pierce, #88221) resin overnight. After extensive washing in purification buffer (50 mM sodium phosphate, 300 mM sodium chloride, 10% (v/v) glycerol, 0.1% DDM, 0.1% CHAPS and 0.2% CHS, pH 8.0 and low imidazole concentrations (20–50 mM), protein was either (1) eluted with purification buffer containing 0.1% DDM, 0.1% CHAPS and 0.2% CHS and 500 mM imidazole (if only purifying for ligand affinity chromatography) or (2) spin labeled overnight by adding 2.5 μL of 340 mM *S*-(1-oxyl-2,2,5,5-tetramethyl-2,5-dihydro-1H-pyrrol-3-yl)methyl methanesulfonothioate (MTSL) (Toronto Research Chemicals, #0875000) (if purifying for EPR). Prior to further chromatography purification and separation, imidazole was removed using a PD-10 desalting column (GE Healthcare, # 17085101). For experiments destined for EPR, after spin labeling, the resin was

extensively washed with several long washes (at least 20 minutes at 4°C) of imidazole-free purification buffer to remove un-reacted spin label before elution.

To purify ligand-active $A_{2A}R$, a ligand affinity column was equilibrated thoroughly in 4 column volumes of purification buffer containing 50 mM sodium phosphate, 300 mM sodium chloride, pH = 8.0, 10% (v/v) glycerol, 0.1% DDM, 0.1% CHAPS, 0.02% CHS. After desalting IMAC-purified receptor, the sample was diluted to 5.5 mL and applied to a 5 mL sample loop on a BioRad Duoflow FPLC which loaded the sample onto the column at a rate of 0.1 mL/min. Inactive receptor was washed from the column by flowing 10 mL of purification buffer at 0.2 mL/min, followed by 16 mL at 0.4 mL/min. Ligand-active receptor was eluted from the column by switching to purification buffer containing 20 mM of low affinity (K_d = 1.6 μM) antagonist theophylline (Sigma, #T1633). For ligand-active variants, the first four 4 mL elution fractions were pooled, concentrated through a 30 kDa molecular weight cutoff centrifugal filter (Millipore, #UFC803096) and passed through a PD-10 desalting column to remove the theophylline prior to EPR.

3.2.3. SDS-PAGE and Western Blotting

10% SDS-PAGE gels were hand-casted in BioRad Criterion empty cassettes (BioRad; #3459902, 3459903). Lysate controls were prepared by lysis of 5 OD cell pellets with 35 μL of YPER (Fisher Scientific, Waltham, MA, USA # 8990) at RT for 20 min, incubation with 2x Laemmli buffer (4% (w/v) SDS, 16% (v/v) glycerol, 0.02% (w/v) bromophenol blue, 167 M Tris, pH 6.8) at 37ºC for 1 h, and centrifugation at 3,000 × g for 1 min to pellet cell debris. Protein samples were prepared by incubation with 2x Laemmli buffer at 37ºC for 30 min. For all samples, 14 μL (for 26-well gel) or 20 μL (for 18-well gel) was loaded per lane, except for

7 μL of Magic Mark XP Western protein ladder (Thermo Scientific, Waltham, MA, USA; # LC5602) as a standard. Electrophoresis was carried out at 120 V for 100 min. Proteins were transferred to 0.2-μm nitrocellulose membranes (BioRad; # 170-4159) via electroblotting using a BioRad Transblot Turbo, mixed MW protocol. Membranes were blocked in Tris-buffered saline with Tween (TBST; 150 mM sodium chloride, 15.2 mM Tris-HCl, 4.6 mM Tris base, pH = 7.4, 0.1% (v/v) Tween 20 (BioRad; # 1706531)) containing 5% (w/v) dry milk, then probed with anti-$A_{2A}R$ antibody, clone 7F6-G5-A2 (Millipore, Burlington, MA, USA; # 05-717) at 1:500 in TBST with 0.5% (w/v) dry milk. Probing with secondary antibody was done with a fluorescent DyLight 550 antibody (Abcam, Cambridge, MA, USA; ab96880) at 1:600 in TBST containing 0.5% (w/v) milk.

For quantitation of protein concentration, BCA assay was applied using Pierce BCA Protein Assay Kit (Thermo Scientific, #23225) following manufacturer's instructions. Alternatively, UV-Vis spectroscopy was employed to measure absorption at 280 nm using a NanoDrop^{TM} 2000 Spectrophotometer (Thermo Scientific, #ND-2000)

3.2.4. Electron Paramagnetic Resonance (EPR) and Quantitation of Spin Labeling Efficiency

For samples that were planned for EPR experiments, the spin labeling reaction was implemented while $A_{2A}R$ was bound to IMAC resin to facilitate sufficient washing steps to remove excess spin label. Solubilized protein samples bound to IMAC resin were spin labeled overnight by adding 2.5 μL of 340 mM *S*-(1-oxyl-2,2,5,5-tetramethyl-2,5-dihydro-1H-pyrrol-3-yl) methylmethanesulfonothioate (MTSL) (Toronto Research Chemicals, #0875000) and gentle mixing. Excess MTSL was removed by washing the resin was extensively with at least

5 washes of 40 mL wash buffer (50 mM sodium phosphate, 300 mM sodium chloride, 10% (v/v) glycerol, 0.1% DDM, 0.1% CHAPS and 0.02% CHS, pH 8.0) for at least 20 minutes at 4°C before elution.

Continuous wave (cw) EPR measurements were performed at RT on a 0.35 T Bruker EMX spectrometer equipped with dielectric cavity (ER4123D). Samples were loaded at a volume of 3.5 µL into a quartz capillary (0.6 mm i.d., 0.84 mm o.d.), which were then sealed on one end with Critoseal® (Oxford Labware; Catalog No. 8889-215003) and the other with beeswax. The experiments were done by irradiating the samples with 6 mW of microwave power at 9.74 GHz using a 2.5 G modulation amplitude, a sweep width of 150 G, and signal averaged over 40 21-second scans.

For quantitation of spin labeling efficiency, a calibration curve was obtained using 4-hydroxy-TEMPO dissolved in buffer (50 mM sodium phosphate, 300 mM sodium chloride, 10% v/v glycerol, pH = 8.0) at various concentrations from 12.5–200 μM. All cw-EPR spectra was background corrected with LabVIEW program Multicomponent by applying interpolation on the absorption spectrum. The amount of spin in each sample was calculated based on the second integral of the spectrum with the new baseline.

3.2.5. Power Saturation Experiment

Continuous-wave EPR (CW-EPR) spectra were recorded on a Bruker EMX spectrometer equipped with a rectangular cavity resonator at a microwave frequency of about 9.75 GHz (X-band). Protein sample volumes of 3 μL (20–100 μM) were inserted into a gas-permeable plastic TPX capillary (Molecular Specialties, Inc.; Catalog No. TPX-2), sealed with

Critoseal® (Oxford Labware; Catalog No. 8889-215003) and sheltered in a TPX holder (Molecular Specialties, Inc.; Catalog No. TPX-H). The solution was equilibrated for 20 min under continuous nitrogen flow (for the deoxygenated control and the sample in Nickel ethylenediamine-*N*,*N*′-diacetic acid (NiEDDA)) or air flow (for the sample in 20% oxygen) around the sample capillary before any spectra was acquired. NiEDDA was synthesized as previously described(Oh et al. 2000). Each sample was measured at room temperature in the presence of nitrogen as a deoxygenated control, 20% oxygen (air), and with the addition of 20 mM NiEDDA. Over a field range of 100 G, 40 scans were acquired for each 2-dB step in the power range of 0.2–200 mW. The modulation amplitude was 1 G and the modulation frequency was 100 kHz. The first integral of the derivative spectrum was plotted against the square root of the incident microwave powered and normalized by the highest first integral value. To determine the spin concentration, double integration of the derivative spectrum was performed and fitted to a calibration curve of 0–200 μM 4-OH TEMPO (4-hydroxy-2,2,6,6-tetramethylpiperidin-1-oxyl).

3.2.6. Construction of an Agonist-Affinity Column for Purification of $A_{2A}R$

Ligand affinity resin was prepared as previously described for purification of active $A_{2A}R$.(O'Malley et al. 2007), (Weiß and Grisshammer 2002) In brief, 8 mL of isopropanol-washed Affigel 10 resin (BioRad, Hercules, CA, USA; #1536099) was mixed gently in an Erlenmeyer flask for 20 h at room temperature with 48 mL of DMSO containing 24 mg of adenosine amine congener (ADAC, high-affinity $A_{2A}R$ agonist, $K_D = 210$ nM; Sigma, St. Louis, MO, USA; #A111). The absorbance at 310 nm of the ADAC-DMSO solution before and after the coupling reaction was measured in 10 mM HCl and compared to a standard curve. The

amount of resin bound to ligand was estimated to be 4.9 μM. The coupling reaction was quenched by washing the resin with DMSO, then with Tris-HCl 50 mM (pH = 7.4), then with 20% (v/v) ethanol. The resin was packed into a Tricorn 10/50 column (GE Healthcare) under pressure via a BioRad Duoflow FPLC (BioRad).

Purification of active $A_{2A}R$ followed the same procedure as that applied for the antagonist-affinity column described in **3.2.2 above**, but instead of theophylline, protein elution was done with 20 mM adenosine (low-affinity $A_{2A}R$ agonist, K_D = 0.7 μM; Sigma; #A9251).

Visualization of the binding of ligands to $A_{2A}R$ was done with PyMOL on the crystal structures of $A_{2A}R$ bound to XAC (PDB ID: 3REY(Doré et al. 2011)) and adenosine (PDB ID: 2YDO(Lebon et al. 2011))

3.3. RESULTS AND DISCUSSION

3.3.1. Cysteine-Free $A_{2A}R$ Variants Showed Significant EPR Background Signals and Biased Ligand Binding

The eight variants identified to have a relative fluorescence greater than 80% of a wild-type $A_{2A}R$ control were selected for further characterization (**Figure 3-3B**). These variants were sub-cloned into the integrating pITy-MC2-10His yeast expression vector for increased expression and purification to facilitate analysis of antagonist (XAC) ligand binding (via a custom ligand affinity column) and EPR measurement. Surprisingly, we found that all the variants exhibited significantly reduced affinity to the XAC column relative to the $A_{2A}R$/C394S control (**Figure 3-4A**) (VSTGTS not shown). These results suggest that the FACS enrichment using an agonist resulted in the enrichment of a library that favored an "active" conformation, but with a reduced affinity for antagonists. Furthermore, continuous wave EPR (CW-EPR) demonstrated that all the variants displayed a noticeable EPR signal. Quantitation of spin labeling efficiency indicated that these variants exhibited a spin labeling efficiency of 1.8–5.9%, except for ISVGSV (21.0%) (**Table 3-1**). Although these values significantly lower than that of the C394S control (23.4%), the result suggested that that at least one of the extracellular disulfide bonds were not completely formed, and thus were available for spin labeling (**Figure 3-4B**).

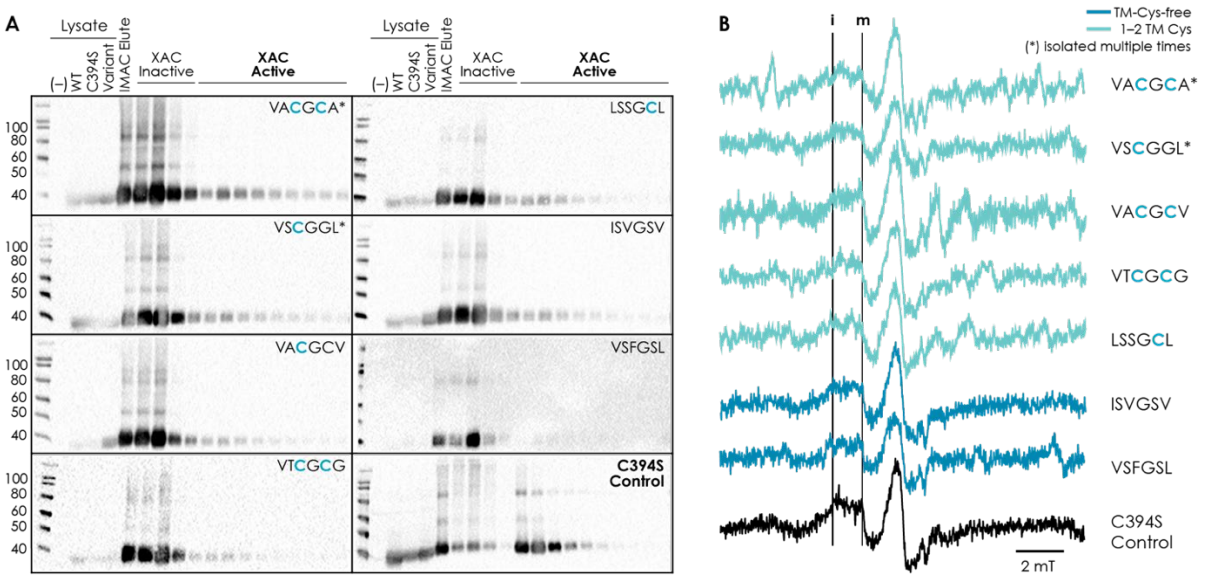

Figure 3-4. Agonist-active TM-Cys-free $A_{2A}R$ Variants Exhibit Reduced Affinity to Antagonist XAC and Incomplete Disulfide Formation. **(A)** Representative Western Blots of $A_{2A}R$ variants purified and analyzed for antagonist binding via xanthine amine congener (XAC) ligand affinity column. Negative control (–) is cell lysate for wild-type BJ5464 S. cerevisiae strain without the $A_{2A}R$ receptor. Positive control (WT) is cell lysate for BJ5464 expressing the wild-type $A_{2A}R$. "XAC Inactive" indicates improperly folded $A_{2A}R$ that has poor/reduced affinity to the XAC ligand affinity column. "XAC Active" indicates receptor that sufficiently bound to the affinity column. (**B**) EPR spectra for spin labeled $A_{2A}R$ library variants.

Table 3-1. Spin labeling efficiency of the various TM-Cys-Free variants of $A_{2A}R$ (VSTGTS not shown) with C394S as the negative control.

Variants	Protein Conc. (μM)	Label Conc. (μM)	Labeling Efficiency (%)
VACGCA	11.7	0.5	4.1
VSCGGL	11.9	0.4	2.9
VACGCV	11.8	0.6	5.5
VTCGCG	11.5	0.6	5.5

Variants	Protein Conc. (μM)	Label Conc. (μM)	Labeling Efficiency (%)
LSSGCL	11.8	0.7	5.9
ISVGSV	11.5	2.4	21.0
VSFGSL	11.4	0.2	1.8
C394S	38.5	9.0	23.4

3.3.2. Power Saturation Experiments Indicated Disruption of Extracellular Disulfide Bonds in Cysteine-Free $A_{2A}R$ Variants

To investigate whether substitution of TM cysteines lead to functional and/or structural modifications, such as the incomplete formation of $A_{2A}R$'s extracellular disulfide bonds, CW-EPR and EPR power saturation experiments upon addition of solvophilic or lipophilic paramagnetic relaxation agents were conducted to yield information about the mobility and solvent accessibility, respectively, of the spin labeled sites in selected $A_{2A}R$ variants. The power saturation experiments were analyzed by plotting the square root of incident microwave power against the normalized EPR signal intensity and observing the change in lineshape of the power saturation curve in the presence of N_2 (deoxygenated control), 21% O_2 (with air), and NiEDDA, where O_2 and NiEDDA act as the paramagnetic relaxation agents to help the spin system absorb more power before reaching the point of saturation of the EPR resonance. In theory, O_2 and NiEDDA only partition into the lipid phase and the solvent phase, respectively. Therefore, the lineshapes of the power saturation curves in the presence of these relaxation agents depend heavily on the environment in which the relaxation agent is enriched. Extracellular cysteines that were not completely disulfide bonded should have greater solvent accessibility compared to the TM cysteines. In this experiment, there was no significant difference in the power saturation curves with O_2 among the selected variants (data not shown), perhaps because the spin system is not buried enough in the lipid phase of the micelles. As such, the O_2 curves were not included.

Previously, it has been shown that wild-type $A_{2A}R$ has a C394 residue in the flexible and solvent-exposed C-terminus that is dominantly spin labeled, and that TM residues C28 and

C254 are partially solvent accessible(Schonenbach et al. 2016). As expected, wild-type $A_{2A}R$ exhibited high mobility (**Figure 3-5A**) and solvent accessibility (**Figure 3-5E**). $A_{2A}R$/C394L lacks this C394 spin label site, and the nitroxide spin label was hypothesized to primarily attach to the TM cysteines that are in the rigid α-helices buried in the lipid phase of the micelles. It was observed that $A_{2A}R$/C394L exhibited much lower mobility (**Figure 3-5B**) and solvent accessibility (**Figure 3-5F**) compared to wild-type $A_{2A}R$, supporting this hypothesis. The reduced solvent accessibility of the spin label is supported with the observed shift to the left of the power saturation curve in the presence of NiEDDA compared to that of $A_{2A}R$-WT (**Figure 3-5F**). A triple mutant, $A_{2A}R$/C394S/C28M/C254S lacking the two most solvent accessible TM cysteines was also analyzed (**Figure 3-5C** and **G**). If the disulfide bonds among the extracellular cysteines were intact, one would expect an EPR profile with reduced mobility and solvent accessibility relative to $A_{2A}R$/C394L, as the spin label should still attach to the rest of the TM cysteines. However, $A_{2A}R$/C394S/C28M/C254S exhibited increased mobility (**Figure 3-5C**) and increased solvent accessibility (**Figure 3-5G**). This data suggests that one or more extracellular disulfide bonds are disrupted in this variant, resulting in the spin labeling of mobile and solvent-exposed extracellular cysteines. To investigate the solvent accessibility of a variant from the $A_{2A}R$ TM-Cys-Free library, variant 53 (ISVGSV) was selected for analysis as it is totally free of TM cysteines with the best agonist binding property (**Figure 3-3B)**. Interestingly, this variant exhibited lower mobility and higher solvent accessibility (**Figure 3-5D** and **H**, respectively) than $A_{2A}R$/C394S/C28M/C254S. These results suggest that different disulfide bond(s) may have been disrupted in comparison to those of $A_{2A}R$/C394S/C28M/C254S, leading to the exposure of a cysteine that is solvent-exposed but displays lower mobility.

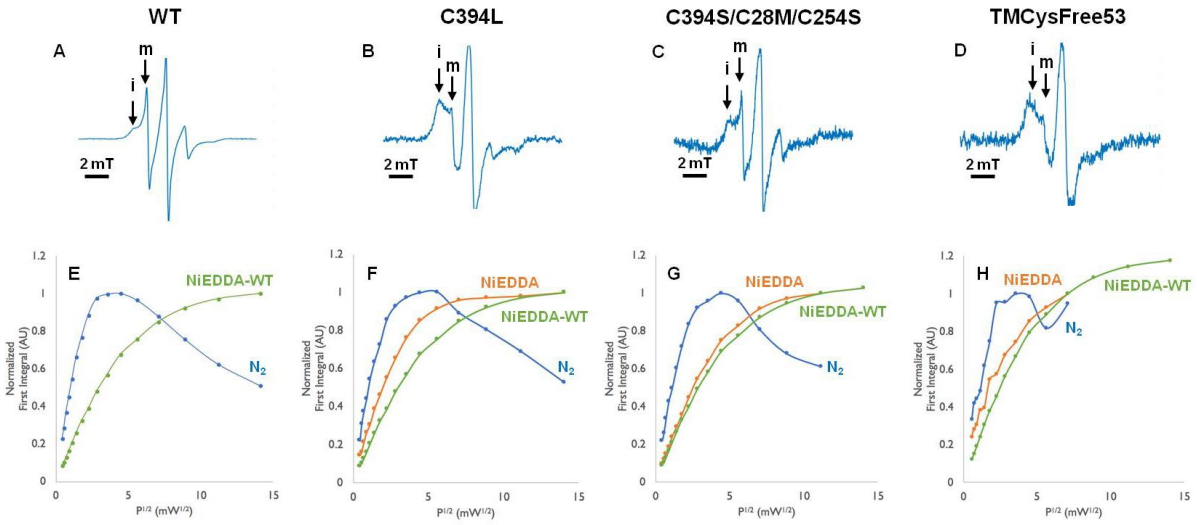

Figure 3-5. Power saturation experiments reveal differences in solvent exposure of spin labeled $A_{2A}R$ variants. **(A–D)** CW-EPR spectra for $A_{2A}R$-WT, $A_{2A}R$-C394L, $A_{2A}R$-C394S/C28M/C254S, and $A_{2A}R$-TM-Cys-Free-53, respectively. The mobile (m) and immobile (i) components in these CW-EPR spectra indicate the mobility of the spin label in these variants. **(E–H)** Power saturation profiles for $A_{2A}R$-WT, $A_{2A}R$-C394L, $A_{2A}R$-C394S/C28M/C254S, and $A_{2A}R$-TM-Cys-Free-53, respectively. The first integral values are normalized by the highest value in each curve and plotted against the square root of microwave power. In **F**, **G**, and **H**, the power curve in the presence of NiEDDA of each variant (orange) is overlaid with that of $A_{2A}R$-WT (green). Solvent accessibility of each variant is assessed by how similar its power curve in NiEDDA is to that of $A_{2A}R$-WT.

3.3.3. TM-Cys-Free $A_{2A}R$ Variants Did Not Bind to Agonist ADAC Due to Steric Hindrance

Since antagonist-affinity chromatography could not be used to purify the agonist-biased TM-Cys-Free variants of $A_{2A}R$, we attempted to construct an agonist-affinity column using adenosine amine congener (ADAC, K_D = 210 nM). $A_{2A}R$-WT was expressed in 1 L of media containing *S. cerevisiae* and purified with IMAC before applied onto the ADAC column (see **3.2.6 above**). In the ligand-affinity chromatogram, fractions 1–8 contained the flow-through that did not bind to ADAC, while fractions 9–17 contained ADAC-active $A_{2A}R$ eluted by the low-affinity agonist adenosine. The protein was detected at 280 nm with a built-in UV detector. Compared with those of the XAC-affinity chromatogram, fractions 1–8 of the ADAC-affinity chromatogram showed significantly larger area under the curve (**Figure 3-6A**). Since the same amount of protein was loaded onto both columns, this result indicated that a substantial amount of protein did not bind to ADAC compared with XAC.

Since the ligand-active fractions 9–17 were saturated by the signals from the ligands, SDS-PAGE followed by Western Blot analysis was required to detect protein in these fractions. The Western Blot on all fractions eluted from the column showed strong bands in the ADAC-inactive fractions, but no protein was observed in the ADAC-active fractions. This is in contrast with the result obtained for XAC-affinity chromatography (**Figure 2-3A**), indicating that the protein could not bind to the agonist ADAC.

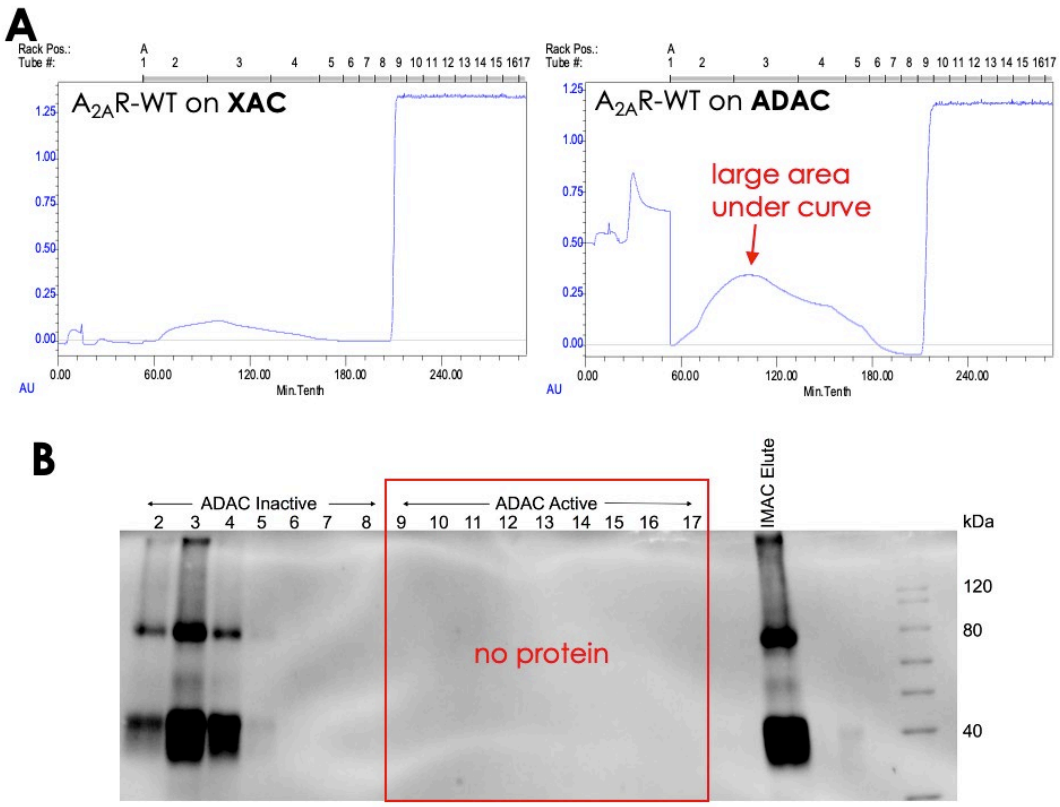

Figure 3-6. The agonist-biased TM-Cys-Free variants of $A_{2A}R$ do not bind to the agonist adenosine amine congener. **(A)** Ligand-affinity chromatograms of $A_{2A}R$-WT bound to XAC and ADAC. The protein is detected at 280 nm wavelength. Fractions 1–8 contain the inactive flow-through, while fractions 9–17 contain the active protein, which is saturated by the signals from the ligands. ADAC-affinity chromatogram (right) shows a much larger area under the curve of the inactive fractions compared with XAC-affinity chromatogram (left). **(B)** Western Blot analysis of SDS-PAGE of all fractions from ADAC-affinity chromatography. No bands were observed in the "ADAC Active" fractions. MagicMark protein ladder (LC5602) is used as the molecular weight standard.

To explain why A_{2A}R-WT could bind to XAC but not to ADAC, PyMOL was used to visualize how these ligands would fit into the binding pocket of A_{2A}R. In order for a ligand to be attached to the Affi-Gel 10 resin used to construct the affinity columns, the ligand must have only one single amine group to ensure uniform attachment, and this amine group must not be buried in the binding pocket of the protein. The crystal structure of A_{2A}R bound to XAC (**Figure 3-7**; PDB ID: 3REY) revealed that the primary amine group on XAC was clearly exposed, suggesting that XAC can be bound to A_{2A}R and attached to the resin at the same time. For ADAC, the crystal structure of A_{2A}R bound to adenosine (**Figure 3-7**; PDB ID: 2YDO) was used, as no structure of A_{2A}R bound to ADAC was available. This structure showed that the entire adenosine molecule was buried inside the binding pocket of A_{2A}R, including the amine group that would be attached to the amine congener upon synthesis of ADAC. Molecular structure of ADAC (**Figure 3-7**) suggested a planar structure at the connection between adenosine and the congener due to electron delocalization. As a result, if ADAC is bound to A_{2A}R, the congener would extend directly into the protein density, making it impossible for ADAC to be bound to A_{2A}R and attached to the resin at the same time. This explains why A_{2A}R could not bind to ADAC-affinity column and why agonist-affinity chromatography is excluded from the purification of A_{2A}R.

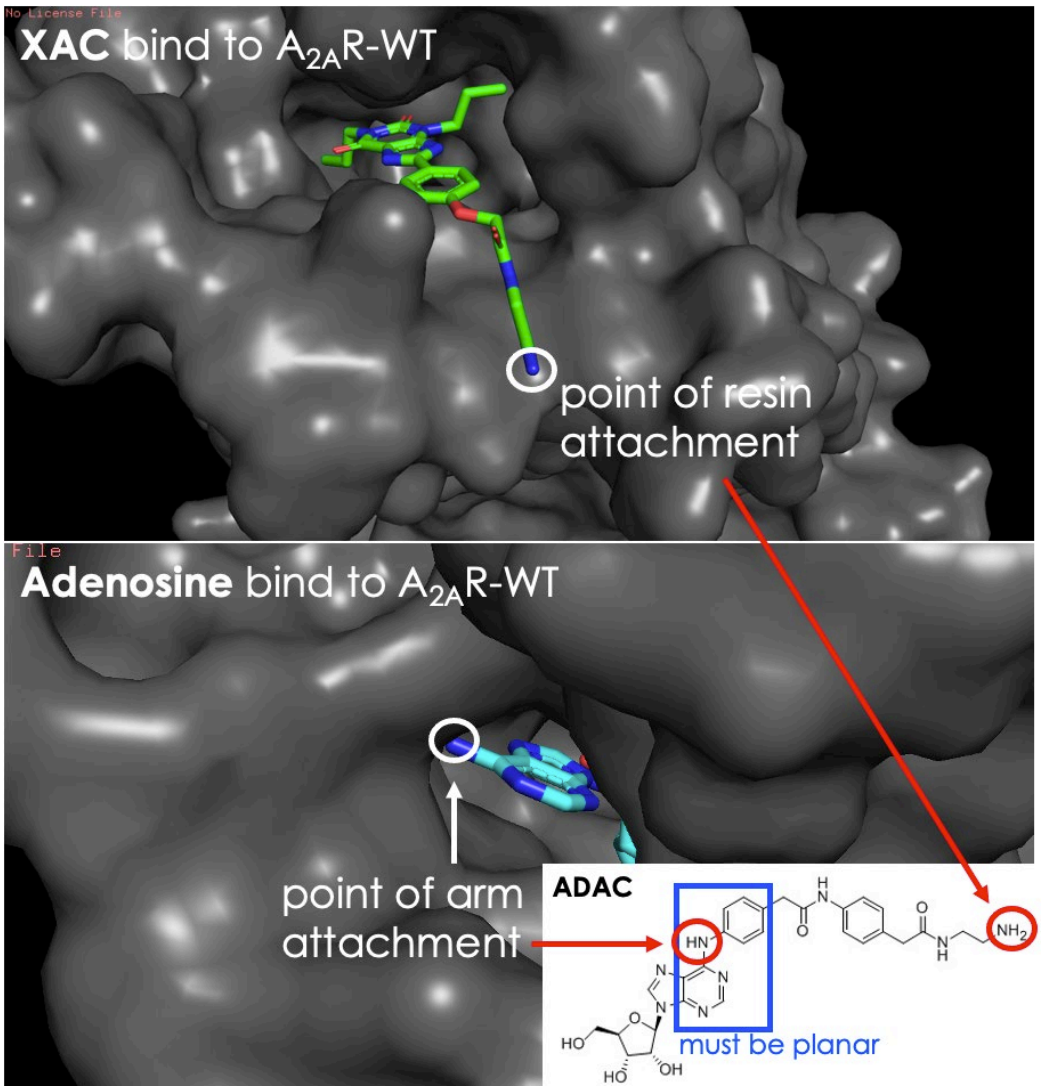

Figure 3-7. Visualization of A_{2A}R-WT bound to XAC (PDB ID: 3REY) and adenosine (PDB ID: 2YDO) with PyMOL. The terminal amine group on XAC is clearly exposed, enabling attachment onto the resin. No crystal structure of A_{2A}R bound to ADAC is available. Based on the structure of A_{2A}R bound to adenosine, the point that would be attached to the amine congener on adenosine is directed towards the protein itself. Due to electron delocalization, attachment of the amine congener creates a planar structure that extends directly into the protein, leaving the terminal amine group unavailable for resin attachment.

3.4. CONCLUSION

To better inform the models and quickly screen all possible amino acid combinations at the six TM cysteine sites, a multi-site saturation $A_{2A}R$ library was enriched via a fluorescent agonist binding FACS assay. The eight variants carried forward for purification and further characterization were found to have significantly reduced affinity to an antagonist affinity column. These results suggested that while the fluorescent agonist FACS screen enriched a library of agonist-active variants, the library was biased toward variants that favor agonist conformation, reducing affinity to antagonists. To further challenge efforts to engineer a TM-Cys-free $A_{2A}R$, power saturation EPR experiments indicated that at least one extracellular disulfide bond is disrupted with the current permutations of TM-cysteine substitutions. Collectively, our findings indicate that $A_{2A}R$'s TM cysteines are not essential for agonist binding, trafficking, or thermodynamic favorability, but play a role in ligand recognition and formation of its extensive extracellular disulfide bond network, suggesting a functional role. Next steps would be to first identify which TM cysteine(s) are critical for maintaining the formation of extracellular disulfide bonds and leverage the information gained by modeling and mutagenesis here to design new variants leaving critical TM cysteines intact.

Chapter 4 | VISUALIZING THE DIMERIC INTERFACE OF THE HUMAN ADENOSINE A_{2A} RECEPTOR USING PARAMAGNETIC RESONANCE AND CRYOGENIC ELECTRON MICROSCOPY

4.1. INTRODUCTION

G protein-coupled receptors (GPCRs), the largest and most diverse superfamily of receptors, are targeted by 40% of all modern drugs due to their implications in numerous diseases(Overington, Al-Lazikani, and Hopkins 2006; Rask-Andersen, Masuram, and Schiöth 2014). Oligomerization of GPCRs can lead to novel functions that are unseen in their monomeric form, altering neurological and pathological behaviors(L. El-Asmar 2004; Barki-Harrington, Luttrell, and Rockman 2003; Shivnaraine et al. 2016; S. P. Lee et al. 2004; H. Liu et al. 2016). $A_{2A}R$ serves as an excellent model to conduct structure-function studies of GPCR oligomerization—this member of the GPCR family can form both homo-oligomers(Canals et al. 2003; Schonenbach et al. 2016; Nguyen et al. 2021) and hetero-oligomers with dopamine D_2 receptor among others(Ferré et al. 2016; Kamiya et al. 2003). The objective of this chapter is to visualize the oligomeric interfaces of the human adenosine A_{2A} receptor ($A_{2A}R$).

$A_{2A}R$ can undergo oligomerization, but the mechanism and functional consequences are not known. As discussed in **Chapter 2**, this unusually long C-terminus of $A_{2A}R$ is necessary for $A_{2A}R$ to form stable oligomers, but its involvement at the molecular level is still unclear. It has also been demonstrated that $A_{2A}R$ can undergo both dimerization and higher-order oligomerization *in vitro*(Nguyen et al. 2021; Schonenbach et al. 2016), but the relationship between the two species is not understood. Mapping the oligomeric interface of

$A_{2A}R$ is the single most crucial step to understand how the C-terminus modulates $A_{2A}R$ oligomerization.

The focus of this chapter is on the structure and properties of $A_{2A}R$ homodimer with intact disordered C-terminus. High-resolution X-ray crystal(V.-P. Jaakola et al. 2008; Doré et al. 2011; Lebon et al. 2011) and cryo-EM(Garcıa-Nafrıa et al. 2018) structures have been successfully obtained of $A_{2A}R$, and solid-state magic angle spinning (MAS) nuclear magnetic resonance (NMR) based structure-function studies of $A_{2A}R$ reported on in several recent publications(Sušac et al. 2018; Eddy et al. 2018; Ye et al. 2016; Prosser et al. 2017), but none of these studies target the full-length WT $A_{2A}R$. X-ray crystallography requires the truncation of its 122-residue long C-terminus in order to enhance the conformational stability and thermostability of the receptor. As the focus of the project is to (i) visualize at the molecular level the oligomer interfaces of $A_{2A}R$ and (ii) eventually its functional consequences, it is compulsory that the full-length receptor be studied.

The strategy presented in this chapter for the structure determination of the $A_{2A}R$ dimers relies on three approaches: (i) determination of the coarse $A_{2A}R$ dimer structure by triangulation of pairwise dipolar EPR distance measurements, (ii) modeling of the overall shape of the $A_{2A}R$ dimer by cryo-EM (5 Å level resolution) and (iii) high-resolution cryo-EM SPA of the $A_{2A}R$ dimer, once sample conditions and types are optimized in (i) and (ii). Dipolar EPR and cryo-EM may currently be the *only* viable tools suitable for structure determination of the wild-type $A_{2A}R$ dimer because they can be used for biomolecular complexes of the size of $A_{2A}R$ dimer (~80 kDa), and importantly, can accommodate partial disorder that is inevitably present with the 122 residue long, intrinsically disordered, C-terminus of $A_{2A}R$. These tools

hence do not require thermostabilizing mutations. Equally important, both tools can acquire structure information of $A_{2A}R$ in biomimetic or native-like membrane environments upon rapid vitrification from solution state. Indeed, resolving the oligomeric interfaces of $A_{2A}R$ with regards to its C-terminus would provide not only ironclad evidence that the C-terminus is crucial for $A_{2A}R$ oligomerization but also information into its molecular mechanism and potentially functional consequences. Such information can also be extended to include the oligomerization of other GPCRs, which may depend on their C-termini and has been inadvertently dismissed by unguided C-terminal truncations.

The challenge for dipolar EPR is that the desired site of $A_{2A}R$ must be unambiguously and fully spin labeled, which is non-trivial for $A_{2A}R$ due to nonspecific labeling of buried cysteine sites, and hence was the focus of **Chapter 3**. The advantage of dipolar EPR is that it will yield intra-protein and intra-dimer distance distributions of the full $A_{2A}R$ ensemble in solution, and is forgiving of imperfect sample conditions, as long as $A_{2A}R$ is spin labeled at the desired sites and intact, making dipolar EPR an ideal first structure screening tool. Here, structure determination by pairwise distance measurements and triangulation will be dramatically enhanced if, for example, the overall shape of the $A_{2A}R$ dimer is known. The global shape can tell us whether the $A_{2A}R$ dimer is tight and intertwined, or a dumbbell like associated between the two $A_{2A}R$ units. This knowledge will help us generate and validate structural models for the $A_{2A}R$ dimers that reconcile the cryo-EM derived overall shape and dipolar EPR-derived intra- and inter-protomers. This is an example showcasing that cryo-EM, even at low resolution, will provide critical and unique insight into the overall dimer shape from the snapshots of vitrified $A_{2A}R$ yielding hundreds of thousands of different orientations.

Once cryo-EM data of sufficient quality is obtained, SPA can be pursued using a high-end cryo-EM instrument.

4.2. MATERIALS AND METHODS

4.2.1. Cloning and Preparation of $A_{2A}R$ in Detergent Micelles

Cloning, expression, and purification of the human adenosine $A_{2A}R$ receptor was performed as described in **2.2 above**. In brief, the multi-integrating pITy plasmid(Parekh, Shaw, and Wittrup 1996), previously used for overexpression of $A_{2A}R$ in *Saccharomyces cerevisiae*(O'Malley et al. 2009), contains a Gal1–10 promoter for galactose-induced expression, a synthetic pre-pro leader sequence which directs protein trafficking(Clements et al. 1991; Parekh, Forrester, and Wittrup 1995), and the yeast alpha terminator. The genes encoding $A_{2A}R$ variants with 10-His C-terminal tag were cloned into pITy downstream of the pre-pro leader sequence, with site-directed mutagenesis done using either splice overlapping extension(Bryksin and Matsumura 2010) or USER cloning using X7 polymerase(Nørholm 2010; Nour-Eldin et al. 2006). The plasmids were then transformed into *S. cerevisiae* strain BJ5464 (MATα ura3-52 trp1 leu2Δ1 his3Δ200 pep4::HIS3 prb1Δ1.6R can1 GAL) (provided by the lab of Anne Robinson at Carnegie Mellon University) using the lithium-acetate/PEG method(Gietz 2014). Transformants were selected on YPD G-418 plates (1% yeast extract, 2% peptone, 2% dextrose, 2.0 mg/mL G-418).

Single *S. cerevisiae* BJ5464 colonies were grown in YPD cultures (1% yeast extract, 2% peptone, 2% dextrose) at 30°C. Expression was induced by transferring the yeast cells into YPG (1% yeast extract, 2% peptone, 2% D-galactose) and grown overnight at 30°C. Cells were

pelleted and lysed with mechanical beads. Receptor was solubilized with a detergent micelle system of DDM (0.1% w/v) + CHAPS (0.1% w/v) + CHS (0.02% w/v). Solubilized protein was incubated with Ni-NTA resin (Pierce; #88221) overnight, washed extensively with low concentrations of imidazole (20–50 mM), and eluted with 500 mM imidazole.

For purification of active $A_{2A}R$, the IMAC-purified receptor was applied on the BioRad Duoflow FPLC for ligand affinity chromatography with xanthine amine congener (XAC, high-affinity $A_{2A}R$ antagonist, K_D = 32 nM; Sigma, St. Louis, MO, USA; #X103). Inactive $A_{2A}R$ was washed from the column before the active $A_{2A}R$ was eluted with 20 mM theophylline (low-affinity $A_{2A}R$ antagonist, K_D = 1.6 μM; Sigma, St. Louis, MO, USA; #T1633). To separate oligomeric species of active $A_{2A}R$, XAC-active receptor was subjected to size exclusion chromatography using a prepacked Tricorn Superdex 200 10/300 GL column (GE Healthcare). Analysis of SDS/PAGE and western blot was done to determine oligomeric states of the eluted $A_{2A}R$.

For samples that were planned for EPR experiments, the spin labeling reaction was implemented while $A_{2A}R$ was bound to IMAC resin to facilitate sufficient washing steps to remove excess spin label. Solubilized protein samples bound to IMAC resin were spin labeled overnight by adding 2.5 μL of 340 mM *S*-(1-oxyl-2,2,5,5-tetramethyl-2,5-dihydro-1H-pyrrol-3-yl) methylmethanesulfonothioate (MTSL) (Toronto Research Chemicals, #0875000) and gentle mixing. Excess MTSL was removed by washing the resin was extensively with at least 5 washes of 40 mL wash buffer (50 mM sodium phosphate, 300 mM sodium chloride, 10% (v/v) glycerol, 0.1% DDM, 0.1% CHAPS and 0.02% CHS, pH 8.0) for at least 20 minutes at

4°C before elution. The receptor was then subjected to ligand-affinity chromatography and SEC if separation of the oligomeric species is required as described in **2.2 above**.

For quantitation of protein concentration, BCA assay was applied using Pierce BCA Protein Assay Kit (Thermo Scientific, #23225) following manufacturer's instructions. Alternatively, UV-Vis spectroscopy was employed to measure absorption at 280 nm using a NanoDrop^{TM} 2000 Spectrophotometer (Thermo Scientific, #ND-2000)

4.2.2. Continuous-Wave EPR

Continuous wave (cw) EPR measurements were performed at RT on a 0.35 T Bruker EMX spectrometer equipped with dielectric cavity (ER4123D). Samples were loaded at a volume of 3.5 μL into a quartz capillary (0.6 mm i.d., 0.84 mm o.d.), which were then sealed on one end with Critoseal® (Oxford Labware; Catalog No. 8889-215003) and the other with beeswax. The experiments were done by irradiating the samples with 6 mW of microwave power at 9.74 GHz using a 2.5 G modulation amplitude, a sweep width of 150 G, and signal averaged over 40 21-second scans.

For quantitation of spin labeling efficiency, a calibration curve was obtained using 4-hydroxy-TEMPO dissolved in buffer (50 mM sodium phosphate, 300 mM sodium chloride, 10% v/v glycerol, pH = 8.0) at various concentrations from 12.5–200 μM. All cw-EPR spectra was background corrected with LabVIEW program Multicomponent by applying interpolation on the absorption spectrum. The amount of spin in each sample was calculated based on the second integral of the spectrum with the new baseline.

4.2.3. Double Electron Electron Microscopy

Prior to DEER analyses, the receptor was exchanged into deuterated buffer (deuterated D_2O, 50 mM sodium phosphate, 10% (v/v) glycerol, 0.1% (w/v) DDM, 0.1% (w/v) CHAPS and 0.02% (w/v) CHS, pH = 8.0). Sodium chloride was added afterwards to achieve the desired ionic strengths.

The DEER experiments were performed with a pulsed Q-band Bruker E580 Elexsys spectrometer, equipped with a Bruker QT-II resonator and a 300 W TWT amplifier with an output power of 10 mW for the recorded data (Applied Systems Engineering, Model 177Ka). The temperature of the cavity was maintained at 65 K using a Bruker/ColdEdge FlexLine Cryostat (Model ER 4118HV-CF100). The bridge is equipped with an Arbitrary Wave Generator to create shaped pulses for increased sensitivity. The samples were made in D_2O buffers with 30 % (v/v) deuterated glycerol (used as the cryoprotectant). To perform an experiment, approximately 40 μL of sample is added to a 3 mm OD, 2 mm ID quartz capillary and flash frozen in liquid nitrogen to preserve sample conformations.

The following 4-pulsed DEER sequence (**Figure 4-1**) was applied to all samples: $\pi_{obs}/2\ -\tau_1\ -\pi_{obs}\ -(t-\pi_{pump})-(\tau_2-t)-\pi_{obs}\ -\tau_2\ -$ echo The DEER signal $V(t)$ is recorded as the integral of the refocused echo as a function of time delay, t, between the Hahn echo and pump pulse. Rectangular observe pulses and chirp pump pulse were used with the following pulse durations: $\pi_{obs}/2$= 11 ns, π_{obs}= 22 ns, π_{pump}= 100 ns. The chirp pump pulse was applied with a frequency width of 60 MHz to excite a distinct spin population, referred to as B spins, while the observe pulse was set 33G up field from the center of the pump frequency range to probe another distinct spin population, A spins. τ_1 was set to 180 ns and τ_2 was set

according to the SNR profile of the dipolar signal. The data was acquired with resolution of 16 ns, 16-step phase cycling, and signal averaged until desirable SNR.

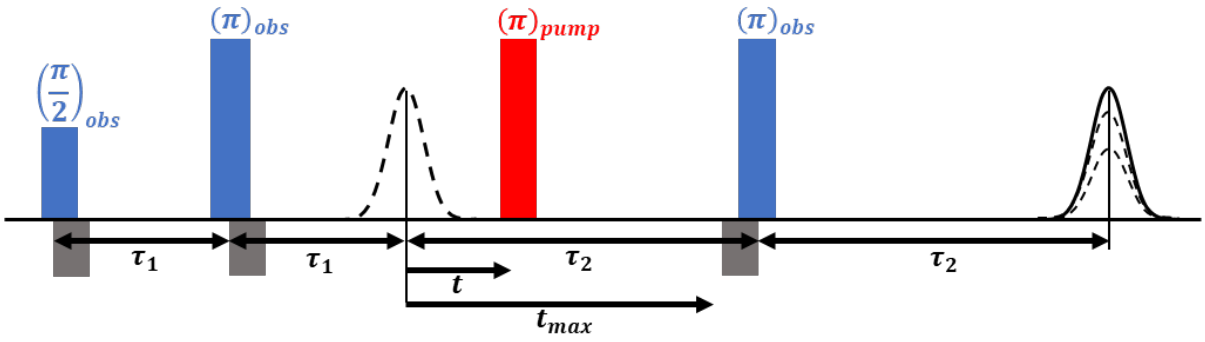

Figure 4-1. Four-pulse DEER sequence. Pump (red) and observer (blue) microwave pulses are used to selectively excite distinct spin populations, A and B. A two pulse Hahn echo is formed by exciting A spins at the observer frequency. A pump pulse is subsequently applied to flip the B spins followed by a varying time delay, $\boldsymbol{t}$, resulting in a modulation of the echo amplitude of A spins. At some delay, $\boldsymbol{\tau_2}$, the echo is refocused by an additional pulse at the observer frequency. The DEER experimental trace, $\boldsymbol{V(t)}$, is the integral of refocused echo as a function of pump pulse position, $\boldsymbol{t}$.

4.2.4. Negative-Staining Electron Microscopy

SEC-separated full-length wild-type $A_{2A}R$ dimer or monomer (0.05 mg/mL or 1 μM) was applied onto a glow-discharged 200-mesh copper Quantifoil 1.2/1.3 grids, or 200-mesh copper C-flat 1.2/1.3 grids. After 2 min of adsorption, the grid was blotted with filter paper to remove the excess sample, immediately washed twice with 50 μL of 0.75% uranyl formate solution for an additional 1 min. The grid was then further blotted with filter paper followed by vacuum aspiration to remove excess stain, and finally examined with either (i) a JEOL-2100F equipped with a direct detector or (ii) ThermoFisher Talos G2, both equipped with a

field emission gun and operated at an acceleration voltage of 200 kV, using a nominal magnification of 94,000x at a pixel size of 2.54 Å.

4.2.5. Cryo-EM Sample Preparation and Screening

Cryo-EM grids were prepared using a Vitrobot Mark IV system. $A_{2A}R$ (3 μL) at a concentration of 0.05 mg/mL was applied onto glow-discharged Quantifoil holey carbon grids (R1.2/1.3, 400 mesh copper) or 300-mesh UltrAuFoil R1.2/1,3 Au gold foil grids. The grids were blotted for 1.5–2 s with a blot force of 0 and 100% humidity before being plunged into ethane cooled by liquid nitrogen. Preliminary screening was done on either (i) a JEOL-2100 equipped or (ii) an Arctica, both operated at an acceleration voltage of 200 kV. Images were recorded at a defocus range from –1.5 to –3.5 μm at a nominal magnification of 36,000x, resulting in a pixel size of 1.114 Å. Each image was dose-fractionated into 42 video frames with a total exposure time of 2.5 s, resulting in a total dose of ~50 electrons/$Å^2$. SerialEM software was used for data collection.

Data analysis was done using RELION 2.0. Briefly, ~4,000 particles were auto picked with a reference particle (particle size: 200; box size: 320). 2D class averages were generated without CTF-correction. From the initial model, the particles were reclassified, generating more 2D averages. After six iterations of 3D refinement, preliminary 3D reconstructed model was generated and superimposed on top of a cryo-EM structure of $A_{2A}R$ monomers (PDB ID: 6GDG).

4.3. RESULTS AND DISCUSSION

4.3.1. MTSL-Labeled C-Terminal Residue C394 Is Immobilized Upon Receptor Oligomerization

Cryo-EM enables high-resolution structure of $A_{2A}R$ dimers, which can reveal information at the molecular level of the interface. However, this technique cannot resolve the intrinsically disordered C-terminus, which has been shown to be critical for $A_{2A}R$ oligomerization in **Chapter 2**. EPR spectroscopy is an excellent tool at probe the dynamics of disordered protein regions.

The first step in applying EPR in structural biology studies is to label the protein and determine the spin labeling efficiency (SLE). Besides the main target that is the C-terminal cysteine C394, $A_{2A}R$ contains six transmembrane cysteines that, as mentioned in **Chapter 3**, cannot be removed without adverse effects on the structure and function of the protein. Therefore, quantitation of SLE was done on the cw-EPR spectra of $A_{2A}R$-WT and the mutant C394S to determine the SLE of residue C394 and of the spurious TM cysteines. The results showed that the SLE of $A_{2A}R$-WT was 70–150%, while that of $A_{2A}R$-C394S was 40–70% (**Figure 4-2**). This indicated that the SLE of residue C394 was 30–80%, comparable with that of the spurious TM cysteines, which was 40–70% in total.

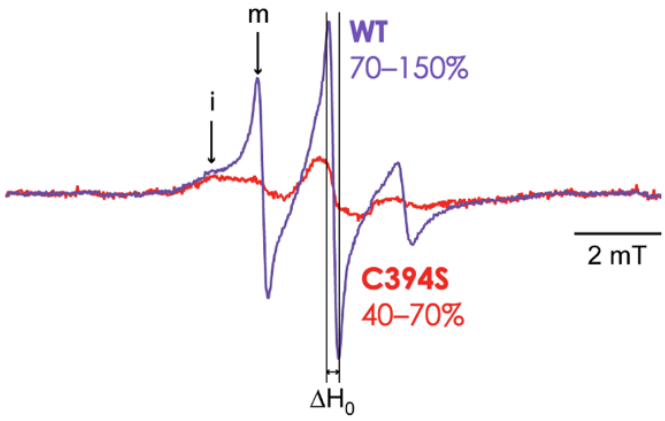

Figure 4-2. CW-EPR spectra for $A_{2A}R$-WT and C394S normalized by protein concentration to emphasize the difference in signal intensity and spin labeling efficiency upon removal of residue C394. Mobile and immobile features are indicated as "m" and "i", respectively. The mobile:immobile ratio indicates tertiary contacts experienced by the side chain of the MTSL label. The center peak linewidth is designated as ΔH_0 as an indicator of side chain mobility.

Moving forward, cw-EPR was performed on SEC-separated $A_{2A}R$-WT monomer, dimer, and high-order oligomers. Their resulted spectra were normalized by the intensity of the center peak to compare the mobile and the immobile features among them. The result showed that the mobile feature progressively diminished as the protein oligomerized, while the immobile feature progressively increased (**Figure 4-3**). This indicated that the mobility of the labeled C-terminal residue C394 decreased upon oligomerization, suggesting that the C-terminus is immobilized and thus directly involved at the oligomeric interface of $A_{2A}R$.

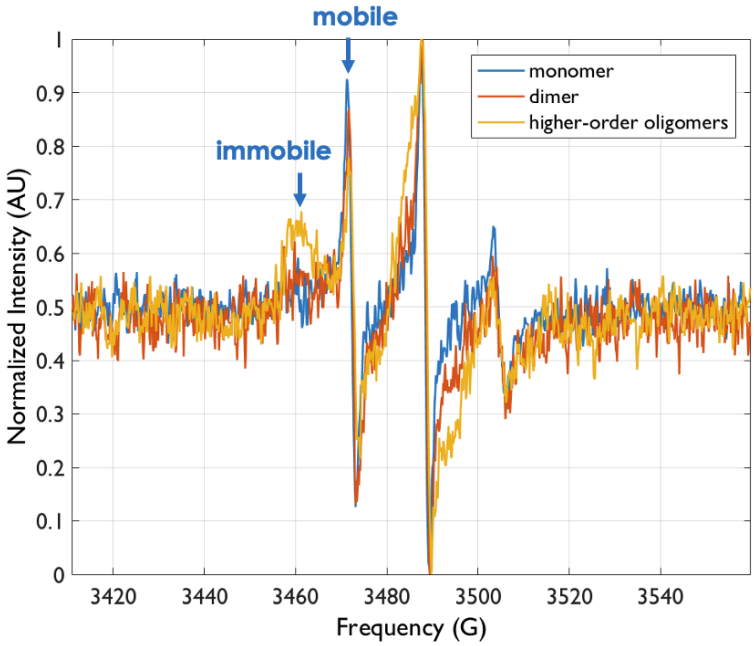

Figure 4-3. CW-EPR measurements of SEC-separated $A_{2A}R$ monomer, dimer, and higher-order oligomers, labeled with MTSL. The spectra are normalized by the intensity of the center peak. Mobile and immobile spectral features are indicated, and the mobile:immobile ratio can indicate tertiary contacts experienced by the side chain of the MTSL label.

4.3.2. DEER Revealed Large C394–C394 Distance in $A_{2A}R$ Oligomers at High Ionic Strength

We next sought to understand how the C-termini were positioned in $A_{2A}R$ oligomers by measuring intermolecular distances with DEER spectroscopy. As demonstrated in **2.3.5 above**, the oligomer levels of $A_{2A}R$ were positively correlated with the ionic strength of the buffer. Herein, we aimed to measure the intermolecular distance between C394 residues $A_{2A}R$-WT oligomers at 0.95 M ionic strength. Two controls were established: the same $A_{2A}R$-WT at 0.15 M ionic strength, which exists predominantly as monomers and thus lacks the intermolecular C394–C394 distance, and the mutant C394S, which lacks residue C394 altogether. The distance distribution was determined using the recently developed Tikhonov regularization of the time-domain DEER decay. The results revealed multiple distance spanning 1.5–4.5 nm in all three samples, suggesting that these distances involved the spurious TM cysteines. On the other hand, a distance at ~5.5 nm was observed only in the WT sample at 0.95 mM ionic strength (**Figure 4-4**). As this was the only sample that exists predominantly as oligomers and is spin labeled at residue C394, this 5.5 nm distance must be an intermolecular distance between two C394 residues in $A_{2A}R$ oligomers. This result suggested that the C394 residues in $A_{2A}R$ oligomers are not in close enough proximity to form disulfide bonds. Together with our finding in **2.3.2 above** that the disulfide linkages that stabilizes $A_{2A}R$ oligomers involve residue C394, such disulfide linkages must be formed between C394 and a different cysteine in the TM regions.

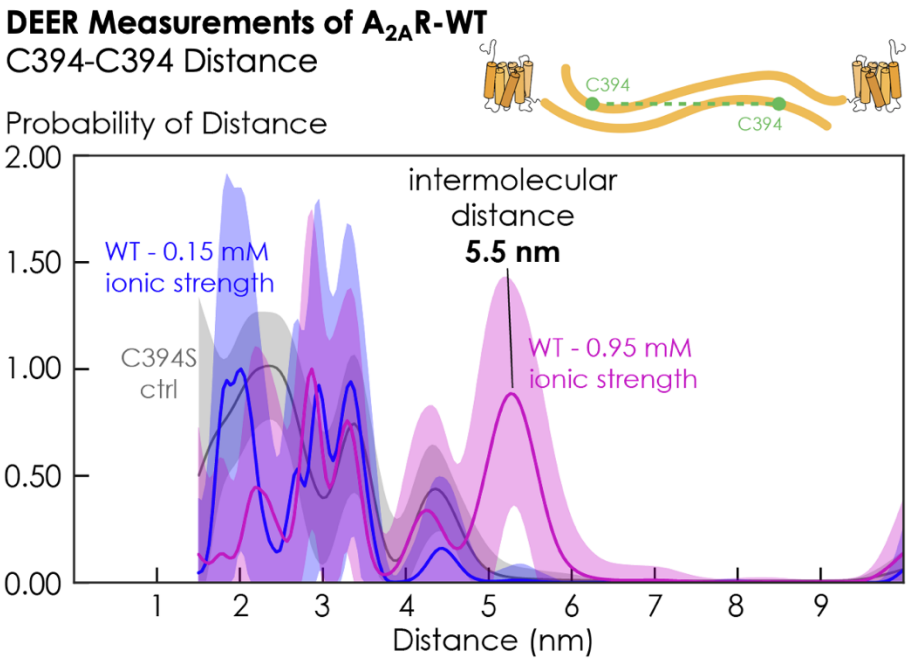

Figure 4-4. Distance distributions from DEER measurements of SEC-separated MTSL-labeled A_{2A}R-WT dimers with at 0.15 mM and 0.95 mM ionic strength. The sample is dominantly labeled at site C394, and hence the targeted distance was the intermolecular distance between residues C394. The mutant C394S is used as a negative control for signals from residue C394. The spectra are denoised with Tikhonov regularization.

4.3.3. Preliminary Cryo-EM 3D Model Revealed a "Dumbbell" Structure of $A_{2A}R$ Dimers Involving the Transmembrane Regions

Although DEER offers valuable insights into the conformation of the dynamic C-terminus in $A_{2A}R$ oligomers, high-resolution structural details of the interfaces could only be observed with cryo-EM. Sample preparation is critical for obtaining high-quality cryo-EM structure, especially for smaller targets such as $A_{2A}R$ dimers. As shown in **Chapter 2**, IMAC, ligand-affinity chromatography, and SEC can be used in tandem to obtain and separate distinct oligomeric species of full-length WT $A_{2A}R$ that are ligand-active. Negative-staining TEM on SEC-separated dimer and monomer of $A_{2A}R$ showed that no significant contaminant was observed in the micrographs, and that the protein particles are highly homogenous in size and shape, which confirmed that the sample purity meets the standard required to obtain cryo-EM images, potentially for SPA (**Figure 4-5**).

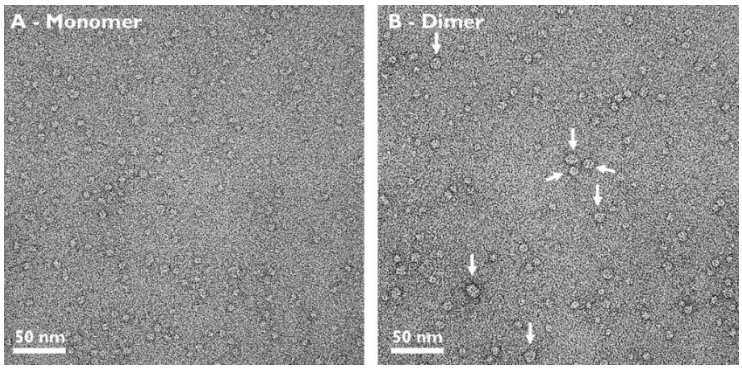

Figure 4-5. TEM images at 100,000X magnification under negative stain of SEC-separated monomer vs. dimer forms of $A_{2A}R$. The image of the monomer fraction **(A)** shows particles of high contrast and consistent size (~7 nm in diameter), while the image of the dimer fraction **(B)** shows significantly larger particles, with white arrows pointing at particles that are ~15 nm in size (particle sizes may vary depending on different orientations on the EM grid). Preliminary data shows that our sample preparation is free of interference from the buffer or contaminants.

Next, preliminary cryo-EM experiment was done on SEC-separated $A_{2A}R$ dimers and monomers using JEOL-2100F TEM with a direct detector. From a reference particle, ~4,000 other particles were auto picked, resulting in the 2D class averages shown in **Figure 4-6**. Refinement of the initial 3D model resulted in a final model of $A_{2A}R$ dimer of ~15-Å resolution with a C2 symmetry and the size approximately two times larger than the superimposed published cryo-EM structure of $A_{2A}R$ monomer (PDB ID: 6GDG[128]). The overall shape of the model suggests that the $A_{2A}R$ dimer is closer to a dumbbell model involving TM regions than one with two separate protomers connected by a C-terminus in between.

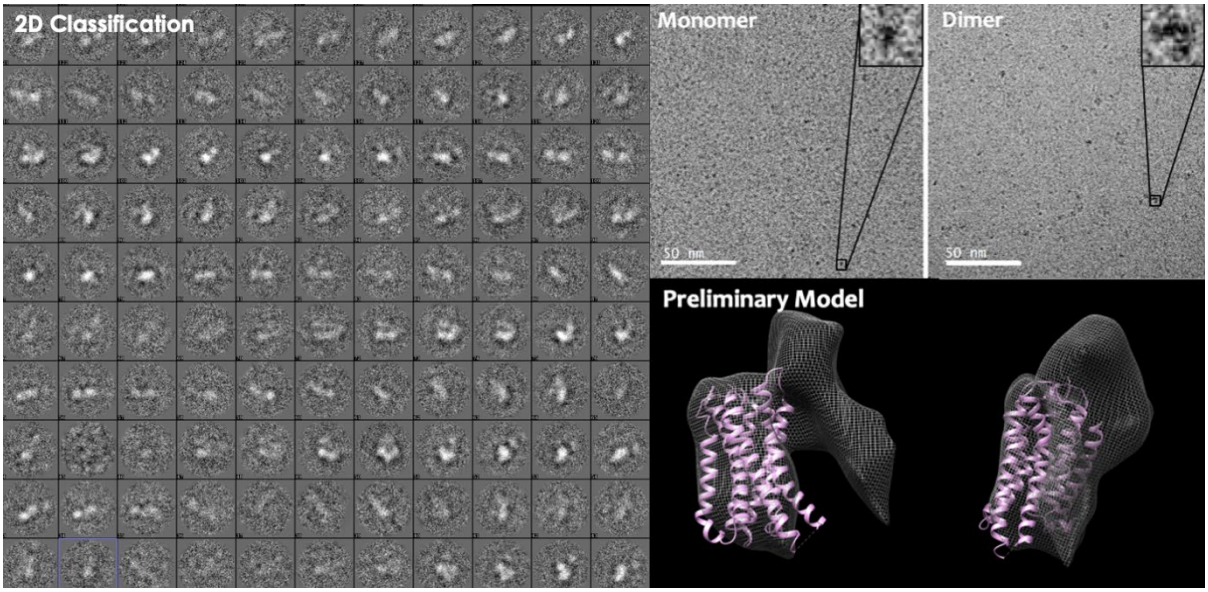

Figure 4-6. Preliminary cryo-EM data collection of SEC-separated $A_{2A}R$ dimers. 2D classification is performed on RELION 2.0 using ~4,000 auto picked particles from a reference. Representative particles of $A_{2A}R$ monomer and dimer are provided. Final model (gray hollow sphere) was found to assume a C2 symmetry with the size approximately two times larger than the cryo-EM structure of $A_{2A}R$ monomer (purple, PDB ID: 6GDG[128]).

4.4. CONCLUSIONS

This study demonstrated the potential of the EPR/cryo-EM combination in resolving interfaces of protein complexes involving an intrinsically disordered region. CW-EPR and DEER indicated that the C-terminus of $A_{2A}R$ is directly involved at its oligomeric interfaces, but in a conformation that excludes C394–C394 disulfide bond formation. Meanwhile, preliminary results from cryo-EM revealed that $A_{2A}R$ dimers exist as a "dumbbell" structure involving TM regions rather two protomers loosely connected by their C-termini. Such structure would allow the function of each $A_{2A}R$ protomer to be allosterically modulated, which has been established to be the main mechanism by which GPCR functions are tuned by receptor oligomerization(Changeux and Christopoulos 2016). The task remaining is to measure distances between other pairs of residues to triangulate the orientation of the C-terminus with respect to the oligomeric interfaces of $A_{2A}R$, as well as improve the resolution of $A_{2A}R$ dimer model obtained with cryo-EM to visualize its interfaces at the molecular level.

Chapter 5 | SOLUBILIZING TRANSMEMBRANE PROTEINS USING STYRENE MALEIC ACID LIPID PARTICLES

5.1. INTRODUCTION

5.1.1. Traditional Membrane Mimetics Are Not Optimal for Membrane Protein Purification

Integral membrane proteins (MPs) are among the most challenging targets in current research in biophysics and structural biology. Carrying out a wide range of vital roles(von Heijne 2007), they represent the majority of pharmacological targets(Overington, Al-Lazikani, and Hopkins 2006), including GPCRs, ~50% of which are druggable(Hauser et al. 2017). Nevertheless, the understanding of MPs in terms of structure and function remains poor compared with water-soluble counterparts. Constituting 20–30% of protein-encoding genes(Fagerberg et al. 2010), MPs are largely underrepresented in the protein data bank (PDB), with less than 2% of all deposited protein structures correspond to MPs(G. Wang and Dunbrack 2003). Owing to the hydrophobic nature of the transmembrane regions, MPs under native conditions are protected from aqueous solution by biomembranes. Structural and functional analyses of MPs thus require the use of membrane mimetics, with much effort directed towards maintaining the stability and activity of these proteins.

Various approaches have been used to extract and stabilize MPs, including the use of detergent micelles, amphipols, lipid bicelles, or nanodiscs bound by membrane scaffold proteins (**Figure 5-1**). These membrane mimetic platforms have been successful to certain extents, yet still have adverse effects on the embedded proteins or on downstream analyses, as detailed below:

- Detergents: It has been a common practice to isolate MPs using detergents(Garavito and Ferguson-Miller 2001), which generally form spherical micelles containing the proteins, detergent molecules, and sometimes lipids(le Maire, Champeil, and Møller 2000; Lichtenberg, Ahyayauch, and Goñi 2013). Despite the undeniable contribution of this approach to the understanding of MPs, detergent-based mimetics have several disadvantages. First, native interactions between the solubilized protein and lipids or other proteins are lost, as detergent molecules lift the protein completely out of its native lipid environment. In the case of GPCRs, it has been well-established that lipids such as cholesterol and phospholipids are essential for the proper functioning of these receptors(Muth, Fries, and Gimpl 2011; Michael A. Hanson et al. 2008; Dawaliby et al. 2015). Second, empirical screening is required to determine the suitable detergent(s) in terms of both composition and concentration for each new case of a protein with unknown characteristics(Privé 2007; Arachea et al. 2012). Third, detergent micelles do not mimic a lipid bilayer very well(Bordag and Keller 2010; Zhou and Cross 2013b), as their single hydrophilic surface is highly curved, their hydrophobic parts are highly disordered, and the monomeric detergent molecules undergo rapid and constant exchange between the micellar and free phase. As a result, this approach removes the lateral pressure exerted by the lipid bilayer on the protein, which is particularly harmful to conformationally dynamic proteins such as GPCRs. Consequently, MPs solubilized in detergent micelles generally show lower stability, higher propensity of aggregation, or even altered function(Quick et al. 2012) and conformation(Zhou and Cross 2013a; Zoonens et al. 2013).

- Amphipols: Consisting of a polyacrylate backbone together with hydrophobic and hydrophilic sidechains(Tribet, Audebert, and Popot 1996), amphipols help overcome a number of adverse effects posed by the use of detergents(Zoonens and Popot 2014). Their monomers exhibit lower exchange rate between the amphipols and solution, which improves the stability of the embedded protein and allows for lower concentrations of amphipols in use. Nevertheless, this platform still lacks an actual lipid bilayer environment.
- Bicelles: This alternative is discoidal structures consisting of phospholipids and detergents in a defined ratio(Dürr, Soong, and Ramamoorthy 2013). The composition can be tuned to achieve different sizes ranging from 8–50 nm in diameter(Vold and Prosser 1996). The larger bicelles are particularly beneficial for nuclear magnetic resonance (NMR) spectroscopy due to their alignability in the magnetic field(Howard and Opella 1996). However, the types of lipids that can form bicelles are limited and their stability is a concern.
- Membrane scaffolding protein (MSP) nanodiscs: In this relatively new approach, MPs are transferred from detergent micelles into lipid nanodiscs bounded by MSPs(Bayburt, Grinkova, and Sligar 2002), which protect the hydrophobic core of the lipids from water. The size of nanodiscs can be controlled by varying the types of MSP, enabling the formation of nanodiscs ranging from 6–17 nm in size(Grinkova, Denisov, and Sligar 2010; Park et al. 2011; X. Wang et al. 2015). As a result, this platform appears to be applicable to a wide variety of proteins, providing relatively high stability(Bayburt and Sligar 2010; Schuler, Denisov, and Sligar 2013). However, the presence of the scaffold protein may interfere with downstream analysis of the

encapsulated protein, especially in experiments involving UV spectroscopy, intrinsic tryptophan fluorescence, or circular dichroism.

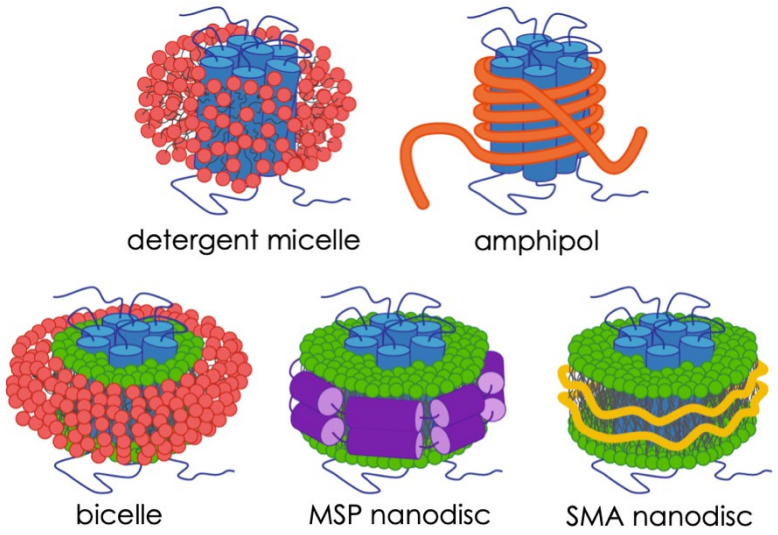

Figure 5-1. Common membrane mimetic platforms for transmembrane protein solubilization. The protein is indicated in blue. Detergent micelle and amphipol are non-bilayer systems, while bicelle, MSP nanodisc, and SMA nanodisc are bilayer systems. (Figure from Dörr, J. M. et al, *Eur. Biophys. J.* **2016**, 45, 3–21.)

The membrane mimetics described above all have one common disadvantage: an initial temporary extraction of proteins from membranes with destabilizing detergents is required, which can potentially be harmful for protein structure and function.

5.1.2. Styrene-Maleic Acid Lipid Particles as the Most Promising New Method for the Studies of MPs

In contrast to micelles, amphipols, bicelles, and MSP nanodiscs, styrene maleic acid lipid particles (SMALPs) (**Figure 5-1**) enable detergent-free isolation of membrane proteins and retention of the native lipid environment(Jamshad, Grimard, et al. 2015; Orwick et al.

2012). Its ability to interact with phospholipids to spontaneously form discoidal structures was first discovered in 2000, rendering this platform useful in drug delivery(Tonge and Tighe 2001) and membrane protein solubilization(Knowles et al. 2009). In fact, they can be inserted into biological membranes to enable direct extraction of integral proteins without transient destabilization of proteins caused by the use of detergent(Long et al. 2013).

In essence, a hydrolysis reaction is required to convert styrene-maleic anhydride into styrene-maleic acid (SMA). SMA is amphipathic in nature due to the presence of the hydrophobic styrene units and the hydrophilic carboxyl/carboxylate groups. The degree of hydrophobicity depends not only on the S:MA ratio but also on pH. Each maleic acid unit in a monomer bears two carboxyl groups with vastly different pKa values: 6 and 10 (**Figure 5-2**).(Banerjee, Pal, and Guha 2012). As a result, at neutral and high pH, most of the maleic acid units will carry at least one negative charge, and electrostatic repulsions between the charged carboxylate groups overwhelms the hydrophobic effect, leading to effective dissolution of SMA in aqueous solution. On the other hand, at pH < 6, the charges on the maleic acid units are lost, allowing the hydrophobic effect to dominate, which leads to precipitation. The nanodiscs formed by SMALPs are ~10 nm in diameter and ~4.6 nm in thickness(Jamshad, Grimard, et al. 2015). The size of these nanodiscs appears to depend not on lipid composition(Scheidelaar et al. 2015) but rather on external factors such as pH, salt concentration, or the composition and chain length of the SMA polymers.

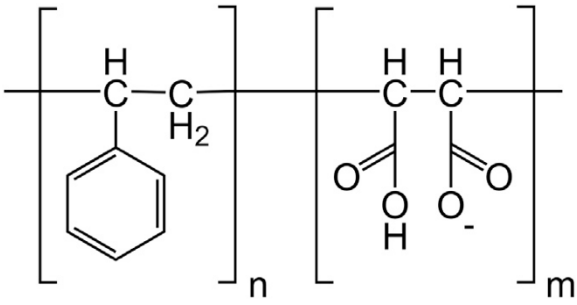

Figure 5-2. Chemical structure of the SMA polymer at 50% ionization. The S:MA ratio (n/m) varies among different types of SMA. (Figure from Scheidelaar et al, *Biophys. J.* **2016**, 111, 1974–1986.)

The interactions between SMA and lipids involve the intercalation of the phenyl groups of SMA in between the lipid acyl chains, as well as the electrostatic interactions between the carboxyl groups and the lipid head groups(Jamshad, Grimard, et al. 2015; Orwick et al. 2012). Scheidelaar et al used turbidimetry to study the kinetics of membrane solubilization by SMA, proposing a three-step model to describe its mode of action(Scheidelaar et al. 2015). These steps involve (1) the binding of SMA to the surface of the lipid bilayer, promoted by increasing the amount of SMA and modulated by electrostatic interactions, (2) the insertion of SMA into the hydrophobic core of the membrane, strongly affected by lipid packing and bilayer thickness, and (3) the solubilization of the bilayer and the simultaneous formation of nanodiscs. In contrast with other membrane mimetic platforms, SMA forms nanodiscs much more efficiently thanks to the small size and rigidity of its phenyl groups, allowing rapid insertion into lipid bilayers with little entropy cost or steric hindrance upon nanodisc formation(Scheidelaar et al. 2015).

SMA polymers have been shown to effectively solubilize MPs directly from intact membranes of bacteria(Postis et al. 2015; Dörr et al. 2014; Swainsbury et al. 2014), yeast(Gulati et al. 2014; Jamshad, Charlton, et al. 2015; Skaar et al. 2015), insect(Gulati et al. 2014), and human cells(Gulati et al. 2014; Jamshad, Charlton, et al. 2015). The MPs that have been successfully captured with SMA range from those with one single α-helix(Paulin et al. 2014) to protein oligomers of up to 36 transmembrane domains(Postis et al. 2015). Once solubilized, the embedded protein can then be purified with SEC, IMAC, among other standard purification techniques. It has been shown that SMALPs are superior to detergent micelles in both function retention and downstream structural analysis for membrane proteins, specifically the *E. coli* multidrug transporter AcrB[135], ATP-binding-cassette transporters[136], and potassium channel KcsA.[137] When it comes to GPCRs, SMALPs have been successfully applied on several members of this class of receptors(Logez et al. 2016; Broecker, Eger, and Ernst 2017; Hall et al. 2018), including $A_{2A}R$, which showed enhanced stability and activity compared with detergent or MSP nanodiscs(Routledge et al. 2020). Among the developed approaches to isolate GPCRs, SMALPs remain the only one that is totally detergent-free, while preserving the native lipid environment along with the lateral pressure it exerts on the embedded receptor.

5.1.3. Limitations of SMALPs

It may appear that SMALPs could become the superior membrane mimetic platform that replaces all the conventional approaches, but much further research is needed to understand and improve SMALPs in many aspects. Since its action involves insertion of the polymers into the lipid bilayer, lipid packing and phospholipid order strongly affects how efficiently SMA solubilizes the membrane. Indeed, SMA has been shown to exhibit low

solubilization efficiency on densely packed membranes(Bell, Frankel, and Bricker 2015; Swainsbury et al. 2017), implying that high overexpression of proteins should be avoided. Next, SMA solubilization depends heavily on pH and ionic strength. The optimal pH range is between 6.4–8.3(Scheidelaar et al. 2016; Grethen et al. 2017), which means one cannot study proteins that are only functional or stable out of this range. Similarly, SMA typically works best at 150–300 mM NaCl(Scheidelaar et al. 2015; 2016; Grethen et al. 2017), potentially limiting the function(Han et al. 2020) or oligomerization (see **2.3.5 above**) of transmembrane proteins.

Another aspect that should be considered is the size of the nanodiscs. Unlike detergent micelles, which simply wrap around the protein and thus are more forgiving when it comes to the size of the protein, SMALP is more rigid, about 10–12 nm in diameter on average. This property of SMALPs may make it difficult to solubilize large proteins, especially those that form high-order oligomeric complexes. Although the size can be controlled by varying the S:MA ratio(Hall et al. 2018; Craig et al. 2016; Tanaka et al. 2015), SMA:protein ratio(Gulati et al. 2014; Smirnova et al. 2016), ionic strength(Gulati et al. 2014; Smirnova et al. 2016; Morrison et al. 2016), or even the types of polymers(Ravula et al. 2018; Oluwole et al. 2017), such efforts are empirical, thus costly and time-consuming.

5.1.4. The Human Adenosine A_{2A} Receptor and the Bacterial Proteorhodopsin as Model Transmembrane Proteins

As outlined in **1.3 above**, the second major aim of the project is to visualize the dimeric interface of $A_{2A}R$. One viable approach is to use cryo-EM to obtain a 3D image of the dimer using single particle analysis (SPA). Compared with detergent micelles, MSP nanodiscs

provide a superior environment for biophysical and structural studies of GPCRs, as they can retain vital GPCR signaling and protein-lipid contacts that is lost in detergent-reconstituted structures(Yin et al. 2020; Y. Lee et al. 2020; Staus et al. 2020). However, as mentioned in **5.1.1 above**, the transient destabilization of protein during the intermediate step of detergent reconstitution could lead to solubilization-induced loss of function. The use of SMALPs offers a promising avenue towards structural analysis of the native form of $A_{2A}R$ dimers with intact structure and function. The goals of this study are (1) to show that $A_{2A}R$ can easily be reconstituted in SMALPs without harmful functional impacts, (2) to demonstrate SMALPs is a better membrane mimetic for $A_{2A}R$ than detergent micelles in terms of generation of cryo-EM images of high quality.

On the other hand, given that the use of SMALPs in studying GPCRs is still in its infancy compared with other well-established approaches (see **5.1.3 above**), it could be challenging to use the limited knowledge of this platform on $A_{2A}R$ dimers, which are inherently small in size (~80 kDa), produced in low yield, and quite delicate in terms of activity and stability. An alternative model protein is proteorhodopsin (PR), a seven-transmembrane proton pump (**Figure 5-3**) that is robust and functional in a wide variety of membrane mimetic environments, including micellar(Idso et al. 2019), bicellar(Tunuguntla et al. 2013; Han et al. 2020; Lindholm et al. 2015), and nanodisc systems(Ranaghan et al. 2011). PR is an important transmembrane protein whose functional properties can be measured as a function of systematic modulation of the extent of oligomerization(Hussain et al. 2015b) or the makeup of the biomimetic environment(Tunuguntla et al. 2013; Lindholm et al. 2015; Han et al. 2020; Idso et al. 2019). Its hexameric form is ~150 kDa in size, which would significantly increase

the contrast of cryo-EM micrographs. Furthermore, PR could be produced in much higher quantity and is much more stable than $A_{2A}R$.

This important bacterial protein uses retinal as chromophore to carry out its fundamental light-activated proton pumping function. Hence, PR's proton transport capacity can be conveniently assessed by using optical absorption of the embedded retinal via two benchmarks: the rate of proton transport and the population of PR's active state. The proton transport rate of PR is measured by time-resolved optical absorbance change after excitation with a pulsed green laser(G. Váró and Lanyi 1991; György Váró et al. 2003; Dioumaev et al. 2002). Photoactivated PR undergoes a series of conformational changes that perturb the local environment of the retinal chromophore, resulting in photo-intermediates that constitute the photochemical reaction cycle. Such transient conformational states, sequentially labeled as *K*, M_1/M_2, *N*, and *PR*', each of which contribute to the overall optical absorbance spectrum, with partially resolved absorbances centered respectively at 555 nm, 410 nm, 560 nm, and 520 nm. Meanwhile, the active population of PR is one in which the primary proton transport depends on the protonation state of its primary proton acceptor D97, *i.e.*, pKa_{D97}(Dioumaev et al. 2002; Beja 2000; Dioumaev et al. 2003; W.-W. Wang et al. 2003). Light-induced isomerization of the embedded retinal enables proton transfer to residue D97, thus requiring the aspartic acid to be deprotonated(Dioumaev et al. 2003). The active form of green-light absorbing PR in the resting state absorbs maximally at around 518 nm, exhibiting a pink color. Conversely, when D97 is protonated and therefore unavailable to accept protons, PR absorbs maximally at around 535 nm, exhibiting a purple color. Given this pH-dependent color transition, the pKa_{D97} of PR can be readily measured via optical absorption spectroscopy as a function of bulk solution pH,

followed by determination of the isosbestic point at 570 nm(Dioumaev et al. 2002; W.-W. Wang et al. 2003; Ikeda, Furutani, and Kandori 2007).

In this study, we studied the proton transport properties of PR in SMALPs compared with in DDM micelles and synthetic POPC/POPG liposomes. The proton transport function of PR was evaluated via measurements of pKa_{D97} and photocycle kinetics. The goal was to test whether SMALPs can solubilize PR efficiently, whether the bulky hexameric form can be encapsulated, and whether its proton transport function is intact.

5.2. MATERIALS AND METHODS

5.2.1. Cloning and Expression of $A_{2A}R$

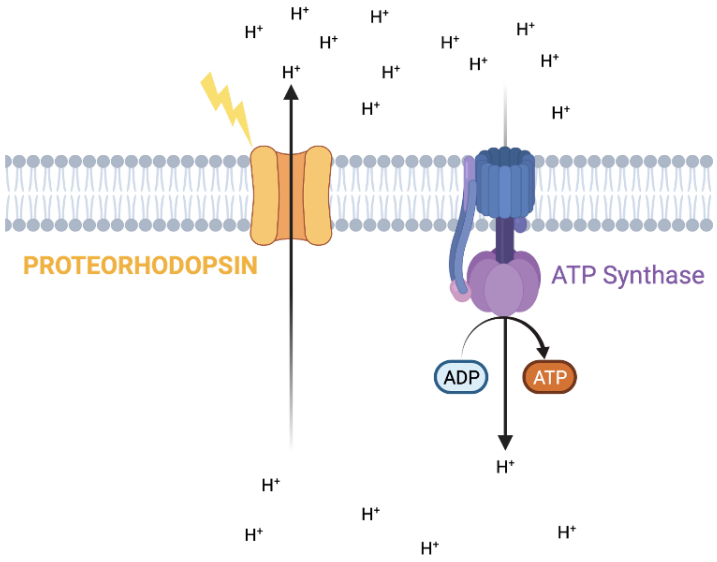

Figure 5-3. Proteorhodopsin acts as a light-activated proton transporter, increasing the proton concentration on the exterior of the cell. ATP synthase is among the proteins that rely on proton gradient to carry out their functions.

Cloning, expression, and purification of the human adenosine $A_{2A}R$ receptor was performed as described in **2.2 above**. In brief, the multi-integrating pITy plasmid(Parekh,

Shaw, and Wittrup 1996), previously used for overexpression of $A_{2A}R$ in *Saccharomyces cerevisiae*(O'Malley et al. 2009), contains a Gal1–10 promoter for galactose-induced expression, a synthetic pre-pro leader sequence which directs protein trafficking(Clements et al. 1991; Parekh, Forrester, and Wittrup 1995), and the yeast alpha terminator. The genes encoding $A_{2A}R$ variants with 10-His C-terminal tag were cloned into pITy downstream of the pre-pro leader sequence, with site-directed mutagenesis done using either splice overlapping extension(Bryksin and Matsumura 2010) or USER cloning using X7 polymerase(Nørholm 2010; Nour-Eldin et al. 2006). The plasmids were then transformed into *S. cerevisiae* strain BJ5464 (MATα ura3-52 trp1 leu2Δ1 his3Δ200 pep4::HIS3 prb1Δ1.6R can1 GAL) (provided by the lab of Anne Robinson at Carnegie Mellon University) using the lithium-acetate/PEG method(Gietz 2014). Transformants were selected on YPD G-418 plates (1% yeast extract, 2% peptone, 2% dextrose, 2.0 mg/mL G-418).

Single *S. cerevisiae* BJ5464 colonies were grown in YPD cultures (1% yeast extract, 2% peptone, 2% dextrose) at 30°C. Expression was induced by transferring the yeast cells into YPG (1% yeast extract, 2% peptone, 2% D-galactose) and grown overnight at 30°C. Cells were pelleted and stored at –80°C.

5.2.2. Solubilization of $A_{2A}R$ with DDM

Cell pellets were lysed with mechanical beads in lysis buffer (50 mM sodium phosphate, 300 mM sodium chloride, 10% (v/v) glycerol, pH = 8.0, 2% (w/v) DDM, 1% (w/v) CHAPS, and 0.2% (w/v) CHS and an appropriate amount of 100x Pierce Halt EDTA-free protease inhibitor (Pierce, Rockford, IL, USA #78439)). Beads were separated using a Kontex column.

Unlysed cells were removed by centrifugation at 3,220 × g for 10 min. Receptor was let solubilized on rotary mixer for 3 hours before cell debris was removed by centrifugation at 10,000 × g for 30 min.

5.2.3. Cloning and Expression of PR

Cysteine-free green-light absorbing PR with a C-terminal 6x His tag, both with and without the E50Q mutant that increased the population of monomeric PR(Maciejko et al. 2015), were expressed and purified using the protocol described previously(Stone et al. 2013; Hussain et al. 2015b). Briefly, site-directed mutagenesis with a two-stage polymerase chain reaction (PCR) technique(W. Wang and Malcolm 1999) was applied to introduce the desired single mutation mentioned above. The PR gene template with desired mutations was then cloned into a pET26b (+) vector (Novagen) for expression in BL21(DE3). PR expression was induced at an optical density of 0.8–1 by adding IPTG (1 mM) and trans-retinal (10 μM). Cells were harvested after 5 hrs of protein expression by centrifugation at 3,000 × g for 10 min at 4°C. Cell pellets were stored at –80°C.

5.2.4. Solubilization of PR with DDM and POPC/POPG

PR-expressing *E. coli* membranes were prepared by lysing the cell pellets with probe-tip sonication in lysis buffer (50 mM KPO_4, 150 mM KCl, 0.02 mg/mL lysozyme, 0.1 mg/mL DNase I, and 2 mM $MgCl_2$, with an appropriate amount of antiproteolytics). Lysate was spun at 100,000 × g to extract the membranes, which were then solubilized overnight in 2% w/v DDM.

Large unilamellar vesicles (LUVs) with desired composition were prepared by a lipid extrusion method. Lipid stocks dissolved in chloroform were purchased from Avanti Polar Lipids (AL) and mixed to achieve a desired molar ratio between different lipid species. The lipid mixture was then dried under a nitrogen stream and further desiccated under vacuum overnight to ensure the removal of residue chloroform. The dried lipids were reconstituted with a HEPES buffer (10 mM HEPES, 150 mM NaCl, pH 6.7), and lipid vesicles were extruded through the Avanti mini-extruder for 19 times using filters with 200 nm pore size. The prepared lipid vesicles were then mixed with DDM surfactant solution to achieve a final DDM concentration 2 times the DDM critical micelle concentration (CMC, 0.0088 w/v %). The mixture was gently shaken for 1 hr to form lipid-surfactant complexes, and the desired type of PR was then added to the mixture with a 1:50 PR-to-lipid molar ratio. The DDM surfactants in PR-lipid-DDM complex were then removed by using six vials of ~160 mg polystyrene BioBeads SM2 (Bio-Rad) to drive the formation of PR liposomes.

5.2.5. Solubilization of $A_{2A}R$ and PR with SMALPs

$A_{2A}R$-expressing *S. cerevisiae* or PR-expressing *E. coli* membranes were prepared by lysing cell pellets in lysis buffer (50 mM Tris-HCl, 10% v/v glycerol, 300 mM NaCl) with mechanical beads (for $A_{2A}R$) or a French press (for PR) at 4°C. Lysate was then centrifuged at 10,000 × g for 30 minutes and then at 100,000 × g for 1 hr to extract the membranes.

SMALP30010P was purchased from Orbiscope (Netherlands). $A_{2A}R$-expressing *S. cerevisiae* or PR-expressing *E. coli* membranes, at a final concentration of 40 mg/mL, were incubated in 50 mM Tris-HCl, 10% glycerol, 300 mM NaCl, 2.5% w/v SMA, pH 8.0 for 20 h at 25°C with gentle rotation. Non-solubilized material was sedimented at 100,000 × g for 1 hr at 4°C to yield a supernatant containing $A_{2A}R$-SMALP or PR-SMALP and a pellet containing non-solubilized proteins. This pellet was resuspended in the same buffer and volume as the supernatant. SDS-PAGE followed by Western Blot with Anti-$A_{2A}R$ or Anti-His antibody was performed on the pellet and the supernatant. Densitometry was then used to determine the relative amount of $A_{2A}R$ or PR, from which SMA solubilization yield was calculated.

5.2.6. Purification of $A_{2A}R$ and PR

Solubilized protein was incubated with Ni-NTA resin (Pierce; #88221) overnight. Protein-resin mixture was then washed extensively in purification buffer containing low imidazole concentrations (20–50 mM). $A_{2A}R$ was eluted into purification buffer containing 500 mM imidazole. Prior to further chromatographic purification, imidazole was removed using a PD-10 desalting column (GE Healthcare, Pittsburgh, PA, USA; # 17085101).

For PR solubilized in DDM or POPC/POPG, the removal of His-tag was done by a tobacco etch virus (TEV) protease (Sigma Aldrich), which recognize and cleave the sequence ENLYFQS in between the C-terminus of PR and the His-tag. His-tag removal reaction was done by first buffer exchanging PR into a 50 mM Tris-HCl buffer (pH 8) with 0.5 μM EDTA, 1 mM DTT and 0.05% w/v DDM after its elution from Ni-NTA resin. Next, TEV protease was added to the PR solution at a protein-to-protein ratio of 1:100 (w/w) and incubated overnight at 4°C with gently mixing. The reacted solution was then buffer exchanged into the 50 mM KPO_4 buffer (pH = 8.2) with 150 mM KCl and 0.05% w/v DDM using the PD-10 desalting column for removing the EDTA, and then combined with the Ni-NTA resin. The mixture was mixed for 5 hours at 4°C to remove the unreacted PR that still has His-tag and residual TEV protease from the solution. The collected solution with Ni-NTA resin removed was the PR product with its His-tag removed.

For purification of active $A_{2A}R$, the IMAC-purified receptor was applied on the BioRad Duoflow FPLC for ligand affinity chromatography with xanthine amine congener (XAC, high-affinity $A_{2A}R$ antagonist, K_D = 32 nM; Sigma, St. Louis, MO, USA; #X103). Inactive $A_{2A}R$ was washed from the column before the active $A_{2A}R$ was eluted with 20 mM theophylline (low-affinity $A_{2A}R$ antagonist, K_D = 1.6 μM; Sigma, St. Louis, MO, USA; #T1633). To separate oligomeric species of active $A_{2A}R$, XAC-active receptor was subjected to size exclusion chromatography using a prepacked Tricorn Superdex 200 10/300 GL column (GE Healthcare). Analysis of SDS/PAGE and western blot was done to determine oligomeric states of the eluted $A_{2A}R$.

5.2.7. SDS-PAGE and Western Blotting of $A_{2A}R$

10% SDS-PAGE gels were hand-casted in BioRad Criterion empty cassettes (BioRad; #3459902, 3459903). Lysate controls were prepared by lysis of 5 OD cell pellets with 35 μL of YPER (Fisher Scientific, Waltham, MA, USA # 8990) at RT for 20 min, incubation with 2x Laemmli buffer (4% (w/v) SDS, 16% (v/v) glycerol, 0.02% (w/v) bromophenol blue, 167 M Tris, pH 6.8) at 37ºC for 1 h, and centrifugation at 3,000 × g for 1 min to pellet cell debris. Protein samples were prepared by incubation with 2x Laemmli buffer at 37ºC for 30 min. For all samples, 14 μL (for 26-well gel) or 20 μL (for 18-well gel) was loaded per lane, except for 7 μL of Magic Mark XP Western protein ladder (Thermo Scientific, Waltham, MA, USA; #LC5602) as a standard. Electrophoresis was carried out at 120 V for 100 min. Proteins were transferred to 0.2-μm nitrocellulose membranes (BioRad; # 170-4159) via electroblotting using a BioRad Transblot Turbo, mixed MW protocol. Membranes were blocked in Tris-buffered saline with Tween (TBST; 150 mM sodium chloride, 15.2 mM Tris-HCl, 4.6 mM Tris base, pH = 7.4, 0.1% (v/v) Tween 20 (BioRad; #1706531)) containing 5% (w/v) dry milk, then probed with anti-$A_{2A}R$ antibody, clone 7F6-G5-A2, mouse monoclonal (Millipore, Burlington, MA, USA; #05-717) at 1:500 in TBST with 0.5% (w/v) dry milk. Probing with secondary antibody was done with a fluorescent anti-mouse IgG H&L DyLight 550 antibody (Abcam, Cambridge, MA, USA; #ab96880) at 1:600 in TBST containing 0.5% (w/v) milk.

Western blot was analyzed with Image Lab 6.1 software (Bio-rad), with built-in tool to define each sample lane and to generate an intensity profile. Peaks were manually selected and integrated with the measure tool to determine the amount of protein present.

5.2.8. BN-PAGE, Western Blot, and SDS-PAGE Analyses of PR

Blue native polyacrylamide gel electrophoresis (BN-PAGE) was performed using an XCell SureLock® Mini-Cell apparatus with NativePAGE™ Bis-Tris Protein Gels having a 3-12% acrylamide gradient (ThermoFisher). PR sample preparation and gel electrophoresis were performed according to the instructions provided by the manufacturer. The destained gel was then imaged with a ChemiDoc MP imaging system (Bio-Rad) using the default protocol for Coomassie blue dyes. Western blotting of BN-PAGE was performed using an XCell II^{TM} Blot Module by following the instructions for Western blotting of NativePAGE™ Gels provided by the manufacturer. The blotted PVDF membrane was rinsed with deionized water and blocked in a TBST buffer containing 5% (w/v) dry milk. The immunodetection was then done by applying HRP conjugated Anti-6X His tag® antibody (Abcam, Cambridge, MA, USA; ab1187) targeted to the six-histidine tag at the N-terminus of PR at 1:5000 in a TBST buffer containing 0.5% (w/v) milk. The membrane was then imaged with a ChemiDoc MP imaging system (Bio-Rad) using the default protocol for chemifluorescence dyes.

SDS-PAGE was performed using a Bio-Rad electrophoresis apparatus with Criterion TGX Stain-Free gels having an 8-16% acrylamide gradient (Bio-Rad). Samples containing ~3 μg PR were incubated at 37^{o}C for 30 minutes to 1 hour with Laemmli buffer (final SDS concentration of 1%), and then centrifuged to remove the unsolubilized portions. The gel was run at 120 V for one hour and imaged with a ChemiDoc MP imaging system (Bio-Rad) using a PR-specific protocol (excitation with green epi light and 695/705 filters to detect emission) based on the fluorescence properties of PR.172 Protein markers (Precision Plus, Bio-Rad) and

total proteins were further imaged using the Stain-Free protocol of ChemiDoc MP. Molecular weight estimates were calculated using the ImageLab software (Bio-Rad).

5.2.9. Optical Absorption Measurements and Analyses of PR

The UV-visible absorption spectra of PR under different conditions were taken by a Shimadzu UV-1800 spectrophotometer. All samples were prepared to have an optical density above 0.3 at 520 nm and an initial volume of 750 μL by diluting the PR sample stocks with the HEPES buffer mentioned above for lipid samples. For each PR sample, the optical absorbance between a wavelength range of 400-750 nm in increments of 0.5 nm were recorded under at least 20 different pHs that spread equally between pH 4 and 10. The pH of each sample was adjusted by titrating with 1 M NaOH (aq.) and 1 M HCl (aq.), and the pH was then measured by Orion Star™ A111 pH benchtop meter (Thermo Fisher Scientific) equipped with an Orion ROSS® Micro pH electrode before each optical absorption measurement. The pKa of PR D97 residue was determined by analyzing the pH-dependent optical absorption transition. The obtained optical absorption spectra under various pH conditions were processed by subtracting each absorption spectrum from the most basic one (pH~10). The differential absorbance at 570 nm, which supposed to be the wavelength that showed the greatest differential absorbance change, was normalized and fitted by the Henderson-Hasselbalch equation. The fitting was done by MATLAB (Mathworks, MA) using home-built codes. The detail of the fitting algorithm and codes was published in our previous study(Idso et al. 2019).

The time-resolved UV-visible measurements were done by a SpectraPhysics Nd:YAG laser with a monochrometer. PR samples were excited by a 532 nm pulse laser with 10 ns

duration, and the PR transient absorbance under various wavelengths were monitored over a time span of 10 μs to 0.5 s by an oscilloscope. The fitting analyses on the transient spectra at 410 nm was done by MATLAB (Mathworks, MA) using home-built codes. The differential absorbance at 410 nm were assumed to be mainly contributed by the blue-shifted M intermediates, both M_1 and M_2 combined, as the absorbance of the other intermediates (*e.g.*, K, N, PR, PR') is significantly lower at this wavelength(György Váró et al. 2003). With this assumption, the growth and decay of the difference spectra at 410 nm represented the accumulation and decay of the M intermediates, respectively. A simplification was made by considering the reverse reactions of the K-M and M-N transitions to be negligible. As a result, a biexponential model for a simple 1st-order two-step consecutive reaction model (**Figure 3C**) could be used to fit the differential absorbance at 410 nm:

$$\Delta Abs_{410nm} = a\frac{k_1}{k_2 - k_1}(e^{-k_1 t} - e^{-k_2 t}),$$

where *a* was a parameter that reflected the magnitude of the differential absorbance, k_1 represented the rate constant of the K–M transition step, and k_2 represented the rate constant of the M–N transition step. The difference absorbance data at 410 nm from **Figure 3A and B** (purple lines) were fitted using the above reaction model (smooth black curves).

5.3. RESULTS

5.3.1. $A_{2A}R$ Can Be Solubilized with SMALPs but Lost Its Affinity to Antagonist

First, we tested how effectively SMALPs can extract $A_{2A}R$ directly from *S. cerevisiae* membranes. After applying SMA on isolated yeast membranes containing $A_{2A}R$, densitometry on Western Blotting analysis was used to determine and compare the concentrations of $A_{2A}R$ in the solubilized supernatant and the non-solubilized pellet (see **5.2.5 above**). SMA solubilization for $A_{2A}R$ from *S. cerevisiae* membranes was found to be ~39% (**Figure 5-4**). Although the yield was not optimal, SMA could encapsulate a sufficient amount of $A_{2A}R$ for further analysis.

The receptor was then bound to Ni-NTA resins, washed extensively with low concentrations of imidazole, eluted with 500 mM of imidazole, then desalted with PD-10 column and sterilized with a 0.22-μm filter. Western Blot analysis was performed on every single step to verify the presence of $A_{2A}R$ (**Figure 5-4**). Clearly, the receptor was present in the final sample prior to ligand-affinity chromatography for isolation of antagonist-active $A_{2A}R$.

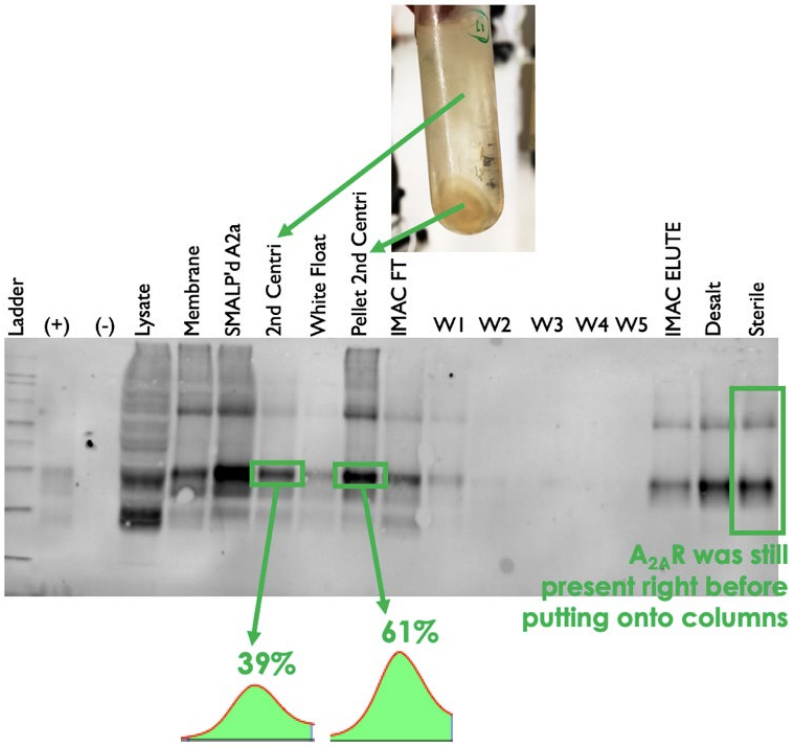

Figure 5-4. Western Blot analysis of SDS-PAGE of $A_{2A}R$ solubilized with SMALPs to track the presence of $A_{2A}R$ at every step from lysis to sterilization prior to ligand-affinity chromatography. Positive ((+) ctrl) and negative ((–) ctrl) controls consist of 5 OD cell lysate of *S. cerevisiae* BJ5464 cells expressing and not expressing $A_{2A}R$ WT, respectively. "SMALP'd A2a" indicates $A_{2A}R$-containing *S. cerevisiae* membranes after SMA application but before ultracentrifugation. "2nd Centri" indicates the supernatant containing solubilized $A_{2A}R$ after ultracentrifugation. "Pellet 2nd Centri" indicates the pellet containing non-solubilized materials. "IMAC FT" and "IMAC Elute" indicate the flow-through and elute from IMAC step. "Desalt" indicates the desalted sample, and "Sterile" indicates the sterilized sample prior to ligand-affinity chromatography. Line densitometry was performed on the bands representing the supernatant containing solubilized $A_{2A}R$ and the pellet containing non-solubilized $A_{2A}R$. MagicMark protein ladder (LC5602) is used as the molecular standard weight.

Next, we tested the ability of the SMA-solubilized $A_{2A}R$ to bind to ligand by performing ligand-affinity chromatography using XAC followed by Western Blot analysis. The results showed that the "active" fractions contain little protein compared with the "inactive" fractions (**Figure 5-5**). This is in contrast with the results obtained in detergent micelles, which showed a significant amount of protein in the "active" fractions. (**Figure 2-3**). This suggests that $A_{2A}R$ solubilized with SMA does not retain its affinity to the antagonist XAC like it does in detergent micelles.

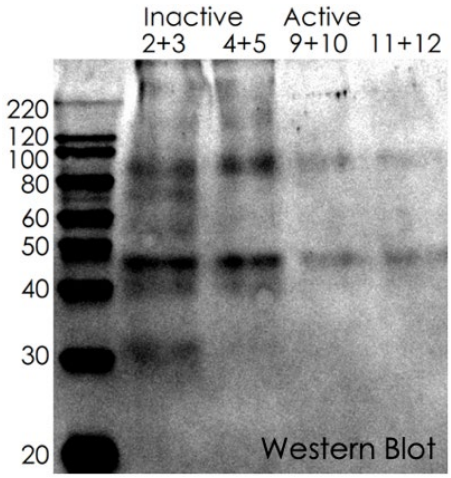

Figure 5-5. Western Blot analysis of SDS-PAGE of $A_{2A}R$ solubilized in SMALPs and in DDM detergent during purification with ligand-affinity column. "XAC inactive" and "XAC active" indicate the fractions that do not and to bind to XAC during the ligand-affinity chromatography step. MagicMark protein ladder (LC5602) is used as the molecular standard weight.

5.3.2. SMALPs Can Extract PR from *E. coli* Membranes but Only the Monomeric Form

Next, we tested how effectively SMALPs can encapsulate PR from *E. coli* membranes. It has been shown that PR-WT exists dominantly as hexamers/pentamers, while the E50Q mutant primarily forms monomers(Hussain et al. 2015a). Therefore, *E. coli* membranes containing PR-WT and PR-E50Q were tested, as the significant difference in size between the hexameric and the monomeric forms of PR could affect the solubilization efficiency. PR-containing *E. coli* membranes were incubated with SMA (4% w/v) overnight at RT, followed by ultracentrifugation to remove the non-solubilized materials. The pellets before and after SMA application were weighed (normalized by the volume of solution before centrifugation) to determine the solubilization efficiency (**Figure 5-6A**). In both cases, the weight of the pellet significantly decreased by 63–66% (**Figure 5-6B**). This indicates that SMA solubilization efficiency on PR-containing *E. coli* membranes is 63–66% and does not depend on the size of the embedded protein.

However, visualization of the supernatant and the pellet of the samples after SMA application showed that in the PR-WT case, the supernatant did not show the pink color characteristic of PR, while the pellet appeared to contain a significant amount of PR. In contrast, the supernatant in the PR-E50Q case showed the distinct red color of PR, while the pellet appeared to contain little PR (**Figure 5-6A**). This suggests that PR-WT was not as effectively encapsulated with SMA as PR-E50Q was, despite the similar solubilization efficiency on the membranes *per se*. Indeed, Western Blot analysis on SDS-PAGE of the final SMA-solubilized samples indicated that only the monomeric form of PR was solubilized in both cases and that the hexameric form of PR-WT was not (**Figure 5-6B**). Furthermore, UV absorption

measurements at 520 nm were used to determine the protein yield for both cases. The results indicated that 1 L of *E. coli* overexpressing PR solubilized with SMALPs yielded 4.0 mg of PR-WT and 72.0 mg of PR-E50Q (**Figure 5-6C**). Clearly, SMA was very effective at encapsulating the monomer-enrich PR-E50Q mutant but could not solubilize the hexamer-dominant PR-WT.

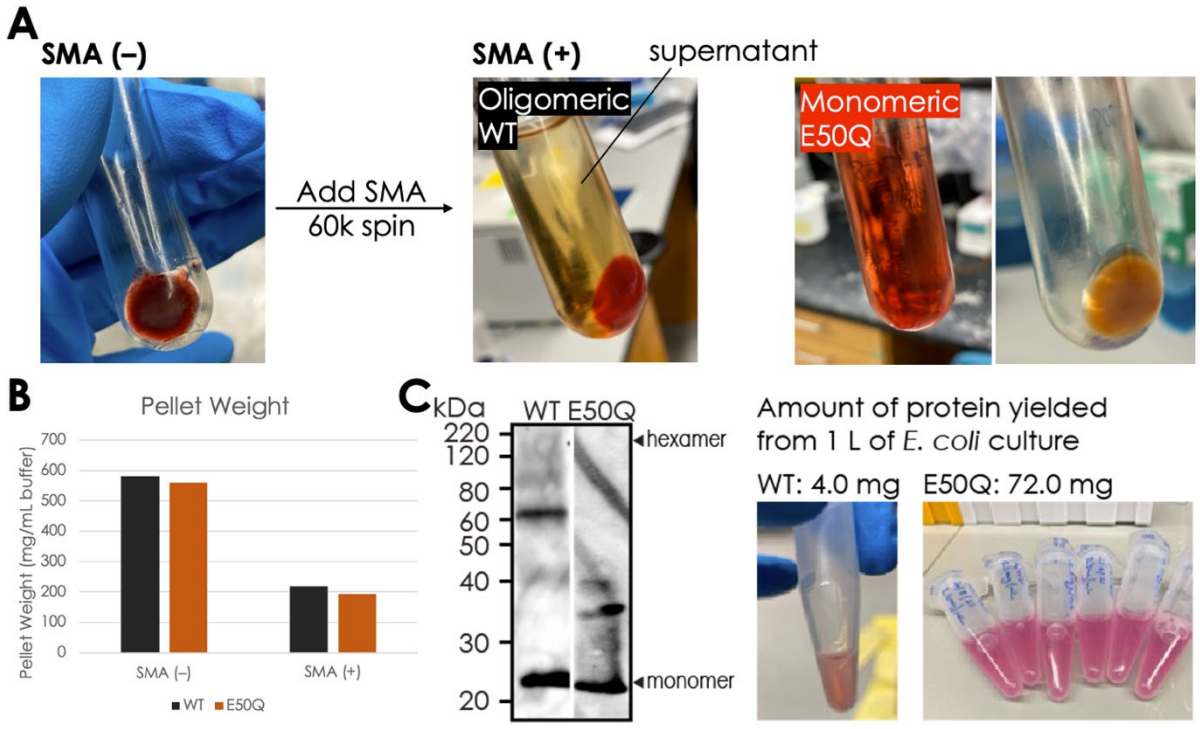

Figure 5-6. SMALPs effectively solubilizes *E. coli* membranes regardless of the size of the embedded protein, but can only capture the monomeric form of PR. **(A)** Visualization of the PR-WT and PR-E50Q samples before and after SMA application. The 60,000 × g ultracentrifugation yields the supernatant, which contains the solubilized materials, and the pellet, which contains the non-solubilized debris. **(B)** The weights of the pellets before and after SMA application of the PR-WT and PR-E50Q samples were normalized by the buffer volume before centrifugation (in mg/mL buffer). **(C)** Western Blot analysis of SDS-PAGE and visualization of SMA-solubilized PR-WT and PR-E50Q samples. MagicMark protein ladder (LC5602) is used as the molecular standard weight.

5.3.3. SMALPs Retains PR's Native Membrane Environment but Disrupt Proton Transport Function

We next explored the functional impact of extracting PR directly from *E. coli* membrane by using SMALPs. The protein transport function of PR solubilized with SMALPs was characterized via pKa_{D97} measurements and photochemical reaction cycle experiments. The monomer-enriched E50Q mutant was used, as the oligomer-dominant PR WT could not be captured due to the limited size of the nanodiscs (see **5.3.2 above**). Our results showed that PR E50Q in SMALPs exhibited a remarkably high pKa_{D97} of 8.9 (**Figure 5-7A**). This is 1.5–2.5 pKa units higher than those of PR E50Q reconstituted in DDM (7.2)(Hussain et al. 2015a) or in POPC/POPG (6.4), indicating that the majority of PR monomers was incapable of proton transport in SMALPs. Note that the fitting was poor for the data at pH < 6 due to the instability of SMALPs at this pH range,(Scheidelaar et al. 2016) in contrast to the quality of pKa_{D97} data of PR reconstituted in other membrane mimetics.

Next, time-resolved UV-visible light spectroscopy experiments was used to evaluate the photocycle kinetics of PR E50Q in DDM micelles and in SMALPs. In DDM, PR-E50Q exhibited well-defined photocycle with differential absorbances that peaked at observable timescales (**Figure 5-7B**). In contrast, the photocycle of PR-E50Q in SMA was found to be severely disrupted, exhibiting absorbance that rapidly diminished over time at all wavelengths examined (**Figure 5-7B**). This indicates that the D97 residue is predominantly protonated, thereby interrupting the native photocycle in which PR would undergo the *M–N* transition. Such disruption of photocycle could be explained by the very high pKa_{D97} of 8.9 for PR E50Q in SMALPs estimated above (**Figure 5-7A**) that would render most of the PR molecules

inactive. This observation however persisted at pH 10.0 (**Figure 5-7B**), indicating that this polymer nanodisc platform interferes with PR's photocycle kinetics, beyond residue D97. Taken together, despite retention of the native *E. coli* membrane, SMALPs appear not to maintain the proton transport capacity of PR, but instead severely reduce its active population and disrupt its photocycle properties.

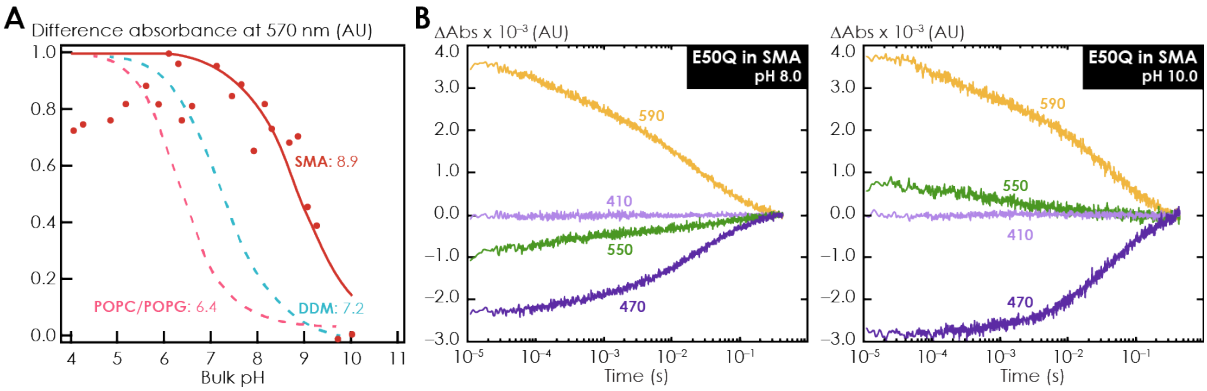

Figure 5-7. (A) pH-dependent absorbance transitions of PR E50Q in SMALPs (solid red line) at 570 nm, compared with those of PR E50Q in DDM detergent (dashed blue line) and in POPC/POPG liposomes (dashed pink line). **(B)** Transient absorbance data of PR E50Q extracted with SMALPs directly from *E. coli* membrane. Measurements were performed at pH 8.0 and 10.0 at ~293 K. The transient absorbance changes at 410, 470, 550, and 590 nm were collected after PR is photoactivated by a green-light pulse laser.

5.4. DISCUSSION

The key finding of this study is that the human adenosine A_{2A} receptor and the bacterial proteorhodopsin both showed altered functional properties when extracted directly from their host membrane environments using SMA. We found that $A_{2A}R$ was successfully solubilized in SMA at a sufficient efficiency (**Figure 5-4**) but lost its affinity to the antagonist XAC (**Figure 5-5**). Additionally, only the monomeric form of PR was encapsulated with SMA, while the oligomeric form was lost (**Figure 5-6**), and the SMA-solubilized PR monomers exhibited an unusually high pKa_{D97} value and a disrupted photocycle (**Figure 5-7**).

The loss of affinity of SMA-solubilized $A_{2A}R$ to XAC might be due to the lack of cholesterol in the nanodisc system. To date, $A_{2A}R$ has been co-crystallized with cholesterol in 38 out of 57 published structures(S. K. Huang et al. 2021). Cholesteryl hemisuccinate (CHS), a cholesterol analog, is crucial for receptor stability and ligand binding in the preparation of $A_{2A}R$ in detergent micelles(O'Malley et al. 2007; 2010b). Since CHS cannot be easily incorporated into SMALPs, $A_{2A}R$ solubilized with this method may exhibit reduced ligand binding affinity. Furthermore, the main sterol in the plasma membranes of *S. cerevisiae* is ergosterol, whereas that in mammalian cells is cholesterol(Opekarová and Tanner 2003; Pucadyil and Chattopadhyay 2006). Therefore, the retention of yeast lipids such as ergosterol with the protein in SMALPs may not be sufficient to maintain the functional properties of $A_{2A}R$.

The oligomeric form of PR could not be encapsulated with SMA perhaps because of the limited size of the nanodiscs formed by this polymer. According to a crystal structure of the hexameric form of blue light-absorbing proteorhodopsin (PDB ID: 4JQ6), the diameter of

hexameric PR is ~91.2 Å, while that of a monomeric PR is ~27.2 Å (**Figure 5-8A**). Although the typical size of a SMALP is also ~100 Å, its mean core diameter is only ~76 ± 4 Å(Jamshad, Grimard, et al. 2015) (**Figure 5-8B**), which renders it difficult to fit a PR hexamer into a SMALP, while a PR monomer can easily be captured and stabilized.

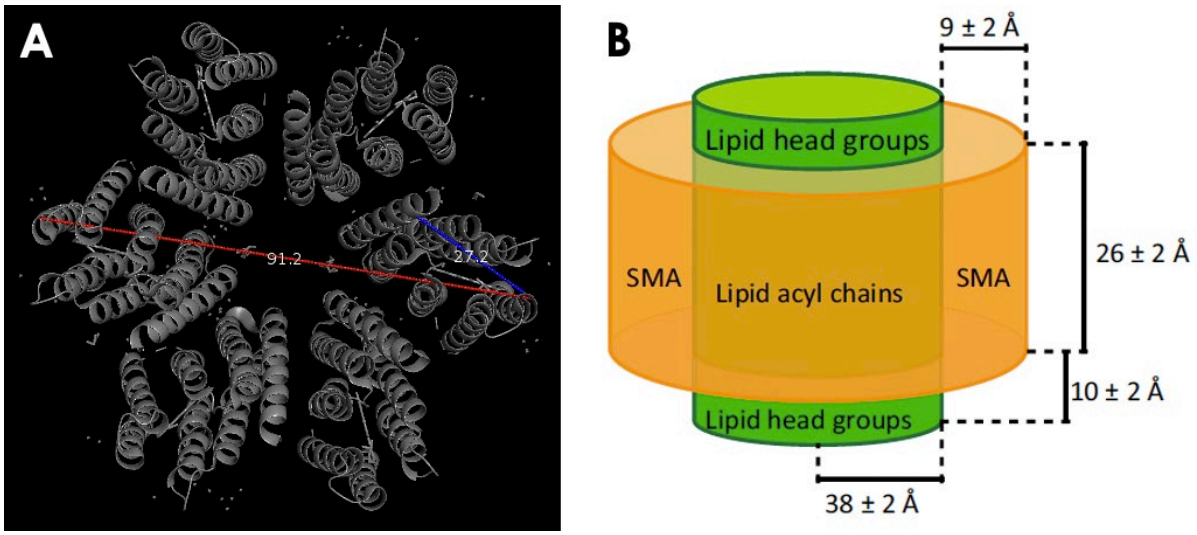

Figure 5-8. **(A)** Measurements of the diameters of PR hexamer and monomer using PyMOL. Measurements are done on the crystal structure of blue light-absorbing proteorhodopsin (PDB ID: 4JQ6). **(B)** Dimensions of styrene-maleic acid lipid particles consisting of DMPC synthetic lipids and a SMA polymer with a S:MA ratio of 2, as determined from small-angle neutron scattering experiments (Figure adapted from Jamshad, M. et al, *Nano Res.* **2015**, 8, 774–789.)

In addition, the pKa_{D97} of PR E50Q mutant in SMA nanodiscs environments is markedly higher than those of PR E50Q in liposomes or micelles (**Figure 5-7A**). As the nanodiscs are formed, the maleic acid moiety must be deprotonated(Tonge and Tighe 2001), which could cause an increase in the local proton concentration around residue D97. As a result, residue D97 could become dominantly protonated, leading to the accelerated decay in photocycle (**Figure 5-7B**). Indeed, a similar trend has been observed with other proteins. In

the *Rubrobacter xylanophilus* rhodopsin RxR, the pKa of K209 has been shown to increase by 1.8 pH units in SMALPs compared with that in DDM(Ueta et al. 2020). Additionally, in the photoreceptor sensory rhodopsin II *Np*SRII of *Natronomonas pharaonic*, an accelerated decay of the *M* photointermediate was found due to the high local proton concentration induced by the maleic acid group of the SMA polymer(Mosslehy et al. 2019) (**Figure 5-2**). Taken together, these results suggest that the charged functional groups of SMALPs could affect membrane protein function via adverse local electrostatic interactions, and therefore it is not a given that SMALP-reconstituted membrane proteins display more native-like function or structure.

5.5. CONCLUSIONS

The discovery that styrene maleic acid copolymers can be used to solubilize native lipid/protein complexes directly from host cells or membranes has sparked a flurry of new research into the potential of this novel platform in membrane protein studies. Our results demonstrated that the functional properties of the human A_{2A} GPCR and the bacterial proteorhodopsin are significantly compromised when solubilized with SMA. By no means of undermining the immense contribution of SMA polymers in membrane protein research, our study simply offers a cautionary tale, suggesting that SMA is not a one-size-fit-all platform, and that empirical testing is required to select the appropriate polymer type for maintaining the native function of the embedded proteins.

Chapter 6 | CONCLUSIONS AND OUTLOOK

6.1. CONCLUSIONS

G protein-coupled receptors play a critical role in a tremendous array of functions in human, and the discovery of their oligomerization has transformed how modern medicine views and targets these receptors. Despite effort put forth to develop novel therapeutic approaches that center around GPCR oligomers, much remains unexplored about the driving factors of their formation as well as their oligomeric interfaces. The dynamic nature of these oligomeric complexes has made it a great challenge to resolve their structures with even well-established technique such as X-ray crystallography, which excludes disordered structural features. Indeed, since the publication of the first crystal structure of GPCR in 2000(Palczewski et al. 2000), fewer than ten of the 113 published unique GPCR structures feature their oligomers. The overall goal of this thesis was to improve the understanding of how protein disorder facilitates GPCR oligomer formation and to address the difficulties that impede structural studies of GPCR oligomers.

Previous research in the Han and O'Malley groups has discovered that the human adenosine A_{2A} receptor forms distinct oligomeric complexes that can be isolated with size-exclusion chromatography and that a C-terminal mutation C394S significantly reduces the oligomer levels of this receptor(Schonenbach et al. 2016). Subsequent work revealed that A_{2A}R oligomers can adopt multiple interconverting interfaces(Song, Duncan, and Sansom 2020), hinting at the role of protein disorder in enabling the formation of these dynamic complexes. With these results in mind, we aimed to understand what drives the association of A_{2A}R homo-oligomers and how its intrinsically disordered C-terminus may facilitate this process. As

protein disorder was discovered to be crucial for the formation of $A_{2A}R$ oligomers and their interfaces need to be visualized at high resolution, we also sought to address the challenges in applying cryogenic electron microscopy (cryo-EM) and double electron electron resonance (DEER) to structural studies of $A_{2A}R$ oligomers. Four main goals of this thesis were summarized as follows:

- Investigate the driving factors of $A_{2A}R$ homo-oligomer formation and the role of the intrinsically disordered C-terminus (**Chapter 2**)
- Examine the structural and functional properties of $A_{2A}R$ variants void of free cysteines for biophysical characterization using electron paramagnetic resonance (EPR) (**Chapter 3**)
- Visualize the dimeric interfaces of $A_{2A}R$ with respect to its C-terminus (**Chapter 4**)
- Characterize the functional properties of $A_{2A}R$ and the bacterial transmembrane proton pump proteorhodopsin (PR) solubilized with styrene maleic acid copolymers (**Chapter 5**)

To accomplish the first goal, strategic mutations and truncations were done on the C-terminus of $A_{2A}R$, followed by assessment of its oligomer levels using size-exclusion chromatography. The C-terminal residue C394 was found to stabilize $A_{2A}R$ oligomers via disulfide linkages, while the charges cluster $^{355}ERR^{357}$ play a role via electrostatic interactions. The oligomer levels of $A_{2A}R$ decrease progressively with the shortening of the C-terminus, with no oligomers observed upon complete truncation. With the help of molecular dynamics simulations, we discovered that $A_{2A}R$ dimerizes via a combination of electrostatic interactions,

hydrogen bonds, and hydrophobic interactions along the length of its C-terminus, enabling the formation of multiple symmetrical and asymmetrical interfaces. Furthermore, $A_{2A}R$ oligomerization were found to be enhanced by increasing ionic strength, revealing the role of depletion interactions as the main driving factor. Turbidity measurements of the stand-alone C-terminus demonstrated that $A_{2A}R$ C-terminus formed self-aggregates in the presence of the salting-out NaCl but not the salting-in GdnHCl, further confirming the role of depletion interactions via the C-terminus in promoting $A_{2A}R$ oligomer formation. These results emphasize for the first time the critical role of the intrinsically disordered C-terminus and depletion interactions in the formation of a GPCR oligomeric complex, offering important insight into the effect of C-terminus modification on receptor oligomerization of $A_{2A}R$ and other GPCRs reconstituted in vitro for biophysical studies.

Once the role of the C-terminus in $A_{2A}R$ oligomerization was uncovered, we tackled the challenges associated with the application of EPR and DEER in studying this disordered structural feature. Much effort has been made in engineering $A_{2A}R$ variants void of free cysteines (TM-Cys-Free) to establish baseline EPR measurements, yet potential structural and functional changes had not been investigated. Using ligand-affinity chromatography and Western Blot analysis, we found that these TM-Cys-Free $A_{2A}R$ variants, selected with an agonist-based fluorescent-activated cell sorting procedure, exhibited reduced affinity to the antagonist xanthine amine congener (XAC). Continuous-wave EPR and specifically power saturation experiments revealed that the simultaneous mutations of the transmembrane cysteines of $A_{2A}R$ led to disruption of various extracellular disulfide bonds, which had been demonstrated to be important for $A_{2A}R$ proper structure and function(De Filippo et al. 2016; O'Malley et al. 2010a). Collectively, these findings suggest that although the transmembrane

cysteines of $A_{2A}R$ are not essential for agonist binding, membrane trafficking, or thermodynamic favorability, they play a crucial role in antagonist ligand recognition as well as formation of its extracellular disulfide linkages. This study also serves as a cautionary tale, highlighting that screening and selecting for GPCR variants with high affinity towards one ligand does not necessarily correlate with intact structure or affinity to other ligands.

Having understood the potential capability as well as pitfalls of applying EPR for structural studies of $A_{2A}R$ oligomers, we next sought to elucidate the conformation of the intrinsically disordered C-terminus with respect to the oligomeric interfaces of the receptor. CW-EPR measurements revealed that the C-terminal residue C394 was immobilized as $A_{2A}R$ formed oligomers, suggesting that the C-terminus is directly involved at the oligomeric interface of the receptor. Results from DEER showed a C394–C394 distance of ~5.5 Å between protomers of SEC-separated $A_{2A}R$ dimers, suggesting that it is not the C394–C394 disulfide bond that stabilizes $A_{2A}R$ dimers. Meanwhile, preliminary screening with negative-staining TEM demonstrated that the SEC-separated $A_{2A}R$ dimers and monomers are homogeneous in size and shape, without contaminant, and of sufficient protein concentration. Early cryo-EM data collection resulted in a ~15-Å resolution 3D structure of $A_{2A}R$ dimers, in which the TM regions appeared to be involved at the interface. Together, these results demonstrated the potential of cryo-EM in combination with DEER in resolving the interfaces of $A_{2A}R$ oligomers at the molecular level, but much further effort is required to improve the data quality.

Finally, since solubilizing $A_{2A}R$ with detergent micelles may alter its native structure and function, we next sought to apply the new detergent-free membrane mimetic platform that is styrene maleic acid (SMA) copolymers. SMA was used to extract directly $A_{2A}R$ from *S.*

cerevisiae membranes and the bacterial proteorhodopsin from *E. coli* membranes. We discovered that $A_{2A}R$ was successfully encapsulated with SMA with acceptable efficiency, but ligand-affinity chromatography revealed that SMA-solubilized $A_{2A}R$ could not bind to the antagonist XAC. For PR, the monomeric form of this receptor was solubilized with SMA at a very high yield, but its hexameric form was lost. Measurements of the pKa of the key proton acceptor D97 demonstrated that PR in SMALPs displayed a pKa_{D97} value 1.5–2.5 units higher than in detergent or liposome environments, implying that its active population is greatly reduced in SMA. Furthermore, measurements of photocycle kinetics revealed that PR's photocycle in SMALPs was severely disrupted. Collectively, despite retention of the native host membranes, SMALPs appeared to have negative impacts on the functional properties of both $A_{2A}R$ and PR, suggesting that this novel membrane mimetic platform should be applied with caution on *in vitro* studies of transmembrane proteins.

In summary, these studies have shown that while it has become clearer how the disordered C-terminus promotes the oligomer formation of $A_{2A}R$, elucidating its role in the oligomerization of other GPCRs remains a task to be explored. Depletion interactions appear to be critical to promote flexible protein-protein association, while EPR combined with cryo-EM carry the unique power in resolving the dynamic and interconverting interfaces of GPCR oligomeric complexes. To that end, the methods and insights described in this work will facilitate the study into how the intrinsically disordered C-terminus enables the oligomerization of other GPCRs.

6.2. FUTURE CONSIDERATIONS

While the studies described in this thesis have collectively advanced the understanding of how intrinsically disorder regions facilitate the dynamic oligomerization of GPCRs, as well as downstream biophysical and structural characterization of their oligomeric interfaces, several avenues are to be explored. The following sections describe the remaining knowledge gap and promising experimental approaches to address the pertinent questions.

6.2.1. Investigating the Functional Consequences of $A_{2A}R$ Oligomerization

One of the major questions that remains is that regarding the functional consequences of $A_{2A}R$ oligomerization. Although $A_{2A}R$ and the associated oligomers are among the most well-studied GPCR complexes, no studies to date have directly investigated how homo-oligomerization may change the functional properties of this receptor. Displacement of the transmembrane domains have been demonstrated to be the hallmark of $A_{2A}R$ activation(Eddy et al. 2018; Sušac et al. 2018; Prosser et al. 2017; Ye et al. 2016), but this aspect has not been demonstrated to show changes upon receptor oligomerization. One of the findings in **Chapter 2** is that truncation of the C-terminus, shown to be critical to $A_{2A}R$ oligomer formation, can lead to structural changes in the heptahelical bundles of $A_{2A}R$ dimers (**Figure 2-14B** and **Figure 2-15**),. In the cellular context, it has been shown that truncation of $A_{2A}R$ C-terminus leads to substantial reduction of G protein binding(Koretz et al. 2021), cAMP accumulation, and signaling response in yeast(A. R. Jain, McGraw, and Robinson 2020). These results hint at potential impact of receptor oligomerization of $A_{2A}R$ conformation, necessitating future investigation into functional outcomes.

Functional changes in $A_{2A}R$ can be verified upon observation of the third intracellular loop (ICL3) connecting H5 and H6 regions. In light-activated transmembrane proteins such as proteorhodopsin (PR), bacteriorhodopsin (BR), and rhodopsin (Rh), this interhelical region when undergoing conformational changes upon light activation reveals a distinctive twisting-and-lifting motion that can be detected by EPR to confirm changes in activity. Such allosteric conformational changes are conserved among GPCRs and can be used as experimental read-out for $A_{2A}R$ activity. In fact, a recent NMR study has identified two residues that exhibit excellent spin labeling efficiency and dynamic profiles (V229 and A289)(Prosser et al. 2017) and are likely candidates for future functional study of $A_{2A}R$. Such dynamic study can be done using again cw-EPR lineshape analysis at 240 GHz to measure this outward movement and how it may change upon receptor oligomerization.

Another strategy is to determine the dissociation constant (K_D) of $A_{2A}R$ for well-characterized ligands such as XAC(Karl-Norbert Klotz 2000), SCH-58261(Ongini et al. 1999), ZM-241385(Karl-Norbert Klotz 2000), CGS-21680(K.-N. Klotz et al. 1997), or NECA(K.-N. Klotz et al. 1997), by applying radioligand binding assays on various $A_{2A}R$ constructs with different oligomeric distributions. Next, downstream signaling of different $A_{2A}R$ oligomeric forms can be evaluated by assessing the synthesis of cyclic AMP in HEK-293 cells(McGraw and Robinson 2017). Since it is crucial that $A_{2A}R$ also be studied in a more native-like environment, these experiments should be carried out in both detergent micelles and SMALPs, should future research improve $A_{2A}R$ ligand binding in the latter, to analyze the effects that membrane environment may have on $A_{2A}R$ function and activity.

6.2.2. Second-Harmonic Generation as a Promising Tool to Probe Conformational Changes of $A_{2A}R$

Despite the power of NMR and EPR in elucidating conformational changes of proteins, these techniques often generate data from signals that are dependent on external factors, such as how the environment is perturbed by the observed conformation. Furthermore, the signal-to-noise ratios of these techniques can be insufficient to distinguish different conformations, especially in the case of GPCRs, which are highly dynamic in nature. On the other hand, second-harmonic generation (SHG), a well-established technique in physics, offers a promising tool to probe structure and function of GPCRs. SHG is a non-linear optical technique that involves the conversion of two photons of equal energy (the fundamental) into one photon of twice the energy (the second harmonic). This second-harmonic light is emitted when SHG-active molecules are immobilized at an interface and irradiated with a fundamental beam. Such SHG is highly sensitive to the orientation of SHG-active molecules and thus can be used to probe conformational changes from subtle to significant in biological molecules. Since proteins do not inherently radiate second-harmonic light, a SHG-active dye molecule needs to be incorporated, conveniently onto cysteine residues through the same chemistry of EPR spin labeling. This aspect makes SHG particularly useful, as the knowledge obtained from **Chapter 3** and **Chapter 4** can be applied to address potential problems associated with simultaneous removal of multiple cysteines and optimize labeling efficiency. The intensity of the SHG signal emitted from the dye molecule depends on the tile angle of the dye relative to the z axis perpendicular to the surface to which the protein is tethered. As a result, conformational changes affect the average orientation of the dye molecule, effectively changing the intensity of SHG light (**Figure 6-1**).

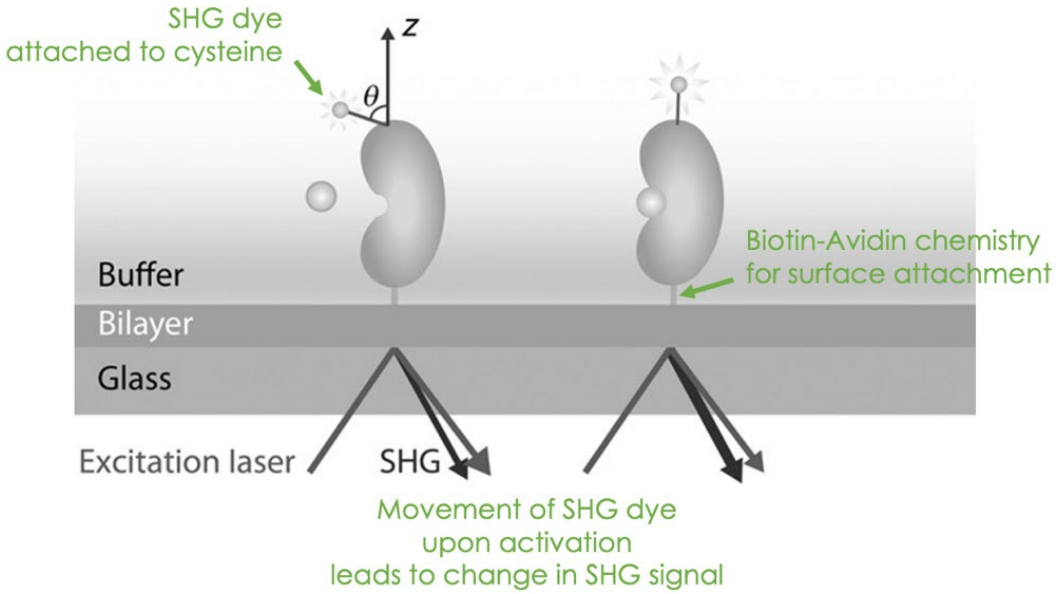

Figure 6-1. Cartoon representation of the experimental setup of SHG assay. A SHG-active dye is conjugated via cysteine to the protein molecule, which is then attached to a supported biotin surface via a Avidin-tag. The SHG intensity is dictated by the angle θ between the transition dipole moment of the dye and the z axis perpendicular to the surface. This change in SHG intensity can be monitored and compared between when the protein is and is not bound to a ligand, indicating conformational changes upon activation. (Figure adapted from Young, T. A. et al, *Methods Enzymol.* **2018**, 610.)

6.2.3. SMA Alternatives with Potential of Retaining Native Functional Properties of $A_{2A}R$ and PR

In **Chapter 5**, we have seen that SMA could successfully encapsulate $A_{2A}R$, but the receptor showed reduced affinity to the antagonist XAC, perhaps due to the lack of cholesterol(O'Malley et al. 2007). CHS has been used as a derivative of cholesterol in the successful solubilization of $A_{2A}R$ in detergent micelles(O'Malley et al. 2007; Schonenbach et al. 2016), but this chemical is not soluble in water and thus cannot be used alongside SMA copolymers for membrane protein solubilization.

Recently, a non-detergent cholesterol derivative called CHEAPS (4-((cholesteryloxy)-4-oxobut-2-enamido)ethyl) dimethylammonio) propane-1-sulfonate) has been developed as a potential solution to the above problem(Trinh et al. 2021). The structure of this chemical involves the linking a cholesterol portion to a zwitterionic sulfobetaine segment via an ester bond (**Figure 6-2**). Despite its low solubility in aqueous solutions, CHEAPS is highly soluble in water containing detergents and amphiphilic polymers, such as DDM and SMA copolymers, likely due to its lack of hydrogen bond donors and acceptors. Specifically, it can be solubilized up to ~44 mg/mL in 5% DDM and ~62 mg/mL in SMA solution (5% w/v in water). On the other hand, CHEAPS exhibits weak absorbance at 280 nm ($A_{280} \sim 0.86 \times 10^3\ M^{-1}\ cm^{-1}$) and thus will not interfere much with protein detection at this wavelength using UV-Vis spectroscopy. Currently, CHEAPS has been shown to successfully replace CHS in maintaining the enzymatic functions of human mitochondrial TSPO, a strict cholesterol-dependent membrane oxygenase(Trinh et al. 2021). These findings demonstrate the potential practicality

of CHEAPS to provide a source of cholesterol in SMA solubilization of $A_{2A}R$ as well as other GPCRs.

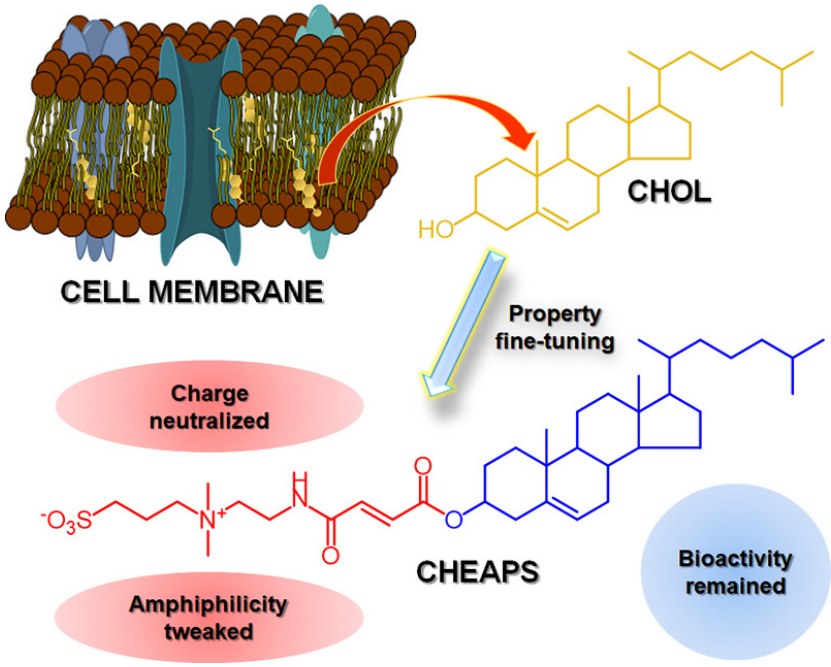

Figure 6-2. The molecular structure of CHEAPS involves linking the cholesterol moiety native in cell membranes with zwitterionic sulfobetaine segment via an ester bond. The lack of hydrogen bond donors and acceptors render this molecule highly soluble in water containing detergents or amphiphilic polymers. (Figure from Trinh, T. K. H. et al, *Biochim Biophys Acta* **2021**, 1865, 129908.)

Additionally, in **Chapter 5**, we have shown that the monomeric form of the bacterial transmembrane proton pump proteorhodopsin was efficiently solubilized with SMA, but its hexameric form was excluded. Our hypothesis was that the size of the nanodiscs formed with SMA2000 was too small to encapsulate the bulky PR hexamers. We also demonstrated that the photocycle of SMA-encapsulated PR monomers was severely disrupted due to heavy protonation of the proton acceptor D97. We hypothesized that the ionization of the maleic acid moiety upon nanodiscs formation causes a significant increase in the local proton concentration

around D97. Due to the above reasons, one possible way to improve SMA solubilization of PR hexamers is to use a different type of amphiphilic polymers that would not release excess protons into solution and would form nanodiscs of larger size.

With that in mind, styrene maleimide quaternary ammonium (SMA-QA)(Ravula et al. 2018) could be the solution to solubilize PR hexamers with intact functional properties. Given the structure shown in **Figure 6-3**, the formation of SMA-QA nanodiscs does not release protons into solution. Furthermore, the size of the nanodiscs formed by SMA-QA can be precisely controlled by varying the concentration of SMA-QA used relative to the wet weight of the membranes. Specifically, SMA-QA at 1.5% w/w forms the typical small 10-nm-diameter nanodiscs, at 1% w/w the intermediate 20-nm-diameter, and at 0.25% w/w the large 30-nm-diameter. Furthermore, the larger nanodiscs of 30 nm diameter allows for slower tumbling in solution and thus alignability in an external magnetic field, making SMA-QA one of the very few types of SMA that are compatible with NMR spectroscopy.

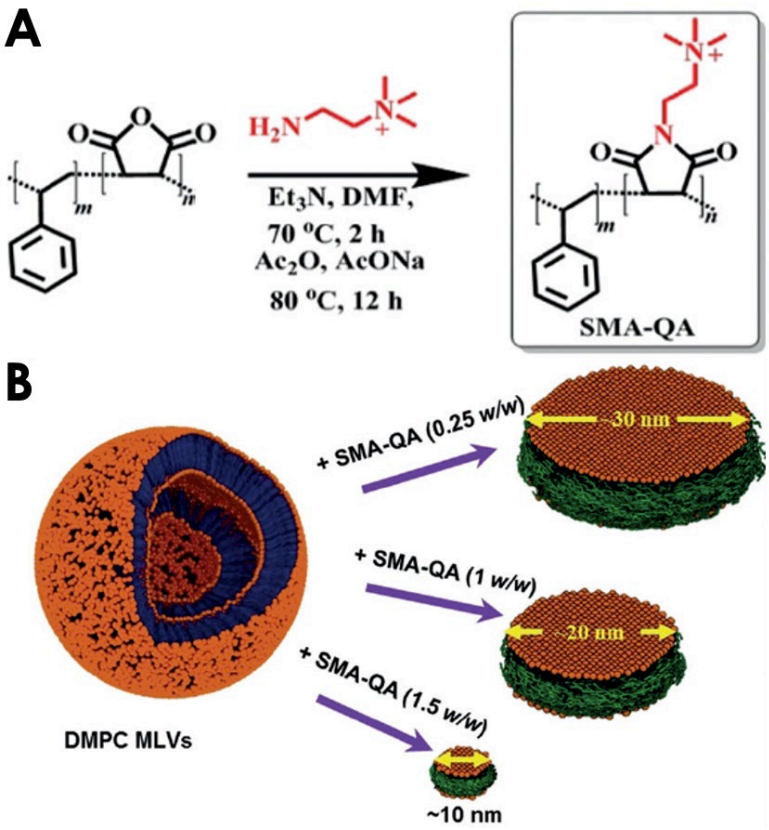

Figure 6-3. (A) Synthesis of SMA-QA polymer by modifications of SMA polymer. The structure of SMA-QA contains a quaternary ammonium moiety that does not increase the local proton concentration when the nanodiscs are formed. **(B)** The size of the nanodiscs formed by SMA-QA can be tuned by varying the concentration of the polymer. (Figure adapted from Ravula, T. et al, *Angew. Chem. Int. Ed.* **2018**, 57, 1342–1345.)

BIBLIOGRAPHY

Abraham, Mark James, Teemu Murtola, Roland Schulz, Szilárd Páll, Jeremy C. Smith, Berk Hess, and Erik Lindahl. 2015. "GROMACS: High Performance Molecular Simulations through Multi-Level Parallelism from Laptops to Supercomputers." *SoftwareX* 1–2 (September): 19–25. https://doi.org/10.1016/j.softx.2015.06.001.

Agnati, L. F. 2003. "Molecular Mechanisms and Therapeutical Implications of Intramembrane Receptor/Receptor Interactions among Heptahelical Receptors with Examples from the Striatopallidal GABA Neurons." *Pharmacological Reviews* 55 (3): 509–50. https://doi.org/10.1124/pr.55.3.2.

Altwaijry, Nojood A., Michael Baron, David W. Wright, Peter V. Coveney, and Andrea Townsend-Nicholson. 2017. "An Ensemble-Based Protocol for the Computational Prediction of Helix–Helix Interactions in G Protein-Coupled Receptors Using Coarse-Grained Molecular Dynamics." *Journal of Chemical Theory and Computation* 13 (5): 2254–70. https://doi.org/10.1021/acs.jctc.6b01246.

Antonini, Angelo, and Roberto Cilia. 2009. "Behavioural Adverse Effects of Dopaminergic Treatments in Parkinson's Disease." *Drug Safety*, 14.

Arachea, Buenafe T., Zhen Sun, Nina Potente, Radhika Malik, Dragan Isailovic, and Ronald E. Viola. 2012. "Detergent Selection for Enhanced Extraction of Membrane Proteins." *Protein Expression and Purification* 86 (1): 12–20. https://doi.org/10.1016/j.pep.2012.08.016.

Armando, Sylvain, Julie Quoyer, Viktorya Lukashova, Arhamatoulaye Maiga, Yann Percherancier, Nikolaus Heveker, Jean-Philippe Pin, Laurent Prézeau, and Michel Bouvier. 2014. "The Chemokine CXC4 and CC2 Receptors Form Homo- and Heterooligomers That Can Engage Their Signaling G-protein Effectors and Barrestin." *The FASEB Journal* 28 (10): 4509–23. https://doi.org/10.1096/fj.13-242446.

Asakura, Sho, and Fumio Oosawa. 1958. "Interaction between Particles Suspended in Solutions of Macromolecules." *Journal of Polymer Science* 33 (126): 183–92. https://doi.org/10.1002/pol.1958.1203312618.

Bagher, Amina M., Robert B. Laprairie, J. Thomas Toguri, Melanie E.M. Kelly, and Eileen M. Denovan-Wright. 2017. "Bidirectional Allosteric Interactions between Cannabinoid Receptor 1 (CB 1) and Dopamine Receptor 2 Long (D 2L) Heterotetramers." *European Journal of Pharmacology* 813 (October): 66–83. https://doi.org/10.1016/j.ejphar.2017.07.034.

Baldwin, R.L. 1996. "How Hofmeister Ion Interactions Affect Protein Stability." *Biophysical Journal* 71 (4): 2056–63. https://doi.org/10.1016/S0006-3495(96)79404-3.

Banerjee, Shubhadeep, Tapan K. Pal, and Sujoy K. Guha. 2012. "Probing Molecular Interactions of Poly(Styrene-Co-Maleic Acid) with Lipid Matrix Models to Interpret the Therapeutic Potential of the Co-Polymer." *Biochimica et Biophysica Acta (BBA) - Biomembranes* 1818 (3): 537–50. https://doi.org/10.1016/j.bbamem.2011.12.010.

Barki-Harrington, Liza, Louis M. Luttrell, and Howard A. Rockman. 2003. "Dual Inhibition of β-Adrenergic and Angiotensin II Receptors by a Single Antagonist: A Functional Role for Receptor–Receptor Interaction In Vivo." *Circulation* 108 (13): 1611–18. https://doi.org/10.1161/01.CIR.0000092166.30360.78.

Bayburt, Timothy H., Yelena V. Grinkova, and Stephen G. Sligar. 2002. "Self-Assembly of Discoidal Phospholipid Bilayer Nanoparticles with Membrane Scaffold Proteins." *Nano Letters* 2 (8): 853–56. https://doi.org/10.1021/nl025623k.

Bayburt, Timothy H., and Stephen G. Sligar. 2010. "Membrane Protein Assembly into Nanodiscs." *FEBS Letters* 584 (9): 1721–27. https://doi.org/10.1016/j.febslet.2009.10.024.

Beaulieu, Jean-Martin, Stefano Espinoza, and Raul R Gainetdinov. 2015. "Dopamine Receptors - IUPHAR Review 13: Dopamine Receptors." *British Journal of Pharmacology* 172 (1): 1–23. https://doi.org/10.1111/bph.12906.

Beja, O. 2000. “Bacterial Rhodopsin: Evidence for a New Type of Phototrophy in the Sea.” *Science* 289 (5486): 1902–6. https://doi.org/10.1126/science.289.5486.1902.

Bell, Adam J., Laurie K. Frankel, and Terry M. Bricker. 2015. “High Yield Non-Detergent Isolation of Photosystem I-Light-Harvesting Chlorophyll II Membranes from Spinach Thylakoids.” *Journal of Biological Chemistry* 290 (30): 18429–37. https://doi.org/10.1074/jbc.M115.663872.

Berthouze, Magali, Lucie Rivail, Alexandre Lucas, Mohammed A. Ayoub, Olivier Russo, Sames Sicsic, Rodolphe Fischmeister, Isabelle Berque-Bestel, Ralf Jockers, and Frank Lezoualc’h. 2007. “Two Transmembrane Cys Residues Are Involved in 5-HT4 Receptor Dimerization.” *Biochemical and Biophysical Research Communications* 356 (3): 642–47. https://doi.org/10.1016/j.bbrc.2007.03.030.

Best, Robert B., Xiao Zhu, Jihyun Shim, Pedro E. M. Lopes, Jeetain Mittal, Michael Feig, and Alexander D. MacKerell. 2012. “Optimization of the Additive CHARMM All-Atom Protein Force Field Targeting Improved Sampling of the Backbone ϕ, ψ and Side-Chain χ_1 and χ_2 Dihedral Angles.” *Journal of Chemical Theory and Computation* 8 (9): 3257–73. https://doi.org/10.1021/ct300400x.

Bjarnadóttir, Thóra K., David E. Gloriam, Sofia H. Hellstrand, Helena Kristiansson, Robert Fredriksson, and Helgi B. Schiöth. 2006. “Comprehensive Repertoire and Phylogenetic Analysis of the G Protein-Coupled Receptors in Human and Mouse.” *Genomics* 88 (3): 263–73. https://doi.org/10.1016/j.ygeno.2006.04.001.

Bockenhauer, Samuel, Alexandre Fürstenberg, Xiao Jie Yao, Brian K. Kobilka, and W. E. Moerner. 2011. “Conformational Dynamics of Single G Protein-Coupled Receptors in Solution.” *The Journal of Physical Chemistry B* 115 (45): 13328–38. https://doi.org/10.1021/jp204843r.

Bonaventura, Jordi, Gemma Navarro, Verònica Casadó-Anguera, Karima Azdad, William Rea, Estefanía Moreno, Marc Brugarolas, et al. 2015. “Allosteric Interactions between Agonists and Antagonists within the Adenosine A_{2A} Receptor-Dopamine D_2 Receptor Heterotetramer.” *Proceedings of the National Academy of Sciences* 112 (27): E3609–18. https://doi.org/10.1073/pnas.1507704112.

Bordag, Natalie, and Sandro Keller. 2010. “α-Helical Transmembrane Peptides: A ‘Divide and Conquer’ Approach to Membrane Proteins.” *Chemistry and Physics of Lipids* 163 (1): 1–26. https://doi.org/10.1016/j.chemphyslip.2009.07.009.

Bordignon, Enrica, and Heinz-Jürgen Steinhoff. 2007. “Membrane Protein Structure and Dynamics Studied by Site-Directed Spin-Labeling ESR.” In *ESR Spectroscopy in Membrane Biophysics*, edited by Marcus A. Hemminga and Lawrence J. Berliner, 129–64. Boston, MA: Springer US. https://doi.org/10.1007/978-0-387-49367-1_5.

Borroto-Escuela, Dasiel O., Manuel Narvaez, Daniel Marcellino, Concepción Parrado, José Angel Narvaez, Alexander O. Tarakanov, Luigi F. Agnati, Zaida Díaz-Cabiale, and Kjell Fuxe. 2010. “Galanin Receptor-1 Modulates 5-Hydroxtryptamine-1A Signaling via Heterodimerization.” *Biochemical and Biophysical Research Communications* 393 (4): 767–72. https://doi.org/10.1016/j.bbrc.2010.02.078.

Borroto-Escuela, Dasiel O., Wilber Romero-Fernandez, Alexander O. Tarakanov, Maricel Gómez-Soler, Fidel Corrales, Daniel Marcellino, Manuel Narvaez, et al. 2010. “Characterization of the A2AR–D2R Interface: Focus on the Role of the C-Terminal Tail and the Transmembrane Helices.” *Biochemical and Biophysical Research Communications* 402 (4): 801–7. https://doi.org/10.1016/j.bbrc.2010.10.122.

Bräuner-Osborne, Hans, Anders A. Jensen, Paul O. Sheppard, Patrick O’Hara, and Povl Krogsgaard-Larsen. 1999. “The Agonist-Binding Domain of the Calcium-Sensing Receptor Is Located at the Amino-Terminal Domain.” *Journal of Biological Chemistry* 274 (26): 18382–86. https://doi.org/10.1074/jbc.274.26.18382.

Bräuner-Osborne, Hans, Petrine Wellendorph, and Anders A Jensen. 2007. “Structure, Pharmacology and Therapeutic Prospects of Family C G-Protein Coupled Receptors.” *Current Drug Targets* 8 (1): 169–84. https://doi.org/10.2174/138945007779315614.

Broecker, Jana, Bryan T. Eger, and Oliver P. Ernst. 2017. “Crystallogenesis of Membrane Proteins Mediated by Polymer-Bounded Lipid Nanodiscs.” *Structure* 25 (2): 384–92. https://doi.org/10.1016/j.str.2016.12.004.

Bryksin, Anton, and Ichiro Matsumura. 2010. “Overlap Extension PCR Cloning: A Simple and Reliable Way to Create Recombinant Plasmids.” *BioTechniques* 48 (6): 463–65. https://doi.org/10.2144/000113418.

Burgueño, Javier, Derek J. Blake, Matthew A. Benson, Caroline L. Tinsley, Christopher T. Esapa, Enric I. Canela, Petronila Penela, et al. 2003. “The Adenosine A $_{2A}$ Receptor Interacts with the Actin-Binding Protein α-Actinin.” *Journal of Biological Chemistry* 278 (39): 37545–52. https://doi.org/10.1074/jbc.M302809200.

Bussi, Giovanni, Davide Donadio, and Michele Parrinello. 2007. “Canonical Sampling through Velocity Rescaling.” *The Journal of Chemical Physics* 126 (1): 014101. https://doi.org/10.1063/1.2408420.

Cabello, Nuria, Jorge Gandía, Daniela C. G. Bertarelli, Masahiko Watanabe, Carme Lluís, Rafael Franco, Sergi Ferré, Rafael Luján, and Francisco Ciruela. 2009. “Metabotropic Glutamate Type 5, Dopamine D $_2$ and Adenosine A $_{2a}$ Receptors Form Higher-Order Oligomers in Living Cells.” *Journal of Neurochemistry* 109 (5): 1497–1507. https://doi.org/10.1111/j.1471-4159.2009.06078.x.

Canals, Meritxell, Javier Burgueño, Daniel Marcellino, Núria Cabello, Enric I. Canela, Josefa Mallol, Luigi Agnati, et al. 2003. “Homodimerization of Adenosine A2A Receptors: Qualitative and Quantitative Assessment by Fluorescence and Bioluminescence Energy Transfer: Homodimerization of Adenosine A2A Receptors.” *Journal of Neurochemistry* 88 (3): 726–34. https://doi.org/10.1046/j.1471-4159.2003.02200.x.

Carpenter, Byron, Rony Nehmé, Tony Warne, Andrew G. W. Leslie, and Christopher G. Tate. 2016. “Structure of the Adenosine A2A Receptor Bound to an Engineered G Protein.” *Nature* 536 (7614): 104–7. https://doi.org/10.1038/nature18966.

Casadó-Anguera, Verònica, Jordi Bonaventura, Estefanía Moreno, Gemma Navarro, Antoni Cortés, Sergi Ferré, and Vicent Casadó. 2016a. “Evidence for the Heterotetrameric Structure of the Adenosine A2A –Dopamine D2 Receptor Complex.” *Biochemical Society Transactions* 44 (2): 595–600. https://doi.org/10.1042/BST20150276.

———. 2016b. “Evidence for the Heterotetrameric Structure of the Adenosine A2A–Dopamine D2 Receptor Complex.” *Biochemical Society Transactions* 44 (2): 595–600. https://doi.org/10.1042/BST20150276.

Cerqueira, Manuel D. 2004. “The Future of Pharmacologic Stress: Selective A2a Adenosine Receptor Agonists.” *The American Journal of Cardiology* 94 (2): 33–40. https://doi.org/10.1016/j.amjcard.2004.04.017.

Changeux, Jean-Pierre, and Arthur Christopoulos. 2016. “Allosteric Modulation as a Unifying Mechanism for Receptor Function and Regulation.” *Cell* 166 (5): 1084–1102. https://doi.org/10.1016/j.cell.2016.08.015.

Cino, Elio A., Mikko Karttunen, and Wing-Yiu Choy. 2012. “Effects of Molecular Crowding on the Dynamics of Intrinsically Disordered Proteins.” Edited by Yaakov Koby Levy. *PLoS ONE* 7 (11): e49876. https://doi.org/10.1371/journal.pone.0049876.

Ciruela, Francisco, Javier Burgueño, Vicent Casadó, Meritxell Canals, Daniel Marcellino, Steven R. Goldberg, Michael Bader, et al. 2004. “Combining Mass Spectrometry and Pull-Down Techniques for the Study of Receptor Heteromerization. Direct Epitope−Epitope Electrostatic Interactions between Adenosine A $_{2A}$ and Dopamine D $_2$ Receptors.” *Analytical Chemistry* 76 (18): 5354–63. https://doi.org/10.1021/ac049295f.

Clements, John M., Graham H. Catlin, Mickhael J. Price, and R.Mark Edwards. 1991. “Secretion of Human Epidermal Growth Factor from Saccharomyces Cerevisiae Using Synthetic Leader Sequences.” *Gene* 106 (2): 267–71. https://doi.org/10.1016/0378-1119(91)90209-T.

Cook, Julia V. F., and Karin A. Eidne. 1997. “An Intramolecular Disulfide Bond between Conserved Extracellular Cysteines in the Gonadotropin-Releasing Hormone Receptor Is Essential for Binding and Activation.” *Endocrinology* 138 (7): 2800–2806. https://doi.org/10.1210/endo.138.7.5233.

Cordomí, Arnau, Gemma Navarro, María S. Aymerich, and Rafael Franco. 2015. “Structures for G-Protein-Coupled Receptor Tetramers in Complex with G Proteins.” *Trends in Biochemical Sciences* 40 (10): 548–51. https://doi.org/10.1016/j.tibs.2015.07.007.

Cordomí, Arnau, Gemma Navarro, Leonardo Pardo, and Rafael Franco. 2020. “Structure of G-Protein-Coupled Receptor Heteromers.” In *GPCRs*, 109–19. Elsevier. https://doi.org/10.1016/B978-0-12-816228-6.00007-6.

Craig, Andrew F., Emily E. Clark, Indra D. Sahu, Rongfu Zhang, Nick D. Frantz, M. Sameer Al-Abdul-Wahid, Carole Dabney-Smith, Dominik Konkolewicz, and Gary A. Lorigan. 2016. “Tuning the Size of Styrene-Maleic Acid Copolymer-Lipid Nanoparticles (SMALPs) Using RAFT Polymerization for Biophysical Studies.” *Biochimica et Biophysica Acta (BBA) - Biomembranes* 1858 (11): 2931–39. https://doi.org/10.1016/j.bbamem.2016.08.004.

Creighton, Thomas E., David A. Hillson, and Robert B. Freedman. 1980. “Catalysis by Protein-Disulphide Isomerase of the Unfolding and Refolding of Proteins with Disulphide Bonds.” *Journal of Molecular Biology* 142 (1): 43–62. https://doi.org/10.1016/0022-2836(80)90205-3.

Cristóvão-Ferreira, Sofia, Gemma Navarro, Marc Brugarolas, Kamil Pérez-Capote, Sandra H. Vaz, Giorgia Fattorini, Fiorenzo Conti, et al. 2013. “A1R–A2AR Heteromers Coupled to Gs and Gi/0 Proteins Modulate GABA Transport into Astrocytes.” *Purinergic Signalling* 9 (3): 433–49. https://doi.org/10.1007/s11302-013-9364-5.

Cvejic, Svetlana, and Lakshmi A Devi. 1997. “Dimerization of the δ Opioid Receptor: Implication for a Role in Receptor Internalization.” *Journal of Biological Chemistry* 272 (43): 26959–64. https://doi.org/10.1074/jbc.272.43.26959.

Daura, Xavier, Karl Gademann, Bernhard Jaun, Dieter Seebach, Wilfred F. van Gunsteren, and Alan E. Mark. 1999. “Peptide Folding: When Simulation Meets Experiment.” *Angewandte Chemie International Edition* 38 (1–2): 236–40. https://doi.org/10.1002/(SICI)1521-3773(19990115)38:1/2<236::AID-ANIE236>3.0.CO;2-M.

Dawaliby, Rosie, Cataldo Trubbia, Cédric Delporte, Matthieu Masureel, Brian K Kobilka, and Cédric Govaerts. 2015. “Allosteric Regulation of G Protein–Coupled Receptor Activity by Phospholipids.” *Nature CHEMICAL BIOLOGY* 12: 7.

De Filippo, Elisabetta, Vigneshwaran Namasivayam, Lukas Zappe, Ali El-Tayeb, Anke C. Schiedel, and Christa E. Müller. 2016. “Role of Extracellular Cysteine Residues in the Adenosine A2A Receptor.” *Purinergic Signalling* 12 (2): 313–29. https://doi.org/10.1007/s11302-016-9506-7.

Dijkman, Patricia M., Oliver K. Castell, Alan D. Goddard, Juan C. Munoz-Garcia, Chris de Graaf, Mark I. Wallace, and Anthony Watts. 2018. “Dynamic Tuneable G Protein-Coupled Receptor Monomer-Dimer Populations.” *Nature Communications* 9 (1). https://doi.org/10.1038/s41467-018-03727-6.

Dioumaev, Andrei K., Leonid S. Brown, Jennifer Shih, Elena N. Spudich, John L. Spudich, and Janos K. Lanyi. 2002. “Proton Transfers in the Photochemical Reaction Cycle of Proteorhodopsin.” *Biochemistry* 41 (17): 5348–58. https://doi.org/10.1021/bi025563x.

Dioumaev, Andrei K., Jennifer M. Wang, Zoltán Bálint, György Váró, and Janos K. Lanyi. 2003. “Proton Transport by Proteorhodopsin Requires That the Retinal Schiff Base Counterion Asp-97 Be Anionic †.” *Biochemistry* 42 (21): 6582–87. https://doi.org/10.1021/bi034253r.

Doré, Andrew S., Nathan Robertson, James C. Errey, Irene Ng, Kaspar Hollenstein, Ben Tehan, Edward Hurrell, et al. 2011. “Structure of the Adenosine A2A Receptor in Complex with

ZM241385 and the Xanthines XAC and Caffeine." *Structure* 19 (9): 1283–93. https://doi.org/10.1016/j.str.2011.06.014.

Dörr, Jonas M., Martijn C. Koorengevel, Marre Schäfer, Alexander V. Prokofyev, Stefan Scheidelaar, Elwin A. W. van der Cruijsen, Timothy R. Dafforn, Marc Baldus, and J. Antoinette Killian. 2014. "Detergent-Free Isolation, Characterization, and Functional Reconstitution of a Tetrameric K^+ Channel: The Power of Native Nanodiscs." *Proceedings of the National Academy of Sciences* 111 (52): 18607–12. https://doi.org/10.1073/pnas.1416205112.

Dorsam, Robert T., and J. Silvio Gutkind. 2007. "G-Protein-Coupled Receptors and Cancer." *Nature Reviews Cancer* 7 (2): 79–94. https://doi.org/10.1038/nrc2069.

Drury, A. N., and A. Szent-Györgyi. 1929. "The Physiological Activity of Adenine Compounds with Especial Reference to Their Action upon the Mammalian Heart1." *The Journal of Physiology* 68 (3): 213–37. https://doi.org/10.1113/jphysiol.1929.sp002608.

Dürr, Ulrich H.N., Ronald Soong, and Ayyalusamy Ramamoorthy. 2013. "When Detergent Meets Bilayer: Birth and Coming of Age of Lipid Bicelles." *Progress in Nuclear Magnetic Resonance Spectroscopy* 69 (February): 1–22. https://doi.org/10.1016/j.pnmrs.2013.01.001.

Ecke, Denise, Theodor Hanck, Mohan E. Tulapurkar, Rainer Schäfer, Matthias Kassack, Rolf Stricker, and Georg Reiser. 2008. "Hetero-Oligomerization of the P2Y11 Receptor with the P2Y1 Receptor Controls the Internalization and Ligand Selectivity of the P2Y11 Receptor." *Biochemical Journal* 409 (1): 107–16. https://doi.org/10.1042/BJ20070671.

Eddy, Matthew T., Ming-Yue Lee, Zhan-Guo Gao, Kate L. White, Tatiana Didenko, Reto Horst, Martin Audet, et al. 2018. "Allosteric Coupling of Drug Binding and Intracellular Signaling in the A2A Adenosine Receptor." *Cell* 172 (1–2): 68-80.e12. https://doi.org/10.1016/j.cell.2017.12.004.

Edelstein, Stuart J., and Jean-Pierre Changeux. 2016. "Biased Allostery." *Biophysical Journal* 111 (5): 902–8. https://doi.org/10.1016/j.bpj.2016.07.044.

Eginton, Christopher, William J. Cressman, Sharrol Bachas, Herschel Wade, and Dorothy Beckett. 2015. "Allosteric Coupling via Distant Disorder-to-Order Transitions." *Journal of Molecular Biology* 427 (8): 1695–1704. https://doi.org/10.1016/j.jmb.2015.02.021.

El-Asmar, L. 2004. "Evidence for Negative Binding Cooperativity within CCR5-CCR2b Heterodimers." *Molecular Pharmacology* 67 (2): 460–69. https://doi.org/10.1124/mol.104.003624.

El-Asmar, Laïla, Jean-Yves Springael, Sébastien Ballet, Eneko Urizar Andrieu, Gilbert Vassart, and Marc Parmentier. 2005. "Evidence for Negative Binding Cooperativity within CCR5-CCR2b Heterodimers." *Molecular Pharmacology* 67 (2): 460–69. https://doi.org/10.1124/mol.104.003624.

Eswar, Narayanan, Ben Webb, Marc A. Marti-Renom, M.S. Madhusudhan, David Eramian, Min-yi Shen, Ursula Pieper, and Andrej Sali. 2006. "Comparative Protein Structure Modeling Using Modeller." *Current Protocols in Bioinformatics* 15 (1): 5.6.1-5.6.30. https://doi.org/10.1002/0471250953.bi0506s15.

Fagerberg, Linn, Kalle Jonasson, Gunnar von Heijne, Mathias Uhlén, and Lisa Berglund. 2010. "Prediction of the Human Membrane Proteome." *PROTEOMICS* 10 (6): 1141–49. https://doi.org/10.1002/pmic.200900258.

Faklaris, Orestis, Martin Cottet, Amandine Falco, Brice Villier, Michel Laget, Jurriaan M. Zwier, Eric Trinquet, Bernard Mouillac, Jean-Philippe Pin, and Thierry Durroux. 2015. "Multicolor Time-resolved Förster Resonance Energy Transfer Microscopy Reveals the Impact of GPCR Oligomerization on Internalization Processes." *The FASEB Journal* 29 (6): 2235–46. https://doi.org/10.1096/fj.14-260059.

Fanelli, Francesca, and Angelo Felline. 2011. "Dimerization and Ligand Binding Affect the Structure Network of A2A Adenosine Receptor." *Biochimica et Biophysica Acta (BBA) - Biomembranes* 1808 (5): 1256–66. https://doi.org/10.1016/j.bbamem.2010.08.006.

Farran, Batoul. 2017. “An Update on the Physiological and Therapeutic Relevance of GPCR Oligomers.” *Pharmacological Research* 117 (March): 303–27. https://doi.org/10.1016/j.phrs.2017.01.008.

Ferré, Sergi, Jordi Bonaventura, Dardo Tomasi, Gemma Navarro, Estefanía Moreno, Antonio Cortés, Carme Lluís, Vicent Casadó, and Nora D. Volkow. 2016. “Allosteric Mechanisms within the Adenosine A2A–Dopamine D2 Receptor Heterotetramer.” *Neuropharmacology* 104 (May): 154–60. https://doi.org/10.1016/j.neuropharm.2015.05.028.

Ferré, Sergi, Vicent Casadó, Lakshmi A. Devi, Marta Filizola, Ralf Jockers, Martin J. Lohse, Graeme Milligan, Jean-Philippe Pin, and Xavier Guitart. 2014. “G Protein–Coupled Receptor Oligomerization Revisited: Functional and Pharmacological Perspectives.” Edited by Mark P. Mattson. *Pharmacological Reviews* 66 (2): 413–34. https://doi.org/10.1124/pr.113.008052.

Ferré, Sergi, Francisco Ciruela, Meritxell Canals, Daniel Marcellino, Javier Burgueno, Vicent Casadó, Joëlle Hillion, et al. 2004. “Adenosine A2A-Dopamine D2 Receptor–Receptor Heteromers. Targets for Neuro-Psychiatric Disorders.” *Parkinsonism & Related Disorders* 10 (5): 265–71. https://doi.org/10.1016/j.parkreldis.2004.02.014.

Ferré, Sergi, Francisco Ciruela, Amina S. Woods, Carme Lluis, and Rafael Franco. 2007. “Functional Relevance of Neurotransmitter Receptor Heteromers in the Central Nervous System.” *Trends in Neurosciences* 30 (9): 440–46. https://doi.org/10.1016/j.tins.2007.07.001.

Ferré, Sergi, Steven R. Goldberg, Carme Lluis, and Rafael Franco. 2009. “Looking for the Role of Cannabinoid Receptor Heteromers in Striatal Function.” *Neuropharmacology* 56 (January): 226–34. https://doi.org/10.1016/j.neuropharm.2008.06.076.

Ferré, Sergi, Marzena Karcz-Kubicha, Bruce T. Hope, Patrizia Popoli, Javier Burgueño, M. Angeles Gutiérrez, Vicent Casadó, et al. 2002. “Synergistic Interaction between Adenosine A2A and Glutamate MGlu5 Receptors: Implications for Striatal Neuronal Function.” *Proceedings of the National Academy of Sciences* 99 (18): 11940–45. https://doi.org/10.1073/pnas.172393799.

Fotiadis, Dimitrios, Beata Jastrzebska, Ansgar Philippsen, Daniel J Müller, Krzysztof Palczewski, and Andreas Engel. 2006. “Structure of the Rhodopsin Dimer: A Working Model for G-Protein-Coupled Receptors.” *Current Opinion in Structural Biology* 16 (2): 252–59. https://doi.org/10.1016/j.sbi.2006.03.013.

Fotiadis, Dimitrios, Yan Liang, Sławomir Filipek, David A. Saperstein, Andreas Engel, and Krzysztof Palczewski. 2003. “Atomic-Force Microscopy Rhodopsin Dimers in Native Disc Membranes.” *Nature* 421 (6919): 127–28. https://doi.org/10.1038/421127a.

Fox, Daniel A., and Linda Columbus. 2013. “Solution NMR Resonance Assignment Strategies for β-Barrel Membrane Proteins: NMR Assignments of β-Barrel Membrane Proteins.” *Protein Science* 22 (8): 1133–40. https://doi.org/10.1002/pro.2291.

Gama, Lucio, Susan G. Wilt, and Gerda E. Breitwieser. 2001. “Heterodimerization of Calcium Sensing Receptors with Metabotropic Glutamate Receptors in Neurons.” *Journal of Biological Chemistry* 276 (42): 39053–59. https://doi.org/10.1074/jbc.M105662200.

Garavito, R. Michael, and Shelagh Ferguson-Miller. 2001. “Detergents as Tools in Membrane Biochemistry.” *Journal of Biological Chemistry* 276 (35): 32403–6. https://doi.org/10.1074/jbc.R100031200.

Garcıa-Nafrıa, Javier, Yang Lee, Xiaochen Bai, Byron Carpenter, and Christopher G Tate. 2018. “Cryo-EM Structure of the Adenosine A2A Receptor Coupled to an Engineered Heterotrimeric G Protein.” *ELife* 7: e35946.

Gaut, James R., and Linda M. Hendershot. 1993. “The Modification and Assembly of Proteins in the Endoplasmic Reticulum.” *Current Opinion in Cell Biology* 5 (4): 589–95. https://doi.org/10.1016/0955-0674(93)90127-C.

George, Susan R., Brian F. O’Dowd, and Samuel P. Lee. 2002. “G-Protein-Coupled Receptor Oligomerization and Its Potential for Drug Discovery.” *Nature Reviews Drug Discovery* 1 (10): 808–20. https://doi.org/10.1038/nrd913.

Ghosh, Anirban, Uddhavesh Sonavane, and Rajendra Joshi. 2014a. “Multiscale Modelling to Understand the Self-Assembly Mechanism of Human B2-Adrenergic Receptor in Lipid Bilayer.” *Computational Biology and Chemistry* 48 (February): 29–39. https://doi.org/10.1016/j.compbiolchem.2013.11.002.

———. 2014b. “Multiscale Modelling to Understand the Self-Assembly Mechanism of Human B2-Adrenergic Receptor in Lipid Bilayer.” *Computational Biology and Chemistry* 48 (February): 29–39. https://doi.org/10.1016/j.compbiolchem.2013.11.002.

Gietz, R. Daniel. 2014. “Yeast Transformation by the LiAc/SS Carrier DNA/PEG Method.” In *Yeast Protocols*, edited by Wei Xiao, 1163:33–44. Methods in Molecular Biology. New York, NY: Springer New York. https://doi.org/10.1007/978-1-4939-0799-1_4.

Gines, S., J. Hillion, M. Torvinen, S. Le Crom, V. Casado, E. I. Canela, S. Rondin, et al. 2000. “Dopamine D1 and Adenosine A1 Receptors Form Functionally Interacting Heteromeric Complexes.” *Proceedings of the National Academy of Sciences* 97 (15): 8606–11. https://doi.org/10.1073/pnas.150241097.

Goldenberg, David P., and Brian Argyle. 2014. “Minimal Effects of Macromolecular Crowding on an Intrinsically Disordered Protein: A Small-Angle Neutron Scattering Study.” *Biophysical Journal* 106 (4): 905–14. https://doi.org/10.1016/j.bpj.2013.12.003.

Golebiewska, Urszula, Jennifer M. Johnston, Lakshmi Devi, Marta Filizola, and Suzanne Scarlata. 2011. “Differential Response to Morphine of the Oligomeric State of μ-Opioid in the Presence of δ-Opioid Receptors.” *Biochemistry* 50 (14): 2829–37. https://doi.org/10.1021/bi101701x.

Gomes, I., A. Gupta, J. Filipovska, H. H. Szeto, J. E. Pintar, and L. A. Devi. 2004. “A Role for Heterodimerization of and Opiate Receptors in Enhancing Morphine Analgesia.” *Proceedings of the National Academy of Sciences* 101 (14): 5135–39. https://doi.org/10.1073/pnas.0307601101.

González-Maeso, Javier, Noelia V. Weisstaub, Mingming Zhou, Pokman Chan, Lidija Ivic, Rosalind Ang, Alena Lira, et al. 2007. “Hallucinogens Recruit Specific Cortical 5-HT2A Receptor-Mediated Signaling Pathways to Affect Behavior.” *Neuron* 53 (3): 439–52. https://doi.org/10.1016/j.neuron.2007.01.008.

“GPCR-EXP for Experimentally-Solved and Predicted GPCR Structures.” 2019. 2019. https://zhanglab.ccmb.med.umich.edu/GPCR-EXP/.

Grace, C. R. R., M. H. Perrin, J. Gulyas, M. R. DiGruccio, J. P. Cantle, J. E. Rivier, W. W. Vale, and R. Riek. 2007. “Structure of the N-Terminal Domain of a Type B1 G Protein-Coupled Receptor in Complex with a Peptide Ligand.” *Proceedings of the National Academy of Sciences* 104 (12): 4858–63. https://doi.org/10.1073/pnas.0700682104.

Grauschopf, Ulla, Hauke Lilie, Konrad Honold, Manfred Wozny, Dietmar Reusch, Angelika Esswein, Wolfgang Schäfer, Karl Peter Rücknagel, and Rainer Rudolph. 2000. “The N-Terminal Fragment of Human Parathyroid Hormone Receptor 1 Constitutes a Hormone Binding Domain and Reveals a Distinct Disulfide Pattern.” *Biochemistry* 39 (30): 8878–87. https://doi.org/10.1021/bi0001426.

Graziano, Giuseppe. 2010. “Hydrophobic Interaction of Two Large Plates: An Analysis of Salting-in/Salting-out Effects.” *Chemical Physics Letters* 491 (1–3): 54–58. https://doi.org/10.1016/j.cplett.2010.03.092.

Grethen, Anne, Abraham Olusegun Oluwole, Bartholomäus Danielczak, Carolyn Vargas, and Sandro Keller. 2017. “Thermodynamics of Nanodisc Formation Mediated by Styrene/Maleic Acid (2:1) Copolymer.” *Scientific Reports* 7 (1): 11517. https://doi.org/10.1038/s41598-017-11616-z.

Grinkova, Y. V., I. G. Denisov, and S. G. Sligar. 2010. “Engineering Extended Membrane Scaffold Proteins for Self-Assembly of Soluble Nanoscale Lipid Bilayers.” *Protein Engineering Design and Selection* 23 (11): 843–48. https://doi.org/10.1093/protein/gzq060.

Grover, Phulwinder K., and Rosemary L. Ryall. 2005. “Critical Appraisal of Salting-Out and Its Implications for Chemical and Biological Sciences.” *Chemical Reviews* 105 (1): 1–10. https://doi.org/10.1021/cr030454p.

Gsponer, Jörg, and M. Madan Babu. 2009. “The Rules of Disorder or Why Disorder Rules.” *Progress in Biophysics and Molecular Biology* 99 (2–3): 94–103. https://doi.org/10.1016/j.pbiomolbio.2009.03.001.

Guitart, Xavier, Gemma Navarro, Estefania Moreno, Hideaki Yano, Ning-Sheng Cai, Marta Sánchez-Soto, Sandeep Kumar-Barodia, et al. 2014. “Functional Selectivity of Allosteric Interactions within G Protein–Coupled Receptor Oligomers: The Dopamine D_1-D_3 Receptor Heterotetramer.” *Molecular Pharmacology* 86 (4): 417–29. https://doi.org/10.1124/mol.114.093096.

Gulati, Sonali, Mohammed Jamshad, Timothy J. Knowles, Kerrie A. Morrison, Rebecca Downing, Natasha Cant, Richard Collins, et al. 2014. “Detergent-Free Purification of ABC (ATP-Binding-Cassette) Transporters.” *Biochemical Journal* 461 (2): 269–78. https://doi.org/10.1042/BJ20131477.

Guo, Wen, Eneko Urizar, Michaela Kralikova, Juan Carlos Mobarec, Lei Shi, Marta Filizola, and Jonathan A Javitch. 2008. “Dopamine D2 Receptors Form Higher Order Oligomers at Physiological Expression Levels.” *The EMBO Journal* 27 (17): 2293–2304. https://doi.org/10.1038/emboj.2008.153.

Hall, Stephen C. L., Cecilia Tognoloni, Jack Charlton, Éilís C. Bragginton, Alice J. Rothnie, Pooja Sridhar, Mark Wheatley, et al. 2018. “An Acid-Compatible Co-Polymer for the Solubilization of Membranes and Proteins into Lipid Bilayer-Containing Nanoparticles.” *Nanoscale* 10 (22): 10609–19. https://doi.org/10.1039/C8NR01322E.

Hammerland, Lance G., Karen J. Krapcho, James E. Garrett, Nousheen Alasti, Benjamin C. P. Hung, Rachel T. Simin, Cynthia Levinthal, Edward F. Nemeth, and Forrest H. Fuller. 1999. “Domains Determining Ligand Specificity for Ca2+Receptors.” *Molecular Pharmacology* 55 (4): 642–48.

Han, Chung-Ta, Jichao Song, Tristan Chan, Christine Pruett, and Songi Han. 2020. “Electrostatic Environment of Proteorhodopsin Affects the PKa of Its Buried Primary Proton Acceptor.” *Biophysical Journal* 118 (8): 1838–49. https://doi.org/10.1016/j.bpj.2020.02.027.

Hanson, M. A., C. B. Roth, E. Jo, M. T. Griffith, F. L. Scott, G. Reinhart, H. Desale, et al. 2012. “Crystal Structure of a Lipid G Protein-Coupled Receptor.” *Science* 335 (6070): 851–55. https://doi.org/10.1126/science.1215904.

Hanson, Michael A., Vadim Cherezov, Mark T. Griffith, Christopher B. Roth, Veli-Pekka Jaakola, Ellen Y.T. Chien, Jeffrey Velasquez, Peter Kuhn, and Raymond C. Stevens. 2008. “A Specific Cholesterol Binding Site Is Established by the 2.8 Å Structure of the Human B2-Adrenergic Receptor.” *Structure* 16 (6): 897–905. https://doi.org/10.1016/j.str.2008.05.001.

Hasbi, Ahmed, Melissa L. Perreault, Maurice Y. F. Shen, Lucia Zhang, Ryan To, Theresa Fan, Tuan Nguyen, Xiaodong Ji, Brian F. O’Dowd, and Susan R. George. 2014. “A Peptide Targeting an Interaction Interface Disrupts the Dopamine D1-D2 Receptor Heteromer to Block Signaling and Function *in Vitro* and *in Vivo* : Effective Selective Antagonism.” *The FASEB Journal* 28 (11): 4806–20. https://doi.org/10.1096/fj.14-254037.

Hauser, Alexander S., Misty M. Attwood, Mathias Rask-Andersen, Helgi B. Schiöth, and David E. Gloriam. 2017. “Trends in GPCR Drug Discovery: New Agents, Targets and Indications.” *Nature Reviews Drug Discovery* 16 (12): 829–42. https://doi.org/10.1038/nrd.2017.178.

Hazell, Georgina G.J., Charles C. Hindmarch, George R. Pope, James A. Roper, Stafford L. Lightman, David Murphy, Anne-Marie O’Carroll, and Stephen J. Lolait. 2012. “G Protein-Coupled Receptors in the Hypothalamic Paraventricular and Supraoptic Nuclei – Serpentine Gateways to Neuroendocrine Homeostasis.” *Frontiers in Neuroendocrinology* 33 (1): 45–66. https://doi.org/10.1016/j.yfrne.2011.07.002.

Heijne, G. von. 2007. “The Membrane Protein Universe: What’s out There and Why Bother?” *Journal of Internal Medicine* 261 (6): 543–57. https://doi.org/10.1111/j.1365-2796.2007.01792.x.

Helenius, Ari, Thorsten Marquardt, and Ineke Braakman. 1992. “The Endoplasmic Reticulum as a Protein-Folding Compartment.” *Trends in Cell Biology* 2 (8): 227–31. https://doi.org/10.1016/0962-8924(92)90309-B.

Herrick-Davis, K., E. Grinde, T. Lindsley, M. Teitler, F. Mancia, A. Cowan, and J. E. Mazurkiewicz. 2015. “Native Serotonin 5-HT2C Receptors Are Expressed as Homodimers on the Apical Surface of Choroid Plexus Epithelial Cells.” *Molecular Pharmacology* 87 (4): 660–73. https://doi.org/10.1124/mol.114.096636.

Hess, Berk, Henk Bekker, Herman J. C. Berendsen, and Johannes G. E. M. Fraaije. 1997. “LINCS: A Linear Constraint Solver for Molecular Simulations.” *Journal of Computational Chemistry* 18 (12): 1463–72. https://doi.org/10.1002/(SICI)1096-987X(199709)18:12<1463::AID-JCC4>3.0.CO;2-H.

Heyda, Jan, Halil I. Okur, Jana Hladílková, Kelvin B. Rembert, William Hunn, Tinglu Yang, Joachim Dzubiella, Pavel Jungwirth, and Paul S. Cremer. 2017. “Guanidinium Can Both Cause and Prevent the Hydrophobic Collapse of Biomacromolecules.” *Journal of the American Chemical Society* 139 (2): 863–70. https://doi.org/10.1021/jacs.6b11082.

Hilairet, Sandrine, Monsif Bouaboula, Dominique Carrière, Gérard Le Fur, and Pierre Casellas. 2003. “Hypersensitization of the Orexin 1 Receptor by the CB1 Receptor: EVIDENCE FOR CROSS-TALK BLOCKED BY THE SPECIFIC CB1 ANTAGONIST, SR141716.” *Journal of Biological Chemistry* 278 (26): 23731–37. https://doi.org/10.1074/jbc.M212369200.

Hilser, V. J., and E. B. Thompson. 2007. “Intrinsic Disorder as a Mechanism to Optimize Allosteric Coupling in Proteins.” *Proceedings of the National Academy of Sciences* 104 (20): 8311–15. https://doi.org/10.1073/pnas.0700329104.

Hino, Tomoya, Takatoshi Arakawa, Hiroko Iwanari, Takami Yurugi-Kobayashi, Chiyo Ikeda-Suno, Yoshiko Nakada-Nakura, Osamu Kusano-Arai, et al. 2012. “G-Protein-Coupled Receptor Inactivation by an Allosteric Inverse-Agonist Antibody.” *Nature* 482 (7384): 237–40. https://doi.org/10.1038/nature10750.

Hinz, Sonja, Gemma Navarro, Dasiel Borroto-Escuela, Benjamin F. Seibt, York-Christoph Ammon, Elisabetta de Filippo, Azeem Danish, et al. 2018. “Adenosine A2A Receptor Ligand Recognition and Signaling Is Blocked by A2B Receptors.” *Oncotarget* 9 (17). https://doi.org/10.18632/oncotarget.24423.

Hofmeister, Franz. 1888. “Zur Lehre Yon Der Wirkung Der Salze.” *Archiv Für Experimentelle Pathologie Und Pharmakologie* 24 (4–5): 247–60.

Howard, Kathleen P., and Stanley J. Opella. 1996. “High-Resolution Solid-State NMR Spectra of Integral Membrane Proteins Reconstituted into Magnetically Oriented Phospholipid Bilayers.” *Journal of Magnetic Resonance, Series B* 112 (1): 91–94. https://doi.org/10.1006/jmrb.1996.0116.

Huang, Jianyun, Shuai Chen, J Jillian Zhang, and Xin-Yun Huang. 2013. “Crystal Structure of Oligomeric B1-Adrenergic G Protein–Coupled Receptors in Ligand-Free Basal State.” *Nature Structural & Molecular Biology* 20 (4): 419–25. https://doi.org/10.1038/nsmb.2504.

Huang, Shuya Kate, Omar Almurad, Reizel J. Pejana, Zachary A. Morrison, Aditya Pandey, Louis-Philippe Picard, Mark Nitz, Adnan Sljoka, and R. Scott Prosser. 2021. “Allosteric Modulation of the Adenosine A2A Receptor by Cholesterol.” *BioRxiv* 2021.09.13.460151 (September). https://doi.org/10.1101/2021.09.13.460151.

Hubbell, Wayne L, Hassane S Mchaourab, Christian Altenbach, and Michael A Lietzow. 1996. “Watching Proteins Move Using Site-Directed Spin Labeling.” *Structure* 4 (7): 779–83. https://doi.org/10.1016/S0969-2126(96)00085-8.

Humphrey, W., A. Dalke, and K. Schulten. 1996. “VMD: Visual Molecular Dynamics.” *Journal of Molecular Graphics* 14 (1): 33–38.

Hunte, Carola, and Hartmut Michel. 2002. “Crystallisation of Membrane Proteins Mediated by Antibody Fragments.” *Current Opinion in Structural Biology* 12 (4): 503–8. https://doi.org/10.1016/S0959-440X(02)00354-8.

Hurst, Dow P., Alan Grossfield, Diane L. Lynch, Scott Feller, Tod D. Romo, Klaus Gawrisch, Michael C. Pitman, and Patricia H. Reggio. 2010. “A Lipid Pathway for Ligand Binding Is Necessary for a Cannabinoid G Protein-Coupled Receptor.” *Journal of Biological Chemistry* 285 (23): 17954–64. https://doi.org/10.1074/jbc.M109.041590.

Hussain, Sunyia, Maia Kinnebrew, Nicole S. Schonenbach, Emily Aye, and Songi Han. 2015a. “Functional Consequences of the Oligomeric Assembly of Proteorhodopsin.” *Journal of Molecular Biology* 427 (6): 1278–90. https://doi.org/10.1016/j.jmb.2015.01.004.

———. 2015b. “Functional Consequences of the Oligomeric Assembly of Proteorhodopsin.” *Journal of Molecular Biology* 427 (6 0 0): 1278–90. https://doi.org/10.1016/j.jmb.2015.01.004.

Hustedt, Eric J., and Albert H. Beth. 1999. “NITROXIDE SPIN-SPIN INTERACTIONS: Applications to Protein Structure and Dynamics.” *Annual Review of Biophysics and Biomolecular Structure* 28 (1): 129–53. https://doi.org/10.1146/annurev.biophys.28.1.129.

Hwang, C, A. Sinskey, and H. Lodish. 1992. “Oxidized Redox State of Glutathione in the Endoplasmic Reticulum.” *Science* 257 (5076): 1496–1502. https://doi.org/10.1126/science.1523409.

Hyde, Alan M., Susan L. Zultanski, Jacob H. Waldman, Yong-Li Zhong, Michael Shevlin, and Feng Peng. 2017. “General Principles and Strategies for Salting-Out Informed by the Hofmeister Series.” *Organic Process Research & Development* 21 (9): 1355–70. https://doi.org/10.1021/acs.oprd.7b00197.

Idso, Matthew N., Naomi R. Baxter, Sirish Narayanan, Evelyn Chang, Julia Fisher, Bradley F. Chmelka, and Songi Han. 2019. “Proteorhodopsin Function Is Primarily Mediated by Oligomerization in Different Micellar Surfactant Solutions.” *The Journal of Physical Chemistry B* 123 (19): 4180–92. https://doi.org/10.1021/acs.jpcb.9b00922.

Ikeda, Daisuke, Yuji Furutani, and Hideki Kandori. 2007. “FTIR Study of the Retinal Schiff Base and Internal Water Molecules of Proteorhodopsin.” *Biochemistry* 46 (18): 5365–73. https://doi.org/10.1021/bi700143g.

Jaakola, Veli-Pekka, Jaime Prilusky, Joel L. Sussman, and Adrian Goldman. 2005. “G Protein-Coupled Receptors Show Unusual Patterns of Intrinsic Unfolding.” *Protein Engineering, Design and Selection* 18 (2): 103–10. https://doi.org/10.1093/protein/gzi004.

Jaakola, V.-P., M. T. Griffith, M. A. Hanson, V. Cherezov, E. Y. T. Chien, J. R. Lane, A. P. IJzerman, and R. C. Stevens. 2008. “The 2.6 Angstrom Crystal Structure of a Human A2A Adenosine Receptor Bound to an Antagonist.” *Science* 322 (5905): 1211–17. https://doi.org/10.1126/science.1164772.

Jain, Abhinav, Claire McGraw, and Anne Robinson. 2020. “The Adenosine A1 and A2A Receptor C-Termini Are Necessary for Activation but Not the Specificity of Downstream Signaling.” Authorea, Inc. https://doi.org/10.22541/au.158532015.55605148.

Jain, Abhinav R., Claire McGraw, and Anne S. Robinson. 2020. “The Specificity of Downstream Signaling for A1 and A2AR Does Not Depend on the C-Terminus, Despite the Importance of This Domain in Downstream Signaling Strength.” *Biomedicines* 8 (12): 603. https://doi.org/10.3390/biomedicines8120603.

Jamshad, Mohammed, Jack Charlton, Yu-Pin Lin, Sarah J. Routledge, Zharain Bawa, Timothy J. Knowles, Michael Overduin, et al. 2015. “G-Protein Coupled Receptor Solubilization and Purification for Biophysical Analysis and Functional Studies, in the Total Absence of Detergent.” *Bioscience Reports* 35 (2): 1–10. https://doi.org/10.1042/BSR20140171.

Jamshad, Mohammed, Vinciane Grimard, Ilaria Idini, Tim J. Knowles, Miriam R. Dowle, Naomi Schofield, Pooja Sridhar, et al. 2015. “Structural Analysis of a Nanoparticle Containing a Lipid Bilayer Used for Detergent-Free Extraction of Membrane Proteins.” *Nano Research* 8 (3): 774–89. https://doi.org/10.1007/s12274-014-0560-6.

Jong, Djurre H. de, Gurpreet Singh, W. F. Drew Bennett, Clement Arnarez, Tsjerk A. Wassenaar, Lars V. Schäfer, Xavier Periole, D. Peter Tieleman, and Siewert J. Marrink. 2013. "Improved Parameters for the Martini Coarse-Grained Protein Force Field." *Journal of Chemical Theory and Computation* 9 (1): 687–97. https://doi.org/10.1021/ct300646g.

Jorgensen, William L., Jayaraman Chandrasekhar, Jeffry D. Madura, Roger W. Impey, and Michael L. Klein. 1983. "Comparison of Simple Potential Functions for Simulating Liquid Water." *The Journal of Chemical Physics* 79 (2): 926–35. https://doi.org/10.1063/1.445869.

Kamiya, Toshio, Osamu Saitoh, Kazuaki Yoshioka, and Hiroyasu Nakata. 2003. "Oligomerization of Adenosine A2A and Dopamine D2 Receptors in Living Cells." *Biochemical and Biophysical Research Communications* 306 (2): 544–49. https://doi.org/10.1016/S0006-291X(03)00991-4.

Kasai, Rinshi S., Shuichi V. Ito, Ryo M. Awane, Takahiro K. Fujiwara, and Akihiro Kusumi. 2018. "The Class-A GPCR Dopamine D2 Receptor Forms Transient Dimers Stabilized by Agonists: Detection by Single-Molecule Tracking." *Cell Biochemistry and Biophysics* 76 (1–2): 29–37. https://doi.org/10.1007/s12013-017-0829-y.

Katritch, Vsevolod, Vadim Cherezov, and Raymond C. Stevens. 2012. "Diversity and Modularity of G Protein-Coupled Receptor Structures." *Trends in Pharmacological Sciences* 33 (1): 17–27. https://doi.org/10.1016/j.tips.2011.09.003.

Klare, Johann P. 2013. "Site-Directed Spin Labeling EPR Spectroscopy in Protein Research." *Biological Chemistry* 394 (10). https://doi.org/10.1515/hsz-2013-0155.

Klein, P., T. Sun, C. Saxe, A. Kimmel, R. Johnson, and P. Devreotes. 1988. "A Chemoattractant Receptor Controls Development in Dictyostelium Discoideum." *Science* 241 (4872): 1467–72. https://doi.org/10.1126/science.3047871.

Klotz, Karl-Norbert. 2000. "Adenosine Receptors and Their Ligands." *Naunyn-Schmiedeberg's Archives of Pharmacology* 362 (4–5): 382–91. https://doi.org/10.1007/s002100000315.

Klotz, K.-N., J. Hessling, J. Hegler, C. Owman, B. Kull, B. B. Fredholm, and M. J. Lohse. 1997. "Comparative Pharmacology of Human Adenosine Receptor Subtypes – Characterization of Stably Transfected Receptors in CHO Cells:" *Naunyn-Schmiedeberg's Archives of Pharmacology* 357 (1): 1–9. https://doi.org/10.1007/PL00005131.

Klug, Candice S., and Jimmy B. Feix. 2008. "Methods and Applications of Site-Directed Spin Labeling EPR Spectroscopy." In *Methods in Cell Biology*, 84:617–58. Elsevier. https://doi.org/10.1016/S0091-679X(07)84020-9.

Knowles, Timothy J., Rachael Finka, Corinne Smith, Yu-Pin Lin, Tim Dafforn, and Michael Overduin. 2009. "Membrane Proteins Solubilized Intact in Lipid Containing Nanoparticles Bounded by Styrene Maleic Acid Copolymer." *Journal of the American Chemical Society* 131 (22): 7484–85. https://doi.org/10.1021/ja810046q.

Koretz, Kirsten S., Claire E. McGraw, Steven Stradley, Ahmed Elbaradei, Noah Malmstadt, and Anne S. Robinson. 2021. "Characterization of Binding Kinetics of A2AR to Gαs Protein by Surface Plasmon Resonance." *Biophysical Journal* 120 (9): 1641–49. https://doi.org/10.1016/j.bpj.2021.02.032.

Kull, Björn, Per Svenningsson, Håkan Hall, and Bertil B Fredholm. 2000. "GTP Differentially Affects Antagonist Radioligand Binding to Adenosine A1 and A2A Receptors in Human Brain." *Neuropharmacology* 39 (12): 2374–80. https://doi.org/10.1016/S0028-3908(00)00081-2.

Kyte, Jack, and Russell F. Doolittle. 1982. "A Simple Method for Displaying the Hydropathic Character of a Protein." *Journal of Molecular Biology* 157 (1): 105–32. https://doi.org/10.1016/0022-2836(82)90515-0.

Lacapère, Jean-Jacques, Eva Pebay-Peyroula, Jean-Michel Neumann, and Catherine Etchebest. 2007. "Determining Membrane Protein Structures: Still a Challenge!" *Trends in Biochemical Sciences* 32 (6): 259–70. https://doi.org/10.1016/j.tibs.2007.04.001.

Lagerström, Malin C., and Helgi B. Schiöth. 2008. “Structural Diversity of G Protein-Coupled Receptors and Significance for Drug Discovery.” *Nature Reviews Drug Discovery* 7 (4): 339–57. https://doi.org/10.1038/nrd2518.

Lappas, Courtney M, Gail W Sullivan, and Joel Linden. 2005. “Adenosine A $_{2A}$ Agonists in Development for the Treatment of Inflammation.” *Expert Opinion on Investigational Drugs* 14 (7): 797–806. https://doi.org/10.1517/13543784.14.7.797.

Larsen, Teresa A, Arthur J Olson, and David S Goodsell. 1998. “Morphology of Protein–Protein Interfaces.” *Structure* 6 (4): 421–27. https://doi.org/10.1016/S0969-2126(98)00044-6.

Lebon, Guillaume, Tony Warne, Patricia C. Edwards, Kirstie Bennett, Christopher J. Langmead, Andrew G. W. Leslie, and Christopher G. Tate. 2011. “Agonist-Bound Adenosine A2A Receptor Structures Reveal Common Features of GPCR Activation.” *Nature* 474 (7352): 521–25. https://doi.org/10.1038/nature10136.

Lee, Samuel P., Christopher H. So, Asim J. Rashid, George Varghese, Regina Cheng, A. José Lança, Brian F. O’Dowd, and Susan R. George. 2004. “Dopamine D1 and D2 Receptor Co-Activation Generates a Novel Phospholipase C-Mediated Calcium Signal.” *Journal of Biological Chemistry* 279 (34): 35671–78. https://doi.org/10.1074/jbc.M401923200.

Lee, Yang, Tony Warne, Rony Nehmé, Shubhi Pandey, Hemlata Dwivedi-Agnihotri, Madhu Chaturvedi, Patricia C. Edwards, et al. 2020. “Molecular Basis of β-Arrestin Coupling to Formoterol-Bound B1-Adrenoceptor.” *Nature* 583 (7818): 862–66. https://doi.org/10.1038/s41586-020-2419-1.

Lefkowitz, Robert J. 2007. “Seven Transmembrane Receptors—A Brief Personal Retrospective.” *Biochimica et Biophysica Acta (BBA) - Biomembranes* 1768 (4): 748–55. https://doi.org/10.1016/j.bbamem.2006.11.001.

Lera Ruiz, Manuel de, Yeon-Hee Lim, and Junying Zheng. 2014. “Adenosine A $_{2A}$ Receptor as a Drug Discovery Target.” *Journal of Medicinal Chemistry* 57 (9): 3623–50. https://doi.org/10.1021/jm4011669.

Liang, Yan, Dimitrios Fotiadis, Sławomir Filipek, David A. Saperstein, Krzysztof Palczewski, and Andreas Engel. 2003. “Organization of the G Protein-Coupled Receptors Rhodopsin and Opsin in Native Membranes.” *Journal of Biological Chemistry* 278 (24): 21655–62. https://doi.org/10.1074/jbc.M302536200.

Lichtenberg, Dov, Hasna Ahyayauch, and Félix M. Goñi. 2013. “The Mechanism of Detergent Solubilization of Lipid Bilayers.” *Biophysical Journal* 105 (2): 289–99. https://doi.org/10.1016/j.bpj.2013.06.007.

Liman, Emily R. 2006. “Use It or Lose It: Molecular Evolution of Sensory Signaling in Primates.” *Pflügers Archiv - European Journal of Physiology* 453 (2): 125–31. https://doi.org/10.1007/s00424-006-0120-3.

Lindholm, Ljubica, Candan Ariöz, Michael Jawurek, Jobst Liebau, Lena Mäler, Åke Wieslander, Christoph von Ballmoos, and Andreas Barth. 2015. “Effect of Lipid Bilayer Properties on the Photocycle of Green Proteorhodopsin.” *Biochimica et Biophysica Acta (BBA) - Bioenergetics* 1847 (8): 698–708. https://doi.org/10.1016/j.bbabio.2015.04.011.

Liu, Haiqing, Yanjun Tian, Bingyuan Ji, Hai Lu, Qing Xin, Yunlu Jiang, Liangcai Ding, Jingmei Zhang, Jing Chen, and Bo Bai. 2016. “Heterodimerization of the Kappa Opioid Receptor and Neurotensin Receptor 1 Contributes to a Novel β-Arrestin-2–Biased Pathway.” *Biochimica et Biophysica Acta (BBA) - Molecular Cell Research* 1863 (11): 2719–38. https://doi.org/10.1016/j.bbamcr.2016.07.009.

Liu, W., E. Chun, A. A. Thompson, P. Chubukov, F. Xu, V. Katritch, G. W. Han, et al. 2012. “Structural Basis for Allosteric Regulation of GPCRs by Sodium Ions.” *Science* 337 (6091): 232–36. https://doi.org/10.1126/science.1219218.

Locker, Jacomine Krijnse, and Gareth Griffiths. 1999. “An Unconventional Role for Cytoplasmic Disulfide Bonds in Vaccinia Virus Proteins.” *Journal of Cell Biology* 144 (2): 267–79. https://doi.org/10.1083/jcb.144.2.267.

Logez, Christel, Marjorie Damian, Céline Legros, Clémence Dupré, Mélody Guéry, Sophie Mary, Renaud Wagner, et al. 2016. “Detergent-Free Isolation of Functional G Protein-Coupled Receptors into Nanometric Lipid Particles.” *Biochemistry* 55 (1): 38–48. https://doi.org/10.1021/acs.biochem.5b01040.

Lohse, M J, P Hein, C Hoffmann, V O Nikolaev, J-P Vilardaga, and M Bünemann. 2009. “Kinetics of G-Protein-Coupled Receptor Signals in Intact Cells: G-Protein-Coupled Receptor Signal Kinetics.” *British Journal of Pharmacology* 153 (S1): S125–32. https://doi.org/10.1038/sj.bjp.0707656.

Long, Ashley R, Catherine C O’Brien, Ketan Malhotra, Christine T Schwall, Arlene D Albert, Anthony Watts, and Nathan N Alder. 2013. “A Detergent-Free Strategy for the Reconstitution of Active Enzyme Complexes from Native Biological Membranes into Nanoscale Discs.” *BMC Biotechnology* 13 (1): 41. https://doi.org/10.1186/1472-6750-13-41.

Luttrell, Louis M., and Robert J. Lefkowitz. 2002. “The Role of β-Arrestins in the Termination and Transduction of G-Protein-Coupled Receptor Signals.” *Journal of Cell Science* 115 (3): 455–65.

Maciejko, Jakob, Michaela Mehler, Jagdeep Kaur, Tobias Lieblein, Nina Morgner, Olivier Ouari, Paul Tordo, Johanna Becker-Baldus, and Clemens Glaubitz. 2015. “Visualizing Specific Cross-Protomer Interactions in the Homo-Oligomeric Membrane Protein Proteorhodopsin by Dynamic-Nuclear-Polarization-Enhanced Solid-State NMR.” *Journal of the American Chemical Society* 137 (28): 9032–43. https://doi.org/10.1021/jacs.5b03606.

Magnani, F., Y. Shibata, M. J. Serrano-Vega, and C. G. Tate. 2008. “Co-Evolving Stability and Conformational Homogeneity of the Human Adenosine A2a Receptor.” *Proceedings of the National Academy of Sciences* 105 (31): 10744–49. https://doi.org/10.1073/pnas.0804396105.

Maire, Marc le, Philippe Champeil, and Jesper V Møller. 2000. “Interaction of Membrane Proteins and Lipids with Solubilizing Detergents.” *Biochimica et Biophysica Acta (BBA) - Biomembranes* 1508 (1–2): 86–111. https://doi.org/10.1016/S0304-4157(00)00010-1.

Malitschek, Barbara, Claude Schweizer, Miranda Keir, Jakob Heid, Wolfgang Froestl, Johannes Mosbacher, Rainer Kuhn, et al. 1999. “The N-Terminal Domain of γ-Aminobutyric AcidBReceptors Is Sufficient to Specify Agonist and Antagonist Binding.” *Molecular Pharmacology* 56 (2): 448–54. https://doi.org/10.1124/mol.56.2.448.

Manglik, Aashish, Andrew C. Kruse, Tong Sun Kobilka, Foon Sun Thian, Jesper M. Mathiesen, Roger K. Sunahara, Leonardo Pardo, William I. Weis, Brian K. Kobilka, and Sébastien Granier. 2012. “Crystal Structure of the M-Opioid Receptor Bound to a Morphinan Antagonist.” *Nature* 485 (7398): 321–26. https://doi.org/10.1038/nature10954.

Marcellino, Daniel, Sergi Ferré, Vicent Casadó, Antonio Cortés, Bernard Le Foll, Carmen Mazzola, Filippo Drago, et al. 2008. “Identification of Dopamine D_1 –D_3 Receptor Heteromers: INDICATIONS FOR A ROLE OF SYNERGISTIC D_1 –D_3 RECEPTOR INTERACTIONS IN THE STRIATUM.” *Journal of Biological Chemistry* 283 (38): 26016–25. https://doi.org/10.1074/jbc.M710349200.

Marenduzzo, Davide, Kieran Finan, and Peter R. Cook. 2006. “The Depletion Attraction: An Underappreciated Force Driving Cellular Organization.” *Journal of Cell Biology* 175 (5): 681–86. https://doi.org/10.1083/jcb.200609066.

Margeta-Mitrovic, Marta, Yuh Nung Jan, and Lily Yeh Jan. 2000. “A Trafficking Checkpoint Controls GABAB Receptor Heterodimerization.” *Neuron* 27 (1): 97–106. https://doi.org/10.1016/S0896-6273(00)00012-X.

Martoňák, R., A. Laio, and M. Parrinello. 2003. “Predicting Crystal Structures: The Parrinello-Rahman Method Revisited.” *Physical Review Letters* 90 (7). https://doi.org/10.1103/PhysRevLett.90.075503.

Martynowycz, Michael W., Anna Shiriaeva, Xuanrui Ge, Johan Hattne, Brent L. Nannenga, Vadim Cherezov, and Tamir Gonen. 2020. “MicroED Structure of the Human Adenosine Receptor Determined from a Single Nanocrystal in LCP.” Preprint. Biophysics. https://doi.org/10.1101/2020.09.27.316109.

McGraw, Claire, and Anne S. Robinson. 2017. “Membrane Cholesterol and the Adenosine A 2a Receptor.” *Biophysical Journal* 112 (3): 33a–34a. https://doi.org/10.1016/j.bpj.2016.11.216.

Milles, Sigrid, Nicola Salvi, Martin Blackledge, and Malene Ringkjøbing Jensen. 2018. “Characterization of Intrinsically Disordered Proteins and Their Dynamic Complexes: From in Vitro to Cell-like Environments.” *Progress in Nuclear Magnetic Resonance Spectroscopy* 109 (December): 79–100. https://doi.org/10.1016/j.pnmrs.2018.07.001.

Mirzadegan, Tara, Gil Benko, Sławomir Filipek, and Krzysztof Palczewski. 2003. “Sequence Analyses of G-Protein-Coupled Receptors: Similarities to Rhodopsin.” *Current Topics*, Biochemistry, 42 (10): 2759–67. https://doi.org/10.1021/bi027224+.

Möller, Jan, Ali Isbilir, Titiwat Sungkaworn, Brendan Osberg, Christos Karathanasis, Vikram Sunkara, Eugene O. Grushevskyi, et al. 2020. “Single-Molecule Analysis Reveals Agonist-Specific Dimer Formation of μ-Opioid Receptors.” *Nature Chemical Biology* 16 (9): 946–54. https://doi.org/10.1038/s41589-020-0566-1.

Monticelli, Luca, Senthil K. Kandasamy, Xavier Periole, Ronald G. Larson, D. Peter Tieleman, and Siewert-Jan Marrink. 2008. “The MARTINI Coarse-Grained Force Field: Extension to Proteins.” *Journal of Chemical Theory and Computation* 4 (5): 819–34. https://doi.org/10.1021/ct700324x.

Morelli, Micaela, Therese Di Paolo, Jadwiga Wardas, Frederic Calon, Danqing Xiao, and Michael A. Schwarzschild. 2007. “Role of Adenosine A2A Receptors in Parkinsonian Motor Impairment and L-DOPA-Induced Motor Complications.” *Progress in Neurobiology* 83 (5): 293–309. https://doi.org/10.1016/j.pneurobio.2007.07.001.

Morrison, Kerrie A., Aneel Akram, Ashlyn Mathews, Zoeya A. Khan, Jaimin H. Patel, Chumin Zhou, David J. Hardy, et al. 2016. “Membrane Protein Extraction and Purification Using Styrene–Maleic Acid (SMA) Copolymer: Effect of Variations in Polymer Structure.” *Biochemical Journal* 473 (23): 4349–60. https://doi.org/10.1042/BCJ20160723.

Mosslehy, Wageiha, Natalia Voskoboynikova, Alexandr Colbasevici, Adrian Ricke, Daniel Klose, Johann P. Klare, Armen Y. Mulkidjanian, and Heinz-Jürgen Steinhoff. 2019. “Conformational Dynamics of Sensory Rhodopsin II in Nanolipoprotein and Styrene–Maleic Acid Lipid Particles.” *Photochemistry and Photobiology* 95 (5): 1195–1204. https://doi.org/10.1111/php.13096.

Motlagh, Hesam N., James O. Wrabl, Jing Li, and Vincent J. Hilser. 2014. “The Ensemble Nature of Allostery.” *Nature* 508 (7496): 331–39. https://doi.org/10.1038/nature13001.

Mullard, Asher. 2014. “2013 FDA Drug Approvals.” *Nature Reviews Drug Discovery* 13 (2): 85–89. https://doi.org/10.1038/nrd4239.

Muth, Sabine, Anja Fries, and Gerald Gimpl. 2011. “Cholesterol-Induced Conformational Changes in the Oxytocin Receptor.” *Biochemical Journal* 437 (3): 541–53. https://doi.org/10.1042/BJ20101795.

Naranjo, Andrea N., Amy Chevalier, Gregory D. Cousins, Esther Ayettey, Emily C. McCusker, Carola Wenk, and Anne S. Robinson. 2015. “Conserved Disulfide Bond Is Not Essential for the Adenosine A2A Receptor: Extracellular Cysteines Influence Receptor Distribution within the Cell and Ligand-Binding Recognition.” *Biochimica et Biophysica Acta (BBA) - Biomembranes* 1848 (2): 603–14. https://doi.org/10.1016/j.bbamem.2014.11.010.

Navarro, Gemma, Paulina Carriba, Jorge Gandí, Francisco Ciruela, Vicent Casadó, Antoni Cortés, Josefa Mallol, Enric I. Canela, Carmen Lluis, and Rafael Franco. 2008. "Detection of Heteromers Formed by Cannabinoid CB $_1$, Dopamine D $_2$, and Adenosine A $_{2A}$ G-Protein-Coupled Receptors by Combining Bimolecular Fluorescence Complementation and Bioluminescence Energy Transfer." *The Scientific World JOURNAL* 8: 1088–97. https://doi.org/10.1100/tsw.2008.136.

Navarro, Gemma, Arnau Cordomí, Marc Brugarolas, Estefanía Moreno, David Aguinaga, Laura Pérez-Benito, Sergi Ferre, et al. 2018. "Cross-Communication between Gi and Gs in a G-Protein-Coupled Receptor Heterotetramer Guided by a Receptor C-Terminal Domain." *BMC Biology* 16 (1). https://doi.org/10.1186/s12915-018-0491-x.

Navarro, Gemma, Arnau Cordomí, Verónica Casadó-Anguera, Estefanía Moreno, Ning-Sheng Cai, Antoni Cortés, Enric I. Canela, et al. 2018. "Evidence for Functional Pre-Coupled Complexes of Receptor Heteromers and Adenylyl Cyclase." *Nature Communications* 9 (1). https://doi.org/10.1038/s41467-018-03522-3.

Navarro, Gemma, Arnau Cordomí, Monika Zelman-Femiak, Marc Brugarolas, Estefania Moreno, David Aguinaga, Laura Perez-Benito, et al. 2016. "Quaternary Structure of a G-Protein-Coupled Receptor Heterotetramer in Complex with Gi and Gs." *BMC Biology* 14 (1). https://doi.org/10.1186/s12915-016-0247-4.

Navarro, Gemma, Sergi Ferré, Arnau Cordomi, Estefania Moreno, Josefa Mallol, Vicent Casadó, Antoni Cortés, et al. 2010. "Interactions between Intracellular Domains as Key Determinants of the Quaternary Structure and Function of Receptor Heteromers." *Journal of Biological Chemistry* 285 (35): 27346–59. https://doi.org/10.1074/jbc.M110.115634.

Nelson, Greg, Mark A. Hoon, Jayaram Chandrashekar, Yifeng Zhang, Nicholas J.P. Ryba, and Charles S. Zuker. 2001. "Mammalian Sweet Taste Receptors." *Cell* 106 (3): 381–90. https://doi.org/10.1016/S0092-8674(01)00451-2.

Ng, Gordon Y. K., Janet Clark, Nathalie Coulombe, Nathalie Ethier, Terence E. Hebert, Richard Sullivan, Stacia Kargman, et al. 1999. "Identification of a GABA $_B$ Receptor Subunit, Gb2, Required for Functional GABA $_B$ Receptor Activity." *Journal of Biological Chemistry* 274 (12): 7607–10. https://doi.org/10.1074/jbc.274.12.7607.

Nguyen, Khanh Dinh Quoc, Michael Vigers, Eric Sefah, Susanna Seppälä, Jennifer Paige Hoover, Nicole Star Schonenbach, Blake Mertz, Michelle Ann O'Malley, and Songi Han. 2021. "Homo-Oligomerization of the Human Adenosine A2A Receptor Is Driven by the Intrinsically Disordered C-Terminus." *ELife* 10 (July): e66662. https://doi.org/10.7554/eLife.66662.

Niebauer, Ronald T., and Anne Skaja Robinson. 2006. "Exceptional Total and Functional Yields of the Human Adenosine (A2a) Receptor Expressed in the Yeast Saccharomyces Cerevisiae." *Protein Expression and Purification* 46 (2): 204–11. https://doi.org/10.1016/j.pep.2005.09.020.

Nobles, Kelly N., Kunhong Xiao, Seungkirl Ahn, Arun K. Shukla, Christopher M. Lam, Sudarshan Rajagopal, Ryan T. Strachan, et al. 2011. "Distinct Phosphorylation Sites on the B2-Adrenergic Receptor Establish a Barcode That Encodes Differential Functions of β-Arrestin." *Sci. Signal.* 4 (185): ra51–ra51. https://doi.org/10.1126/scisignal.2001707.

Nørholm, Morten HH. 2010. "A Mutant Pfu DNA Polymerase Designed for Advanced Uracil-Excision DNA Engineering." *BMC Biotechnology* 10 (1): 21. https://doi.org/10.1186/1472-6750-10-21.

Nour-Eldin, Hussam H., Bjarne G. Hansen, Morten H. H. Nørholm, Jacob K. Jensen, and Barbara A. Halkier. 2006. "Advancing Uracil-Excision Based Cloning towards an Ideal Technique for Cloning PCR Fragments." *Nucleic Acids Research* 34 (18): e122–e122. https://doi.org/10.1093/nar/gkl635.

Oakley, Robert H., Stéphane A. Laporte, Jason A. Holt, Larry S. Barak, and Marc G. Caron. 2001. "Molecular Determinants Underlying the Formation of Stable Intracellular G Protein-Coupled Receptor-β-Arrestin Complexes after Receptor Endocytosis*." *Journal of Biological Chemistry* 276 (22): 19452–60. https://doi.org/10.1074/jbc.M101450200.

Oakley, Robert H., Stéphane A. Laporte, Jason A. Holt, Larry S. Barak, Marc G. Caron, and §. 1999. "Association of β-Arrestin with G Protein-Coupled Receptors during Clathrin-Mediated Endocytosis Dictates the Profile of Receptor Resensitization." *Journal of Biological Chemistry* 274 (45): 32248–57. https://doi.org/10.1074/jbc.274.45.32248.

Oh, Kyoung Joon, Christian Altenbach, R. John Collier, and Wayne L. Hubbell. 2000. "Site-Directed Spin Labeling of Proteins: Applications to Diphtheria Toxin." In *Bacterial Toxins*, by Otto Holst, 145:147–69. New Jersey: Humana Press. https://doi.org/10.1385/1-59259-052-7:147.

O'Hara, Patrick J., Paul O. Sheppard, Henning Thógersen, Domenick Venezia, Betty A. Haldeman, Vicki McGrane, Khaled M. Houamed, Christian Thomsen, Teresa L. Gilbert, and Eileen R. Mulvihill. 1993. "The Ligand-Binding Domain in Metabotropic Glutamate Receptors Is Related to Bacterial Periplasmic Binding Proteins." *Neuron* 11 (1): 41–52. https://doi.org/10.1016/0896-6273(93)90269-W.

Oliveira, Paulo A. de, James A. R. Dalton, Marc López-Cano, Adrià Ricarte, Xavier Morató, Filipe C. Matheus, Andréia S. Cunha, et al. 2017. "Angiotensin II Type 1/Adenosine A 2A Receptor Oligomers: A Novel Target for Tardive Dyskinesia." *Scientific Reports* 7 (1). https://doi.org/10.1038/s41598-017-02037-z.

Oluwole, Abraham Olusegun, Bartholomäus Danielczak, Annette Meister, Jonathan Oyebamiji Babalola, Carolyn Vargas, and Sandro Keller. 2017. "Solubilization of Membrane Proteins into Functional Lipid-Bilayer Nanodiscs Using a Diisobutylene/Maleic Acid Copolymer." *Angewandte Chemie International Edition* 56 (7): 1919–24. https://doi.org/10.1002/anie.201610778.

O'Malley, Michelle A., Tzvetana Lazarova, Zachary T. Britton, and Anne S. Robinson. 2007. "High-Level Expression in Saccharomyces Cerevisiae Enables Isolation and Spectroscopic Characterization of Functional Human Adenosine A2a Receptor." *Journal of Structural Biology* 159 (2): 166–78. https://doi.org/10.1016/j.jsb.2007.05.001.

O'Malley, Michelle A., J. Dominic Mancini, Carissa L. Young, Emily C. McCusker, David Raden, and Anne S. Robinson. 2009. "Progress toward Heterologous Expression of Active G-Protein-Coupled Receptors in *Saccharomyces Cerevisiae* : Linking Cellular Stress Response with Translocation and Trafficking." *Protein Science* 18 (11): 2356–70. https://doi.org/10.1002/pro.246.

O'Malley, Michelle A., Andrea N. Naranjo, Tzvetana Lazarova, and Anne S. Robinson. 2010a. "Analysis of Adenosine A $_2$ a Receptor Stability: Effects of Ligands and Disulfide Bonds." *Biochemistry* 49 (43): 9181–89. https://doi.org/10.1021/bi101155r.

———. 2010b. "Analysis of Adenosine A $_2$ a Receptor Stability: Effects of Ligands and Disulfide Bonds." *Biochemistry* 49 (43): 9181–89. https://doi.org/10.1021/bi101155r.

Ongini, E., Silvio Dionisotti, Stefania Gessi, E. Irenius, and Bertil B. Fredholm. 1999. "Comparison of CGS 15943, ZM 241385 and SCH 58261 as Antagonists at Human Adenosine Receptors:" *Naunyn-Schmiedeberg's Archives of Pharmacology* 359 (1): 7–10. https://doi.org/10.1007/PL00005326.

Opekarová, M, and W Tanner. 2003. "Specific Lipid Requirements of Membrane Proteins—a Putative Bottleneck in Heterologous Expression." *Biochimica et Biophysica Acta (BBA) - Biomembranes* 1610 (1): 11–22. https://doi.org/10.1016/S0005-2736(02)00708-3.

Orwick, Marcella C., Peter J. Judge, Jan Procek, Ljubica Lindholm, Andrea Graziadei, Andreas Engel, Gerhard Gröbner, and Anthony Watts. 2012. "Detergent-Free Formation and Physicochemical Characterization of Nanosized Lipid-Polymer Complexes: Lipodisq." *Angewandte Chemie* 124 (19): 4731–35. https://doi.org/10.1002/ange.201201355.

Overington, John P., Bissan Al-Lazikani, and Andrew L. Hopkins. 2006. "How Many Drug Targets Are There?" *Nature Reviews Drug Discovery* 5 (12): 993–96. https://doi.org/10.1038/nrd2199.

Overton, Mark C., and Kendall J. Blumer. 2000. "G-Protein-Coupled Receptors Function as Oligomers in Vivo." *Current Biology* 10 (6): 341–44. https://doi.org/10.1016/S0960-9822(00)00386-9.

Palczewski, Krzysztof, Takashi Kumasaka, Tetsuya Hori, Craig A Behnke, Hiroyuki Motoshima, Brian A Fox, Isolde Le Trong, et al. 2000. “Crystal Structure of Rhodopsin: A G Protein–Coupled Receptor” 289: 8.

Palle, Venkata P, Elfatih O Elzein, Scott A Gothe, Zhihe Li, Zhenhai Gao, Stephanie Meyer, Brent Blackburn, and Jeff A Zablocki. 2002. “Structure–Affinity Relationships of the Affinity of 2-Pyrazolyl Adenosine Analogues for the Adenosine A2A Receptor.” *Bioorg. Med. Chem. Lett.*, 5.

Pándy-Szekeres, Gáspár, Christian Munk, Tsonko M Tsonkov, Stefan Mordalski, Kasper Harpsøe, Alexander S Hauser, Andrzej J Bojarski, and David E Gloriam. 2018. “GPCRdb in 2018: Adding GPCR Structure Models and Ligands.” *Nucleic Acids Research* 46 (D1): D440–46. https://doi.org/10.1093/nar/gkx1109.

Parekh, R.N., Kathy J. Forrester, and D. Wittrup. 1995. “Multicopy Overexpression of Bovine Pancreatic Trypsin Inhibitor Saturates the Protein Folding and Secretory Capacity of Saccharomyces Cerevisiae.” *Protein Expression and Purification* 6 (4): 537–45. https://doi.org/10.1006/prep.1995.1071.

Parekh, R.N., M.R. Shaw, and K.D. Wittrup. 1996. “An Integrating Vector for Tunable, High Copy, Stable Integration into the Dispersed Ty δ Sites of Saccharomyces Cerevisiae.” *Biotechnology Progress* 12 (1): 16–21. https://doi.org/10.1021/bp9500627.

Park, Sang Ho, Sabrina Berkamp, Gabriel A. Cook, Michelle K. Chan, Hector Viadiu, and Stanley J. Opella. 2011. “Nanodiscs versus Macrodiscs for NMR of Membrane Proteins.” *Biochemistry* 50 (42): 8983–85. https://doi.org/10.1021/bi201289c.

Paulin, Sarah, Mohammed Jamshad, Timothy R Dafforn, Jorge Garcia-Lara, Simon J Foster, Nicola F Galley, David I Roper, Helena Rosado, and Peter W Taylor. 2014. “Surfactant-Free Purification of Membrane Protein Complexes from Bacteria: Application to the Staphylococcal Penicillin-Binding Protein Complex PBP2/PBP2a.” *Nanotechnology* 25 (28): 285101. https://doi.org/10.1088/0957-4484/25/28/285101.

Periole, Xavier, Marco Cavalli, Siewert-Jan Marrink, and Marco A. Ceruso. 2009. “Combining an Elastic Network With a Coarse-Grained Molecular Force Field: Structure, Dynamics, and Intermolecular Recognition.” *Journal of Chemical Theory and Computation* 5 (9): 2531–43. https://doi.org/10.1021/ct9002114.

Periole, Xavier, Adam M. Knepp, Thomas P. Sakmar, Siewert J. Marrink, and Thomas Huber. 2012. “Structural Determinants of the Supramolecular Organization of G Protein-Coupled Receptors in Bilayers.” *Journal of the American Chemical Society* 134 (26): 10959–65. https://doi.org/10.1021/ja303286e.

Perlman, Jeffrey H., Wei Wang, Daniel R. Nussenzveig, and Marvin C. Gershengorn. 1995. “A Disulfide Bond between Conserved Extracellular Cysteines in the Thyrotropin-Releasing Hormone Receptor Is Critical for Binding.” *Journal of Biological Chemistry* 270 (42): 24682–85. https://doi.org/10.1074/jbc.270.42.24682.

Pin, J.-P., R. Neubig, M. Bouvier, L. Devi, M. Filizola, J. A. Javitch, M. J. Lohse, et al. 2007. “International Union of Basic and Clinical Pharmacology. LXVII. Recommendations for the Recognition and Nomenclature of G Protein-Coupled Receptor Heteromultimers.” *Pharmacological Reviews* 59 (1): 5–13. https://doi.org/10.1124/pr.59.1.5.

Pollack, A.E., and J.S. Fink. 1995. “Adenosine Antagonists Potentiate D2 Dopamine-Dependent Activation of Fos in the Striatopallidal Pathway.” *Neuroscience* 68 (3): 721–28. https://doi.org/10.1016/0306-4522(95)00168-I.

Popot, J. L., and D. M. Engelman. 1990. “Membrane Protein Folding and Oligomerization: The Two-Stage Model.” *Biochemistry* 29 (17): 4031–37. https://doi.org/10.1021/bi00469a001.

Postis, Vincent, Shaun Rawson, Jennifer K. Mitchell, Sarah C. Lee, Rosemary A. Parslow, Tim R. Dafforn, Stephen A. Baldwin, and Stephen P. Muench. 2015. “The Use of SMALPs as a Novel Membrane Protein Scaffold for Structure Study by Negative Stain Electron Microscopy.”

Biochimica et Biophysica Acta (BBA) - Biomembranes 1848 (2): 496–501. https://doi.org/10.1016/j.bbamem.2014.10.018.

Pratt, Lawrence R., and David Chandler. 1977. "Theory of the Hydrophobic Effect." *The Journal of Chemical Physics* 67 (8): 3683–3704. https://doi.org/10.1063/1.435308.

Prezeau, Laurent, Marie-Laure Rives, Laëtitia Comps-Agrar, Damien Maurel, Julie Kniazeff, and Jean-Philippe Pin. 2010. "Functional Crosstalk between GPCRs: With or without Oligomerization." *Current Opinion in Pharmacology* 10 (1): 6–13. https://doi.org/10.1016/j.coph.2009.10.009.

Privé, Gilbert G. 2007. "Detergents for the Stabilization and Crystallization of Membrane Proteins." *Methods* 41 (4): 388–97. https://doi.org/10.1016/j.ymeth.2007.01.007.

Prosser, R. Scott, Libin Ye, Aditya Pandey, and Alexander Orazietti. 2017. "Activation Processes in Ligand-Activated G Protein-Coupled Receptors: A Case Study of the Adenosine A2A Receptor." *BioEssays* 39 (9): 1700072. https://doi.org/10.1002/bies.201700072.

Pucadyil, Thomas J., and Amitabha Chattopadhyay. 2006. "Role of Cholesterol in the Function and Organization of G-Protein Coupled Receptors." *Progress in Lipid Research* 45 (4): 295–333. https://doi.org/10.1016/j.plipres.2006.02.002.

Qin, Kou, Chunmin Dong, Guangyu Wu, and Nevin A Lambert. 2011. "Inactive-State Preassembly of Gq-Coupled Receptors and Gq Heterotrimers." *Nature Chemical Biology* 7 (10): 740–47. https://doi.org/10.1038/nchembio.642.

Qin, Sanbo, and Huan-Xiang Zhou. 2013. "Effects of Macromolecular Crowding on the Conformational Ensembles of Disordered Proteins." *The Journal of Physical Chemistry Letters* 4 (20): 3429–34. https://doi.org/10.1021/jz401817x.

Quick, Matthias, Lei Shi, Britta Zehnpfennig, Harel Weinstein, and Jonathan A Javitch. 2012. "Experimental Conditions Can Obscure the Second High-Affinity Site in LeuT." *Nature Structural & Molecular Biology* 19 (2): 207–11. https://doi.org/10.1038/nsmb.2197.

Ranaghan, Matthew J., Christine T. Schwall, Nathan N. Alder, and Robert R. Birge. 2011. "Green Proteorhodopsin Reconstituted into Nanoscale Phospholipid Bilayers (Nanodiscs) as Photoactive Monomers." *Journal of the American Chemical Society* 133 (45): 18318–27. https://doi.org/10.1021/ja2070957.

Rashid, A. J., C. H. So, M. M. C. Kong, T. Furtak, M. El-Ghundi, R. Cheng, B. F. O'Dowd, and S. R. George. 2007. "D1-D2 Dopamine Receptor Heterooligomers with Unique Pharmacology Are Coupled to Rapid Activation of Gq/11 in the Striatum." *Proceedings of the National Academy of Sciences* 104 (2): 654–59. https://doi.org/10.1073/pnas.0604049104.

Rask-Andersen, Mathias, Surendar Masuram, and Helgi B. Schiöth. 2014. "The Druggable Genome: Evaluation of Drug Targets in Clinical Trials Suggests Major Shifts in Molecular Class and Indication." *Annual Review of Pharmacology and Toxicology* 54 (1): 9–26. https://doi.org/10.1146/annurev-pharmtox-011613-135943.

Rasmussen, Søren G. F., Brian T. DeVree, Yaozhong Zou, Andrew C. Kruse, Ka Young Chung, Tong Sun Kobilka, Foon Sun Thian, et al. 2011. "Crystal Structure of the B2 Adrenergic Receptor–Gs Protein Complex." *Nature* 477 (7366): 549–55. https://doi.org/10.1038/nature10361.

Ravula, Thirupathi, Nathaniel Z. Hardin, Sudheer Kumar Ramadugu, Sarah J. Cox, and Ayyalusamy Ramamoorthy. 2018. "Formation of PH-Resistant Monodispersed Polymer-Lipid Nanodiscs." *Angewandte Chemie International Edition* 57 (5): 1342–45. https://doi.org/10.1002/anie.201712017.

Robberecht, Patrick, Philippe Gourlet, Philippe Neef, Marie-Claire Woussen-Colle, Marie-Claire Vandermeers-Piret, Andre Vandermeers, and Jean Christophe. 1992. "Structural Requirements for the Occupancy of Pituitary Adenylate-Cyclase-Activating-Peptide (PACAP) Receptors and Adenylate Cyclase Activation in Human Neuroblastoma NB-OK-1 Cell Membranes. Discovery of PACAP(6-38) as a Potent Antagonist." *European Journal of Biochemistry* 207 (1): 239–46. https://doi.org/10.1111/j.1432-1033.1992.tb17043.x.

Robbins, Melanie J., Andrew R. Calver, Alexander K. Filippov, Warren D. Hirst, Robert B. Russell, Martyn D. Wood, Shabina Nasir, et al. 2001. "GABA $_{B2}$ Is Essential for G-Protein Coupling of the GABA $_{B}$ Receptor Heterodimer." *The Journal of Neuroscience* 21 (20): 8043–52. https://doi.org/10.1523/JNEUROSCI.21-20-08043.2001.

Romano, Carmelo, Wan-Lin Yang, and Karen L. O'Malley. 1996. "Metabotropic Glutamate Receptor 5 Is a Disulfide-Linked Dimer." *Journal of Biological Chemistry* 271 (45): 28612–16. https://doi.org/10.1074/jbc.271.45.28612.

Romo, T.D., and A. Grossfield. 2009. "LOOS: An Extensible Platform for the Structural Analysis of Simulations." In *2009 Annual International Conference of the IEEE Engineering in Medicine and Biology Society*, 2332–35. Minneapolis, MN: IEEE. https://doi.org/10.1109/IEMBS.2009.5335065.

Römpler, Holger, Claudia Stäubert, Doreen Thor, Angela Schulz, Michael Hofreiter, and Torsten Schöneberg. 2007. "G Protein-Coupled Time Travel: Evolutionary Aspects of GPCR Research." *Molecular Interventions* 7 (1): 17–25. https://doi.org/doi: 10.1124/mi.7.1.5.

Routledge, Sarah J., Mohammed Jamshad, Haydn A. Little, Yu-Pin Lin, John Simms, Alpesh Thakker, Corinne M. Spickett, et al. 2020. "Ligand-Induced Conformational Changes in a SMALP-Encapsulated GPCR." *Biochimica et Biophysica Acta (BBA) - Biomembranes* 1862 (6): 183235. https://doi.org/10.1016/j.bbamem.2020.183235.

Rozenfeld, Raphael, and Lakshmi A. Devi. 2007. "Receptor Heterodimerization Leads to a Switch in Signaling: B-arrestin2-mediated ERK Activation by M-δ Opioid Receptor Heterodimers." *The FASEB Journal* 21 (10): 2455–65. https://doi.org/10.1096/fj.06-7793com.

Runge, Steffen, Christian Gram, Hans Bräuner-Osborne, Kjeld Madsen, Lotte B. Knudsen, and Birgitte S. Wulff. 2003. "Three Distinct Epitopes on the Extracellular Face of the Glucagon Receptor Determine Specificity for the Glucagon Amino Terminus." *Journal of Biological Chemistry* 278 (30): 28005–10. https://doi.org/10.1074/jbc.M301085200.

Saaranen, Mirva J., and Lloyd W. Ruddock. 2013. "Disulfide Bond Formation in the Cytoplasm." *Antioxidants & Redox Signaling* 19 (1): 46–53. https://doi.org/10.1089/ars.2012.4868.

Scheidelaar, Stefan, Martijn C. Koorengevel, Juan Dominguez Pardo, Johannes D. Meeldijk, Eefjan Breukink, and J. Antoinette Killian. 2015. "Molecular Model for the Solubilization of Membranes into Nanodisks by Styrene Maleic Acid Copolymers." *Biophysical Journal* 108 (2): 279–90. https://doi.org/10.1016/j.bpj.2014.11.3464.

Scheidelaar, Stefan, Martijn C. Koorengevel, Cornelius A. van Walree, Juan J. Dominguez, Jonas M. Dörr, and J. Antoinette Killian. 2016. "Effect of Polymer Composition and PH on Membrane Solubilization by Styrene-Maleic Acid Copolymers." *Biophysical Journal* 111 (9): 1974–86. https://doi.org/10.1016/j.bpj.2016.09.025.

Schindler, Charles W, Marzena Karcz-Kubicha, Eric B Thorndike, Christa E Müller, Srihari R Tella, Sergi Ferré, and Steven R Goldberg. 2005. "Role of Central and Peripheral Adenosine Receptors in the Cardiovascular Responses to Intraperitoneal Injections of Adenosine A $_{1}$ and A $_{2A}$ Subtype Receptor Agonists." *British Journal of Pharmacology* 144 (5): 642–50. https://doi.org/10.1038/sj.bjp.0706043.

Schonenbach, Nicole S., Sunyia Hussain, and Michelle A. O'Malley. 2015. "Structure and Function of G Protein-Coupled Receptor Oligomers: Implications for Drug Discovery: Studying GPCR Oligomer Function." *Wiley Interdisciplinary Reviews: Nanomedicine and Nanobiotechnology* 7 (3): 408–27. https://doi.org/10.1002/wnan.1319.

Schonenbach, Nicole S., Monica D. Rieth, Songi Han, and Michelle A. O'Malley. 2016. "Adenosine A2a Receptors Form Distinct Oligomers in Protein Detergent Complexes." *FEBS Letters* 590 (18): 3295–3306. https://doi.org/10.1002/1873-3468.12367.

Schuler, Mary A., Ilia G. Denisov, and Stephen G. Sligar. 2013. "Nanodiscs as a New Tool to Examine Lipid–Protein Interactions." In *Lipid-Protein Interactions*, edited by Jörg H. Kleinschmidt,

974:415–33. Methods in Molecular Biology. Totowa, NJ: Humana Press. https://doi.org/10.1007/978-1-62703-275-9_18.

Schwarzschild, Michael A., Luigi Agnati, Kjell Fuxe, Jiang-Fan Chen, and Micaela Morelli. 2006. "Targeting Adenosine A2A Receptors in Parkinson's Disease." *Trends in Neurosciences* 29 (11): 647–54. https://doi.org/10.1016/j.tins.2006.09.004.

Sharma, Naveen, Ajay Suresh Akhade, and Ayub Qadri. 2013. "Sphingosine-1-Phosphate Suppresses TLR-Induced CXCL8 Secretion from Human T Cells." *Journal of Leukocyte Biology* 93 (4): 521–28. https://doi.org/10.1189/jlb.0712328.

Shivnaraine, Rabindra V, Brendan Kelly, Krishana S Sankar, Dar'ya S Redka, Yi Rang Han, Fei Huang, Gwendolynne Elmslie, et al. 2016. "Allosteric Modulation in Monomers and Oligomers of a G Protein-Coupled Receptor." *ELife* 5 (May). https://doi.org/10.7554/eLife.11685.

Skaar, Karin, Henryk J. Korza, Michael Tarry, Petra Sekyrova, and Martin Högbom. 2015. "Expression and Subcellular Distribution of GFP-Tagged Human Tetraspanin Proteins in Saccharomyces Cerevisiae." Edited by Andreas Hofmann. *PLOS ONE* 10 (7): e0134041. https://doi.org/10.1371/journal.pone.0134041.

Smirnova, Irina A., Dan Sjöstrand, Fei Li, Markus Björck, Jacob Schäfer, Henrik Östbye, Martin Högbom, et al. 2016. "Isolation of Yeast Complex IV in Native Lipid Nanodiscs." *Biochimica et Biophysica Acta (BBA) - Biomembranes* 1858 (12): 2984–92. https://doi.org/10.1016/j.bbamem.2016.09.004.

Song, Wanling, Anna L. Duncan, and Mark S.P. Sansom. 2020. "GPCR Oligomerisation Modulation by Conformational State and Lipid Interactions Revealed by MD Simulations and Markov Models." Preprint. Biophysics. https://doi.org/10.1101/2020.06.24.168260.

Soranno, Andrea, Iwo Koenig, Madeleine B. Borgia, Hagen Hofmann, Franziska Zosel, Daniel Nettels, and Benjamin Schuler. 2014. "Single-Molecule Spectroscopy Reveals Polymer Effects of Disordered Proteins in Crowded Environments." *Proceedings of the National Academy of Sciences* 111 (13): 4874–79. https://doi.org/10.1073/pnas.1322611111.

Stanasila, Laura, Jean-Baptiste Perez, Horst Vogel, and Susanna Cotecchia. 2003. "Oligomerization of the α_{1a} - and α_{1b} -Adrenergic Receptor Subtypes: POTENTIAL IMPLICATIONS IN RECEPTOR INTERNALIZATION." *Journal of Biological Chemistry* 278 (41): 40239–51. https://doi.org/10.1074/jbc.M306085200.

Staus, Dean P., Hongli Hu, Michael J. Robertson, Alissa L. W. Kleinhenz, Laura M. Wingler, William D. Capel, Naomi R. Latorraca, Robert J. Lefkowitz, and Georgios Skiniotis. 2020. "Structure of the M2 Muscarinic Receptor–β-Arrestin Complex in a Lipid Nanodisc." *Nature* 579 (7798): 297–302. https://doi.org/10.1038/s41586-020-1954-0.

Stone, Katherine M., Jeda Voska, Maia Kinnebrew, Anna Pavlova, Matthias J.N. Junk, and Songi Han. 2013. "Structural Insight into Proteorhodopsin Oligomers." *Biophysical Journal* 104 (2): 472–81. https://doi.org/10.1016/j.bpj.2012.11.3831.

Strange, Philip G. 2005. "Oligomers of D₂ Dopamine Receptors: Evidence From Ligand Binding." *Journal of Molecular Neuroscience* 26 (2–3): 155–60. https://doi.org/10.1385/JMN:26:2-3:155.

Sun, Bingfa, Priti Bachhawat, Matthew Ling-Hon Chu, Martyn Wood, Tom Ceska, Zara A. Sands, Joel Mercier, Florence Lebon, Tong Sun Kobilka, and Brian K. Kobilka. 2017. "Crystal Structure of the Adenosine A2A Receptor Bound to an Antagonist Reveals a Potential Allosteric Pocket." *Proceedings of the National Academy of Sciences* 114 (8): 2066–71. https://doi.org/10.1073/pnas.1621423114.

Sušac, Lukas, Matthew T. Eddy, Tatiana Didenko, Raymond C. Stevens, and Kurt Wüthrich. 2018. "A2A Adenosine Receptor Functional States Characterized by 19F-NMR." *Proceedings of the National Academy of Sciences*, November, 201813649. https://doi.org/10.1073/pnas.1813649115.

Swainsbury, David J. K., Stefan Scheidelaar, Rienk van Grondelle, J. Antoinette Killian, and Michael R. Jones. 2014. “Bacterial Reaction Centers Purified with Styrene Maleic Acid Copolymer Retain Native Membrane Functional Properties and Display Enhanced Stability.” *Angewandte Chemie International Edition* 53 (44): 11803–7. https://doi.org/10.1002/anie.201406412.

Swainsbury, David J.K., Stefan Scheidelaar, Nicholas Foster, Rienk van Grondelle, J. Antoinette Killian, and Michael R. Jones. 2017. “The Effectiveness of Styrene-Maleic Acid (SMA) Copolymers for Solubilisation of Integral Membrane Proteins from SMA-Accessible and SMA-Resistant Membranes.” *Biochimica et Biophysica Acta (BBA) - Biomembranes* 1859 (10): 2133–43. https://doi.org/10.1016/j.bbamem.2017.07.011.

Szasz, Cs., A. Alexa, K. Toth, M. Rakacs, J. Langowski, and P. Tompa. 2011. “Protein Disorder Prevails under Crowded Conditions.” *Biochemistry* 50 (26): 5834–44. https://doi.org/10.1021/bi200365j.

Tabor, Alina, Siegfried Weisenburger, Ashutosh Banerjee, Nirupam Purkayastha, Jonas M. Kaindl, Harald Hübner, Luxi Wei, et al. 2016. “Visualization and Ligand-Induced Modulation of Dopamine Receptor Dimerization at the Single Molecule Level.” *Scientific Reports* 6 (1). https://doi.org/10.1038/srep33233.

Takahashi, K., K. Tsuchida, Y. Tanabe, M. Masu, and S. Nakanishi. 1993. “Role of the Large Extracellular Domain of Metabotropic Glutamate Receptors in Agonist Selectivity Determination.” *Journal of Biological Chemistry* 268 (26): 19341–45.

Takeda, Shigeki, Shiro Kadowaki, Tatsuya Haga, Hirotomo Takaesu, and Shigeki Mitaku. 2002. “Identi¢cation of G Protein-Coupled Receptor Genes from the Human Genome Sequence.” *FEBS Letters*, 5.

Tanaka, Masafumi, Akira Hosotani, Yuka Tachibana, Minoru Nakano, Kenji Iwasaki, Toru Kawakami, and Takahiro Mukai. 2015. “Preparation and Characterization of Reconstituted Lipid–Synthetic Polymer Discoidal Particles.” *Langmuir* 31 (46): 12719–26. https://doi.org/10.1021/acs.langmuir.5b03438.

Tanford, C. 1978. “The Hydrophobic Effect and the Organization of Living Matter.” *Science* 200 (4345): 1012–18. https://doi.org/10.1126/science.653353.

Tanford, Charles. 1980. *The Hydrophobic Effect: Formation of Micelles and Biological Membranes*. 2nd ed. J. Wiley.

The PyMOL Molecular Graphics System, Version 2.0 Schrödinger, LLC. n.d.

Thévenin, Damien, Tzvetana Lazarova, Matthew F. Roberts, and Clifford R. Robinson. 2005. “Oligomerization of the Fifth Transmembrane Domain from the Adenosine A $_{2A}$ Receptor.” *Protein Science* 14 (8): 2177–86. https://doi.org/10.1110/ps.051409205.

Thomas, Andrew S., and Adrian H. Elcock. 2007. “Molecular Dynamics Simulations of Hydrophobic Associations in Aqueous Salt Solutions Indicate a Connection between Water Hydrogen Bonding and the Hofmeister Effect.” *Journal of the American Chemical Society* 129 (48): 14887–98. https://doi.org/10.1021/ja073097z.

Thompson, Rebecca F., Matt Walker, C. Alistair Siebert, Stephen P. Muench, and Neil A. Ranson. 2016. “An Introduction to Sample Preparation and Imaging by Cryo-Electron Microscopy for Structural Biology.” *Methods* 100 (May): 3–15. https://doi.org/10.1016/j.ymeth.2016.02.017.

Thorner, Jeremy. 1980. *The Molecular Biology of the Yeast Saccharomyces Cerevisiae: Life Cycle and Inheritance*. Cold Spring Harbor, New York: Cold Spring Harbor Laboratory.

Thorsen, Thor Seneca, Rachel Matt, William I. Weis, and Brian K. Kobilka. 2014. “Modified T4 Lysozyme Fusion Proteins Facilitate G Protein-Coupled Receptor Crystallogenesis.” *Structure* 22 (11): 1657–64. https://doi.org/10.1016/j.str.2014.08.022.

Timsit, Youri, Fréderic Allemand, Claude Chiaruttini, and Mathias Springer. 2006. “Coexistence of Two Protein Folding States in the Crystal Structure of Ribosomal Protein L20.” *EMBO Reports* 7 (10): 1013–18. https://doi.org/10.1038/sj.embor.7400803.

Tonge, S.R, and B.J Tighe. 2001. “Responsive Hydrophobically Associating Polymers: A Review of Structure and Properties.” *Advanced Drug Delivery Reviews* 53 (1): 109–22. https://doi.org/10.1016/S0169-409X(01)00223-X.

Torres, Jaume, Tim J. Stevens, and Montserrat Samsó. 2003. “Membrane Proteins: The ‘Wild West’ of Structural Biology.” *Trends in Biochemical Sciences* 28 (3): 137–44. https://doi.org/10.1016/S0968-0004(03)00026-4.

Torvinen, M. 2004. “Adenosine A2A Receptor and Dopamine D3 Receptor Interactions: Evidence of Functional A2A/D3 Heteromeric Complexes.” *Molecular Pharmacology* 67 (2): 400–407. https://doi.org/10.1124/mol.104.003376.

Tovo-Rodrigues, L., A. Roux, M.H. Hutz, L.A. Rohde, and A.S. Woods. 2014. “Functional Characterization of G-Protein-Coupled Receptors: A Bioinformatics Approach.” *Neuroscience* 277 (September): 764–79. https://doi.org/10.1016/j.neuroscience.2014.06.049.

Tribet, C., R. Audebert, and J.-L. Popot. 1996. “Amphipols: Polymers That Keep Membrane Proteins Soluble in Aqueous Solutions.” *Proceedings of the National Academy of Sciences* 93 (26): 15047–50. https://doi.org/10.1073/pnas.93.26.15047.

Trinh, Thi Kim Hoang, Weihua Qiu, Meg Thornton, Everett E. Carpenter, and Youzhong Guo. 2021. “A Property Fine-Tuned Sulfobetaine Cholesterol Derivative for Membrane Protein Structural Biology.” *Biochimica et Biophysica Acta (BBA) - General Subjects* 1865 (7): 129908. https://doi.org/10.1016/j.bbagen.2021.129908.

Tsai, Chung-Jung, Shuo Liang Lin, Haim J. Wolfson, and Ruth Nussinov. 1997. “Studies of Protein-Protein Interfaces: A Statistical Analysis of the Hydrophobic Effect: Protein-Protein Interfaces: The Hydrophobic Effect.” *Protein Science* 6 (1): 53–64. https://doi.org/10.1002/pro.5560060106.

Tsai, Chung-Jung, and Ruth Nussinov. 1997. “Hydrophobic Folding Units at Protein-Protein Interfaces: Implications to Protein Folding and to Protein-Protein Association.” *Protein Science* 6 (7): 1426–37. https://doi.org/10.1002/pro.5560060707.

Tunuguntla, Ramya, Mangesh Bangar, Kyunghoon Kim, Pieter Stroeve, Caroline M. Ajo-Franklin, and Aleksandr Noy. 2013. “Lipid Bilayer Composition Can Influence the Orientation of Proteorhodopsin in Artificial Membranes.” *Biophysical Journal* 105 (6): 1388–96. https://doi.org/10.1016/j.bpj.2013.07.043.

Ueta, Tetsuya, Keiichi Kojima, Tomoya Hino, Mikihiro Shibata, Shingo Nagano, and Yuki Sudo. 2020. “Applicability of Styrene-Maleic Acid Copolymer for Two Microbial Rhodopsins, RxR and HsSRI.” *Biophysical Journal* 119 (9): 1760–70. https://doi.org/10.1016/j.bpj.2020.09.026.

Vallano, Antoni, Víctor Fernandez-Duenas, Consuelo Pedros, Josep Maria Arnau, and Francisco Ciruela. 2011. “An Update on Adenosine A2A Receptors as Drug Target in Parkinson’s Disease.” *CNS & Neurological Disorders - Drug Targets* 10 (6): 659–69. https://doi.org/10.2174/187152711797247803.

Váró, G., and J.K. Lanyi. 1991. “Distortions in the Photocycle of Bacteriorhodopsin at Moderate Dehydration.” *Biophysical Journal* 59 (2): 313–22. https://doi.org/10.1016/S0006-3495(91)82225-1.

Váró, György, Leonid S. Brown, Melinda Lakatos, and Janos K. Lanyi. 2003. “Characterization of the Photochemical Reaction Cycle of Proteorhodopsin.” *Biophysical Journal* 84 (2): 1202–7. https://doi.org/10.1016/S0006-3495(03)74934-0.

Vegt, Nico F. A. van der, and Divya Nayar. 2017. “The Hydrophobic Effect and the Role of Cosolvents.” *The Journal of Physical Chemistry B* 121 (43): 9986–98. https://doi.org/10.1021/acs.jpcb.7b06453.

Vidi, Pierre-Alexandre, Jiji Chen, Joseph M.K. Irudayaraj, and Val J. Watts. 2008. “Adenosine A $_{2A}$ Receptors Assemble into Higher-Order Oligomers at the Plasma Membrane.” *FEBS Letters* 582 (29): 3985–90. https://doi.org/10.1016/j.febslet.2008.09.062.

Vilardaga, Jean-Pierre, Viacheslav O Nikolaev, Kristina Lorenz, Sébastien Ferrandon, Zhenjie Zhuang, and Martin J Lohse. 2008. "Conformational Cross-Talk between A2A-Adrenergic and μ-Opioid Receptors Controls Cell Signaling." *Nature Chemical Biology* 4 (2): 126–31. https://doi.org/10.1038/nchembio.64.

Viñals, Xavier, Estefanía Moreno, Laurence Lanfumey, Arnau Cordomí, Antoni Pastor, Rafael de La Torre, Paola Gasperini, et al. 2015. "Cognitive Impairment Induced by Delta9-Tetrahydrocannabinol Occurs through Heteromers between Cannabinoid CB1 and Serotonin 5-HT2A Receptors." Edited by Eric J. Nestler. *PLOS Biology* 13 (7): e1002194. https://doi.org/10.1371/journal.pbio.1002194.

Vold, Regitze R., and R.Scott Prosser. 1996. "Magnetically Oriented Phospholipid Bilayered Micelles for Structural Studies of Polypeptides. Does the Ideal Bicelle Exist?" *Journal of Magnetic Resonance, Series B* 113 (3): 267–71. https://doi.org/10.1006/jmrb.1996.0187.

Waldhoer, M., J. Fong, R. M. Jones, M. M. Lunzer, S. K. Sharma, E. Kostenis, P. S. Portoghese, and J. L. Whistler. 2005. "A Heterodimer-Selective Agonist Shows in Vivo Relevance of G Protein-Coupled Receptor Dimers." *Proceedings of the National Academy of Sciences* 102 (25): 9050–55. https://doi.org/10.1073/pnas.0501112102.

Wallin, Erik, and Gunnar Von Heijne. 1998. "Genome-Wide Analysis of Integral Membrane Proteins from Eubacterial, Archaean, and Eukaryotic Organisms: Membrane Protein Topology." *Protein Science* 7 (4): 1029–38. https://doi.org/10.1002/pro.5560070420.

Wang, G., and R. L. Dunbrack. 2003. "PISCES: A Protein Sequence Culling Server." *Bioinformatics* 19 (12): 1589–91. https://doi.org/10.1093/bioinformatics/btg224.

Wang, Wei-Wu, Oleg A. Sineshchekov, Elena N. Spudich, and John L. Spudich. 2003. "Spectroscopic and Photochemical Characterization of a Deep Ocean Proteorhodopsin." *Journal of Biological Chemistry* 278 (36): 33985–91. https://doi.org/10.1074/jbc.M305716200.

Wang, Wenyan, and Bruce A. Malcolm. 1999. "Two-Stage PCR Protocol Allowing Introduction of Multiple Mutations, Deletions and Insertions Using QuikChangeTM Site-Directed Mutagenesis." *BioTechniques* 26: 680–82.

Wang, Xiaoming, Zongjun Mu, Yan Li, Yunchen Bi, and Yujuan Wang. 2015. "Smaller Nanodiscs Are Suitable for Studying Protein Lipid Interactions by Solution NMR." *The Protein Journal* 34 (3): 205–11. https://doi.org/10.1007/s10930-015-9613-2.

Wassenaar, Tsjerk A., Kristyna Pluhackova, Rainer A. Böckmann, Siewert J. Marrink, and D. Peter Tieleman. 2014. "Going Backward: A Flexible Geometric Approach to Reverse Transformation from Coarse Grained to Atomistic Models." *Journal of Chemical Theory and Computation* 10 (2): 676–90. https://doi.org/10.1021/ct400617g.

Weis, William I, and Brian K Kobilka. 2008. "Structural Insights into G-Protein-Coupled Receptor Activation." *Current Opinion in Structural Biology* 18 (6): 734–40. https://doi.org/10.1016/j.sbi.2008.09.010.

Weiß, H. Markus, and Reinhard Grisshammer. 2002. "Purification and Characterization of the Human Adenosine A2a Receptor Functionally Expressed in Escherichia Coli: Purification and Characterization of A2a Receptor." *European Journal of Biochemistry* 269 (1): 82–92. https://doi.org/10.1046/j.0014-2956.2002.02618.x.

White, Julia H., Alan Wise, Martin J. Main, Andrew Green, Neil J. Fraser, Graham H. Disney, Ashley A. Barnes, Piers Emson, Steven M. Foord, and Fiona H. Marshall. 1998. "Heterodimerization Is Required for the Formation of a Functional GABAB Receptor." *Nature* 396 (6712): 679–82. https://doi.org/10.1038/25354.

Wicky, Basile I. M., Sarah L. Shammas, and Jane Clarke. 2017. "Affinity of IDPs to Their Targets Is Modulated by Ion-Specific Changes in Kinetics and Residual Structure." *Proceedings of the National Academy of Sciences* 114 (37): 9882–87. https://doi.org/10.1073/pnas.1705105114.

Woods, Amina S., and Sergi Ferré. 2005. “Amazing Stability of the Arginine−Phosphate Electrostatic Interaction.” *Journal of Proteome Research* 4 (4): 1397–1402. https://doi.org/10.1021/pr050077s.

Wu, Beili, Ellen Y.T. Chien, Clifford D. Mol, Gustavo Fenalti, Wei Liu, Vsevolod Katritch, Ruben Abagyan, et al. 2010. “Structures of the CXCR4 Chemokine GPCR with Small-Molecule and Cyclic Peptide Antagonists.” *Science* 300: 1066–71. https://doi.org/doi: 10.1126/science.1194396.

Xie, Zhidong, Samuel P. Lee, Brian F. O’Dowd, and Susan R. George. 1999. “Serotonin 5-HT1B and 5-HT1D Receptors Form Homodimers When Expressed Alone and Heterodimers When Co-Expressed.” *FEBS Letters* 456 (1): 63–67. https://doi.org/10.1016/S0014-5793(99)00918-7.

Xu, Fei, Huixian Wu, Vsevolod Katritch, Gye Won Han, Kenneth A Jacobson, Zhan-Guo Gao, Vadim Cherezov, and Raymond C Stevens. 2011. “Structure of an Agonist-Bound Human A2A Adenosine Receptor” 332: 7.

Xue, Li, Xavier Rovira, Pauline Scholler, Han Zhao, Jianfeng Liu, Jean-Philippe Pin, and Philippe Rondard. 2015. “Major Ligand-Induced Rearrangement of the Heptahelical Domain Interface in a GPCR Dimer.” *Nature Chemical Biology* 11 (2): 134–40. https://doi.org/10.1038/nchembio.1711.

Yang, Zhen. 2009. “Hofmeister Effects: An Explanation for the Impact of Ionic Liquids on Biocatalysis.” *Journal of Biotechnology* 144 (1): 12–22. https://doi.org/10.1016/j.jbiotec.2009.04.011.

Yao, Lina, Maria Pia Arolfo, Douglas P Dohrman, Zhan Jiang, Peidong Fan, Sara Fuchs, Patricia H Janak, Adrienne S Gordon, and Ivan Diamond. 2002. “Beta-Gamma Dimers Mediate Synergy of Dopamine D2 and Adenosine A2 Receptor-Stimulated PKA Signaling and Regulate Ethanol Consumption.” *Cell* 109: 733–43.

Ye, Libin, Ned Van Eps, Marco Zimmer, Oliver P. Ernst, and R. Scott Prosser. 2016. “Activation of the A2A Adenosine G-Protein-Coupled Receptor by Conformational Selection.” *Nature* 533 (7602): 265–68. https://doi.org/10.1038/nature17668.

Yin, Jie, Kuang-Yui M. Chen, Mary J. Clark, Mahdi Hijazi, Punita Kumari, Xiao-chen Bai, Roger K. Sunahara, Patrick Barth, and Daniel M. Rosenbaum. 2020. “Structure of a D2 Dopamine Receptor–G-Protein Complex in a Lipid Membrane.” *Nature* 584 (7819): 125–29. https://doi.org/10.1038/s41586-020-2379-5.

Yodh, A. G., K. Lin, J. C. Crocker, A. D. Dinsmore, R. Verma, and P. D. Kaplan. 2001. “Entropically Driven Self–Assembly and Interaction in Suspension.” Edited by J. Hansen, P. N. Pusey, and P. B. Warren. *Philosophical Transactions of the Royal Society of London. Series A: Mathematical, Physical and Engineering Sciences* 359 (1782): 921–37. https://doi.org/10.1098/rsta.2000.0810.

Yoshioka, K., O. Saitoh, and H. Nakata. 2001. “Heteromeric Association Creates a P2Y-like Adenosine Receptor.” *Proceedings of the National Academy of Sciences* 98 (13): 7617–22. https://doi.org/10.1073/pnas.121587098.

Zangi, Ronen, Morten Hagen, and B. J. Berne. 2007. “Effect of Ions on the Hydrophobic Interaction between Two Plates.” *Journal of the American Chemical Society* 129 (15): 4678–86. https://doi.org/10.1021/ja068305m.

Zeng, Fu-Yue, and Jürgen Wess. 1999. “Identification and Molecular Characterization of M3 Muscarinic Receptor Dimers.” *Journal of Biological Chemistry* 274 (27): 19487–97. https://doi.org/10.1074/jbc.274.27.19487.

Zezula, J, and M Freissmuth. 2009. “The A2A-Adenosine Receptor: A GPCR with Unique Features?: The A2A-Adenosine Receptor.” *British Journal of Pharmacology* 153 (S1): S184–90. https://doi.org/10.1038/sj.bjp.0707674.

Zhang, Peisu, Peter S Johnson, Christian Zollner, Wenfei Wang, Zaijie Wang, Anita E Montes, Brian K Seidleck, Carrie J Blaschak, and Christopher K Surratt. 1999. “Mutation of Human m Opioid

Receptor Extracellular '"Disulfide Cysteine"' Residues Alters Ligand Binding but Does Not Prevent Receptor Targeting to the Cell Plasma Membrane," 10.

Zhou, Huan-Xiang, and Timothy A. Cross. 2013a. "Modeling the Membrane Environment Has Implications for Membrane Protein Structure and Function: Influenza A M2 Protein: Influence on M2 Protein by Membrane Mimetics." *Protein Science* 22 (4): 381–94. https://doi.org/10.1002/pro.2232.

———. 2013b. "Influences of Membrane Mimetic Environments on Membrane Protein Structures." *Annual Review of Biophysics* 42 (1): 361–92. https://doi.org/10.1146/annurev-biophys-083012-130326.

Zhu, Xiangyang, and Jürgen Wess. 1998. "Truncated V2 Vasopressin Receptors as Negative Regulators of Wild-Type V2 Receptor Function." *Biochemistry* 37 (45): 15773–84. https://doi.org/10.1021/bi981162z.

Zoonens, Manuela, Jeffrey Comer, Sandrine Masscheleyn, Eva Pebay-Peyroula, Christophe Chipot, Bruno Miroux, and François Dehez. 2013. "Dangerous Liaisons between Detergents and Membrane Proteins. The Case of Mitochondrial Uncoupling Protein 2." *Journal of the American Chemical Society* 135 (40): 15174–82. https://doi.org/10.1021/ja407424v.

Zoonens, Manuela, and Jean-Luc Popot. 2014. "Amphipols for Each Season." *The Journal of Membrane Biology* 247 (9–10): 759–96. https://doi.org/10.1007/s00232-014-9666-8.

Zosel, Franziska, Andrea Soranno, Karin J. Buholzer, Daniel Nettels, and Benjamin Schuler. 2020. "Depletion Interactions Modulate the Binding between Disordered Proteins in Crowded Environments." *Proceedings of the National Academy of Sciences* 117 (24): 13480–89. https://doi.org/10.1073/pnas.1921617117.